Louisiana State University
LSU Digital Commons

LSU Doctoral Dissertations | Graduate School

2007

Design, Synthesis, And Conformational Studies Of Peptides Containing Î±,Î±-Disubstituted amino acids

Jia Wang
Louisiana State University and Agricultural and Mechanical College

Follow this and additional works at: https://digitalcommons.lsu.edu/gradschool_dissertations

 Part of the Chemistry Commons

Recommended Citation
Wang, Jia, "Design, Synthesis, And Conformational Studies Of Peptides Containing Î±,Î±-Disubstituted amino acids" (2007). *LSU Doctoral Dissertations*. 1761.
https://digitalcommons.lsu.edu/gradschool_dissertations/1761

This Dissertation is brought to you for free and open access by the Graduate School at LSU Digital Commons. It has been accepted for inclusion in LSU Doctoral Dissertations by an authorized graduate school editor of LSU Digital Commons. For more information, please contactgradetd@lsu.edu.

DESIGN, SYNTHESIS, AND CONFORMATIONAL STUDIES OF PEPTIDES CONTAINING ALPHA, ALPHA-DISUBSTITUTED AMINO ACIDS

A Dissertation

Submitted to the Graduate Faculty of the
Louisiana State University and
Agricultural and Mechanical College
in partial fulfillment of the
requirements for the degree of
Doctor of Philosophy

in

The Department of Chemistry

by
Jia Wang
B.S., Dalian University, 1996
August, 2007

ACKNOWLEDGEMENTS

I would like to thank my research advisor, Dr. Robert Hammer, for his guidance, knowledge and support. I would also like to thank my advisory committee members, Dr. William Crowe, Dr. Andrew Maverick, Dr. Graca Vicente and Dr. Jack Losso for their time and valuable suggestions. I acknowledge Dr. Timothy Keiderling at University of Illinois at Chicago for his insight advice.

Thanks are also due to my colleagues, for their friendship and a lot of laughter.

Most of all my appreciation is for my parents and my husband for their endless love, encouragement, and sacrifice.

TABLE OF CONTENTS

LIST OF TABLES

LIST OF FIGURES

LIST OF ABBREVIATIONS

ααAA	$C^{\alpha,\alpha}$-disubstituted amino acid
Aβ	β-amyloid peptide
Aib	α-aminoisobutyric acid
Ac	acetyl
Ala	alanine
Asn	asparagine
Bn	benzyl
Boc	tert-butyloxycarbonyl
CD	circular dichroism
COSY	homonuclear correlated spectroscopy
d	doublet
DBU	1,8-diazobicyclo[4.5.0]undec-7-ene
DCC	dicyclohexylcarbodiimide
DCE	1,2-dichloroethane
Deg	$C^{\alpha,\alpha}$-diethylglycine
Dibg	$C^{\alpha,\alpha}$-diisobutylglycine
DIEA	diisopropylethylamine
DMF	N,N-dimethylformamide
DMAP	dimethylaminopyridine
Dpg	$C^{\alpha,\alpha}$-dipropylglycine
Equiv.	equivalents
Et_2O	diethyl ether

EtOAc	ethyl acetate
EtOH	ethanol
Fmoc	9-fluorenylmethoxycarbonyl
GHP	Gellman hairpin peptide
Glu	glutamic acid
HATU	O-(7-azabenzotriazol-1-yl)-1,1,3,3-tetramethyluronium hexafluorophosphate
HBTU	O-(1-benzotriazol-1-yl)-1,1,3,3-tetramethyluronium hexafluorophosphate
HOAt	1-hydroxy-7-azabenzotriazole
HOBt	1-hydroxybenzotriazole
HPLC	high performance liquid chromatography
HSQC	heteronuclear single quantum correlation
HMBC	heteronuclear multiple bond coherence
i-Bu	isobutyl
Lys	lysine
m	multiplet
M	molar
MALDI	matrix assisted laser desorption ionization
MHz	megahertz
mL	milliliter
mM	millimolar
mmol	millimole
MTPACl	α-methoxy-α-trifluoromethyl-phenylacetyl chloride

nm	nanometer
NMR	nuclear magnetic resonance
NOE	nuclear overhauser effect
NOESY	nuclear overhauser effect spectroscopy
PAL	5-(4-aminomethyl-3,5-dimethoxyphenoxy)valeric acid
PB	phosphate buffer
PEG-PS	polyethylene glycol–polystyrene (graft resin support)
PTC	phase transfer catalyst
PyAOP	7-azabenzotriazolyoxytris(pyrrolidino)phosphonium hexafluorophosphate
PyBOP	1-benzotriazolyoxytris(pyrrolidino)phosphonium hexafluorophosphate
q	quartet
ROESY	rotating frame overhauser enhancement spectroscopy
s	singlet
SPPS	solid phase peptide synthesis
t	triplet
t-Bu	*tert*-butyl
TBAB	tetrabutylammonium bromide
TBTU	*N*-[(1*H*-benzotriazol-1-yl)(dimethylamino)methylene]-*N*-methylmethanaminium tetrafluoroborate;
TFA	trifluoroacetic acid
THF	tetrahydrofuran
TIPS	triisopropylsilane
Thr	threonine

TMS-Cl	trimethylsilyl chloride
TOCSY	total correlated spectroscopy
Trt	triphenylmethyl (trityl)
Tyr	tyrosine
UV	ultraviolet spectroscopy
Val	valine
VCD	vibrational circular dicroism

ABSTRACT

$C^{\alpha,\alpha}$-disubstituted amino acids ($\alpha\alpha$AAs) are widely utilized to conformationally constrain peptides. Several pentapeptides containing dipropylglycine (Dpg) at alternating positions and their α-amino acid counterpart L-norvaline (Nva) analogues were synthesized to fully investigate the impact of Dpg on peptide backbone structure in aqueous solution. CD, VCD and NMR spectral analysis suggest that Dpg containing peptides adopt more ordered structures relative to their Nva containing analogues. The central residues (Ala, Thr, Tyr, Val) and the charged side-chains of Glu and Lys play important roles in the degree of peptide folding. Hydrophobic and branched residues (Val, Tyr) at the central position of the peptide produce greater folding as judged by CD and NMR. Temperature-dependent NMR analysis ($\Delta\delta/\Delta T$ NH) of Ac-Glu-Dpg-Tyr-Dpg-Lys-NH_2 suggests a series of i→i+3 hydrogen bonds between the N-terminal acetyl carbonyl and the Tyr^3 NH, and the Glu^1 carbonyl and the Dpg^4 NH. The solution conformation of Ac-Glu-Dpg-Tyr-Dpg-Lys-NH_2 calculated from NMR-derived constraints shows a 3_{10}-helical structure (two repetitive type-III β-turns) at residues 1-4, which is supported by 2D NMR, CD and VCD spectra. Analysis of NMR-derived models of these peptides suggest that there is a strong hydrophobic interaction of the pro-*S* propyl side chain of Dpg^2 and the Tyr^3 side-chain that may be a strong stabilizing force of the peptide folding in water.

$C^{\alpha,\alpha}$-diisobutylglycine(Dibg) was synthesized via palladium catalyzed allylation reaction with an excellent overall yield and incorporated into various positions of a model β-hairpin peptide GHP in order to determine the effectiveness of the $\alpha\alpha$AAs as design elements in both the strand and turn portions of β-hairpins. CD and NMR data of Dibg

containing peptides showed Dibg residue can contribute to the stability of the strand portion of a β-hairpin peptide and destabilize the β-turn in the GHP. The sheet stabilizing effect of Dibg may be due to the strong propensity of Dibg to have a fully extended conformation(ϕ/ψ= 180°). Several chiral amino esters were prepared with high enantioselectivity by alkylation of the corresponding Schiff bases under chiral phase-transfer condition. The enantiomeric excess of these chiral amino esters was efficiently determined by ^{19}F-NMR analysis of the corresponding diastereomeric Mosher amides.

CHAPTER 1: INTRODUCTION

1.1 Protein Structure

The 20 most common naturally occurring amino acids differ only in the side chains attached to the α-carbon. The difference of side chains is what is responsible for the structural variation and functional diversity of peptides or proteins. The three-dimensional structure of a protein is crucial to its physical, chemical and biological properties. In nature, proteins adopt unique folded conformations that optimize their biological function. Thus, a good understanding of fundamental forces that determine peptide secondary structure will contribute our ability to design new peptides with specific structure and function.

Protein structure has been classified into four different levels. Primary structure is the amino acid sequence in the protein chain. Secondary structure consists of a regularly repeating regional structure such as α-helix, β-sheet, turns, and random coil. Tertiary structure is the folding of secondary structure elements of a single peptide chain to give an overall fold or 3D structure. Quaternary structure is the spatial arrangement of the individual peptide chain resulting from the interactions between two or more individual polypeptide chains. Protein structures are stabilized by both covalent interactions which are responsible for the formation of amide bonds and three noncovalent interactions: electrostatic interactions, hydrogen bonds, and van der Waals interactions which are responsible for stabilization of the higher level of structures, such as secondary, tertiary or quaternary structures.

The peptide bond possesses partial double-bond character which is depicted by a resonance structure (Figure 1.1) that leads to a planar and rigid amide group. The

resonance form of the amide bond also demonstrates that the peptide bond itself is polarized such that the oxygen is a hydrogen bond acceptor and the N-H bond is a hydrogen bond donor. Hydrogen bonding interactions are a main force in stabilizing the secondary structures of peptides and proteins.

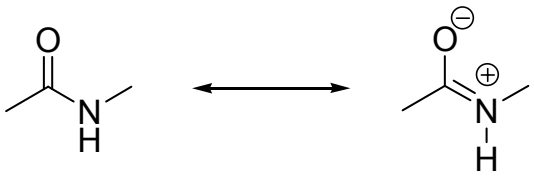

Figure 1.1 Resonance structure of the amide bond

Peptides form different secondary structures based upon the spatial arrangement of amide groups dictated by the backbone conformation. The conformation of a peptide backbone is characterized by a set of torsional angles ϕ and ψ with respect to the amide plane, in which ϕ is the rotation about the C^{α}-N bond and ψ is the rotation around the C^{α}-CO bond(Figure 1.2). Different peptide conformations are associated with specific ranges of ϕ and ψ values. Table 1.1 lists the typical torsional angles associated with the various types of helical and β-sheet conformations.

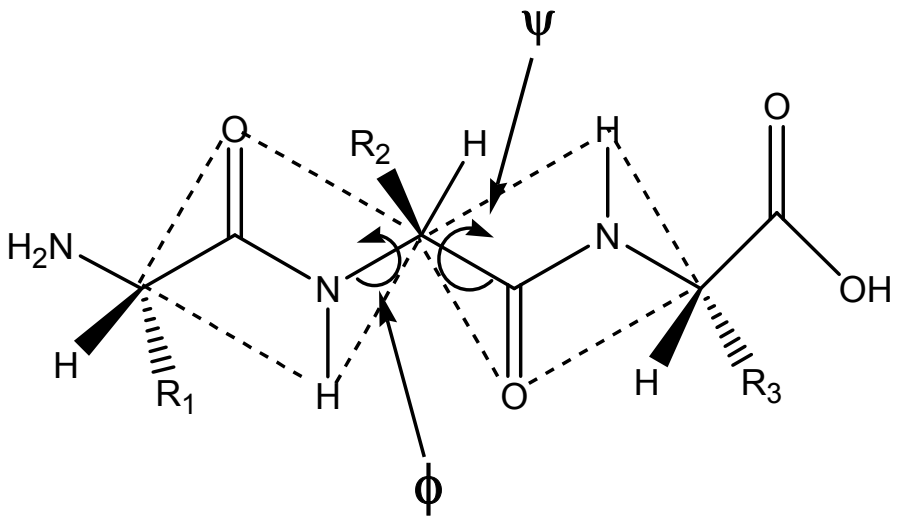

Figure 1.2 Torsional angles of the peptide backbone

Table 1.1 Torsional angles for helices and β-sheets [a]

Conformation	ϕ	ψ	Residues per turn/repeat
α-Helix (right handed)	-57°	-47°	3.6
α-Helix (left handed)	57°	47°	3.6
3_{10}–Helix	-60°	-30°	3.0
Parallel β-sheet	-119°	113°	2.0
Antiparallel β-sheet	-139°	135°	2.0

[a] Angles taken from IUPAC-IUB Commission on Biochemical Nomenclature (1970)

Helices are one of the most common types of secondary structure in proteins in which amino acid residues are wrapped around a central axis to form an approximately cylindrical surface with intramolecuar hydrogen bonds parallel to the helix axis. The α-helix has 3.6 residues per turn, stabilized by intramolecular hydrogen bonding between CO of residue i and the NH of residue i+4. The distance between adjacent amino acids is 1.5 Å. The 3_{10}-helix contains 3 residues per turn, stabilized by intramolecuar hydrogen bonding between CO of residue i and the NH of residue i+3. The distance between adjacent amino acids is 2.0 Å. The uniform alignments of amide groups with hydrogen bonded carbonyl groups in the helix generate helix dipole moment with a net positive charge at the N-terminus and a net negative charge at the C-terminus which is an important property for helical conformations. Baldwin et al. have shown that charged groups play a critical role in helix stability in aqueous solution by interaction with a nearby dipole of the helix.[1] This interaction will stabilize helical structures if the two have opposite charge and will be helix-destabilizing when the two possess the same charge. This phenomenon has been noted as the charged group-helix dipole interaction.

The second main type of secondary structure is β-sheet, which form a sheet like structure in a zigzag format stabilized by intermolecular hydrogen bonding between two adjacent peptide strands, whereas in the helical structure the hydrogen bondings are between NH and CO in the same strand. The distance between adjacent amino acids is 3.5 Å. Two types of β-sheets exist, parallel β-sheet and antiparallel β-sheet, having polypeptide strands either parallel or antiparallel to each other.

The third main type of secondary structure in protein is turns. β-Turn and γ-turn contain consecutive four and three amino acid residues respectively, where the polypeptide chain folds back on itself by nearly 180 degrees. β-Turns are stabilized by a hydrogen bond between the carbonyl of the residue *i* and the NH of the residue *i + 3* as shown in Figure 1.3. While γ-turns are stabilized by a hydrogen bond between the carbonyl of the residue *i* and the NH of the residue *i + 2.* It is these chain reversals which give a protein its globularity rather than linearity. Lewis et al. found that 25% of β-turns do not possess the hydrogen bond.[2] Therefore the broadened definition of β-turns is that the distance between the alpha carbon of residue i and the alpha carbon of residue i+3 should be less than 7 Å. It should be noted that the type-III β-turn possesses the same torsional angles as a 3_{10} helix structure. Thus, the type-III β-turn is equivalent to a 3_{10} helix. The common β-turns and their characteristic torsional angles are listed in Table 1.2.

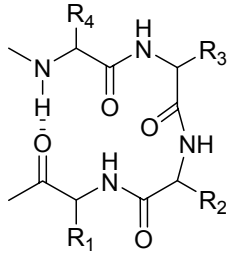

Figure 1.3 β-Turn structure, hydrogen bonds are indicated by dotted lines

Table 1.2 Typical torsional angles for various β-turns[a]

Conformation	Torsional Angle (degrees)[b]				Residures per turn/repeat
	ϕ_{i+1}	ϕ_{i+2}	ψ_{i+1}	ψ_{i+2}	3
Type-I	-60	-90	-30	0	3
Type-I'	+60	+90	+30	0	3
Type-II	-60	+80	+120	0	3
Type-II'	+60	-80	-120	0	3
Type-III	-60	-60	-30	-30	3

[a] For β-turn, the torsional angles from two consecutive amino acid residues i+1 and i+2 in the middle of the turn are used to define the structure.
[b] Torsional angels taken from Ref 3.[3]

1.2 Commonly Used Techniques for Conformational Analysis of Peptides

The three-dimensional structure of peptides can provide valuable information on their properties and biological functions. Circular dichroism (CD), fourier transform infrared (FTIR), and nuclear magnetic resonance (NMR) analysis are commonly used spectroscopic techniques to interpret peptide structures in solution.

- **Circular Dichroism (CD) Study of Peptide Conformation**

Circular dichroism (CD) spectroscopy has been widely used to probe peptide secondary structure in solution. Circular dichroism spectroscopy measures the difference between the absorption of left- and right-handed circularly polarized light by a chiral molecule.[4] The interaction between transition moments leads to CD and the geometrical relation between amide groups in different secondary structures leads to the characteristic CD spectra of different secondary structures. There are two types of CD spectroscopies: circular dichroism due to electronic transitions is referred to as CD(also as ECD) and that due to vibrational transitions as VCD. Most CD measurements are reported in molar

ellipticity as: $[\theta] = 100\ \theta / C*l$ in the unit of deg cm^2dmol^{-1} where C and l are the molar concentration of the sample and pathlength in cm, respectively.

CD spectra of peptides in the far-UV (190-250 nm) region are dominated by the amide chromophores and reflect primarily the conformation of the peptide backbone, which is diagnostic for the peptide secondary structure. CD spectra of peptides in the near-UV (250-300 nm) region are the contributions of aromatic and sulfur-containing side chains. Some CD spectra show a positive interfering band around 224 nm for the aromatic side chains and a negative band around 228 nm for sulfur-containing side chains. In most cases, a CD spectrum below 260 nm is governed by the amide chromophore, and the side-chain contribution is negligible.[5]

α-Helices are characterized by double minima at 210 nm (π-π* transitions) and 222 nm (n-π* transitions); β-sheets show a single, broad, negative band at 212 nm (n-π* transitions) and a positive band near 195 nm; random coils exhibit a strong, negative band at 195 nm. A typical β-turn CD spectrum exhibits a negative band near 225 nm(n-π* transitions), a strong positive π-π* transition between 200 nm and 205 nm.[6] CD is a quick method that requires only small amount of peptide, and thus can be used to survey the effects of differing pH, temperature and solvent conditions on peptide conformations. CD experiments are carried out in solution phase that is important for the study of biological systems because it can provide the structure in a near physiological condition. CD is dependent upon a cooperative effect of the amide transitions and thus is positionally averaged and doesn't give site-specific information.

- **Fourier Transform Infrared (FTIR)**

Amide I and amide II regions in FTIR are often utilized to extract secondary structural

information of peptides from amide stretching bands.[7] Amide I band results from stretching vibrations of the backbone carbonyl groups and amide II band results from the N-H bending vibration. The frequency of the vibration is determined by the nature of the hydrogen bonding and backbone conformations. α-Helices show the amide I band at about 1655 cm^{-1} and the amide II band at 1540 cm^{-1}; β-sheets exhibit the amide I band at 1630 cm^{-1} and the amide II band at 1520 cm^{-1} ; random coils show the amide I and II at 1660 and 1535 cm^{-1} respectively. FTIR spectroscopy in some cases can give information on the relative populations of various folded conformations in solution.

- **NMR Analysis of Peptide Secondary Structure**

The determination of peptide structures by nuclear magnetic resonance (NMR) has come into wide use in the last twenty years. The technique uses peptide samples in aqueous solution, rather than crystals. Thus it can provide the structure close to physiological conditions. Parameters such as nuclear overhauser effect (NOE), rotating frame overhauser enhancement (ROE), chemical shift deviation from the random coil conformation, temperature coefficients of amide protons, and coupling constant have been routinely used in the elucidation of peptide structures by NMR.

NOE and ROE can detect distances of pairs of protons less than 5 **Å**. The interproton distances serve as NMR restraints and are used to construct a three-dimensional structure of a peptide through molecular dynamics and energy minimization methods. The NOE connectivities can also provide information on the types of conformations present in solution because different peptide conformations are associated with specific NOE connectivity patterns. Sequential $d_{NN}(i,i+1)$ NOE connectivities, medium-range NOE connectivities $d_{\alpha N}(i,i+2)$, and $d_{\alpha N}(i,i+3)$ are observed, if the peptide

has a significant population of turns or helices, whereas long range NOE connectivities and strong sequential $d_{\alpha N}(i,i+1)$ NOE connectivities with the absence of $d_{NN}(i,i+1)$ NOEs are observed if the peptide adopts an extended conformation.[8]

α-Proton chemical shifts have been proven to be highly sensitive to peptide backbone conformation. They experience upfield shifts relative to the random coil structure when in a helical or turn structure and exhibit downfield shifts from the random coil value when in a β-sheet structure.[9] Carbon chemical shifts of α-carbons and carbonyl carbons are also conformationally dependent, with residues in helical structures showing downfield shifts and with residues in β-sheet structures showing upfield shifts relative to the random coil values.

Wishart and coworkers have demonstrated that "chemical shift index" ($\Delta\delta_{H\alpha} = \delta_{H\alpha(observed)} - \delta_{H\alpha(random\ coil)}$) provides qualitative insight on secondary structure. A group of three or more residues with $\Delta\delta_{H\alpha} > 0.1$ ppm are considered to be β-strands. A group of residues containing four or more residues with $\Delta\delta_{H\alpha} < 0.1$ indicate helical or turn structures.[9] Gellman et al. and Searle et al. have reported that α-proton resonances are reliable reporters for the quantitative analysis of β-hairpin populations.[10-12] The β-hairpin populations can be quantitatively determined in aqueous solution by comparison of the chemical shifts of α-proton in the sheet portion or the diastereotopic glycine α-protons of the peptide of interest relative to those of reference compound representing the unfolded and fully folded states by using the following equations:

$$f = (\delta_{observed} - \delta_{unfolded})/(\delta_{fully\ folded} - \delta_{unfolded})$$

$$f = \Delta\delta Gly_{observed} / \Delta\delta_{fully\ folded}$$

where f = mole fraction of hairpin folded and $\delta_{observed}$ is the chemical shift of α-hydrogens

of the sheet portion or glycine α-protons observed experimentally, $\delta_{unfolded}$ is the chemical shift of the α-proton in the fully unfolded state, and $\delta_{fully\ folded}$ is the chemical shift of the α-proton in the fully folded state. The extent of folding can be related to the equilibrium constant K, by the following equation, K = f/(1-f). The free energy change can then be determined from $\Delta G = -RT \ln K$.

The chemical shift of the amide proton resonance depends upon the temperature; the temperature dependences of amide proton chemical shifts (temperature coefficients) are frequently measured to locate intramolecular hydrogen-bonds.[13] Hydrogen-bonded (exchange-protected) amide protons typically display reduced temperature coefficients with respect to non-hydrogen bonded, solvent exposed amide protons.

Coupling constants $^3J_{HNH\alpha}$ are dependent on the angle between amide proton and α-proton and can be converted to the dihedral angle ϕ based on Karplus equation:[14] $^3J_{HNH\alpha} = 6.51\cos^2(\phi-60°)-1.76\cos(\phi-60°)+1.60$. The calculated ϕ with a +/-10° limit are often introduced as torsion angle restraints for structural calculation.

COSY enables one to see correlations between coupled protons. TOCSY correlates all protons within the same spin system. ROESY correlates protons that are close to each other in space, typically 4.5 Å or less. HSQC correlates protons with their directly attached carbon nuclei. HMBC detects long range coupling between proton and carbon on these two and three bond couplings. HSQC-TOCSY spectrum correlates one-bond ^1H-^{13}C couplings and shows these correlations throughout an entire spin system.[15]

1.3 Fmoc Solid Phase Peptide Synthesis

Solid phase peptide synthesis (SPPS) introduced by Robert Bruce Merrifield in 1963 has been significantly advanced over the past five decades and has greatly

facilitated the synthesis of peptides and small proteins.[16] Dr. Merrifield was awarded the 1984 Nobel Chemistry Prize for the invention of SPPS. The basic principle of SPPS is the construction of a peptide chain on an insoluble polymeric support via stepwise coupling of suitably protected amino acids to the solid support. The polypeptide chain is then extended one amino acid at a time from the C to N-terminus. Since the insolubility of polymers allows purification simply by wash and filtration, it can save an enormous amount time and effort on peptide synthesis and purification. It also produces high yield, high purity peptides in comparison with solution phase peptide synthesis. Fmoc SPPS introduced in 1970s has made the SPPS safer to carry out relative to the original Boc form SPPS by avoiding the use of hydrofluoric acid. Fmoc SPPS is now the most commonly used technique for peptide synthesis in research laboratories. The principles of Fmoc solid phase synthesis are illustrated in Figure 1.4.

- **Protecting groups used in Fmoc SPPS**

In Fmoc SPPS, excess amino acids and activating reagents are used to drive each coupling reaction to completion. Reactive functional side chain groups and the amino group of amino acids need to be protected in order to prevent the formation of undesired side products. Fmoc group is used for temporary protection of α-amino group and is removed before each coupling by piperidine to form dibenzofulvene via a β-elimination mechanism as shown in Figure 1.5. The dibenzofulvene is then scavenged by piperidine to afford the piperidine-dibenzofulvene adduct which is UV visible and is used to monitor the progress of coupling reactions in the Fmoc solid phase peptide synthesis quantitatively. Acid labile side chain protecting group, such as Pbf, Boc, t-butyl, and

trityl, are removed using TFA at the same time as cleavage of the peptide off the resin as shown in Figure 1.6.

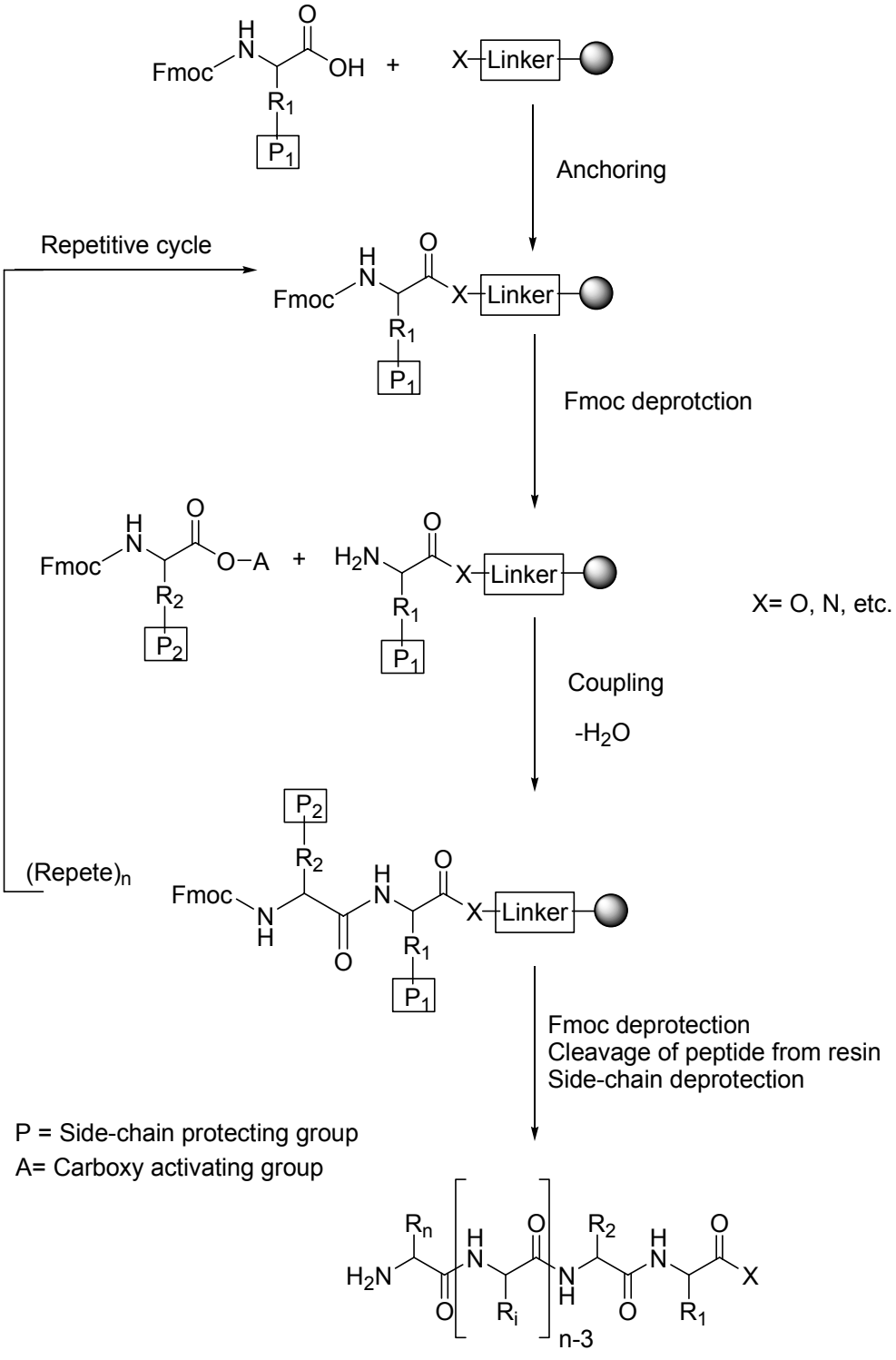

Figure 1.4 Stepwise synthetic route for the Fmoc solid phase peptide synthesis

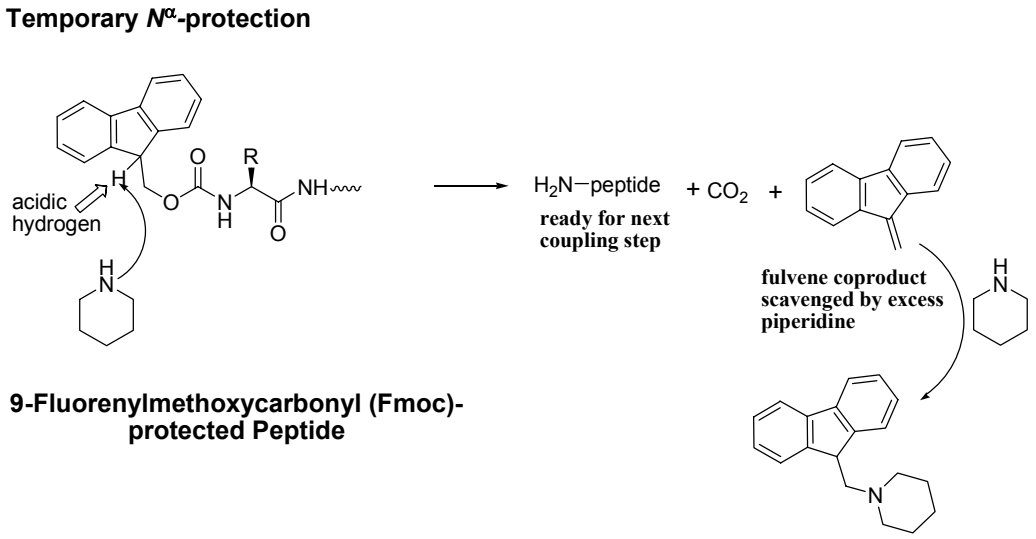

Figure 1.5 Piperidine mediated Fmoc deprotection

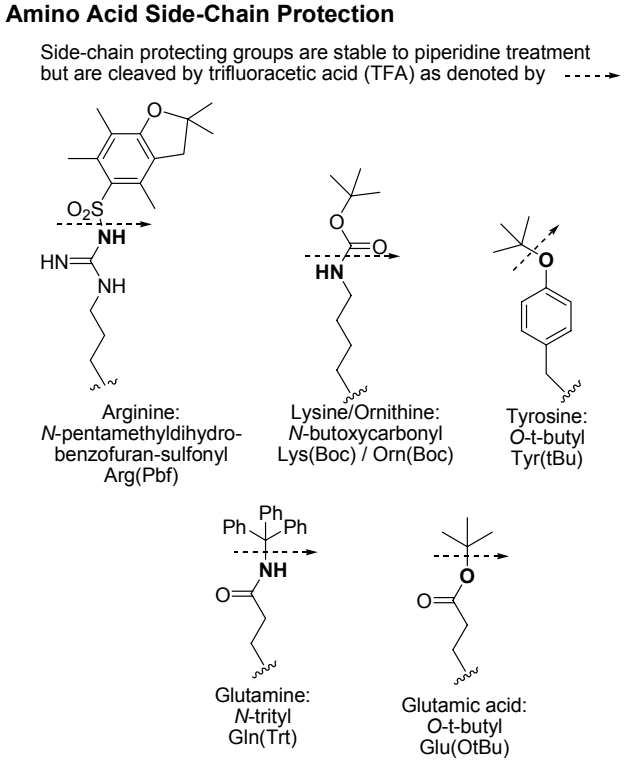

Figure 1.6 The commonly used protecting groups for the Fmoc SPPS

- **Peptide Coupling Reagents**

The effective acylation of amino group to form the amide bond requires carboxyl group of incoming amino acids to be activated. Traditionally, this activating step is

carried out with dicyclohexylcarbodiimide (DCC) which activates the carboxyl group by the formation of a highly reactive species O-acylisourea which can lead to racemization and undergo a rearrangement to give unreactive species. Thus, 1-hydroxy-benzotrizaole, (HOBt)[17] or 1-hydroxy-7-azabenzotriazole (HOAt)[18] has been used as an additive to capture active species and give the corresponding esters which are less reactive and less tend to racemization. [18] In the last decade, coupling reagents uronium and phosphonium salts based on hydroxybenzotriazole derivatives such as HATU, HBTU, TBTU, PyAOP and PyBOP have been widely used for in situ carboxyl activation as shown in Figure 1.7.[19,20] These reagents activate the carboxyl group by converting Fmoc-amino acids in the presence of a tertiary base such as DIEA to their corresponding active OAt or OBt esters in situ.

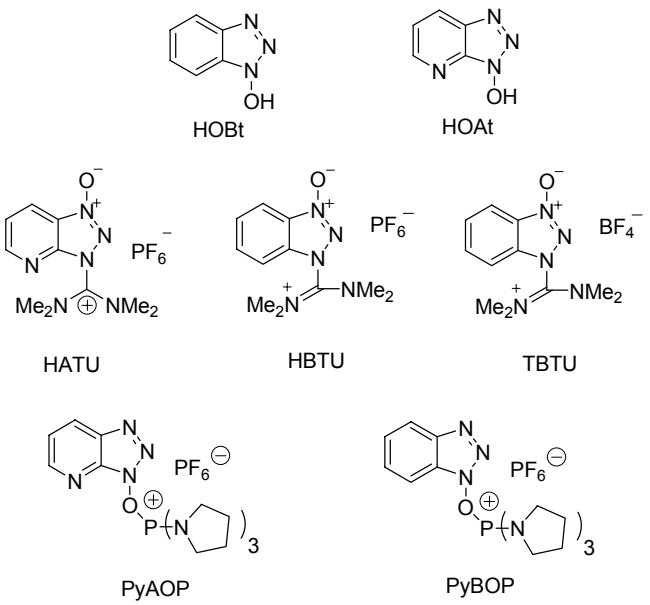

Figure 1.7 Uronium and phosphonium activating reagents

PyAOP is more reactive than PyBOP, and used to effectively incorporate sterically hindered amino acids such as Aib and Dpg into the peptide sequence. PyAOP and PyBOP are preferred to their uronium counterparts such as HATU and HBTU

because uronium can block amino terminus for further peptide chain assembly through formation of a tetramethyl-guanidinated residue at amino terminus.[21] Symmetrical anhydrides, the pre-formed activated amino acid derivatives are ideal reagents for incorporation of hindered amino acids. These symmetrical anhydrides can be prepared by reaction of 2 equivalents of Fmoc-amino acids with 1 equivalent DCC in CH_2Cl_2.

1.4 Design of Synthetic Peptides Containing ααAAs as Inhibitors for Protein Conformational Diseases

$C^{\alpha,\alpha}$–disubstituted amino acids (ααAAs) have been widely recognized as a means of introducing backbone conformational constraints in peptides and used as stereochemical directors of polypeptide chain folding.[22] Conformationally constrained peptides often have improved activity, bio-stability, and bioavailability.[23, 24] Peptide-based and peptide mimetic-based drugs provide significant medical relief and chemotherapy for a number of ailments including AIDS,[25] and prostate cancer.[26]

Protein or polypeptides conformational misfoldings from normal protein geometries to β-sheet conformation are thought to be key pathogenic factors in several protein conformational diseases, including Alzheimer's disease (AD), diabetes type II, Parkinson diseases and prion disorders,[27-31] in which the misfolded protein self-aggregates to amyloid fibrils and deposits as amyloid plaques in diverse organs promoting tissue damage and organ dysfunction. The interruption of the formation of the β-sheet conformation of the amyloid peptide by ααAA-containing peptides has been shown to be a promising therapeutic approach to development of the fibrilization inhibitory drug.

Our group has recently developed a novel ααAA-containing peptide-based approach for disrupting the hydrogen bonding network in amyloid-β peptide (Aβ) and inhibiting the formations of fibril or protofibril,[32] which leads the formation of amyloid plaques,

the proposed causative agent leading to the progression of Alzheimer's disease and brain cell death. The ααAAs with side chain larger than ethyl have been shown to stabilize extended peptide conformations. The hypothesis of the Hammer group design of inhibitors of Aβ fibril formation is that peptides containing steric hindered α,α−disubstituted amino acids (ααAAs) in the hydrophobic core of Aβ can interact with Aβ by hydrogen bonding as well as by side-chain interactions, but hydrogen bonding was blocked on the opposite edge. Thus, further aggregation of Aβ into toxic protofibril or fibril was prevented as shown in Figure 1.8.

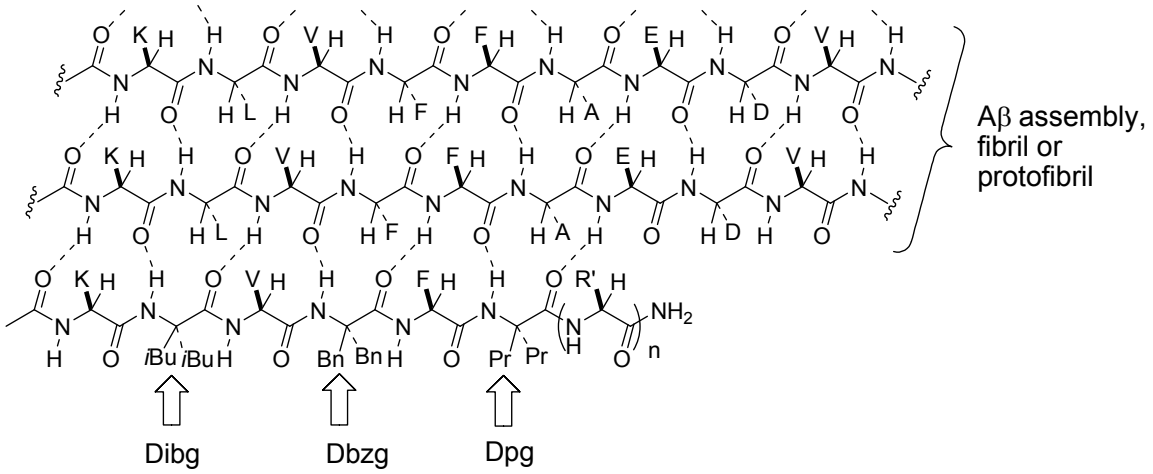

Figure 1.8 Design of peptides with ααAAs as blockers of Aβ assembly

Conformational preferences of Aib have been characterized in a variety of peptides. The presence of two sterically bulky methyl groups on the α-carbon greatly restricts the rotational freedom of the backbone torsional angles ϕ and ψ and strongly favors helical conformations. The very high tendency of Aib to induce helical conformations has been used to design of helical inhibitors to disrupt the formation of β-sheet structure. Formaggio et al. have demonstrated that a single amino acid replacement

of Val at position 2 with Aib in the protected pentapeptide benzyloxycarbony-Leu-Val-Phe-Phe-Asp(*Ot*Bu)-*Ot*Bu, which corresponds residue 17 to residue 21 of the amyloid-β peptide, induces helical structure and completely disrupt the β-sheet structure of this amyloid-β peptide fragment in organic solvent.[33]

Aib has also proven to be a good β-sheet breaker amino acid; it disrupts β-sheet structure in a variety of peptides.[22, 34] Therefore, Aib has been used as β-breaker element for the design of peptide-based inhibitor for amyloid fibril formation in protein conformational diseases. Gazit et al. have elegantly designed an Aib-containing peptide to inhibit human islet peptide hIAPP amyloid fibrillization by preventing the β-sheet formation.[35] hIAPP, a 37 amino acid hormone peptide, accumulates as islet amyloid fibrils and deposits in the pancreas of type II diabetes patients. The inhibitor peptide was based on the amino acid sequence, Ala-Asn-Phe-Leu-Val-His, which corresponds to residue 13 to residue 18 of the hydrophobic core of hIAPP peptide. Fibrillization can be inhibited by replacing alanine (residue 13) and leucine (residue 16) with Aib. This designed inhibitor has shown a high affinity for the hIAPP molecule and exhibits significant inhibition toward fibril formation of hIAPP peptide determined by electron microscopy (EM), Congo red (CR) birefringence, and FTIR spectroscopy assays.

1.5 References

1. Shoemaker, K. R.; Kim, P. S.; York, E. J.; Stewart, J. M.; Baldwin, R. L., Tests of the Helix Dipole Model for Stabilization of α-Helices. *Nature* **1987,** 326, 563-567.

2. Lewis, P. N.; Momany, F. A.; Scheraga, H. A., Chain Reversals in Proteins. *Biochim. Biophys. Acta* **1973,** 303, 211-229.

3. Smith, J. A.; Pease, L. G., Reverse Turns in Peptides and Proteins. *Crc Critical Reviews in Biochemistry* **1980,** 8, 315-399.

4. Sreerama, N.; Woody, R. W., Computation and analysis of protein circular dichroism spectra. In *Numerical Computer Methods, Pt D*, 2004; Vol. 383, pp 318-351.

5. Krittanai, C.; Johnson, W. C., Correcting the circular dichroism spectra of peptides for contributions of absorbing side chains. *Anal. Biochem.* **1997,** 253, 57-64.

6. Rodger, A.; Norden, B., *Circular Dichroism and Linear Dichroism*. 1997.

7. Miyazawa, T.; Blout, E. R., Infrared Spectra of Polypeptides in Various Conformations - Amide I and II Bands. *J. Am. Chem. Soc.* **1961,** 83, 712-719.

8. Wuthrich, K., *NMR of Proteins and Nucleic Acids*. 1986; p 304.

9. Wishart, D. S.; Sykes, B. D.; Richards, F. M., Relationship between Nuclear Magnetic Resonance Chemical Shift and Protein Secondary Structure. *Journal of Molecular Biology* **1991,** 222, 311-333.

10. Griffiths-Jones, S. R.; Maynard, A. J.; Searle, M. S., Dissecting the stability of a β-hairpin peptide that folds in water: NMR and molecular dynamics analysis of the β-turn and β-strand contributions to folding. *Journal of Molecular Biology* **1999,** 292, 1051-1069.

11. Syud, F. A.; Espinosa, J. F.; Gellman, S. H., NMR-based quantification of β-sheet populations in aqueous solution through use of reference peptides for the folded and unfolded states. *J. Am. Chem. Soc.* **1999,** 121, 11577-11578.

12. Searle, M. S.; Griffiths-Jones, S. R.; Skinner-Smith, H., Energetics of weak interactions in a β-hairpin peptide: Electrostatic and hydrophobic contributions to stability from lysine salt bridges. *J. Am. Chem. Soc.* **1999,** 121, 11615-11620.

13. Kopple, K. D.; Ohnishi, M.; Go, A., Conformations of Cyclic Peptides .3. Cyclopentaglycyltyrosyl and Related Compounds. *J. Am. Chem. Soc.* **1969,** 91, 4264-4272.

14. Vuister, G. W.; Bax, A., Quantitative J Correlation - a New Approach for Measuring Homonuclear 3-Bond $J_{HNH\alpha}$ Coupling-Constants in N^{15}-Enriched Proteins. *J. Am. Chem. Soc.* **1993,** 115, 7772-7777.

15. Silverstein, R. M.; Webster, F. X.; Kiemie, D., *Spectrometric Identification of Organic Compounds, 7th Edition*. 2002.

16. Merrifield, R. B., Solid Phase Peptide Synthesis .1. Synthesis of a Tetrapeptide. *J. Am. Chem. Soc.* **1963,** 85, 2149-2154.

17. Konig, W.; Geiger, R., A New Method for Synthesis of Peptides - Activation of Carboxyl Group with Dicyclohexylcarbodiimide Using 1-Hydroxybenzotriazoles as Additives. *Chemische Berichte-Recueil* **1970,** 103, 788-790.

18. Carpino, L. A., 1-Hydroxy-7-Azabenzotriazole - an Efficient Peptide Coupling Additive. *J. Am. Chem. Soc.* **1993,** 115, 4397-4398.

19. Coste, J.; Lenguyen, D.; Castro, B., Pybop - a New Peptide Coupling Reagent Devoid of Toxic by-Product. *Tetrahedron Lett.* **1990,** 31, 205-208.

20. Albericio, F.; Cases, M.; Alsina, J.; Triolo, S. A.; Carpino, L. A.; Kates, S. A., On the use of PyAOP, a phosphonium salt derived from HOAt, in solid-phase peptide synthesis. *Tetrahedron Lett.* **1997,** 38, 4853-4856.

21. Story, S. C.; Aldrich, J. V., Side-Product Formation During Cyclization with HBTU on a Solid Support. *International Journal of Peptide and Protein Research* **1994,** 43, 292-296.

22. Toniolo, C.; Crisma, M.; Formaggio, F.; Peggion, C., Control of peptide conformation by the Thorpe-Ingold effect (C^{α}-tetrasubstitution). *Biopolymers* **2001,** 60, 396-419.

23. Dentino, A. R.; Raj, P. A.; Bhandary, K. K.; Wilson, M. E.; Levine, M. J., Role of Peptide Backbone Conformation on Biological-Activity of Chemotactic Peptides. *J. Biol. Chem.* **1991,** 266, 18460-18468.

24. Prasad, S.; Rao, R. B.; Bergstrand, H.; Lundquist, B.; Becker, E. L.; Balaram, P., Conformation-activity correlations for chemotactic tripeptide analogs incorporating dialkyl residues with linear and cyclic alkyl sidechains at position 2. *International Journal of Peptide and Protein Research* **1996,** 48, 312-318.

25. Leung, D.; Abbenante, G.; Fairlie, D. P., Protease inhibitors: current status and future prospects. *J. Med. Chem.* **2000,** 43, 305-341.

26. Stricker, H. J., Luteinizing hormone-releasing hormone antagonists in prostate cancer. *Urology* **2001,** 58, 24-27.

27. Sunde, M.; Blake, C. C. F., From the globular to the fibrous state: protein structure and structural conversion in amyloid formation. *Q. Rev. Biophys.* **1998,** 31, 1-37.

28. Rochet, J. C.; Lansbury, P. T., Amyloid fibrillogenesis: themes and variations. *Curr. Opin. Struct. Biol.* **2000,** 10, 60-68.

29. Gazit, E., The "Correctly folded" state of proteins: Is it a metastable state? *Angewandte Chemie-International Edition* **2001,** 41, 257-259.

30. Soto, C., Unfolding the role of protein misfolding in neurodegenerative diseases. *Nature Reviews Neuroscience* **2003,** 4, 49-60.

31. Stefani, M.; Dobson, C. M., Protein aggregation and aggregate toxicity: new insights into protein folding, misfolding diseases and biological evolution. *Journal of Molecular Medicine-JMM* **2003,** 81, 678-699.

32. Etienne, M. A.; Aucoin, J. P.; Fu, Y. W.; McCarley, R. L.; Hammer, R. P., Stoichiometric inhibition of amyloid β-protein aggregation with peptides containing alternating α,α-disubstituted amino acids. *J. Am. Chem. Soc.* **2006,** 128, 3522-3523.

33. Formaggio, F.; Bettio, A.; Moretto, V.; Crisma, M.; Toniolo, C.; Broxterman, Q. B., Disruption of the β-sheet structure of a protected pentapeptide, related to the β-amyloid sequence 17-21, induced by a single, helicogenic C^{α}-tetrasubstituted α-amino acid. *Journal of Peptide Science* **2003,** 9, 461-466.

34. Karle, I. L.; Balaram, P., Structural Characteristics of α-Helical Peptide Molecules Containing Aib Residues. *Biochemistry* **1990,** 29, 6747-6756.

35. Gilead, S.; Gazit, E., Inhibition of amyloid fibril formation by peptide analogues modified with α-aminoisobutyric acid. *Angewandte Chemie-International Edition* **2004,** 43, 4041-4044.

CHAPTER 2

SHORT FOLDED PEPTIDES IN AQUEOUS SOLUTION: ROLE OF α,α-DISUBSTITUTED AMINO ACID AND CENTRAL RESIDUES ON PENTAPEPTIDE STRUCTURES

2.1 Introduction

Design, synthesis, and conformational analysis of short peptides that fold into defined structures have greatly improved our understanding of protein folding[1-4] and stability, and have produced a number of breakthroughs in biologically active materials with enhanced potential to fight diseases.[5, 6] $C^{\alpha,\alpha}$–disubstituted amino acids (ααAAs) are widely utilized to conformationally constrain peptides and to stabilize particular secondary structures. Short peptide sequences, which generally would not be structured, can be induced to fold by the introduction of ααAAs into the sequence. ααAAs affect this folding by acting as stereochemical directors of polypeptide backbone conformation, through the phenomenon commonly referred to as the Thorpe-Ingold effect, or the gem dialkyl effect.[7]

A large body of research shows that Aib (α-aminoisobutyric acid or α,α-dimethylglycine) favors helical conformations in a wide variety of peptides of differing lengths and sequences.[8, 9] The presence of two methyl groups on the α-carbon restricts the rotational freedom of the backbone torsional angles ϕ and ψ, and tends to constrain the backbone torsional angles to favor formation of 3_{10} ($\phi = \pm 57°$, $\psi = \pm 30°$) and α ($\phi = \pm 63°$, $\psi = \pm 42°$) helices. The high helical propensity of Aib has been utilized by nature to make helical antimicrobial peptides.[10] Additionally Aib has been utilized in de novo design helical peptides with antimicrobial activity and design helical inhibitors against HIV-1 virus entry into cells.[6] Aib has also proven to be a good β-sheet breaker amino acid, therefore it is used as a beta-breaker element for the inhibition of amyloid fibril formation

by human islet amyloid polypeptide (hIAPP), which is associated with the pathogenesis of type II diabetes.[11]

Less is known about the conformation of peptides containing ααAAs with side-chains larger than methyl group, such as Deg (diethylglycine), Dpg (di–n-propylglycine), and Dbg (di-n-butylglycine). These amino acids are unique in that they have been shown to adopt both extended and helical conformations, depending on their sequence context, length, and environmental factors.[12-30] In the case of Aib, conformational energy calculations suggest that helical conformations are significantly more stable than fully extended conformations. In contrast, the higher dialkylglycines have similar energy minima in both the fully extended (ϕ, $\psi \sim \pm 180^{o}$) and helical conformations.[7] The coexistence of a fully extended conformation and a helical conformation in single crystals of the peptide Boc-Leu-Dpg-Val-OMe agrees well with those theoretical calculations.[30] There are no studies to date that fully explain the context-dependent conformational preference of these ααAAs and their influence on neighboring residues. Previous studies relied heavily on solid-state structures of peptides crystallized from organic solvents, which may deviate from solution conformations of ααAA-containing peptides in aqueous (physiologically relevant) medium.[31]

In short water-soluble peptides, the water molecules compete very effectively with the intramolecular hydrogen-bonding between the carbonyl and amide groups of peptide backbone. Early calculation and experimental results suggest that short linear peptides would not adopt ordered structures in water; as a result, the general belief for many years was that short water-soluble peptides adopt random coil conformations in water. With the improvements for the experimental techniques, Dyson et al. demonstrated

that small peptides with four to six residues adopt β-turn conformations in water.[32] In correlation with statistical studies on β-turn probability performed by Chou and Fasman, Dyson et al. also demonstrated that β-turn conformational propensity is dependent on the local amino acid sequence, rather than on medium- to long-range interactions. Toniolo et al. reported the first two water soluble 3_{10}-helical peptides, which contain five residues of highly helical inducing α,α-disubstituted amino acids, either α-aminoisobutyric acids(Aib) or isovalines(Iva) with two water-solubilizing, azacrown-functionalized α-amino acids, L-2-amino-3[1-(1,4,7-triazacyclononyl)]propanoic acid(ATANP).[33, 34] The 3_{10}-helical conformation of the heptapeptides was mainly attributed to high Aib and Iva content and main chain length favoring helical conformation.

The conformational analyses of Dpg containing peptides have only been conducted in organic solvents and solid states. It is necessary to fully investigate the impact of Dpg on peptide backbone structure in biocompatible aqueous solution. For this reason, several pentapeptides containing Dpg and its α-amino acid counterpart L-norvaline (Nva) at alternating positions (Table 2.1) were synthesized using solid phase Fmoc chemistry and their conformational preferences were analyzed in aqueous phosphate buffer. Glutamic acid and lysine residues were incorporated at each end of the peptide sequence to probe the potential conformational effects resulting from charge-charge, or charge-dipole interactions. Residues with different conformation preferences such as alanine, threonine, tyrosine, and valine were incorporated at the central position (residue 3) of the peptides to examine the sequence effect in stabilizing extended or helical conformations. Charge-dipole interactions were analyzed by switching the order of glutamic acid and lysine. The conformation of these peptides was initially probed by

CD. Several of the more structured peptides were further investigated by multi-dimensional NMR techniques which indicated that several of the Dpg-containing peptides were likely helical in structure. Conformations of the peptide containing Tyr at the central residue, Ac-Glu-Dpg-Tyr-Dpg-Lys-NH_2 constructed via ^1H NMR-based structure calculations show that this peptide has a type-III turn or 3_{10} helix geometry.

2.2 Results and Discussion

2.2.1 Peptide Synthesis

Table 2.1 Primary sequences of Dpg and Nva peptides[a]

Peptide Name	Sequence
EE-Dpg-Y	Ac-Glu-Dpg-Tyr-Dpg-Glu-NH_2
EK-Dpg-Y	Ac-Glu-Dpg-Tyr-Dpg-Lys-NH_2
KK-Dpg-Y	Ac-Lys-Dpg-Tyr-Dpg-Lys-NH_2
KE-Dpg-Y	Ac-Lys-Dpg-Tyr-Dpg-Glu-NH_2
EK-Dpg-T	Ac-Glu-Dpg-Thr-Dpg-Lys-NH_2
EK-Dpg-A	Ac-Glu-Dpg-Ala-Dpg-Lys-NH_2
EK-Dpg-V	Ac-Glu-Dpg-Val-Dpg-Lys-NH_2
EK-Aib-Y	Ac-Glu-Aib-Tyr-Aib-Lys-NH_2
EK-Nva-Y	Ac-Glu-Nva-Tyr-Nva-Lys-NH_2
EK-Nva-T	Ac-Glu-Nva-Thr-Nva-Lys-NH_2
EK-Nva-A	Ac-Glu-Nva-Ala-Nva-Lys-NH_2
EK-Nva-V	Ac-Glu-Nva-Val–Nva-Lys-NH_2

[a] EK-Dpg-T and EK-Nva-T were synthesized by Yanwen Fu.

Peptides were synthesized using standard solid-phase Fmoc chemistry on Fmoc-

PAL-PEG-PS resin. The primary sequences of Dpg and Nva containing peptides are listed in Table 2.1. Our group has previously found that coupling Dpg to the peptide sequence could be greatly improved at elevated temperatures, thus the coupling of Dpg containing peptides were carried out at 50 ºC using PyAOP activation. For these difficult couplings, we prefer the phosphonium-based coupling reagent over uronium reagents like HATU and HBTU as it avoids chain termination via guanidinium form at amino terminus.[35] A particular difficult peptide to synthesize is EK-Dpg-V due to the steric hindrance between Val and Dpg residues. Double coupling of Val^3 to Dpg^4 and Dpg^2 to Val^3 is necessary to avoid the deletion sequence. After the last amino acid coupling, acetylation of the N-terminus of all peptides was carried out manually with acetic anhydride in DMF.

2.2.2 Conformational Analysis by Circular Dichroism (CD)

Minimum and maximum ellipticities and corresponding wavelength of CD spectra for Dpg and Nva peptides are listed in Table 2.2.

Variation of the sequence, as detailed in Table 2.1, incorporation of glutamic acid or lysine residues at residue 1 and residue 5 of EE-Dpg-Y, EK-Dpg-Y, KK-Dpg-Y, and KE-Dpg-Y was designed to evaluate the potential conformational effects resulting from residue-residue charged side chain interactions or charge-dipole interactions. The EE-Dpg-Y, KK-Dpg-Y, KE-Dpg-Y exhibit similar CD spectra at pH 7.0 with a negative band at about 190 nm, a positive band near 200 nm, and a weak negative band at 230 nm as shown in Figure 2.1. The CD spectrum of EK-Dpg-Y has the same sign pattern, but is much more intense so that its positive band at 200 nm and negative band at 230 nm gives it characteristics that have been previously attributed to a β-turn conformation,[36] but may

but may also arise from the aromatic group of Tyr. The intensity difference may be due to side chain interactions between negatively charged Glu side chain(Glu^-) or positively charged Lys side chain(Lys^+) or interactions between charged side chains and a helix dipole in EK-Dpg-Y. Reversal of Glu and Lys residues in KE-Dpg-Y reduces the structure of the peptide, which may be due to interactions of the Glu and Lys with a helix dipole in EK-Dpg-Y that stabilizes a turn structure.[37, 38] The helix dipole moment is an important property of helices that is generated by the uniform alignments of hydrogen bonds in the helix. Baldwin and coworkers have shown that charged groups play a critical role in stabilizing helices in aqueous solution.[37] Helical structures are stabilized if the side-chain group and pole of the helix have opposite charges, e.g. Glu^- on the N-terminus and Lys^+ on the C-terminus. This phenomenon has been noted as the charged group-helix dipole interaction.

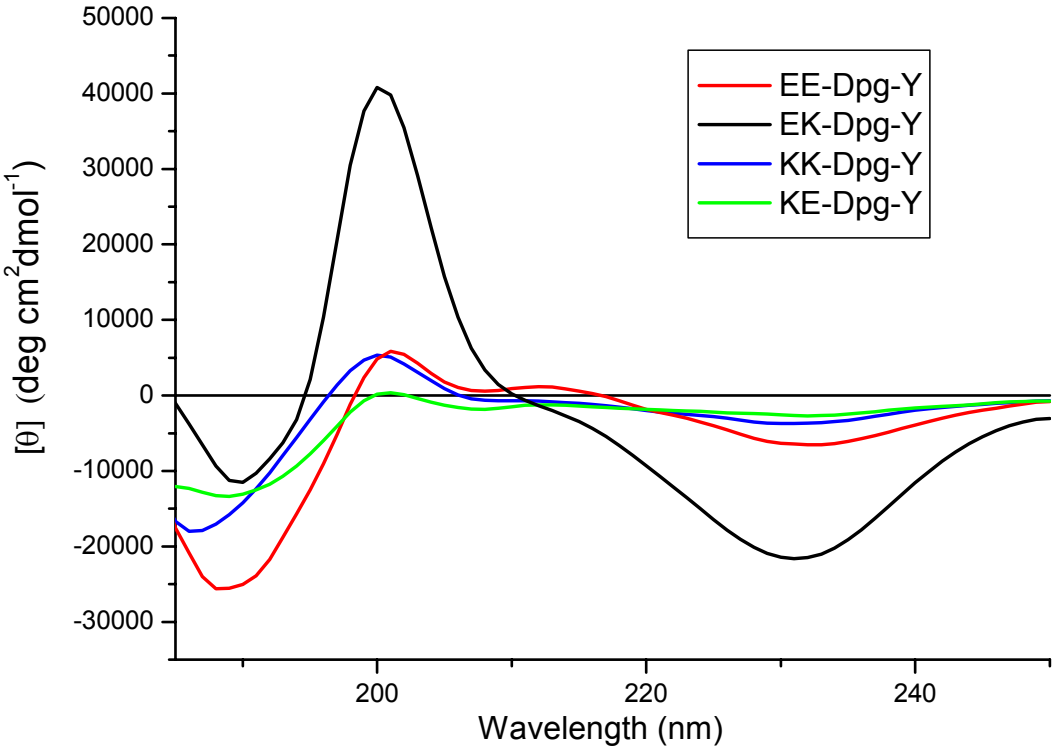

Figure 2.1 CD spectra of 100 μM peptide concentration of EE-Dpg-Y, EK-Dpg-Y, KK-Dpg-Y, and KE-Dpg-Y in 10 mM phosphate buffer, pH 7.0, recorded at 20°C.

Table 2.2 Minimum and maximum ellipticities and corresponding wavelength of CD spectra for Dpg and Nva containing peptides

Peptide Name	Min/Max		Min/Max	
	λ (nm)	θx(10^3)	λ (nm)	θx(10^3)
EE-Dpg-Y	201	5.82	232	-6.53
EK-Dpg-Y	200	40.8	231	-21.6
KK-Dpg-Y	200	5.35	230	-3.70
KE-Dpg-Y	201	0.36	232	-2.69
EK-Dpg-T	192	-5.30	226	-2.01
EK-Dpg-A	194	-20.0	229	-5.28
EK-Dpg-V	201	-20.3	226	-12.9
EK-Aib-Y	200	2.48	230	-5.65
EK-Nva-Y	195	-7.52	223	-1.03
EK-Nva-T	197	-13.7	226	-1.38
EK-Nva-A	198	-36.6	227	-5.15
EK-Nva-V	197	-11.7	224	-1.37

To further test the hypothesis that EK-Dpg-Y is stabilized by the interactions of Glu^- and Lys^+ with a helix dipole in EK-Dpg-Y, CD measurements of EK-Dpg-Y were carried out in phosphate buffer solutions at differing pH values as shown in Figure 2.2.

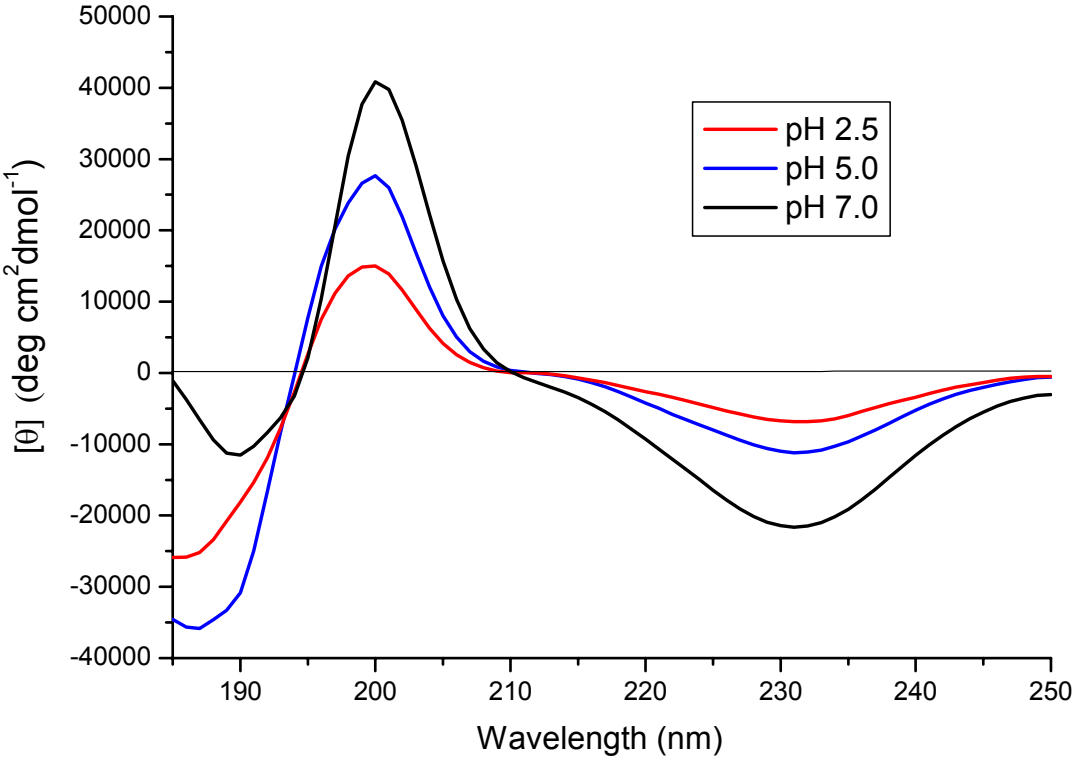

Figure 2.2 pH dependent CD spectra of 100 μM peptide concentration of EK-Dpg-Y in 10 mM phosphate buffer at differing pH, recorded at 20 °C.

A systematic reduction of molar ellipticity values at 200 nm and less negative bands at 230 nm were observed when the pH value was decreased. This phenomenon indicates a reduction of ordered structures at lower pH presumably due to the conversion of Glu^- to Glu^0 and the loss of the favorable interaction between side-chain of Glu and the helix dipole in this peptide.

Conformational preferences of Aib have been characterized in a variety of peptides. It is well established that Aib, is a strong promoter of alpha and 3_{10} helical

conformations. EK-Aib-Y was synthesized in which Dpg residues were replaced by Aib to investigate if Aib and Dpg possess the similar structural effects on the peptide conformation in the aqueous media.

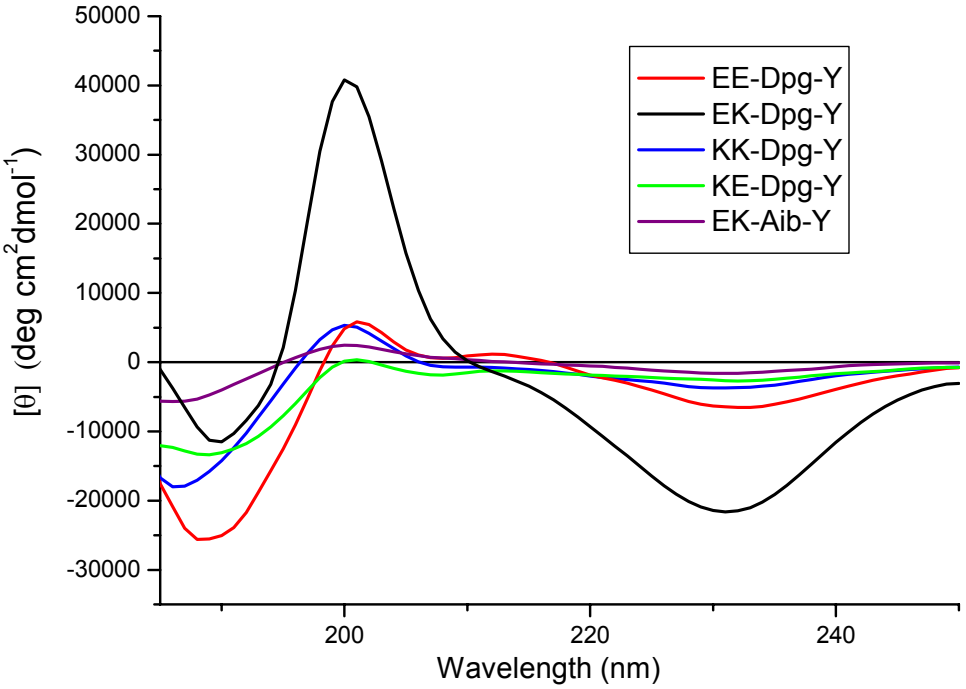

Figure 2.3 CD spectra of 100 μM peptide concentration of EE-Dpg-Y, EK-Dpg-Y, KK-Dpg-Y, KE-Dpg-Y, and EK-Aib-Y in 10 mM phosphate buffer, pH 7.0, recorded at 20°C.

The CD spectrum of EK-Aib-Y displays a diminishing positive band at 200 nm and a weaker negative band at 230 nm compared to EK-Dpg-Y, EE-Dpg-Y, and KK-Dpg-Y, suggesting that Aib destabilizes the structure as shown in Figure 2.3.

To further investigate the ααAA impacts on the peptide backbone conformation, L-norvaline (Nva) analogs were prepared. The CD spectrum of EK-Nva-Y has no near-UV structure and only a negative minimum at 195 nm indicative of a random coil structure as illustrated in Figure 2.4.

The CD spectra of the EK-Dpg-T, EK-Nva-T, EK-Dpg-A, and EK-Nva-A are dominated by negative bands at ~197 nm indicative of mostly random coil structures as

shown in Figure 2.5. The negative band near 197 nm is stronger for EK-Nva-T than for EK-Dpg-T and the same is true for EK-Nva-A as compared to EK-Dpg-A, suggesting that Dpg residues impose backbone constraints in comparison with Nva containing peptides. These results also suggest that the hydrophobic central residue may play an important role in these peptide structures since with the central Tyr residue the CD has a distinctly different shape.

The CD spectrum of EK-Dpg-V shows two minima at 202 nm and 227 nm which suggests that EK-Dpg-V adopts a different, possibly turn-like structure. The CD spectrum of EK-Nva-V has a negative band at 197 nm consistent with a coil-like structure as illustrated in Figure 2.6.

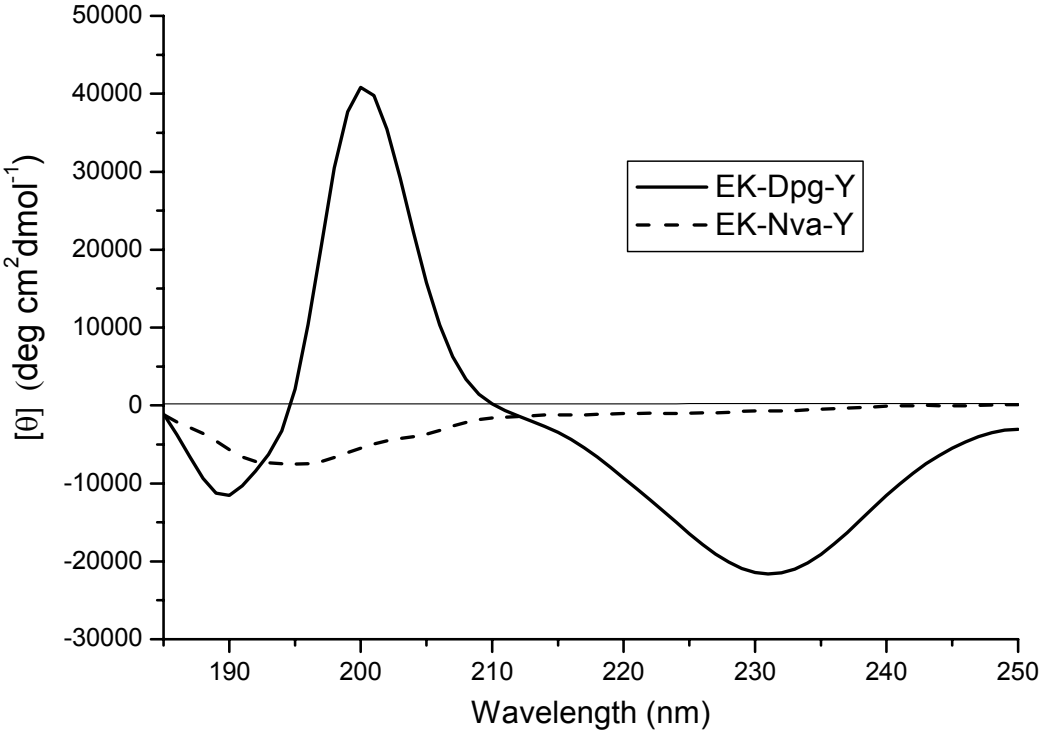

Figure 2.4 CD spectra of 100 μM peptide concentration of EK-Dpg-Y and EK-Nva-Y, in 10 mM phosphate buffer, recorded at 20 °C.

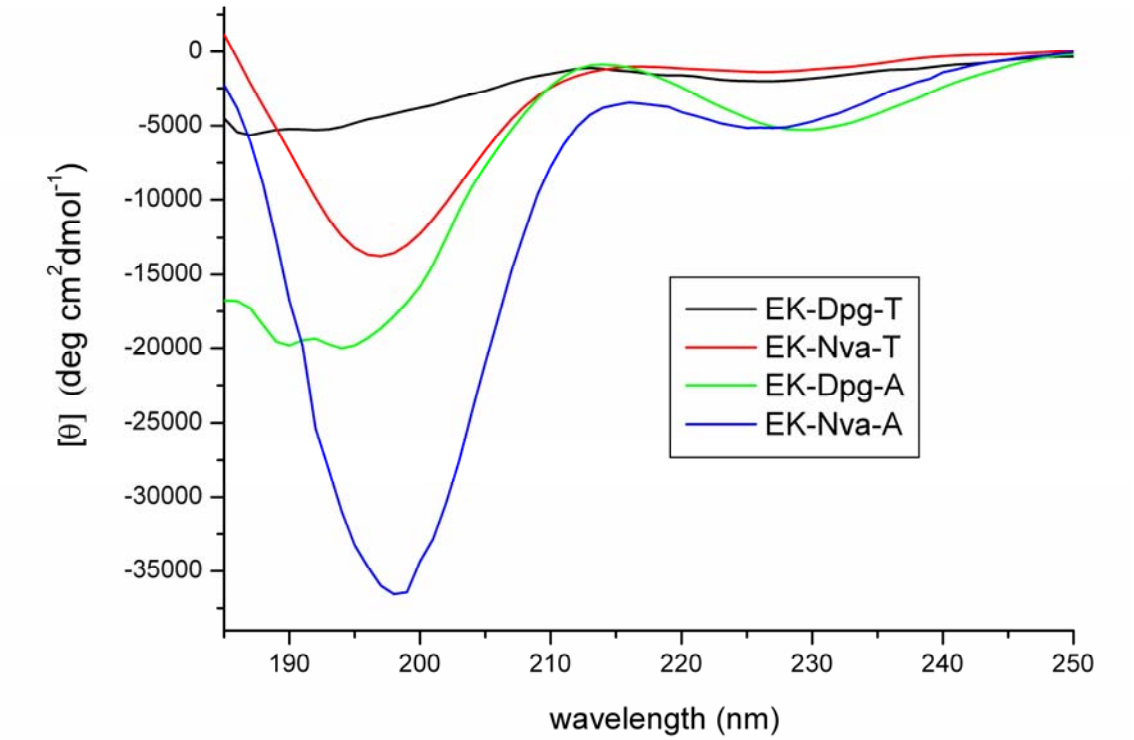

Figure 2.5 CD spectra of 100 μM peptide concentration of EK-Dpg-T, EK-Nva-T, EK-Dpg-A, and EK-Nva-A in 10 mM phosphate buffer, recorded at 20 °C.

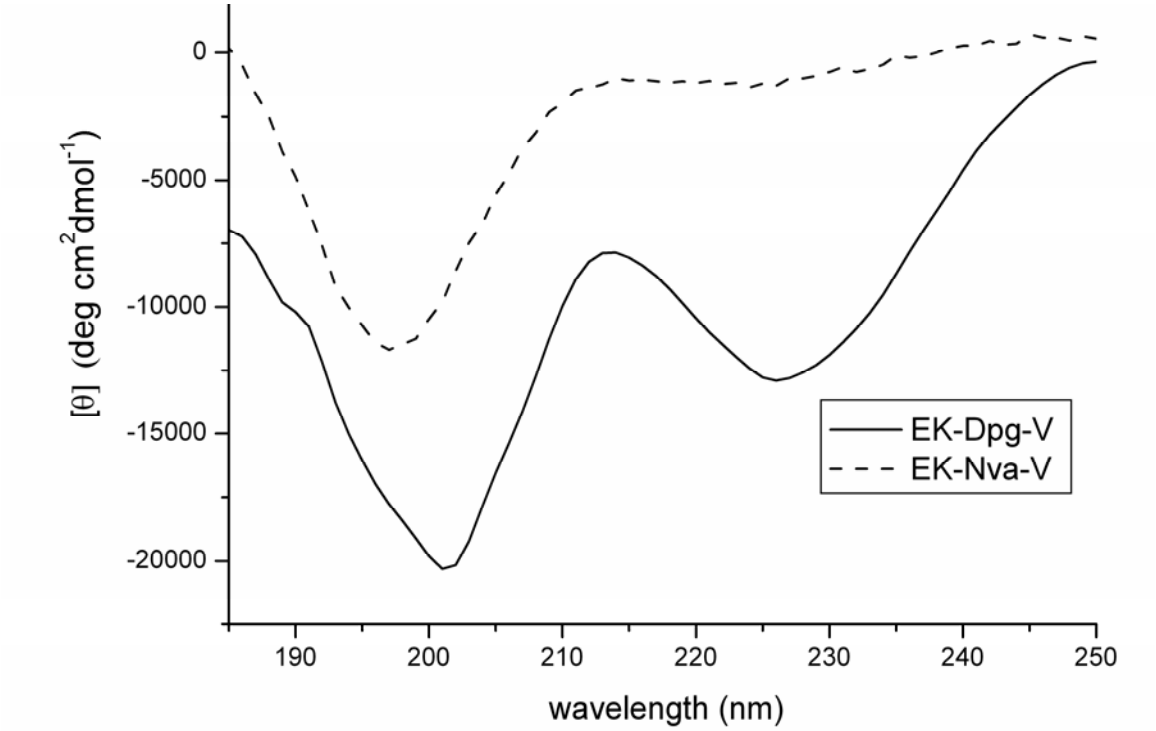

Figure 2.6 CD spectra of 100 μM peptide concentration of EK-Dpg-V and EK-Nva-V in 10 mM phosphate buffer, recorded at 20 °C.

The concentration dependence studies for both EK-Dpg-Y and KE-Dpg-Y were carried out at peptide concentrations of 100, 250, 500 μM in phosphate buffer at pH 7, The CD spectra are concentration independent for both peptides, indicating stable secondary structures and no aggregation in the two peptides. The temperature dependence study of EK-Dpg-Y shows unchanged CD bands under measured temperature indicting a stable secondary structure is preserved over temperatures. The temperature dependence study of KE-Dpg-Y shows decreasing of the maximum at 200 nm over the temperature, indicating instability of this peptide at higher temperature.

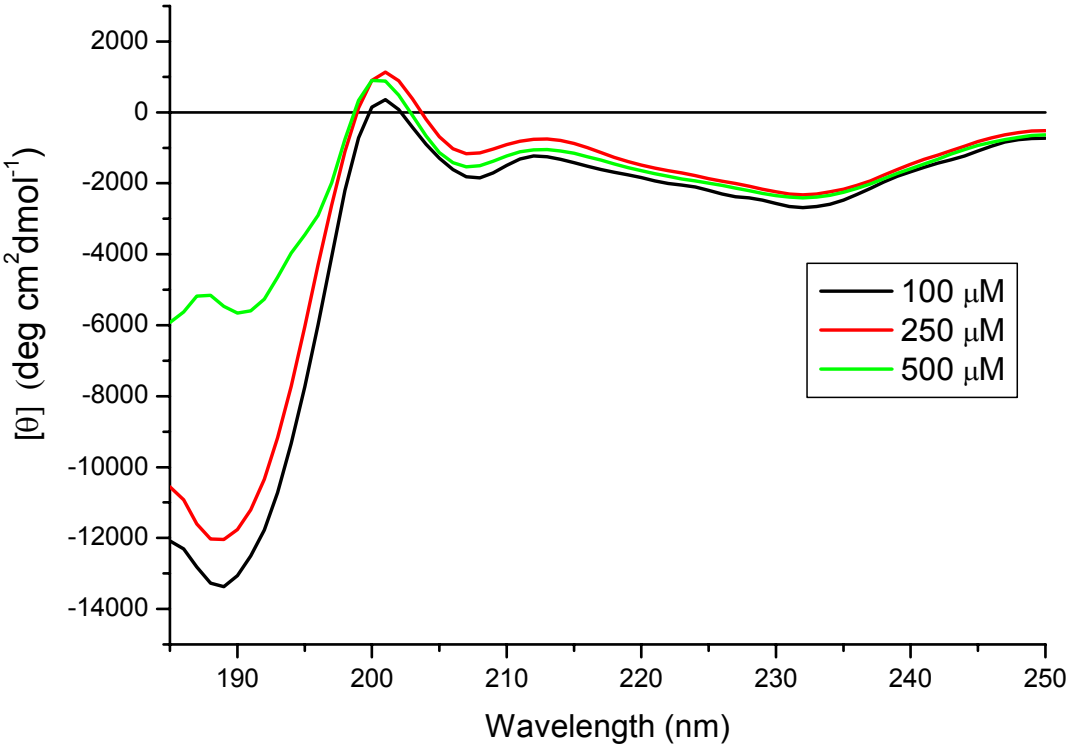

Figure 2.7 The concentration dependent study of the CD spectra of KE-Dpg-Y in 10 mM of phosphate buffer, 20 ºC.

The concentration dependence study for EK-Aib-Y was carried out at peptide concentrations of 100 μM, 250 μM and 500 μM in phosphate buffer at pH 7. A red shift occurs form 200 nm to 202 nm as increasing the concentration, indicating the secondary structure is not stable as shown in Figure 2.8.

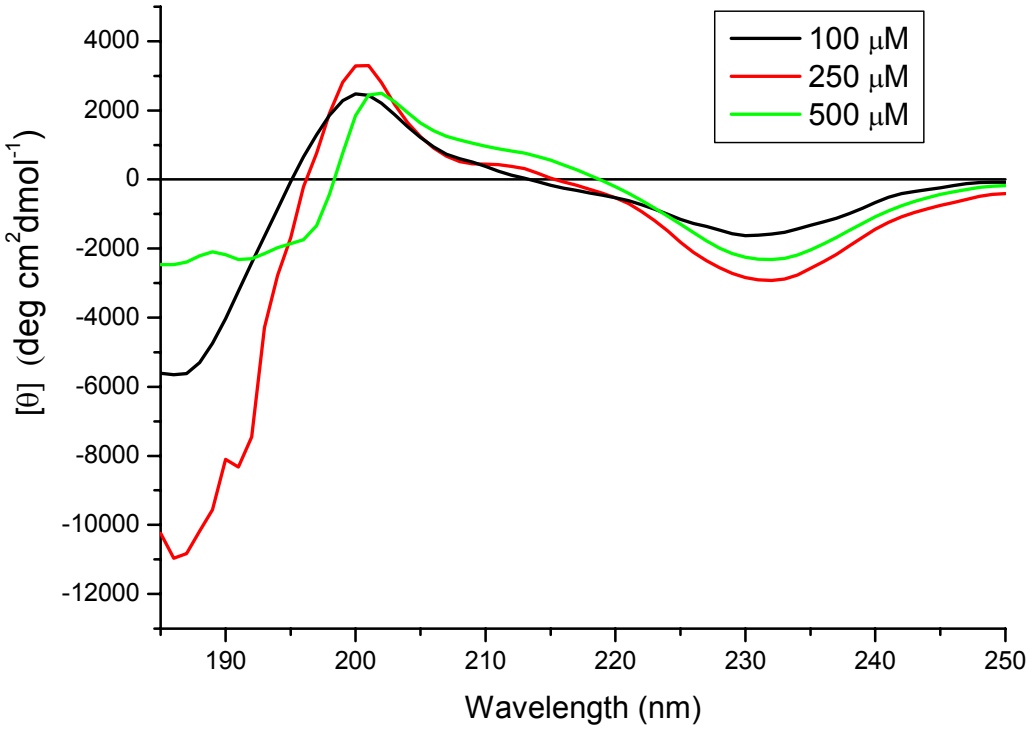

Figure 2.8 The concentration dependent study of the CD spectra of EK-Aib-Y in 10 mM of phosphate buffer, 20 ºC.

CD spectra of peptides in the near-UV (250-300 nm) region are the contributions of aromatic and sulfur-containing side chains. Some CD spectra show a positive interfering band around 224 nm for the aromatic side chain and a negative band around 228 nm for sulfur-containing side chains.[39] In most cases, a CD spectrum below 260 nm is governed by the amide chromophore, and the side-chain contribution is negligible.

2.2.3 Conformational Analysis by IR and VCD[a]

By comparison, the IR and VCD spectra for the EK-Dpg-Y, KE-Dpg-Y, EK-Dpg-V, and EK-Aib-Y peptides are quite similar as shown in Figure 2.9 and Figure 2.10 repectively. The amide I absorbance peaks at ~1637 cm^{-1} in both the FTIR and the VCD is quite weak for both but has a positive couplet shape, which would be consistent with a partial, local 3_{10} helical conformation. These data are inconsistent with a disordered form

for either and with a large difference in their structures. The side-chains, particularly Tyr do not interfere with IR or VCD measurements.

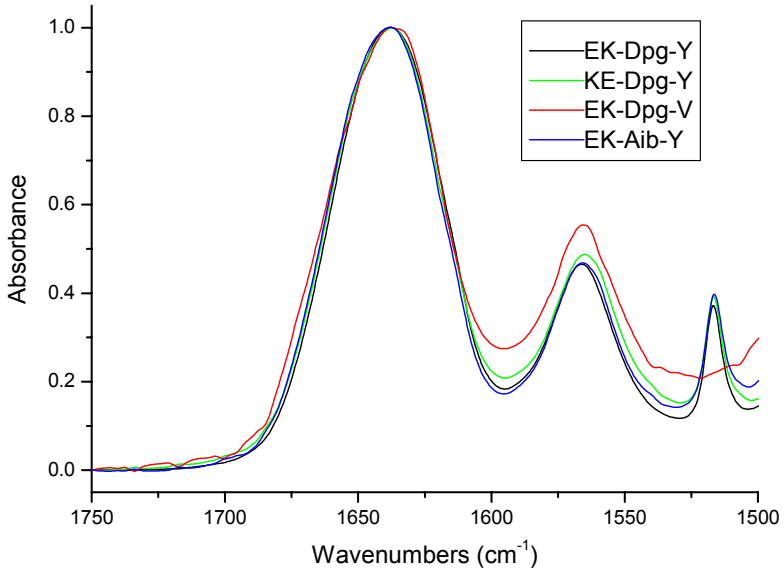

Figure 2.9 Amide I′ absorbance (1637 cm^{-1}) and tyrosine band (1516 cm^{-1}) FTIR spectra for 40 mM of EK-Dpg-Y, KE-Dpg-Y, EK-Dpg-V, and EK-Aib-Y. Each band was normalized to a maximum of 1.0 for comparison.

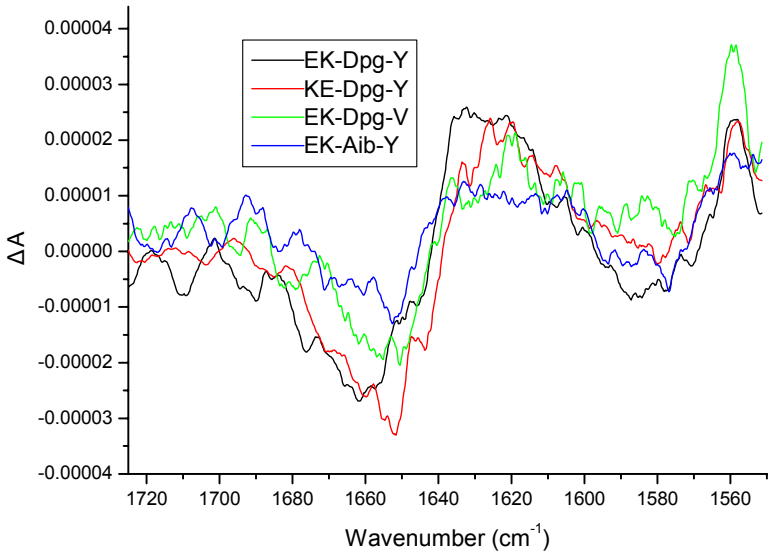

Figure 2.10 VCD spectra of 40 mM of EK-Dpg-Y, KE-Dpg-Y, EK-Dpg-V, and EK-Aib-Y

[a] IR and VCD were run by Ling Wu at University of Illinois at Chicago.

2.2.4 ^{1}H and ^{13}C NMR Resonance Assignments

The ultimate goal of the NMR experiment is to obtain proton-proton distances (from ROESY) and other restraints(e.g. $^{3}J_{HNH\alpha}$) to be used in 3D structure calculations. As a precursor to this thought protons much first be assigned.

^{1}H and ^{13}C NMR resonance assignments of EK-Dpg-Y were obtained using the combination of DQF-COSY, TOCSY, ROESY, HSQC, HSQC-TOCSY, and HMBC spectra. The first step in the ^{1}H NMR resonance assignment of EK-Dpg-Y is the identification of the ^{1}H spin systems of the individual amino acid residues for Glu^{1}, Tyr^{3}, and Lys^{5} via through-bond ^{1}H-^{1}H connectivities using COSY and TOCSY spectra. (Figure 2.12 and blue arrows in Figure 2.11) The different spin systems of the 20 proteinogenic amino acids usually show a characteristic connectivity pattern of cross peaks. Tyr can be readily identified by the NH-H_{β} cross peaks where H_{β}s of Tyr^{3} have characteristic chemical shifts at 2.85 ppm and 3.24 ppm due to the aromatic effect. Lys^{5} can be differentiated from Glu^{1} by cross peaks of NH-H_{ε} and NH-H_{δ} since Glu does not possess H_{δ} and H_{ε}. The chemical shifts of $Lys^{5}H_{\varepsilon}$ and $Lys^{5}H_{\delta}$ are 2.97 ppm and 1.70 ppm respectively. Dpg^{2} and Dpg^{4} can not be identified using TOSCY spectra because the amide protons of Dpg^{2} and Dpg^{4} did not show any connectivities to the other protons in their individual spin systems due to the lack of alpha protons.

The second step in the ^{1}H NMR resonance assignment is to sequentially connect each amino acid residue to its neighboring ones using ROESY experiment. The ROE cross-peaks between amide proton of residue *i+1* and H_{α} of residue *i* can be observed in ROESY spectrum because the distance between them is less than 5 Å.

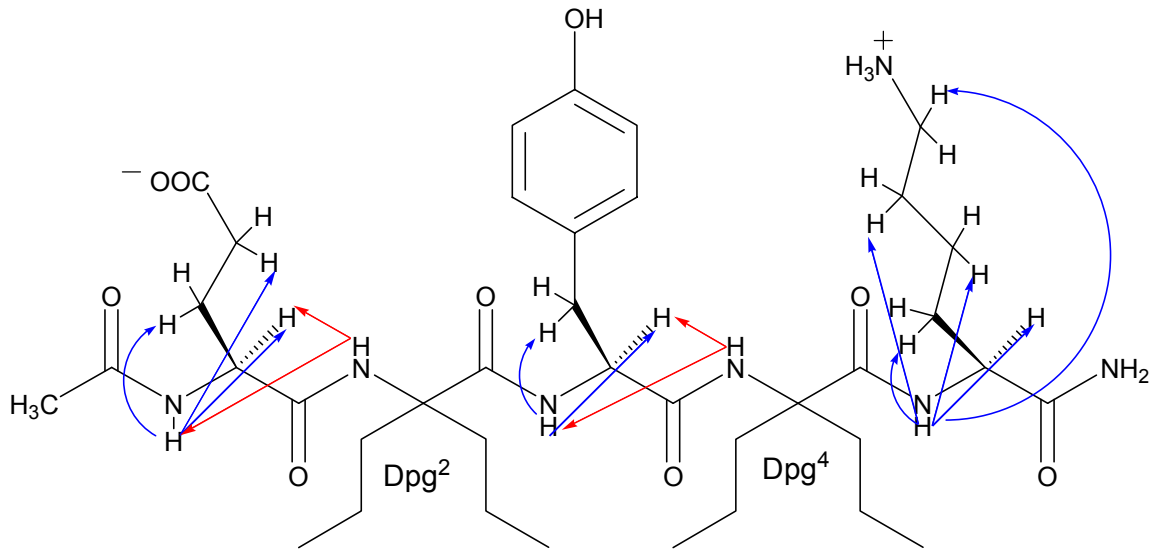

Intraresidual TOCSY couplings Sequential ROESY couplings

Figure 2.11 Intraresidual TOCSY and sequential ROESY couplings

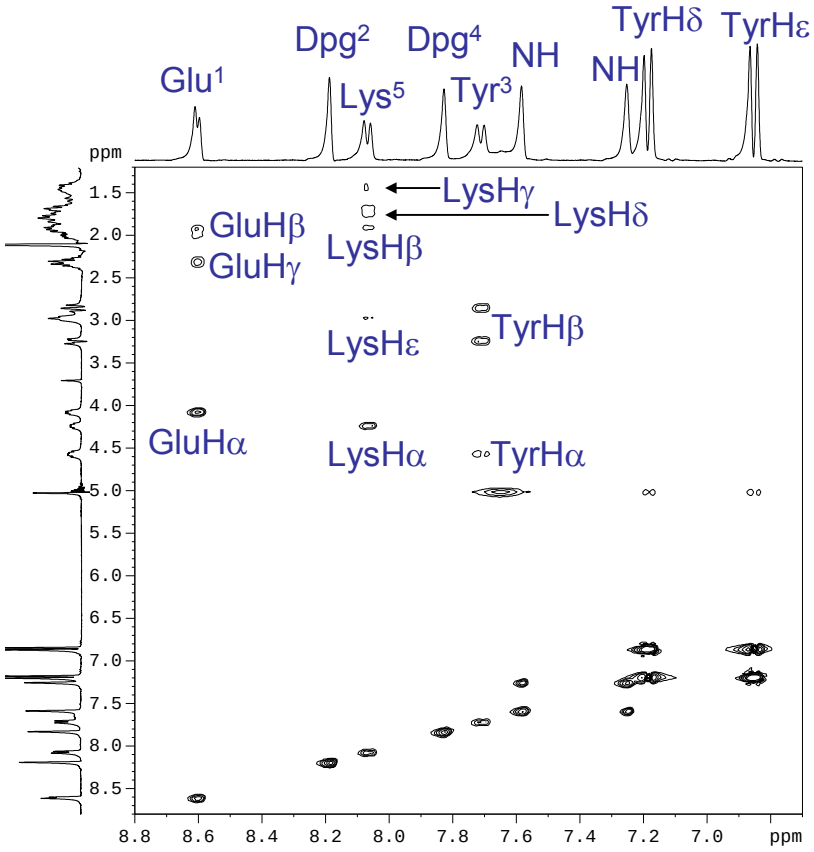

Figure 2.12 Portion of 400 MHz TOCSY spectrum of EK-Dpg-Y in 30 mM phosphate buffer (H_2O: D_2O 9:1), pH 7.0 at 278 K

Amide protons of Dpg[2] and Dpg[4] can be identified through the sequential ROE couplings from the already identified neighboring amino acids. The NH which has the chemical shift of 8.18 ppm shows ROE connectivities with Glu[1]NH and Glu[1]H_α, indicating this NH belongs to Dpg[2]. (Figure 2.13 and red arrows in Figure 2.11) The NH which has the chemical shift of 7.82 ppm shows ROE connectivities with Lys[5]NH and Tyr[3]H_α, indicating this NH corresponds to Dpg[4].

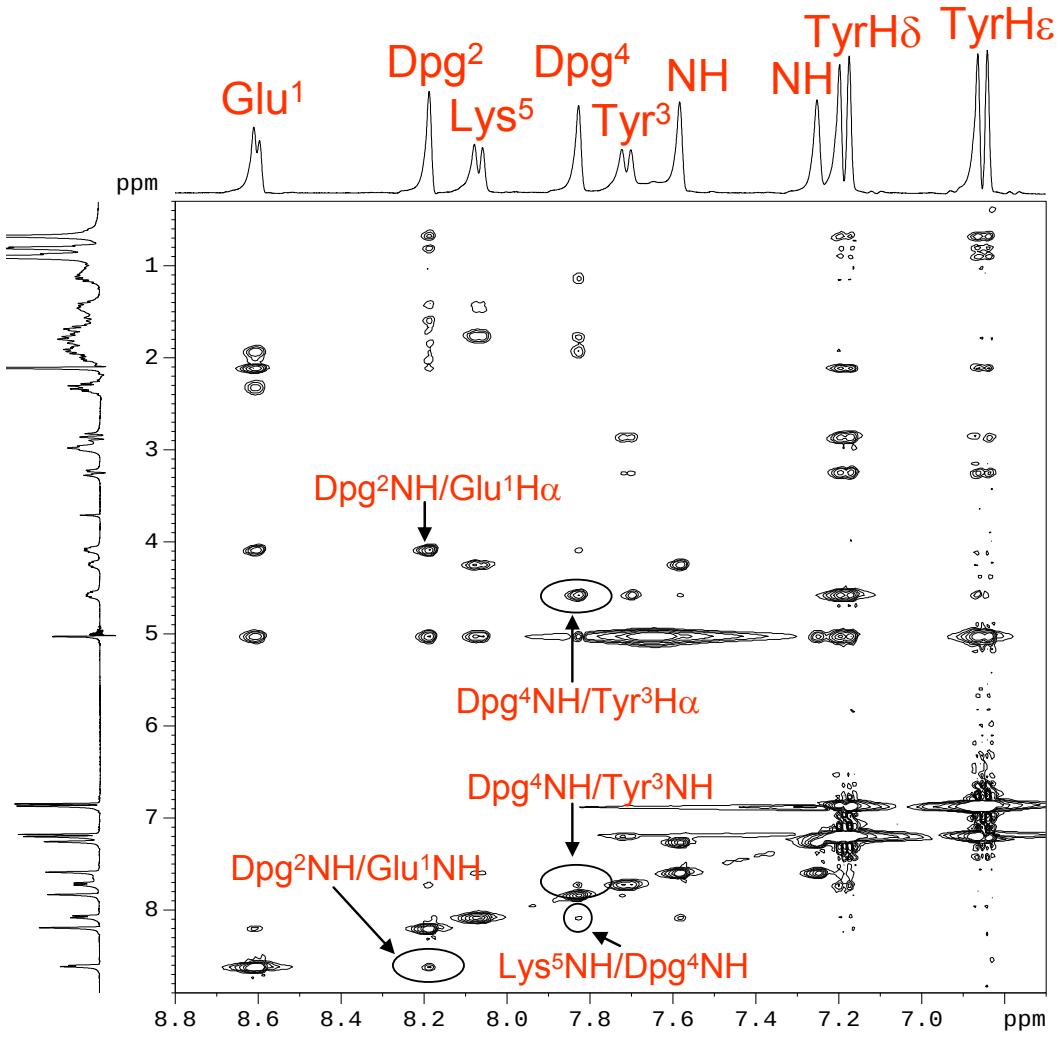

Figure 2.13 Portion of 400 MHz ROESY spectrum of EK-Dpg-Y in 30 mM phosphate buffer (H_2O: D_2O 9:1), pH 7.0 at 278 K.

The third step in ^{1}H NMR resonance assignment of EK-Dpg-Y is to identity the four propyl groups from the two Dpg residues. The side chains of the two dipropyl glycine residues are indistinguishable using DQF-COSY, TOCSY and ROESY, thus HSQC, HSQC-TOCSY, and HMBC 2D experiments were performed to identify the four propyl groups. HMBC gives two cross peaks between amide proton of Dpg^2 and its two C_β at 38.9 ppm(side-chain A) and 36.4 ppm (side-chain B) respectively. This C_β at 38.9 shows a cross-peak with its H_γ and H_δ of Dpg^2 residue at 0.67 from HSQC-TOCSY which enabled the assignment of propyl side chain A of Dpg^2 residue. The C_β at 36.4 shows a cross-peak with its delta proton at 0.79 which allowed the assignment of propyl side chain B for Dpg^2 residue. Two sets of diastereotopic protons from the beta carbons of propyl side-chain A and propyl side-chain B of Dpg^2 reside were readily identified from HSQC spectra through the correlations of one bond ^{1}H-^{13}C coupling.

HMBC displays a cross-peak correlating amide proton of Dpg^4 to its C_β at 37.0 ppm. This C_β displays a cross-peak with its gamma and delta protons of Dpg^4 residue at 1.12 and 0.88 respectively from HSQC-TOCSY which enabled the assignment for the two propyl groups of Dpg^4 residue. The diastereotopic beta protons of propyl side-chain C and propyl side-chain D of Dpg^4 are overlapping based on the integration of HSQC peak volume.

The C-terminal amide protons were determined from a cross-peak of H_α of Lys with a NH at 7.25 ppm using HMBC. The NH proton identified at 7.25 ppm had a cross-peak in TOCSY with another amide proton at 7.58 ppm supporting an amide proton coupling pattern. Integration ratio of the two protons is 1:1. This correlation excludes the possibility of NH proton from the side-chain of Lys; because HMBC allows the

correlation at most 4 bonds away and thus the correlations between alpha proton of Lys with its side-chain NH_3 are too far away to be observed. Overlaps were observed for the alpha carbons of Glu and Tyr, C_α of residue 2 (Dpg^2) and residue 4 (Dpg^4) respectively in HSQC spectra. HSQC–TOCSY further confirms the assignments by enabling us to see one bond ^1H-^{13}C coupling throughout an entire spin system. The ^1H resonance chemical shift assignments, coupling constants and ^{13}C resonance chemical shift assignments for EK-Dpg-Y are summarized in Table 2.3 and Table 2.4 respectively.

Table 2.3 ^1H Chemical shifts[a] and coupling constants of EK-Dpg-Y peptide in phosphate buffer, pH 7.0, at 278 K

Residues	NH	H_α	H_β	Others	$^3J_{HNH\alpha}$
$Acety^0$				CH_3 2.10	
Glu^1	8.60	4.06	1.94 2.02	H_γ 2.31	5.0
Dpg^2	8.18	—	1.43, 1.59 1.71, 1.84	H_γ 0.67, H_δ 0.67 H_γ 1.04, H_δ 0.79	—
Tyr^3	7.71	4.56	2.85 3.24	H_δ 7.18, H_ε 6.85	6.9
Dpg^4	7.82	—	1.78 1.93	H_γ 1.12, H_δ 0.88	—
Lys^5	8.07	4.22	1.92 1.79	H_γ 1.46, H_δ 1.70 H_ε 2.97	7.3
Amide	7.25 7.58				

[a]Chemical shifts are referenced to internal DSS at 0 °C, pH 7.

Table 2.4 ^{13}C Chemical shifts for EK-Dpg-Y

Residue	**^{13}C Chemical Shift (ppm)**						
	C=O	C_α	C_β	C_γ	C_δ	C_ε	C_ζ
Acetyl	177.2	24.0					
Glu^1	176.4	58.0	29.4	36.0	182.0		
Dpg^2	178.6	66.0	38.6 36.6	18.6 18.2	15.6 16.0		
Tyr^3	175.2	58.0	37.8	130.0	132.0	118.0	155.0
Dpg^4	178.8	66.0	37.2 37.2	18.6 18.6	16.0 16.0		
Lys^5	179.4	56.0	31.8	24.8	28.4	41.6	

2.2.5 Conformational Analysis by NMR

2.2.5.1 Chemical Shift Deviations

The assignments of ^{1}H chemical shifts for the EK-Dpg-Y peptide are summarized in Table 2.3. Those for the H_α in peptides are well-known to be highly conformationally dependent. In helical and turn conformations, α-protons exhibit an upfield shift with respect to random coil conformation whereas a downfield shift indicates of a β-sheet structure.[40] Chemical shift deviations of H_α and NH from random coil values for the EK-Dpg-Y and EK-Dpg-V are summarized in Table 2.5. H_α of both EK-Dpg-Y and EK-Dpg-V experience upfield shift, suggesting that the EK-Dpg-Y and EK-Dpg-V may adopt helical or turn conformations. However the effects of ααAAs on H_α chemical shifts have not been fully studied, chemical shift data alone are not enough to provide the information on the nature of the conformations.

Table 2.5 H_α and NH NMR chemical shift deviation for EK-Dpg-Y and EK-Dpg-V[a]

	EK-Dpg-Y	
Residue	H_α CSD ($\Delta\delta$, ppm)[b]	NH CSD ($\Delta\delta$, ppm)[c]
Glu	-0.28	0.03
Tyr	-0.02	-0.53
Lys	-0.09	-0.40
	EK-Dpg-V	
Glu	-0.16	0.13
Val	-0.21	-0.37
Lys	-0.13	-0.34

a. since Dpg is not standard proteinic residue, and has no H_α, there are no reference values for which CSD can be computed.

b. H_α chemical shift deviations were calculated from peptide data at 25 ºC and random coil data at 25 ºC from Wishart et al.[41]
c. NH chemical shift deviations were calculated from peptide data at 25 ºC and random coil data at 25 ºC from Wishart et al.[41]

Carbon chemical shifts of C_α and carbonyl carbons are conformationally sensitive and these shifting tendencies for carbon nuclei are opposite in direction to those found for the α and amide protons, with residues in helical structures showing downfield shifts and with residues in β-sheet showing upfield shifts relative to random coil conformation. Chemical shift deviations of α- and carbonyl carbon from random coil values for the EK-Dpg-Y are summarized in Table 2.6. Both α-carbon and carbonyl carbons of EK-Dpg-Y display downfield shift, suggesting that the EK-Dpg-Y may adopt helical or turn conformations.

Table 2.6 α-Carbon and carbonyl carbon NMR chemical shift deviations for EK-Dpg-Y[a]

Residue	EK-Dpg-Y	
	C_α CSD(Δδ, ppm)[a]	C=O CSD (Δδ, ppm)[a]
Glu	3.1	2.0
Tyr	2.4	0.4
Lys	0.8	3.2

[a.] C_α and C=O chemical shift deviations were calculated from peptide data at 5 ºC and random coil data at 25 ºC from Wishart et al.[41]

2.2.5.2 Amide Proton Temperature Coefficients

The temperature dependence of amide proton chemical shifts (temperature coefficients) are frequently measured to provide valuable information on intramolecular hydrogen-bonding formation. Hydrogen-bonded NHs typically display reduced temperature coefficients with respect to those in random coil structures.[42] Temperature

coefficients of NH resonances for EK-Dpg-Y are shown in Table 2.7. The Dpg^2 residue has $\Delta\delta/\Delta T$ of -7.8, while Dpg^4 has $\Delta\delta/\Delta T$ of -3.4. The substantial difference of $\Delta\delta/\Delta T$ values between them and the small absolute values of $\Delta\delta/\Delta T$ of the Dpg^4 N-H suggest that it may participate in the formation of the hydrogen bond. In addition, the chemical shifts of amide protons involved in hydrogen bonding experience upfield shift with respect to the amide protons exposed to water.[43] The amide proton chemical shift of Dpg^4 at 7.82 ppm is significantly upfield shifted compared to Dpg^2 amide proton at 8.18. The Tyr^3 NH possesses a reduced temperature coefficient compared to the random coil temperature coefficient of -9.32 and the amide proton of Tyr^3 shows significant upfield shift from random coil by 0.53 ppm as shown in table 2.5, thus indicating it may also form of a hydrogen bond.

Table 2.7 Temperature coefficients of NH resonances for EK-Dpg-Y in phosphate buffer, pH 7.0

EK-Dpg-Y	Observed $\Delta\delta/\Delta T$ (ppb/K)	Reported Random Coil $\Delta\delta/\Delta T$ (ppb/K)
Glu^1	-7.2	-7.01
Dpg^2	-7.8	_
Tyr^3	-5.8	-9.32
Dpg^4	-3.4	_
Lys^5	-8.6	-7.87
NH downfield (C-terminus)	-7.5	_
NH upfield (C-terminus)	-7.2	_

Table 2.8 shows the temperature coefficients of N-H resonances for KE-Dpg-Y. The Dpg^2 residue has $\Delta\delta/\Delta T$ of -7.2, while Dpg^4 has $\Delta\delta/\Delta T$ of -4.5. The

Δδ/ΔT difference between the two residues is 2.7 which is much smaller than the difference of 4.4 in EK-Dpg-Y, suggesting Dpg[4] NH in KE-Dpg-Y may be accessible to the solvent. The Tyr[3] N-H has a lowered temperature coefficient of -5.3 compared to the random coil temperature coefficient of -9.32, thus indicating it may participate in intramolecular hydrogen bonding. The ^{1}H NMR spectra of amide NH for EK-Dpg-Y and KE-Dpg-Y over the temperatures of 278 K to 303 K are shown in Figure 2.14 and Figure 2.15 respectively.

Table 2.8 Temperature coefficients of NH resonances for KE-Dpg-Y in phosphate buffer

KE-Dpg-Y	Observed $\Delta\delta/\Delta T$ (ppb/K)	Reported Random Coil $\Delta\delta/\Delta T$ (ppb/K)
Lys[1]	-8.0	-7.87
Dpg[2]	-7.2	_
Tyr[3]	-5.3	-9.32
Dpg[4]	-4.5	_
Glu[5]	-6.0	-7.01
NH downfield (C-terminus)	-5.5	_

Table 2.9 illustrates the temperature coefficients of N-H resonances for EK-Dpg-V. The valine NH has a reduced temperature coefficient of -5.5 compared to the random coil temperature coefficient of -8.35; however, the difference between them is only 2.85, suggestive of a moderately solvent shielded proton. The temperature coefficients of NH resonances for EK-Aib-Y are given in Table 2.10. The temperature coefficients of Tyr[3] and Lys[5] cannot be measured due to the overlap of amide protons of Tyr[3] and Lys[5].

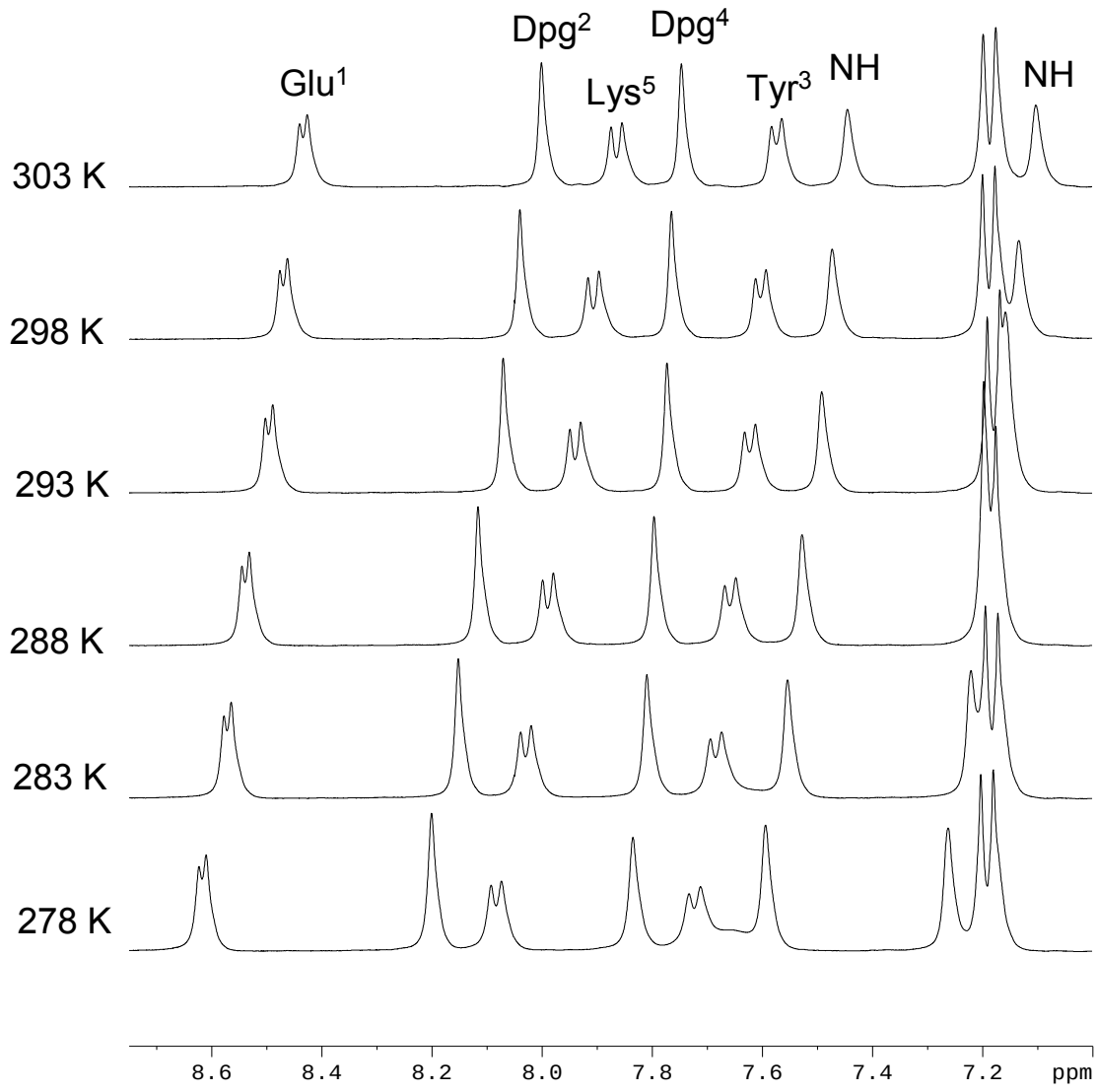

Figure 2.14 400 MHz ^{1}H NMR of amide NH of 10 mM EK-Dpg-Y in 30 mM phosphate buffer (H_2O: D_2O 9:1) at various temperatures, pH 7.0

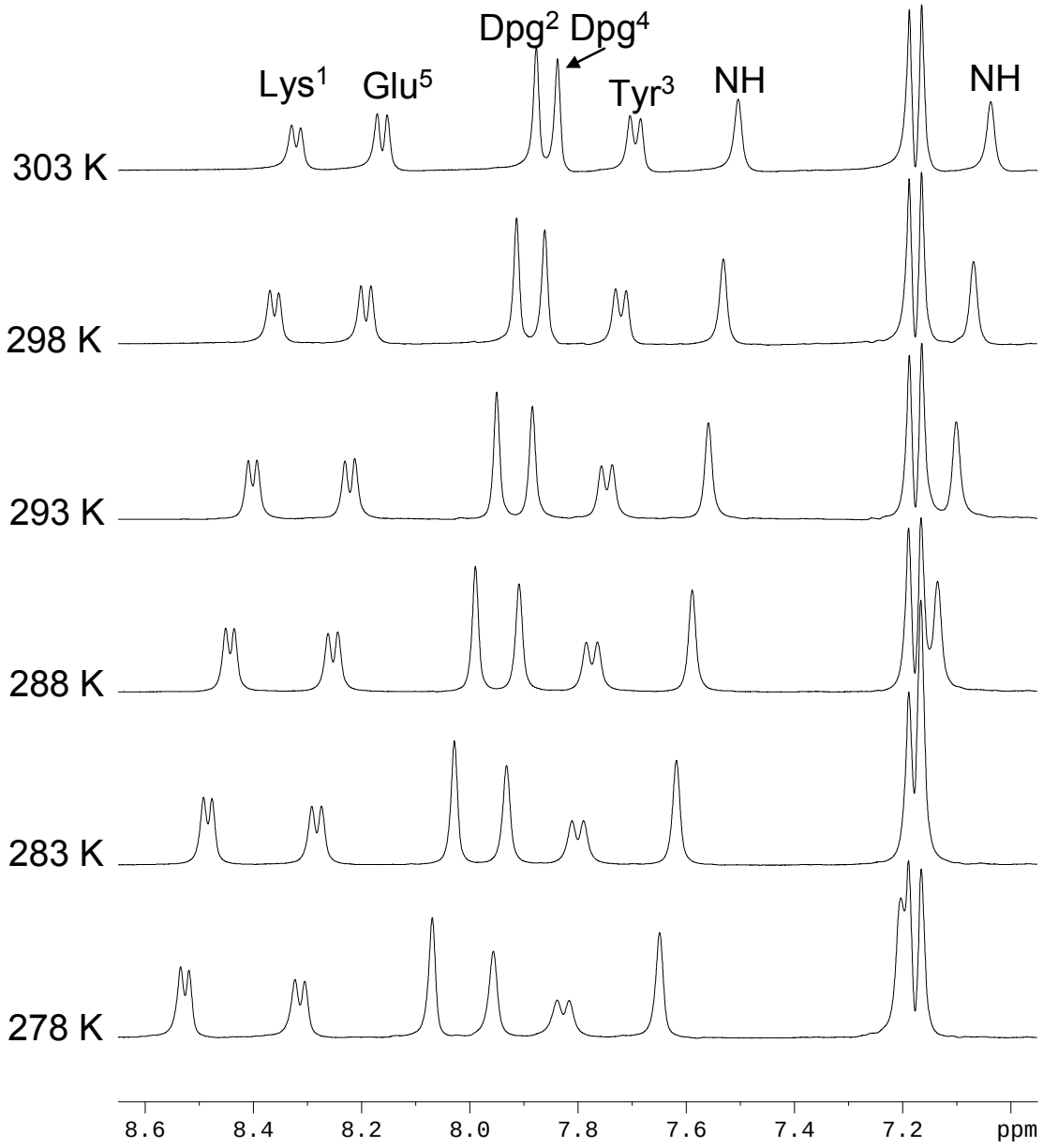

Figure 2.15 400 MHz ^{1}H NMR of amide NH of 10 mM KE-Dpg-Y in 30 mM phosphate buffer (H_2O: D_2O 9:1) at various temperatures, pH 7.0

Table 2.9 Temperature coefficients of NH resonances for EK-Dpg-V in phosphate buffer, pH 7.0

EK-Dpg-V	Observed $\Delta\delta/\Delta T$ (ppb/K)	Reported Random Coil $\Delta\delta/\Delta T$ (ppb/K)
Glu[1]	-6.5	-7.01
Dpg[2]	-8.0	_
Val[3]	-5.5	-8.35
Dpg[4]	-9.2	_
Lys[5]	-6.3	-7.87
NH downfield (C-terminus)	-7.0	_

Table 2.10 Temperature coefficients of NH resonances for EK-Aib-Y in phosphate buffer, pH 7.0

EK-Aib-Y	Observed $\Delta\delta/\Delta T$ (ppb/K)	Reported Random Coil $\Delta\delta/\Delta T$ (ppb/K)
Glu[1]	-5.8	-7.01
Aib[2]	-7.2	_
Tyr[3]	_	-9.32
Aib[4]	-4.1	_
Lys[5]	_	-7.87
NH downfield (C-terminus)	-3.7	_
NH upfield (C-terminus)	-4.0	_

2.2.5.3 NOE Connectivities

The NOE connectivities provide information on the types of conformations present in solution because different peptide conformations are associated with specific patterns of NOE connectivities.[44] Sequential $d_{NN}(i,i+1)$ NOE connectivities, medium-range NOE connectivities $d_{\alpha N}(i,i+2)$, and $d_{\alpha N}(i,i+3)$ are observed, if the peptide has a significant population of turns or helices. Whereas strong sequential $d_{\alpha N}(i,i+1)$ NOE connectivities with the absence of $d_{NN}(i,i+1)$ NOEs are observed if the peptide adopts an extended conformation.[32] The NH-NH region of the ROESY spectrum and the H_α-NH region of the 2D ROESY NMR spectra for EK-Dpg-Y are shown in Figure 2.16 and 2.17 respectively. EK-Dpg-Y shows strong sequential d_{NN} $(i,i+1)$ NOE connectivities throughout the entire sequence of this peptide indicating the presence of the helical conformation (Figure 2.16). Medium-range NOEs $d_{\alpha N}$ $(i,i+2)$ between the residue Glu[1] and Tyr[3], between CH_3 of acetyl group and Dpg[2], medium-range $d_{\alpha N}$ $(i,i+3)$ NOE

between the Glu[1] and Dpg[4] (Figure 2.17) are observed, indicating significant population of turn or helical backbone conformation. The cross-peaks of $d_{\alpha N}(2, 4)$ between Glu and Tyr and cross-peak between acetyl CH_3 proton and Dpg[2] NH and reduced temperature coefficient of Tyr[3] NH indicate a β-turn structure from acetyl to Tyr[3] with an intramolecular 4→1 hydrogen bonding between the acetyl carbonyl oxygen and Tyr[3] NH. The cross-peak of $d_{\alpha N}(1, 4)$ between Glu[1] and Dpg[4] and reduced temperature coefficient of the Dpg[4] NH suggest another β-turn from residue Glu[1] to Dpg[4] with a presence of a 4→1 hydrogen bonding between carbonyl of Glu[1] and Dpg[4] NH. The pattern of NOE connectivities for EK-Dpg-Y is identical at both 278 K and 298 K, suggesting that the solution structure of EK-Dpg-Y is stable over temperatures and the high population of the structure is still preserved at higher temperature 298 K.

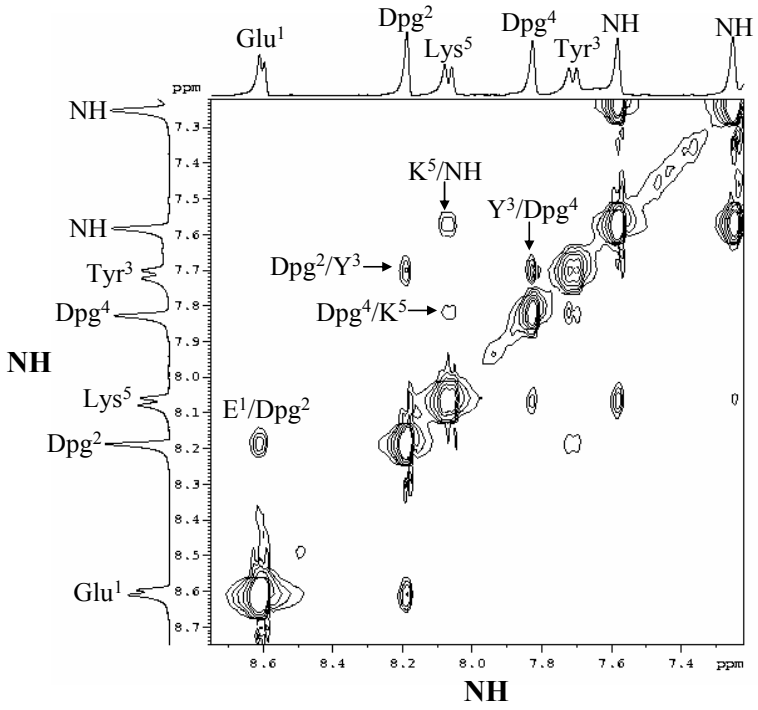

Figure 2.16 NH-NH region of the 400 MHz ROESY spectrum of 10 mM EK-Dpg-Y in 30 mM phosphate buffer (H_2O: D_2O 9:1), pH 7.0 at 278 K. A spin-lock mixing time of 400 ms was used

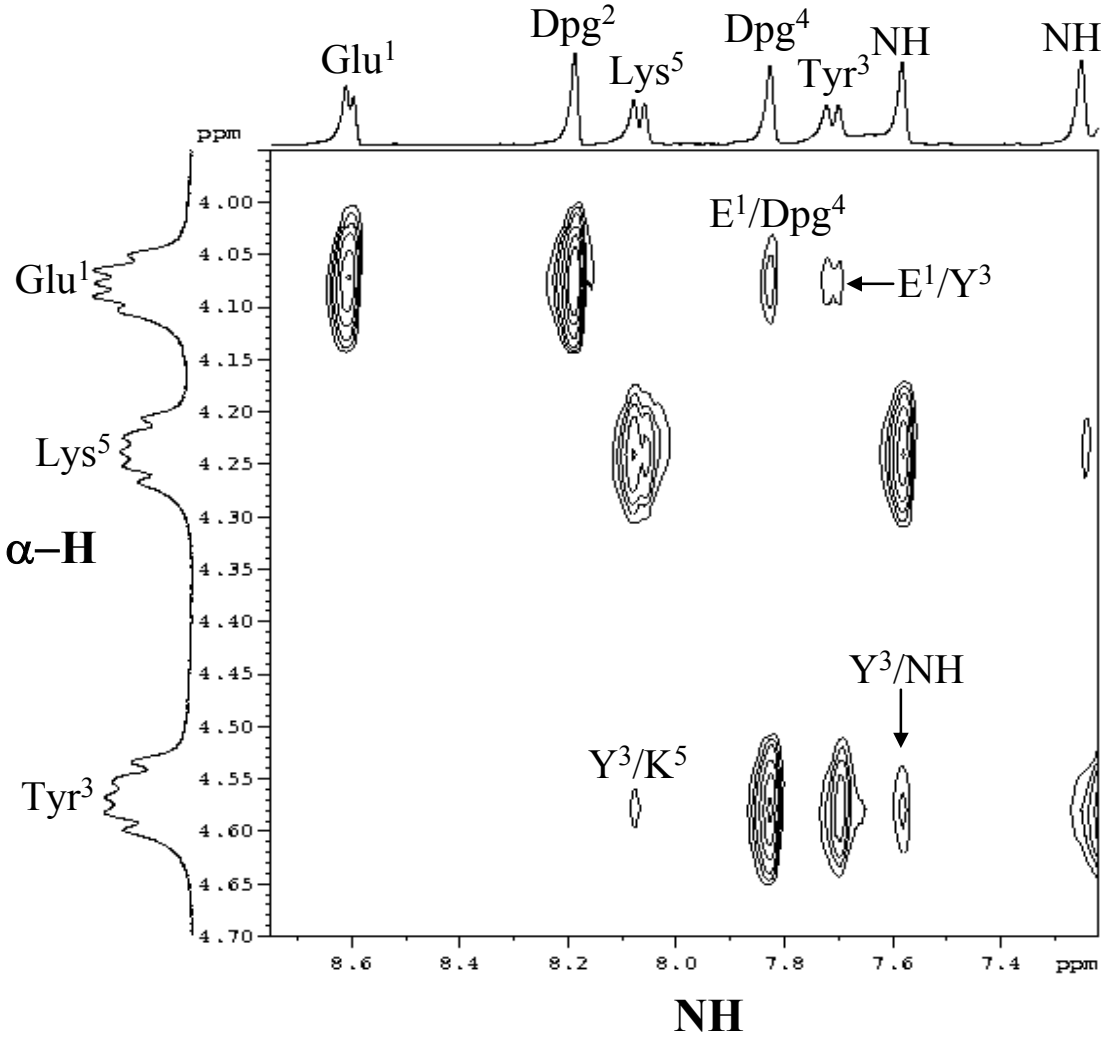

Figure 2.17 H_α-NH region of the 400 MHz ROESY spectrum of 10 mM EK-Dpg-Y in 30 mM phosphate buffer (H_2O: D_2O 9:1), pH 7.0 at 278 K. A spin-lock mixing time of 400 ms was used

The observed NMR NOEs for EK-Dpg-Y are summarized schematically in Figure 2.18.

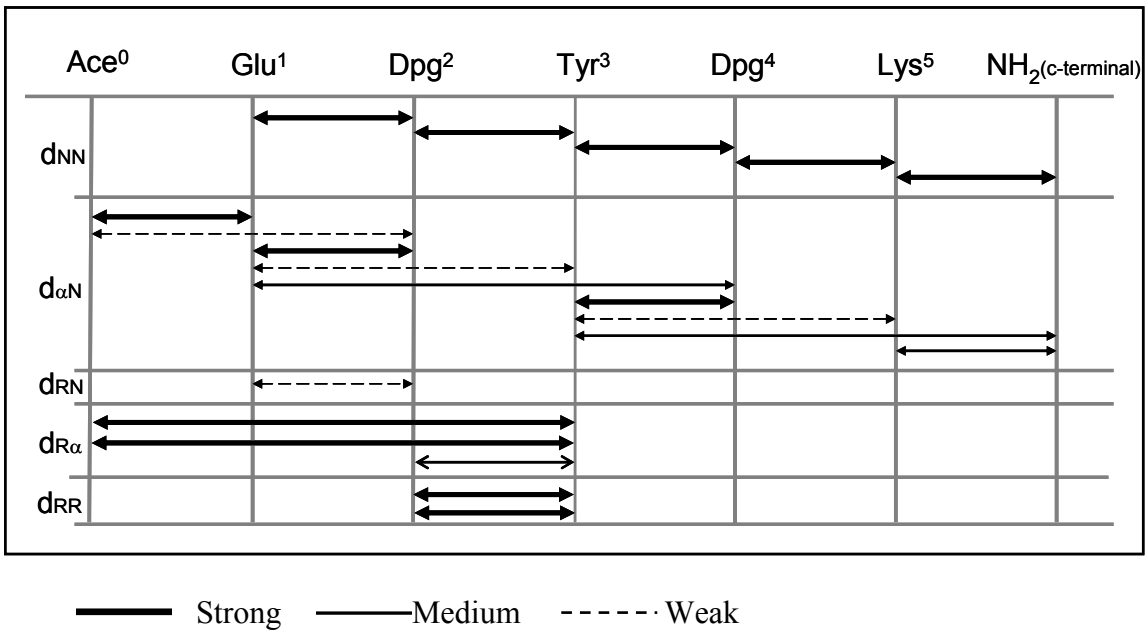

Figure 2.18 Summary of ROEs for EK-Dpg-Y. The thickness of the lines reflects the relative NOE intensities. d_{NN} refers to the NH-NH ROE, $d_{\alpha N}$ refers to the H_α-NH ROE, d_{RN} refers to side chain-NH ROE, $d_{R\alpha}$ refers to side chain-H_α ROE and d_{RR} refers to side chain-side chain ROE.

EK-Dpg-V shows sequential d_{NN} (i,i+1) NOEs over the entire sequence of this peptide suggesting backbone dihedral angles are in the helical or turn region of conformational space (Figure 2.19) which is consistent with the CD result. The medium-range NOE $d_{\alpha N}$ (i,i+2) between the residue Val^3 and Lys^5 is also observed (Figure 2.20); however, the other medium-range NOEs can not be assigned because the overlap of Glu and Lys alpha protons.

KE-Dpg-Y shows strong sequential $d_{\alpha N}$(i,i+1) NOEs over the entire length of the sequence and only one sequential d_{NN} (i,i+1) NOE between Lys^1 and Dpg^2 as shown in Figure 2.21 and Figure 2.22. This peptide also exhibits no medium-range H_α-NH NOEs (Figure 2.22) suggesting it is less structured than EK-Dpg-Y which is in good agreement with the CD results of this peptide. In EK-Dpg-A, NH-NH NOEs between Dpg^2 and Ala^3, between Lys and C-terminal NH are the only two NOEs identifiable because of the overlapping of the amide protons of Ala^3, Lys^5 and Dpg^4, and also some of the NOEs are too proximate to the diagonal to be assigned unambiguously as shown in Figure 2.23. The complete overlap of H_αs of Glu, Ala and Lys makes the assignment of H_α-NH NOEs impossible in this peptide as illustrated in Figure 2.24. In EK-Aib-Y, the observation of the strong sequential $d_{\alpha N}$ (i,i+1) NOEs between Glu^1 and Aib^2, between Tyr^3 and Aib^4, and between Lys^5 and NH of C-terminus indicating that backbone dihedral angles are in the β-sheet region of conformational space as shown in Figure 2.26. The two NOEs in the NH-NH region can not be assigned unambiguously due to the overlap of amide protons of Tyr^3 and Lys^5 as illustrated in Figure 2.25.

The NOE connectivities other than NH-NH and H_α-NH NOEs observed for the peptides KE-Dpg-Y, EK-Dpg-V, and EK-Aib-Y are as follows: In KE-Dpg-Y, strong

medium range NOEs between CH_3 of acetyl^0 and Tyr$^3H_\delta$, between CH_3 of acetyl^0 and Tyr$^3H_\varepsilon$, between Dpg$^2H_\gamma$, H_δ with Tyr$^3H_\delta$ and Tyr$^3H_\varepsilon$ respectively were observed, NOE between Dpg$^4H_\gamma$ and Tyr$^3H_\delta$ was also observed. In EK-Dpg-V, NOEs from the Dpg side chains and Val side chain can not be assigned unambiguously due to the overlap between Dpg$^2H_\gamma$ and Val$^3H_\gamma$ and the overlap between Dpg$^2H_\beta$, Dpg$^4H_\beta$ and Lys$^5H_\beta$. In EK-Aib-Y, NOEs between two Aib$^2H_\beta$ and Tyr$^3H_\delta$, and only one Aib$^4H_\beta$ and Tyr$^3H_\varepsilon$ were observed, NOE between CH_3 of acetyl^0 and Tyr$^3{}_\delta$ was also observed.

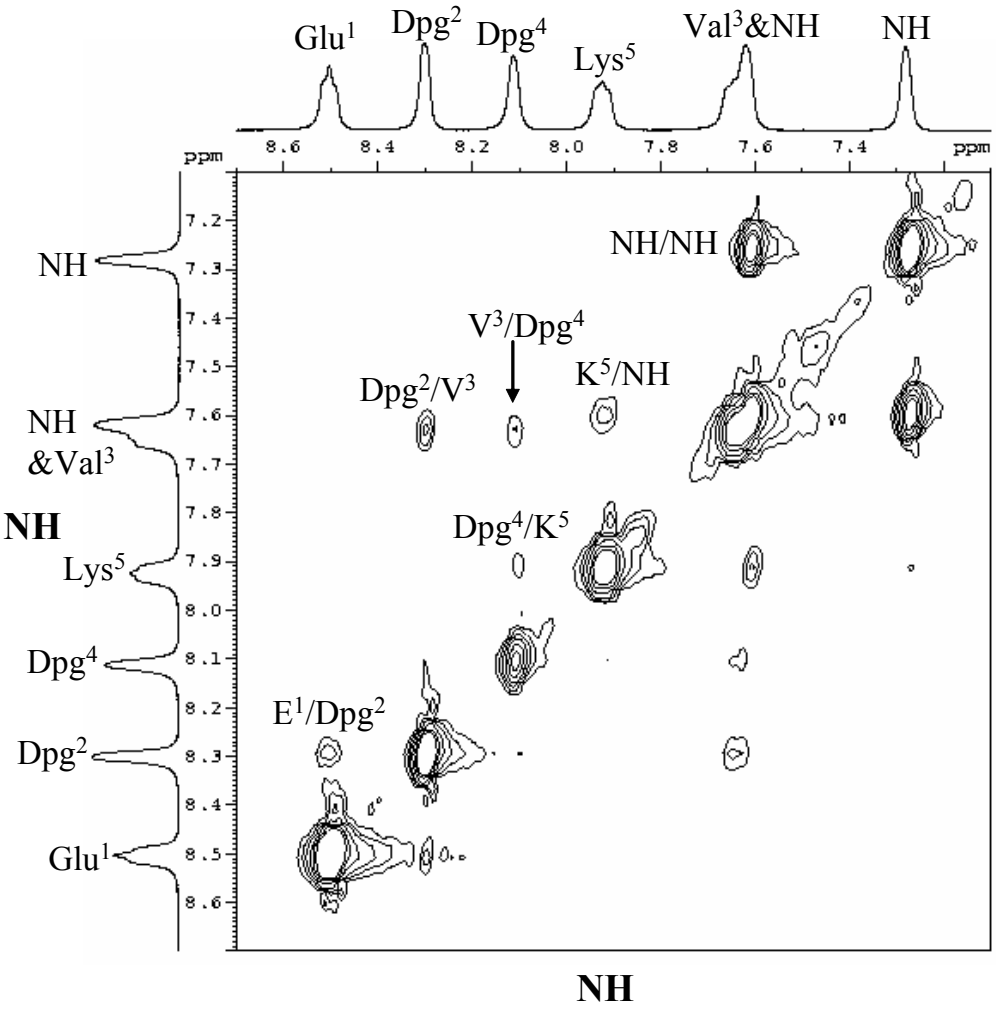

Figure 2.19 NH-NH region of the 400 MHz ROESY spectrum of 10 mM EK-Dpg-V in 30 mM phosphate buffer (H_2O: D_2O 9:1), pH 7.0 at 278 K. A spin-lock mixing time of 400 ms was used.

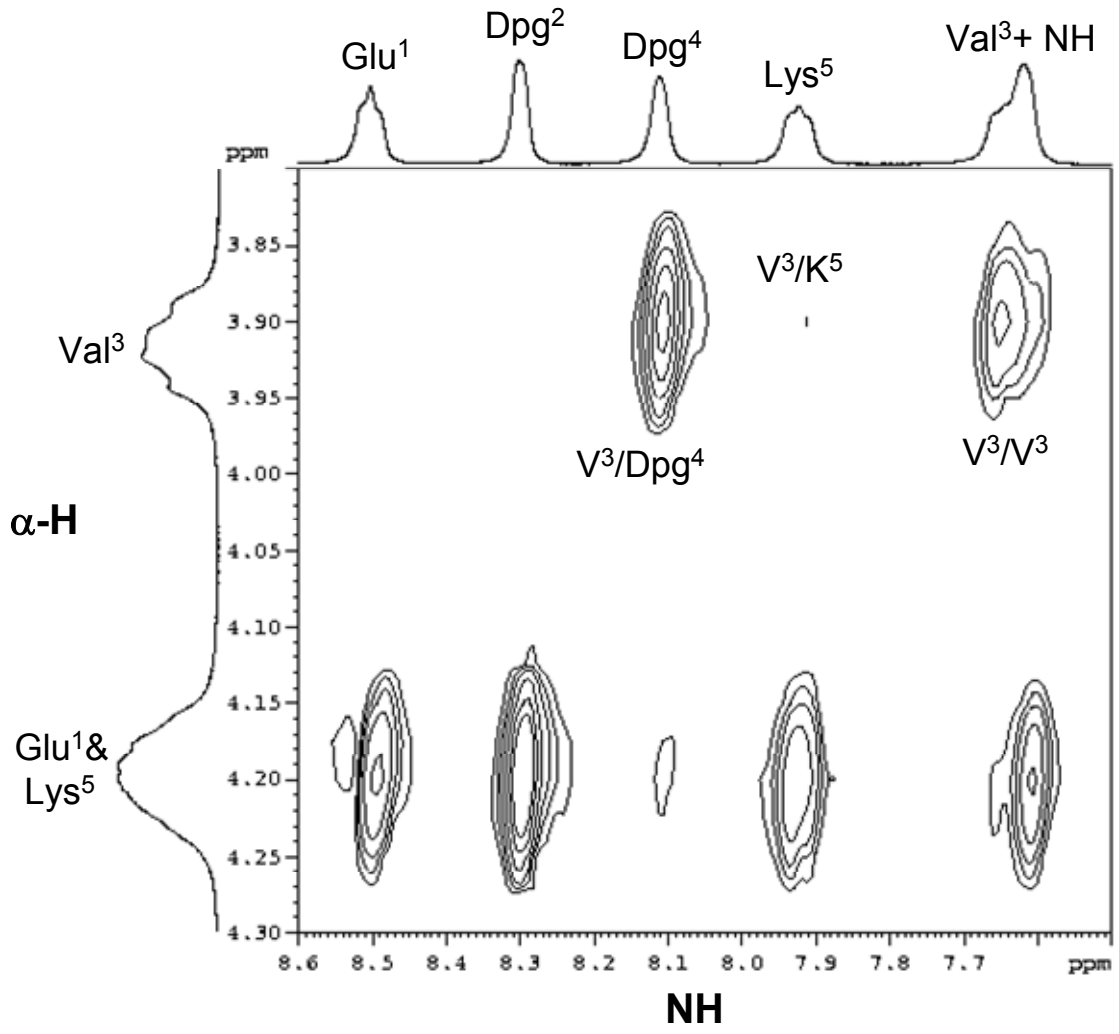

Figure 2.20 H_α-NH region of the 400 MHz ROESY spectrum of 10 mM EK-Dpg-V in 30 mM phosphate buffer (H_2O: D_2O 9:1), pH 7.0 at 278 K. A spin-lock mixing time of 400 ms was used.

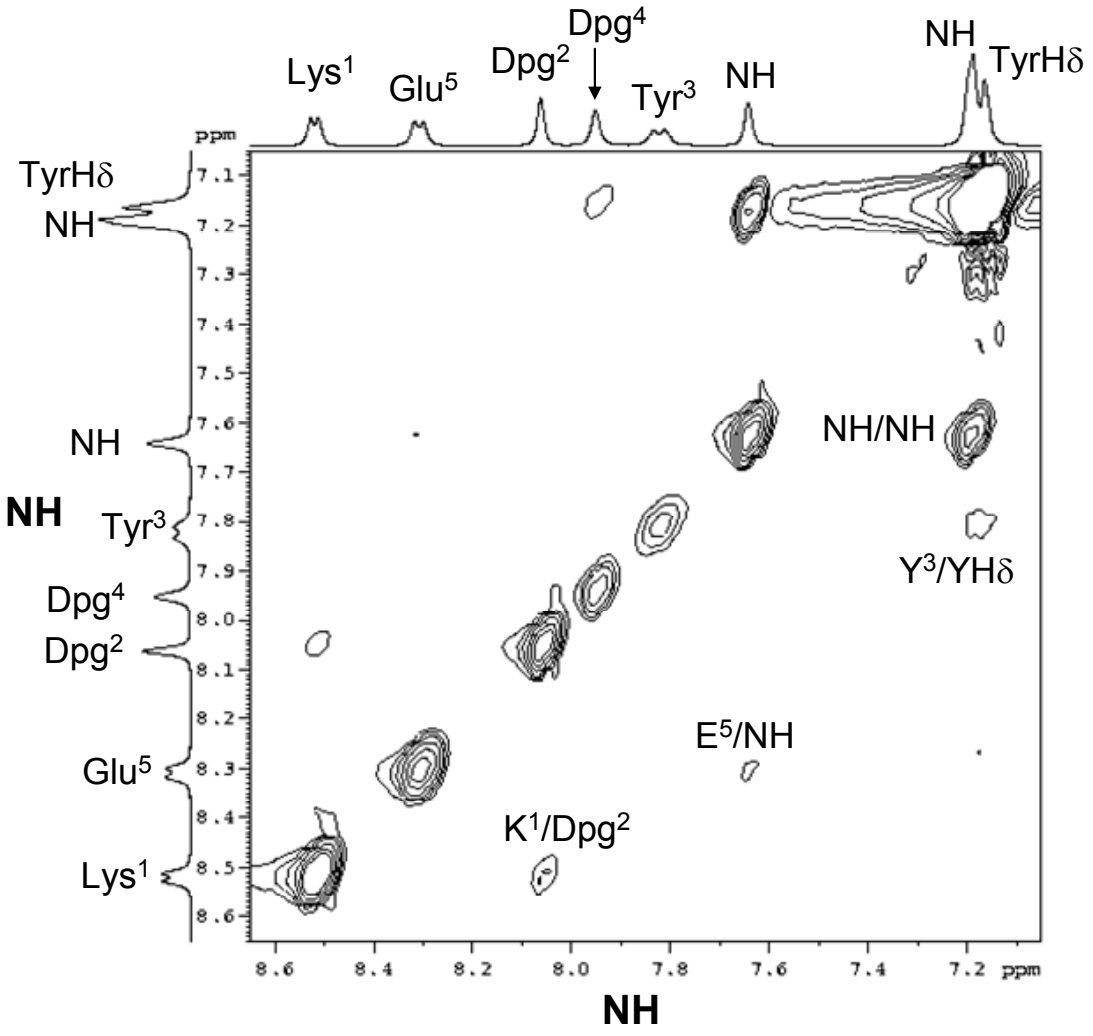

Figure 2.21 NH-NH region of the 400 MHz ROESY spectrum of 10 mM KE-Dpg-Y in 30 mM phosphate buffer (H_2O: D_2O 9:1), pH 7.0 at 278 K. A spin-lock mixing time of 400 ms was used.

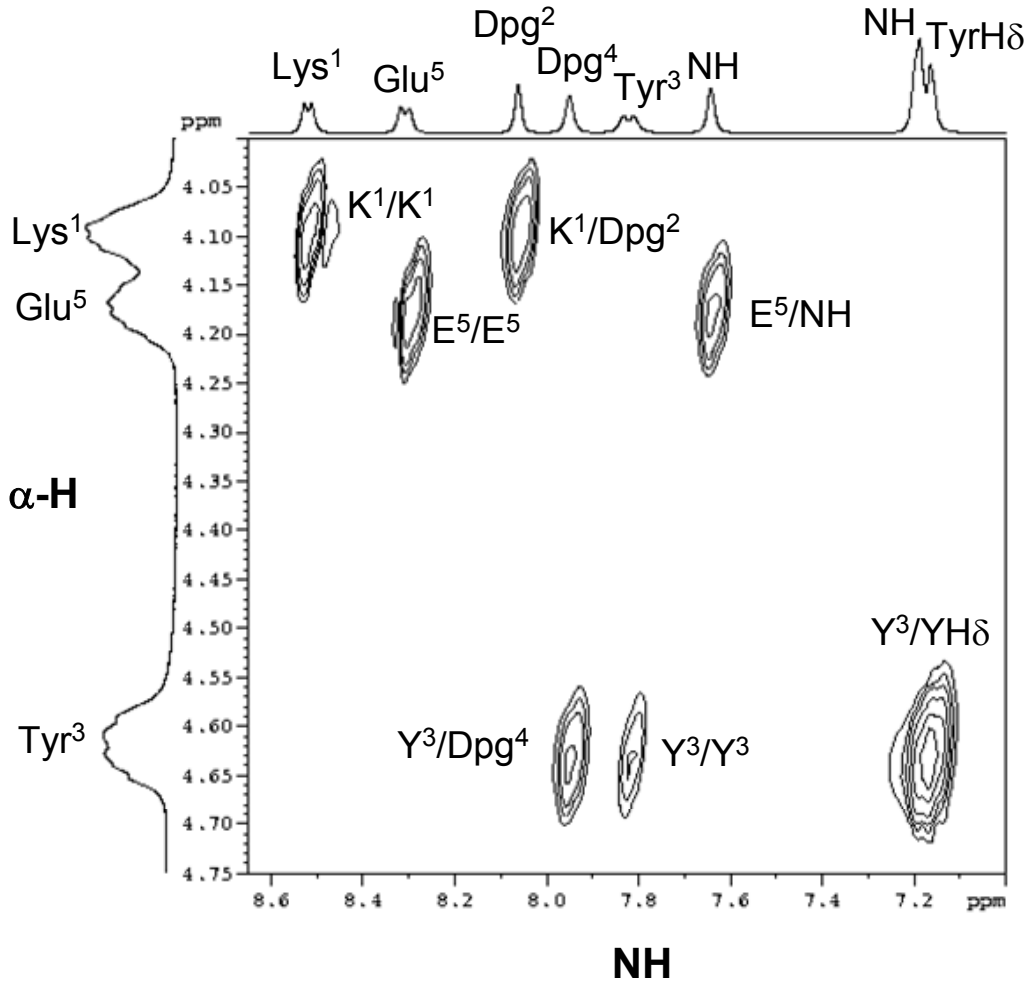

Figure 2.22 H_α-NH region of the 400 MHz ROESY spectrum of 10 mM KE-Dpg-Y in 30 mM phosphate buffer (H_2O: D_2O 9:1), pH 7.0 at 278 K. A spin-lock mixing time of 400 ms was used.

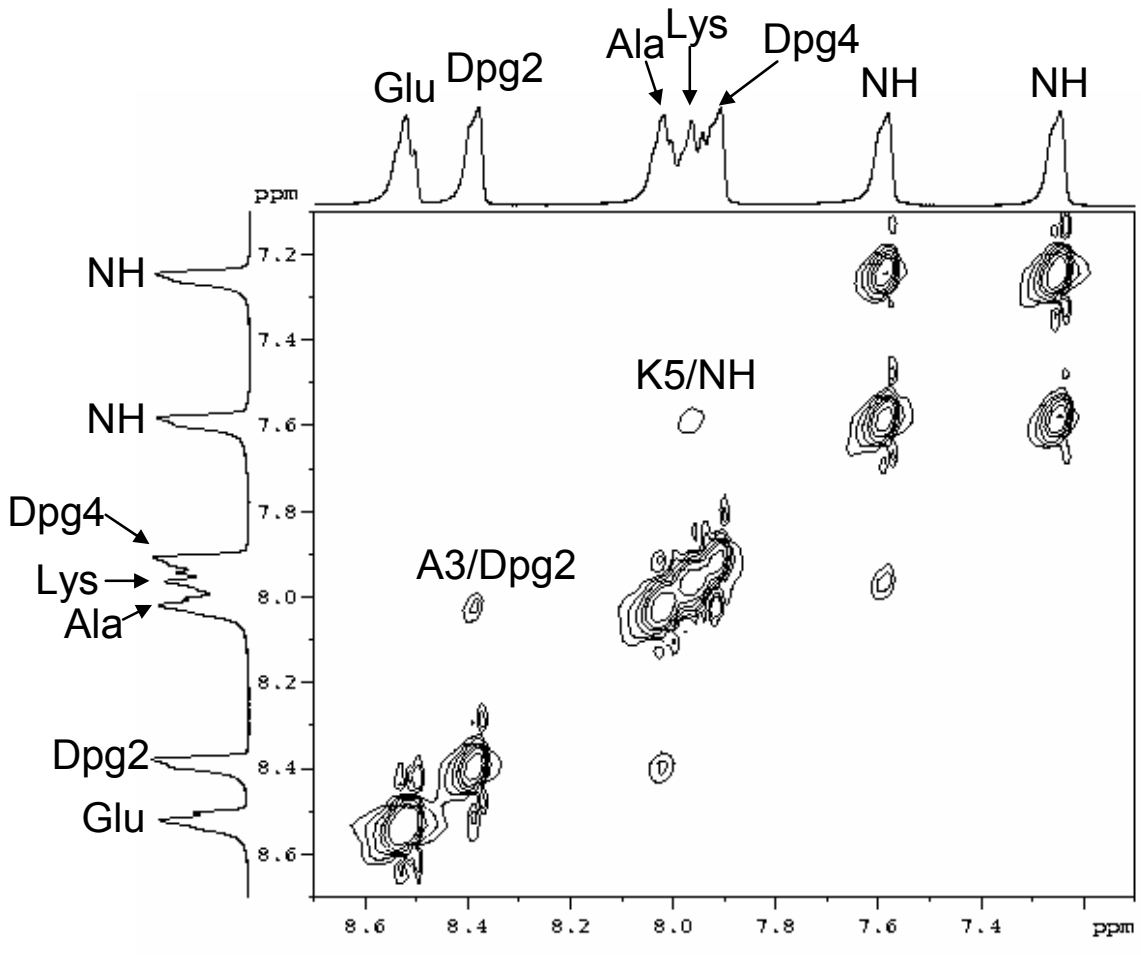

Figure 2.23 NH-NH region of the 400 MHz ROESY spectrum of 10 mM EK-Dpg-A in 30 mM phosphate buffer (H_2O: D_2O 9:1), pH 7.0 at 278 K. A spin-lock mixing time of 400 ms was used.

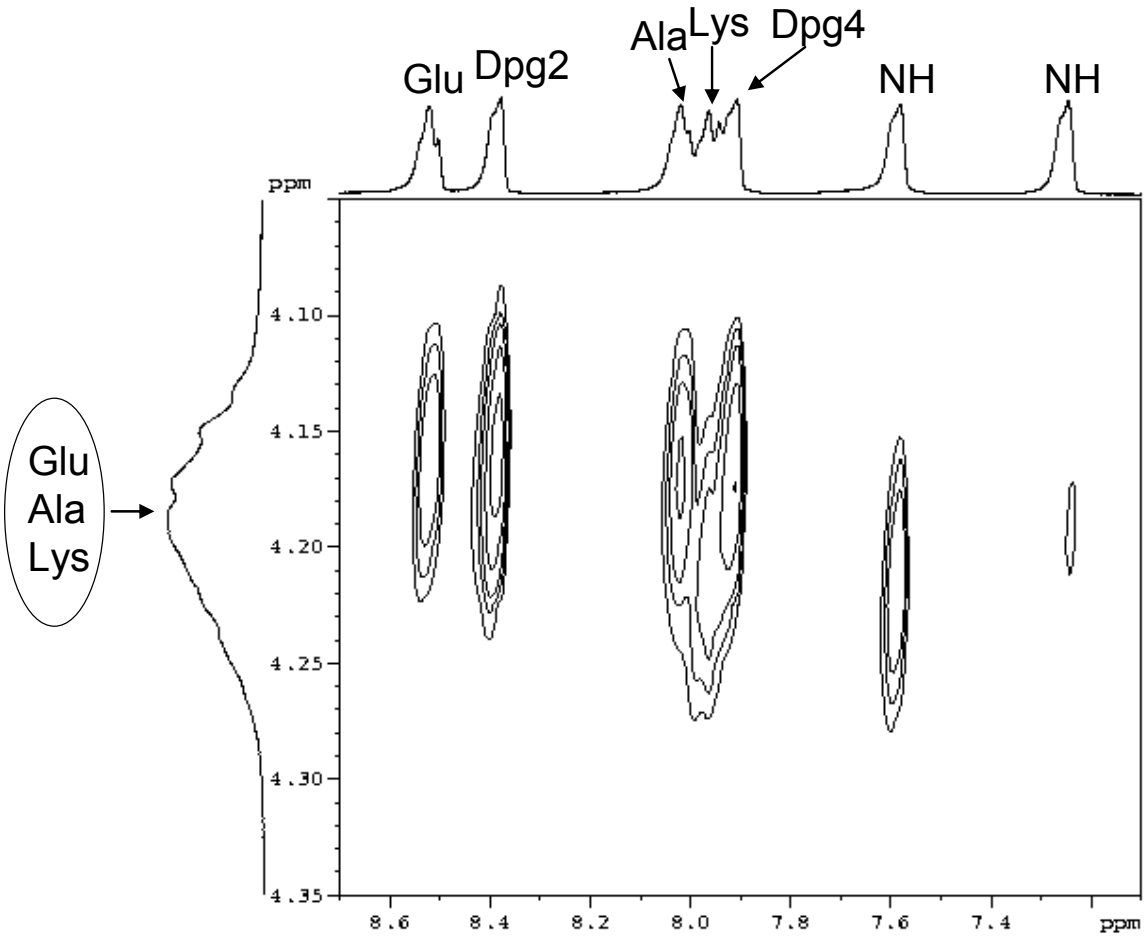

Figure 2.24 H_α-NH region of the 400 MHz ROESY spectrum of 10 mM EK-Dpg-A in 30 mM phosphate buffer (H_2O: D_2O 9:1), pH 7.0 at 278 K. A spin-lock mixing time of 400 ms was used.

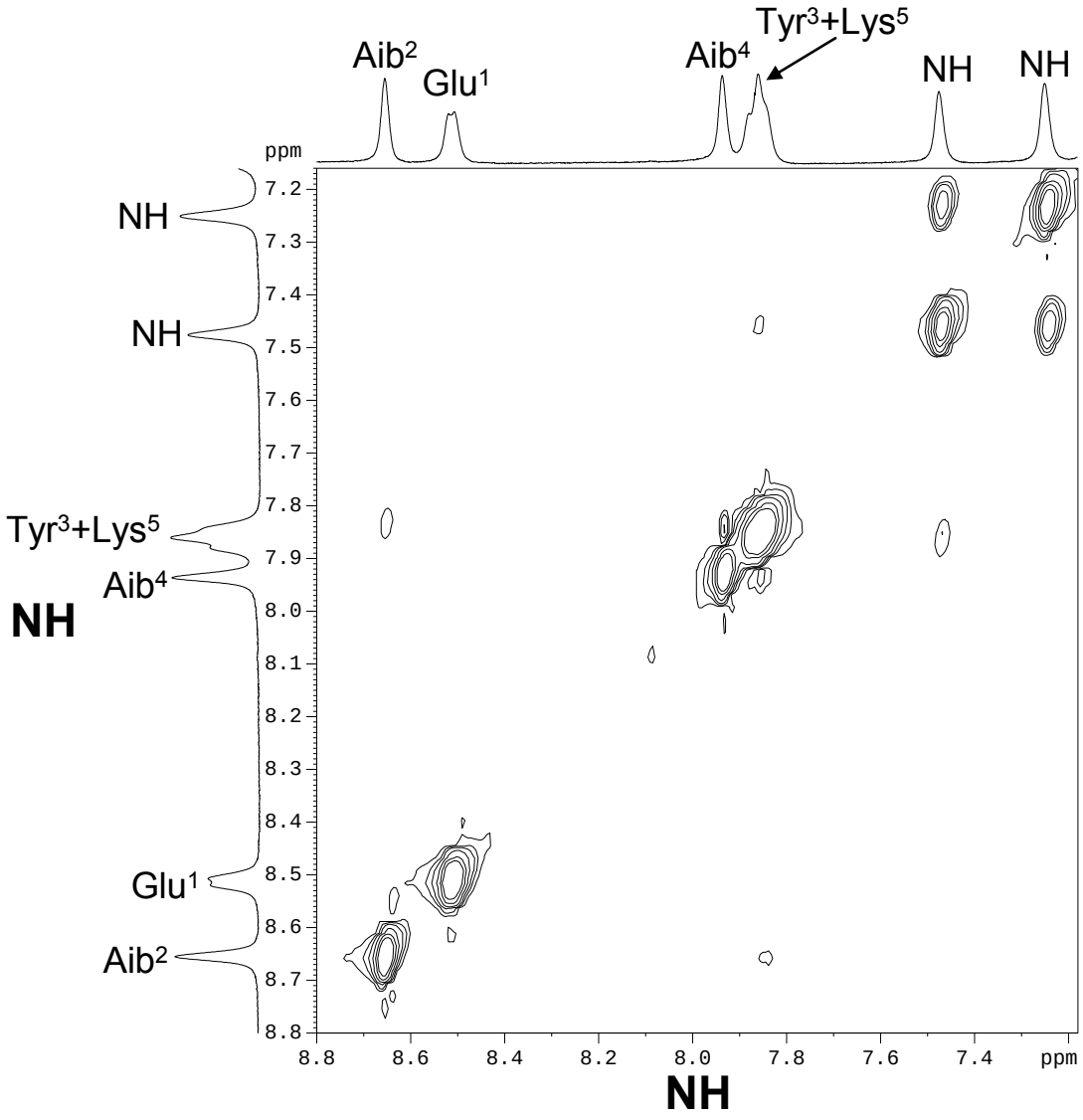

Figure 2.25 NH-NH region of the 400 MHz ROESY spectrum of 10 mM EK-Aib-Y in 30 mM phosphate buffer (H_2O: D_2O 9:1), pH 7.0 at 278 K. A spin-lock mixing time of 400 ms was used.

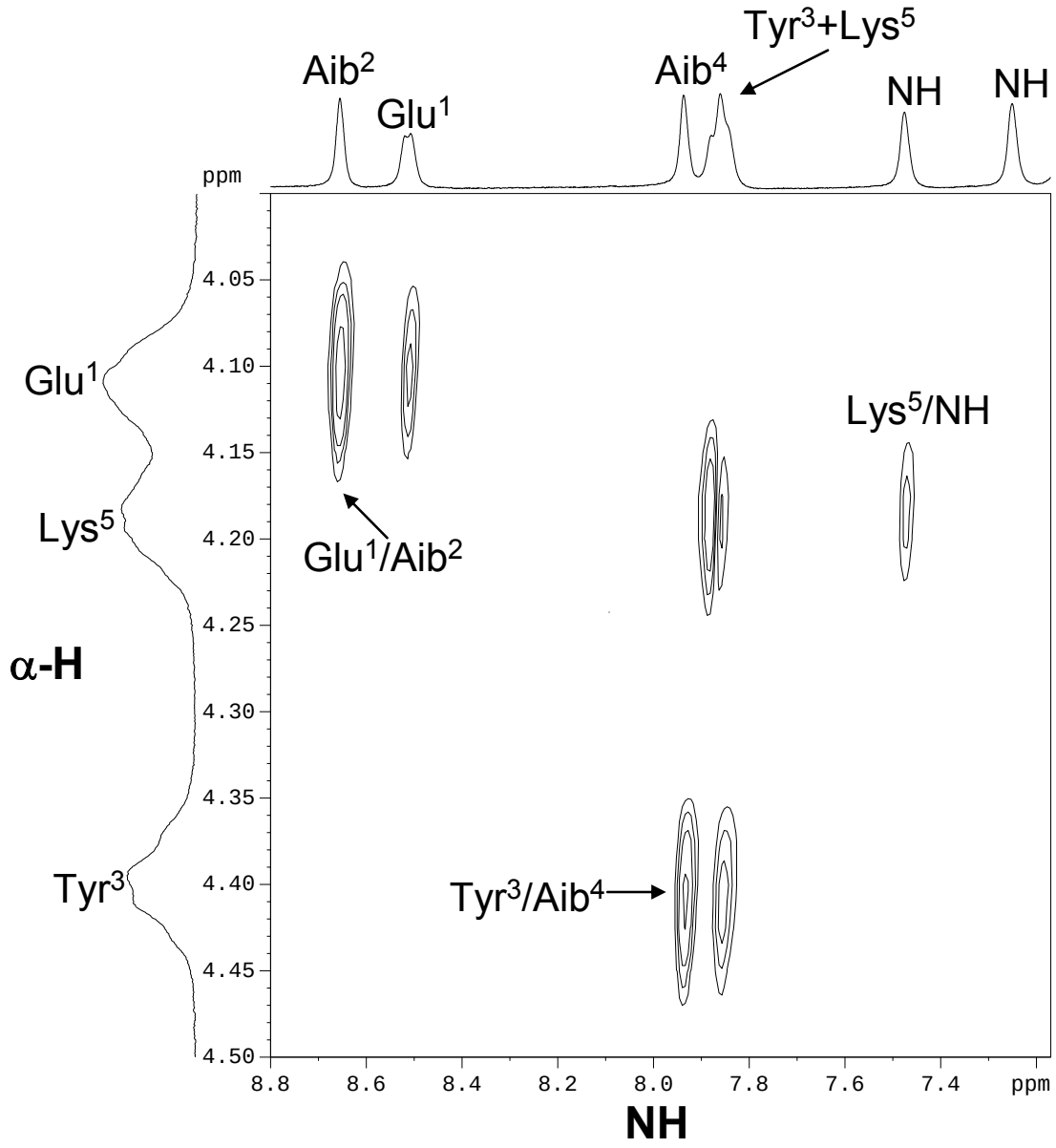

Figure 2.26 H_α-NH region of the 400 MHz ROESY spectrum of 10 mM EK-Aib-Y in 30 mM phosphate buffer (H_2O: D_2O 9:1), pH 7.0 at 278 K. A spin-lock mixing time of 400 ms was used.

2.2.6 Structural Analysis of EK-Dpg-Y

The optical spectra, CD and VCD are consistent in suggestion that the EK-Dpg-Y pentapeptide has a partially helical or turn-like structure. The NMR H_α chemical shifts, C_α and C=O chemical shift are consistent with helical or turn conformations and the N-H temperature dependence NMR analysis($\Delta\delta/\Delta T$) further confirms the Tyr^3 and Dpg^4 residues are H-bonded with N-terminal acetyl carbonyl and Glu^1 carbonyl respectively. Our data for NOE values and coupling constants can further be used to constrain a normal NMR structure analysis.

Structures calculated by MD simulated annealing using experimental restraints from the ROE and HNHA data superimpose well for the backbone atom positions from the N-terminus until the C-terminal Dpg^4 residue, as shown for the low variance in the ϕ dihedral angle for the Glu^1, Dpg^2 ,Tyr^3 and Dpg^4 residues noted in Table 2.11. The overlay of side-chains follows a similar pattern where Glu^1, Dpg^2, Tyr^3, and Dpg^4 are well structured while Lys^5 seems flexible and unstructured with side-chains having no particular conformation as shown in Figure 2.27. The Tyr^3 ring packs tightly against Dpg^2 and is well structured indicating that there is a strong hydrophobic interaction of the Tyr^3 side-chain and the pro-*S* propyl side chain of Dpg^2. This hydrophobic interaction may be a strong stabilizing force of the peptide folding in water. The order in the ensemble for the N-terminal Ace^0 is due to packing with Tyr^3 as well. Backbone hydrogen bonds found between the NH of Tyr^3 and the carbonyl of the Ac group and between NH of Dpg^4 and the carbonyl of Glu^1 most likely play a critical role in the stability of this peptide turn as illustrated in Table 2.12.

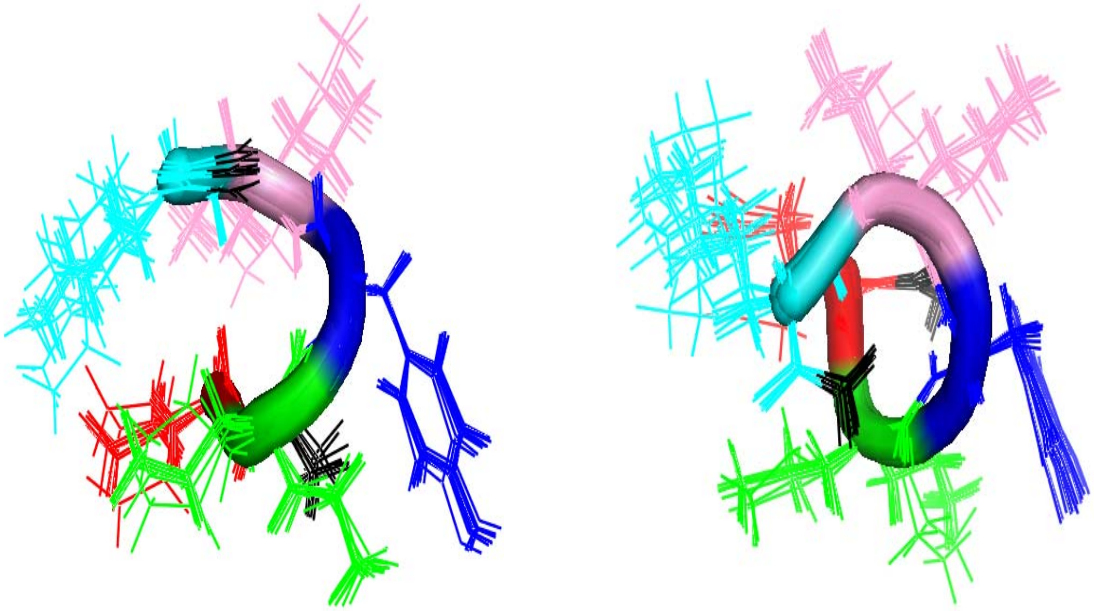

a b

Figure 2.27 Overlay of 10 structures of the EK-Dpg-Y calculated from ROE restrained molecular dynamics simulated annealing. a: side view, b: top view. Each residue is displayed in the different color: Ace^{0}(black), Glu^{1}(red), Dpg^{2}(green), Tyr^{3}(blue), Dpg^{4}(pink), Lys^{5}(cyan) and NH_2(black).

The secondary structure for the mean was evaluated within MOLMOL and is found to adopt a short 3_{10}-helix from residues 0-4, while the C-terminus is frayed. This is evident from the cyan colored backbone trace in Figure 2.27b. A comparison of the average torsional angles for the 10 lowest energy structures(Table 2.11) and the apparent H-bond lengths(Table 2.12) also illustrate that the ordered region of the peptide adopts a helical structure.

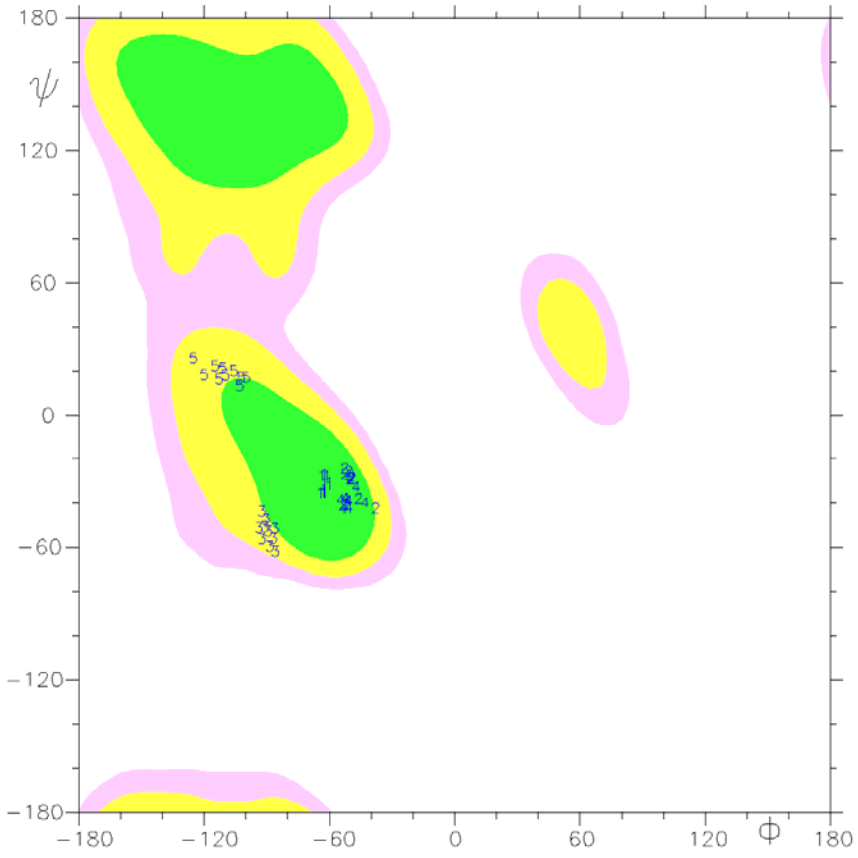

Figure 2.28 The Ramachandran plot of EK-Dpg-Y

The Ramachandran plot of EK-Dpg-Y is shown in Figure 2.28, which gives possible conformations of ϕ and ψ dihedral angles. All of the dihedral angles ϕ and ψ for EK-Dpg-Y are in the right-handed helical region of conformational space.

Table 2.11 Average dihedral angles, standard deviations are given in parentheses. An angle τ represents N-C_α-C(O) angle

	Glu1	Dpg2	Tyr3	Dpg4	Lys5
ϕ	-62.5 (1.3)	-49.1 (4.3)	-90.0 (2.8)	-51.1 (3.4)	-111 (8.1)
ψ	-31.7 (3.4)	-30.0 (5.7)	-53.1 (5.5)	-39.1(2.8)	19.1 (3.5)
χ_1	-69.2 (45)	47.8 (37) 81.2 (48)	-47.1 (3.4)	43.6 (53) -170 (37)	-61.2 (3.7)
χ_2	-173 (4.3)		-158 (93)		-178 (39)
χ_3	-3.50 (92)				-177 (69)
χ_4					164 (48)
χ_5					-78 (99)
χ_6			-178 (117)		
τ	111(0.31)	113(0.68)	111(0.15)	112(0.82)	111(0.18)

Table 2.12 Backbone H-bonds and the distance between the ring group of Tyr^3 and the side chain of Dpg^2

	Distance Å
O (Ac) – HN (Tyr^3)	2.37 (0.28)
O (Ac) – HN (Dpg^4)	3.15 (0.90)
O (Glu^2) – HN (Dpg^4)	2.59 (0.43)
O (Glu^2) – HN (Lys^5)	3.00 (1.28)
Cγ1 (Dpg^2) - Cγ (Tyr^3)	4.18 (0.49)

X-ray crystallography studies suggest that most peptides containing Dpg favor helical conformations and only a few favors extended structures.[21-23, 26-30] Karle et al. showed that when incorporated into a poor helix promoting sequence, the hexapeptide Boc-Gly-Dpg-Gly-Gly-Dpg-Gly-NHMe adopts a helical conformation in crystal structure.[21] The substantial retention of the helical conformation was observed in apolar solvent $CDCl_3$, whereas, in the strongly solvating solvent DMSO, an unfolded conformation was observed based on NMR data. The helical conformation is stabilized by the intramolecular hydrogen bonding involving residues 4-6 and the terminal NHMe in $CDCl_3$. The unfolded structure in DMSO is due to the solvent invasion which destabilizes intramolecularly hydrogen bonded backbone conformations indicated by the

high temperature coefficients ($\Delta\delta/\Delta T$). This suggests that solvents play an important role in the formation of the peptide conformation.

Dpg coupled to the highly helical promoting alanine in the tripeptide Boc-Ala-Dpg-Ala-OMe adopts a helical conformation in crystal state, whereas in DMSO the tripeptide adopts extended conformation.[18, 24] It suggests that differences between solid and solution state conformation do occur. Herein, we present the first reported use of aqueous solutions in elucidating secondary conformations of Dpg containing peptides.

Theoretical calculations reveal a strong dependence on the bond angle N-C^{α}-CO (τ) with $\tau > 105°$ favoring helical conformations and $\tau < 105°$ favoring extended conformations.[45-47] The crystal structures of Dpg containing peptides have also been shown to have τ angles in this range. Indeed the MD simulated annealing gave the τ angles of the two Dpg residues for EK-Dpg-Y larger than 110° as illustrated in Table 2.11, which indicates that these residues are in the helical conformation.

2.3 Conclusions

In conclusion, CD, VCD and NMR spectral analysis suggest that Dpg containing peptides adopt more ordered structures relative to their Nva containing analogues. The central residues (Ala, Val, Thr, Tyr) and the charged side-chains of Glu and Lys play important roles in the degree of peptide folding. Hydrophobic and branched residues (Val, Tyr) at the central position of the peptide produce greater folding as judged by CD and NMR. Despite the high tendency of Aib to induce helical conformation, CD and NMR data suggest that EK-Aib-Y is less structured compared to EK-Dpg-Y. This suggests that the stabilizing force for the pentapeptide EK-Dpg-Y folding in water may arise from strong hydrophobic interaction between side-chains of Dpg^2 and Tyr^3 rather than the

amino acid propensity for helical conformations. Temperature-dependent NMR analysis of NH resonances ($\Delta\delta/\Delta T$) for Ac-Glu-Dpg-Tyr-Dpg-Lys-NH_2 suggests a series of i→i+3 hydrogen bonds between the N-terminal acetyl carbonyl and the Tyr^3 NH, and the Glu^1 carbonyl and the Dpg^4 NH. The solution conformation of Ac-Glu-Dpg-Tyr-Dpg-Lys-NH_2 calculated from NMR-derived restraints shows a 3_{10}-helical structure (two repetitive type-III β-turns), which is supported by 2D NMR, CD and VCD spectra. Analysis of NMR-derived models of these peptides suggest that there is a strong hydrophobic interaction of the pro-*S* propyl side chain of Dpg^2 and the Tyr^3 side-chain that may be a strong stabilizing force of the peptide folding in water.

2.4 Experimental

- **Synthesis and Purification of Peptides**

Peptides were synthesized using standard solid-phase Fmoc chemistry on Fmoc-PAL-PEG-PS resin (Applied Biosystems) in continuous-flow mode on an Applied Biosystems Pioneer peptide synthesizer. The primary sequences of Dpg and Nva containing peptides are listed in Table 2.1.

The Fmoc amino acids utilized were Fmoc-Glu(tBu)-OH, Fmoc-Dpg-OH, Fmoc-Tyr(tBu)-OH, Fmoc-Lys(Boc)-OH, Fmoc-Ala-OH, Fmoc-Val-OH, Fomc-Thr(tBu)-OH, Fmoc-Nva-OH and Fmoc-Aib-OH. Deprotection of Fmoc group was achieved using Reagent B (Piperidine-DBU-DMF, 2:2:96 v/v). The step-wise coupling of each amino acid was performed in DMF using 4 eq of amino acids, 4 eq of PyAOP, and 8 eq of DIEA. Couplings for Dpg containing peptides were performed at an elevated temperature of 50ºC due to the difficult coupling of the Dpg to the peptide sequence. Acetylation of the N-terminus of Dpg and Nva peptides was carried out via manual synthesis, where the

resin was treated with excess 0.2 M of Ac_2O in 0.28 M of DIEA/DMF solution (16 equiv) for 2 h, followed by rinsing with DMF and DCM, the resin was dried under high vacuum for 4h. The peptide was cleaved off the solid support with concomitant deprotection of side chains using standard cleavage solution (trifluoroacetic acid-triisopropylsilane-water-phenol, 88:2:5:5 v/v) for 2 hours.

- **TFA-Mediated Peptide Cleavage**

Precipitation Method: the resulting filtrate was precipitated with cold ether overnight. The precipitate was then washed with cold diethyl ether and centrifuged at 40, 000 rpm for ten minutes (3 x). Ether was decanted off and the pellet was allowed to dry under high vacuum for 5 hours to yield the crude peptide.

Extraction Method: the resulting filtrate was diluted with cold 30% acetic acid solution, washed with cold diethyl ether (3 x 50 mL), and lyophilized to yield the crude peptide.

Crude peptides were purified by reverse-phase high-performance liquid chromatography (HPLC) on a Waters Delta-Pak C_{18} column (15 μm, 300Å, 8 x 100 mm) with a gradient from 90% A (H_2O, 0.1%TFA) and 10% B (CH_3CN, 0.1% TFA) to 30% A and 70% B over 60 mins at a flow rate of 1mL/min. Semi preparative conditions were carried out using a Waters preparative Delta-Pak C_{18} column (15 μm, 300 Å, 25x100 mm) at a flow rate of 20 mL/min. The homogeneity (> 99%) was confirmed by analytical reverse-phase HPLC monitoring at the wavelength of 220 nm with the scan wavelength from 200 to 400 nm using a Vydac C_{18} column (5 μm, 4.6 x 250 mm) and identity of the peptides was determined by matrix-assisted laser desorption ionization-time of flight (MALDI-TOF) on a Bruker Proflex III instrument with XMASS software Net peptide concentration determined by quantitative amino acid analysis. Amino acid analysis was

performed on a Dionex AAA-Direct system composed of a GS50 Gradient Pump, an AS50 Autosampler, and an ED50 Electrochemical Detector.

Table 2.13 Analytical HPLC retention time and corresponding MALDI results

Peptide	Retention time(min)	MALDI $(M+H)^+$ m/z	
		Calculated	observed
EK-Dpg-Y	37.1	762.9	762.4
KE-Dpg-Y	25.0	762.9	762.9
EK-Dpg-A	46.7	670.8	671.1
EK-Dpg-V	43.8	698.5	698.2
EK-Nva-A	37.1	586.4	585.8
EK-Nva-V	37.9	614.7	614.4
EK-Aib-Y	27.6	650.7	650.4

- **Circular Dichroism Spectroscopy**

CD spectra were recorded on an Aviv 60DS circular dichroism spectrometer with Igor plotting software using a 1mm path-length quartz cell for samples. The CD spectra are averages of three scans, collected at 1.00 nm intervals from 250 to 190 nm, recorded at 20 °C. Samples were prepared by dilution of a stock solution of peptide sample (~1 mM) in phosphate buffer (10 mM, pH =7) to acquire the working solution of 100-500 μM peptide concentration. All spectra were corrected by subtraction of the buffer background and are presented as molar ellipticity [θ] in units of (deg cm^2 $dmol^{-1}$).

- **Infrared Absorption and Vibrational CD**

IR spectra were obtained on an FTS-60A (Digilab/Varian Randolf, MA) FTIR for peptides that were lyophilized from 10% DCl (to remove TFA) and redissolved in D_2O based 0.01 M phosphate buffer. Samples were placed in a demountable cell (homemade) with CaF_2 windows separated by a 50 or 100 μm spacer. A pathlength(spacer) of 100 μm was used. Temperature was controlled by flow from a software controlled bath (Neslab RTE 11).

VCD spectra were obtained on a dispersive instrument, whose design and operation are detailed in the literature,[48] using the same samples and cells. VCD spectra of these peptides were very weak, are the average of 8 scans with a 10 sec time constant and needed optimized correction for baseline (obtained from identical scans of just buffer in a similar cell) to reveal the amide I pattern.

- **NMR Spectroscopy**

NMR data for EK-Dpg-Y was acquired from 13.6 mM EK-Dpg-Y in 30 mM potassium phosphate buffer (H_2O: D_2O 9:1) with 0.05 mM DSS as internal NMR chemical shift reference standard. All experiments were performed at 278 K on a Bruker DPX operating at 400 MHz. The COSY, TOCSY, and ROESY experiments were acquired with spectral widths of 4800*4800 Hz and 2048*512 complex acquisition points in the direct and indirect dimensions respectively. All spectra were zero filled once in the t1 dimension and weighted by a square cosine bell function. Several TOCSY spectra were recorded with 16 transients per increment and mixing times of 18, 36, 72 and 144 ms.[49] The ROESY experiment was recorded with 56 scans per increment and a mixing time of 400 ms.

Two dimensional HSQC, HSQC-TOCSY and HMBC spectra were collected on a Varian INOVA with a proton Larmor frequency of 500 MHz. Water suppression for the HSQC and HSQC-TOCSY was accomplished through 'WET'.[50] Spectral widths are 8000Hz*21400Hz for proton and carbon dimension, respectively and were acquired with 2400*512 complex points, with 64 scans per increment. Also, an 80ms spin lock was used for the HSQC-TOCSY. Gaussian line broadening was used for each of these spectra as well as having used linear prediction in t1 for the HSQC-TOCSY. The HMBC, were recorded with spectral widths of 6500*30200 Hz for proton and carbon dimensions, respectively along with 2048*1024 complex points and 48 scans per increment. Linear prediction was performed once in the carbon dimension while a Gaussian window function was used for line broadening. Long range coupling constants 10 Hz and 6 Hz are used, respectively. Long range coupling constants are important parameters for HMBC. If they are set incorrectly, the long range coupling cross peaks may disappear. The difficult part here is that the long range coupling constants are not fixed but variable in a range. Therefore we choose 2 constants to get needed information, which is not available from using just one constant value.

The temperature coefficients of the amide protons were measured by collecting a series of 1D spectra on a Bruker DPX operating at 400 MHz. The spectra were recorded at six different temperatures ranging from 5 °C to 30 °C in 5 deg increments. All spectra were processed using XWINNMR 2.6 on a Silicon Graphics computer.

- **Structure Calculations**[a]

The ROESY experiments yielded a total of 59 interproton distance restraints which were classified into upper bounds of 3.5, 4.5 and 6.0 Å depending on cross peak

volumes and are calibrated from fixed atomic distances within the molecule. A lower bound of 1.8 Å was used in all cases as well. Additionally, a single φ restraint was determined from the HNHA data based on the criteria (φ = -120 ± 45° if $^{3}J_{HNH\alpha}$ >7.5 Hz; φ = -50 ± 45° if $^{3}J_{HNH\alpha}$ <6.0 Hz).

For incorporation of Dpg into simulated annealing procedure employed for NMR structure determination, a new monomer needed to be created. The extended conformation of a Dpg containing peptide crystal structure (CSD refcode: WOZZIL) was used as a starting point. This extended structure was used to obtain RESP charges by using Gaussian 03 and RESP program in AMBER 8 package.

An extended model of EK-Dpg-Y was built within the LEAP module of AMBER. Partial charges for the Dpg residue were obtained by employing a restrained electrostatic potential (RESP), which is consistent with the Amber force field (ff99sb).[51,52] All subsequent molecular dynamics (MD) calculations were performed using a generalized Born continuous solvation model.[53]

A total of 500 starting structures were generated in AMBER 8, by running unrestrained MD for 3ps, during which the temperature is ramped to 300 K and then back down to 20 K. Next the structures were subjected to a round of restrained simulated annealing for 20 ps, during which the temperature was ramped to 1000 K (8 ps) and then cooled to 0 K (12 ps). The experimentally derived restraints were ramped from 20% to full value during the first 12 ps and held at full value until the end of the run. During the calculations, the NOE distance, ^{3}J dihedral and the ω constraints were applied with force constants of 20 kcal mol^{-1} Å^{-1}, 500 kcal mol^{-1} rad^{-2}, 1000 kcal mol^{-1} rad^{-2}, respectively. Bond angle and chirality restraints were also applied at a constant value of 1000 kcal mol^{-}

[1] rad [-2] throughout the simulation. The simulated annealing protocol was repeated twice more for a total production run of 60 ps. The 10 unique structures with the lowest AMBER and restraint violation energies were then selected for further analysis. The program Suppose was used to overlay the structures which were found to be well ordered (r.m.s. deviation of 0.29 Å for backbone heavy atoms). The graphics were generated with the program MOLMOL.[54]

[a] Structure calculations were performed by Dr. Dan McElheny at UIC.

Table 2.14 Structure determination statistics

NMR restraints	
Distance restraints	41
Intraresidue	18
Sequential ($\|i-j\|=1$)	14
Medium range ($1<\|i-j\|\leq 4$)	9
Long range ($\|i-j\|>4$)	0
Ambiguous	0
Torsion angle restraints	
φ[a]	1
Structure statistics (10 structures)	
Energies	
Mean AMBER energy	-177±16 kcal mol^{-1}
Mean restraint violation energy	7±1 kcal mol^{-1}
R.m.s deviations from ideal covalent geometry	
Bond lengths[b]	0.012 Å
Bond angles[b]	1.78°
Ramchandran statistics[c]	
Most favored	86.7
Allowed	13.3
Disallowed	0.0
Atomic r.m.s deviations (Å)$^{-1}$	
Backbone atoms	0.11
All heavy atoms	0.56

[a]Determined from ^{3}J measurements. [b]Torsional and distance restraint violations. [c]As evaluated using the program PROCHECK[55]

2.5 References

1. Lacroix, E.; Kortemme, T.; Lopez de la Paz, M.; Serrano, L., The design of linear peptides that fold as monomeric β-sheet structures. *Curr. Opin. Struct. Biol.* **1999,** 9, 487-493.

2. Gellman, S. H., Minimal model systems for β-sheet secondary structure in proteins. *Current opinion in chemical biology* **1998,** 2, 717-725.

3. Carulla, N.; Woodward, C.; Barany, G., BetaCore, a designed water soluble four-stranded antiparallel β-sheet protein. *Protein Science* **2002,** 11, 1539-1551.

4. Gibbs, A. C.; Bjorndahl, T. C.; Hodges, R. S.; Wishart, D. S., Probing the Structural Determinants of Type II' β-Turn Formation in Peptides and Proteins. *J. Am. Chem. Soc.* **2002,** 124, 1203-1213.

5. Lai, J. R.; Huck, B. R.; Weisblum, B.; Gellman, S. H., Design of Non-Cysteine Containing Antimicrobial β-Hairpins: Structure-Activity Relationship Studies with Linear Protegrin-1 Analogues. *Biochemistry* **2002,** 41, 12835-12842.

6. Sia, S. K.; Carr, P. A.; Cochran, A. G.; Malashkevich, V. N.; Kim, P. S., Short constrained peptides that inhibit HIV-1 entry. *Proc. Natl. Acad. Sci. U. S. A.* **2002,** 99, 14664-14669.

7. Toniolo, C.; Crisma, M.; Formaggio, F.; Peggion, C., Control of peptide conformation by the Thorpe-Ingold effect (C^{α}-tetrasubstitution). *Biopolymers* **2001,** 60, 396-419.

8. Prasad, B. V. V.; Balaram, P., The stereochemistry of peptides containing α-aminoisobutyric acid. *Critical Reviews in Biochemistry* **1984,** 16, 307-348.

9. Karle, I. L.; Balaram, P., Structural Characteristics of α-Helical Peptide Molecules Containing Aib Residues. *Biochemistry* **1990,** 29, 6747-6756.

10. Pandey, R. C.; Cook, J. C.; Rinehart, K. L., Structures of Peptide Antibiotics Emerimicins Iii and Iv. *J. Am. Chem. Soc.* **1977,** 99, 5205-5206.

11. Gilead, S.; Gazit, E., Inhibition of amyloid fibril formation by peptide analogues modified with α-aminoisobutyric acid. *Angewandte Chemie-International Edition* **2004,** 43, 4041-4044.

12. Benedetti, E.; Diblasio, B.; Pavone, V.; Pedone, C.; Bavoso, A.; Toniolo, C.; Bonora, G. M.; Leplawy, M. T.; Hardy, P. M., Preferred Structures of Constrained Peptides from Achiral α,α-Dialkylated Glycyl Residues with Acyclic Side-Chains. *J. Biosci.* **1985,** 8, 253-262.

13. Toniolo, C., Structural Versatility of Homo-Peptides from $C^{\alpha,\alpha}$-Dialkylated Glycines. *British Polymer Journal* **1986,** 18, 221-225.

14. Toniolo, C.; Benedetti, E., Old and New Structures from Studies of Synthetic Peptides Rich in $C^{\alpha,\alpha}$-Disubstituted Glycines. *Isi Atlas of Science-Biochemistry* **1988,** 1, 225-230.

15. Toniolo, C., Structure of Conformationally Constrained Peptides - from Model Compounds to Bioactive Peptides. *Biopolymers* **1989,** 28, 247-257.

16. Toniolo, C.; Benedetti, E., Structures of Polypeptides from α-Amino Acids Disubstituted at the α-Carbon. *Macromolecules* **1991,** 24, 4004-4009.

17. Kaul, R.; Banumathi, S.; Velmurugan, D.; Ravikumar, K.; Rao, R. B.; Balaram, P., Context-dependent conformation of diethylglycine residues in peptides. *Journal of Peptide Research* **2000,** 55, 271-278.

18. Kaul, R.; Banumathi, S.; Velmurugan, D.; Rao, R. B.; Balaram, P., Conformational choice at alpha,alpha-di-n-propylglycine residues: Helical or fully extended structures? *Biopolymers* **2000,** 54, 159-167.

19. Vijayalakshmi, S.; Rao, R. B.; Karle, I. L.; Balaram, P., Comparison of helix-stabilizing effects of α,α-dialkyl glycines with linear and cycloalkyl side chains. *Biopolymers* **2000,** 53, 84-98.

20. Prasad, S.; Rao, R. B.; Balaram, P., Contrasting Solution Conformations of Peptides Containing α,α-Dialkylated Residues with Linear and Cyclic Side-Chains. *Biopolymers* **1995,** 35, 11-20.

21. Karle, I. L.; Kaul, R.; Rao, R. B.; Raghothama, S.; Balaram, P., Stereochemical analysis of higher α,α-dialkylglycine containing peptides. Characterization of local helical conformations at dipropylglycine residues and observation of a novel hydrated multiple β-turn structure in crystals of a glycine rich peptide. *J. Am. Chem. Soc.* **1997,** 119, 12048-12054.

22. Karle, I. L.; Gurunath, R.; Prasad, S.; Kaul, R.; Rao, R. B.; Balaram, P., Peptide Design - Structural Evaluation of Potential Nonhelical Segments Attached to Helical Modules. *J. Am. Chem. Soc.* **1995,** 117, 9632-9637.

23. Karle, I. L.; Rao, R. B.; Prasad, S.; Kaul, R.; Balaram, P., Nonstandard Amino Acids in Conformational Design of Peptides - Helical Structures in Crystals of 5-10-Residue Peptides Containing Dipropylglycine and Dibutylglycine. *J. Am. Chem. Soc.* **1994,** 116, 10355-10361.

24. Crisma, M.; Valle, G.; Toniolo, C.; Prasad, S.; Rao, R. B.; Balaram, P., β-Turn Conformations in Crystal-Structures of Model Peptides Containing α,α-Di-n-Propylglycine and α,α-Di-n-Butylglycine. *Biopolymers* **1995,** 35, 1-9.

25. Diblasio, B.; Pavone, V.; Isernia, C.; Pedone, C.; Benedetti, E.; Toniolo, C.; Hardy, P. M.; Lingham, I. N., A Helical Dpg Homo-Peptide. *Journal of the Chemical Society-Perkin Transactions 2* **1992**, 523-526.

26. Karle, I. L.; Rao, R. B.; Kaul, R.; Prasad, S.; Balaram, P., Peptide design: Crystal structure of a helical peptide module attached to a potentially nonhelical amino terminal segment. *Biopolymers* **1996,** 39, 75-83.

27. Datta, S.; Kaul, R.; Rao, R. B.; Shamala, N.; Balaram, P., Stereochemistry of linking segments in the design of helix-helix motifs in peptides. Crystallographic comparison of a glycyl-dipropylglycyl-glycyl segment in a tripeptide and a 14-residue peptide. *Journal of the Chemical Society-Perkin Transactions 2* **1997**, 1659-1664.

28. Bonora, G. M.; Toniolo, C.; Diblasio, B.; Pavone, V.; Pedone, C.; Benedetti, E.; Lingham, I.; Hardy, P., Folded and Extended Structures of Homooligopeptides from α,α-Dialkylated α-Amino Acids - an Infrared Absorption and Hydrogen Nuclear Magnetic Resonance Study. *J. Am. Chem. Soc.* **1984,** 106, 8152-8156.

29. Dentino, A. R.; Raj, P. A.; Bhandary, K. K.; Wilson, M. E.; Levine, M. J., Role of Peptide Backbone Conformation on Biological-Activity of Chemotactic Peptides. *J. Biol. Chem.* **1991,** 266, 18460-18468.

30. Prasad, S.; Mitra, S.; Subramanian, E.; Velmurugan, D.; Rao, R. B.; Balaram, P., Coexistence of Folded and Extended Conformations of a Tripeptide Containing α,α-Di-n-Propylglycine in Crystals. *Biochem. Biophys. Res. Commun.* **1994,** 198, 424-430.

31. Benevides, J. M.; Wang, A. H. J.; Vandermarel, G. A.; Vanboom, J. H.; Thomas, G. J., Crystal and Solution Structures of the B-DNA Dodecamer D(CGCAAATTTGCG) Probed by Raman Spectroscopy - Heterogeneity in the Crystal Structure Does Not Persist in the Solution Structure. *Biochemistry* **1988,** 27, 931-938.

32. Dyson, H. J.; Rance, M.; Houghten, R. A.; Lerner, R. A.; Wright, P. E., Folding of Immunogenic Peptide-Fragments of Proteins in Water Solution .1. Sequence Requirements for the Formation of a Reverse Turn. *Journal of Molecular Biology* **1988,** 201, 161-200.

33. Formaggio, F.; Crisma, M.; Rossi, P.; Scrimin, P.; Kaptein, B.; Broxterman, Q. B.; Kamphuis, J.; Toniolo, C., The first water-soluble 3_{10}-helical peptides. *Chemistry-a European Journal* **2000,** 6, 4498-4504.

34. Toniolo, C.; Formaggio, F.; Tognon, S.; Broxterman, Q. B.; Kaptein, B.; Huang, R.; Setnicka, V.; Keiderling, T. A.; McColl, I. H.; Hecht, L.; Barron, L. D., The complete

chirospectroscopic signature of the peptide 3_{10}-helix in aqueous solution. *Biopolymers* **2004,** 75, 32-45.

35. Story, S. C.; Aldrich, J. V., Side-Product Formation During Cyclization with HBTU on a Solid Support. *International Journal of Peptide and Protein Research* **1994,** 43, 292-296.

36. Rodger, A.; Norden, B., *Circular Dichroism and Linear Dichroism*. 1997.

37. Shoemaker, K. R.; Kim, P. S.; York, E. J.; Stewart, J. M.; Baldwin, R. L., Tests of the Helix Dipole Model for Stabilization of α-Helices. *Nature* **1987,** 326, 563-567.

38. Fairman, R.; Shoemaker, K. R.; York, E. J.; Stewart, J. M.; Baldwin, R. L., Further Studies of the Helix Dipole Model Effects of a Free α-NH^{3+} or α-COO^- Group on Helix Stability. *Proteins-Structure Function and Genetics* **1989,** 5, 1-7.

39. Krittanai, C.; Johnson, W. C., Correcting the circular dichroism spectra of peptides for contributions of absorbing side chains. *Anal. Biochem.* **1997,** 253, 57-64.

40. Wishart, D. S.; Sykes, B. D.; Richards, F. M., Relationship between Nuclear Magnetic Resonance Chemical Shift and Protein Secondary Structure. *Journal of Molecular Biology* **1991,** 222, 311-333.

41. Wishart, D. S.; Bigam, C. G.; Holm, A.; Hodges, R. S.; Sykes, B. D., H^1, C^{13} and N^{15} Random Coil NMR Chemical Shifts of the Common Amino-Acids .1. Investigations of Nearest-Neighbor Effects. *Journal of Biomolecular NMR* **1995,** 5, 67-81.

42. Kopple, K. D.; Ohnishi, M.; Go, A., Conformations of Cyclic Peptides .3. Cyclopentaglycyltyrosyl and Related Compounds. *J. Am. Chem. Soc.* **1969,** 91, 4264-4272.

43. Rose, G. D.; Gierasch, L. M.; Smith, J. A., Turns in Peptides and Proteins. *Adv. Protein Chem.* **1985,** 37, 1-109.

44. Wuthrich, K., *NMR of Proteins and Nucleic Acids*. 1986; p 304.

45. Benedetti, E.; Toniolo, C.; Hardy, P.; Barone, V.; Bavoso, A.; Diblasio, B.; Grimaldi, P.; Lelj, F.; Pavone, V.; Pedone, C.; Bonora, G. M.; Lingham, I., Folded and Extended Structures of Homooligopeptides from α,α-Dialkylated Glycines - a Conformational Energy Computation and X-Ray-Diffraction Study. *J. Am. Chem. Soc.* **1984,** 106, 8146-8152.

46. Barone, V.; Lelj, F.; Bavoso, A.; Diblasio, B.; Grimaldi, P.; Pavone, V.; Pedone, C., Conformational Behavior of α,α-Dialkylated Peptides. *Biopolymers* **1985,** 24, 1759-1767.

47. Cirilli, M.; Coiro, V. M.; Di Nola, A.; Mazza, F., Relationship between conformation and geometry as evidenced by molecular dynamics simulation of $C^{\alpha,\alpha}$-dialkylated glycines. *Biopolymers* **1998,** 46, 239-244.

48. Keiderling, T. A.; Kubelka, J.; Hilario, J., Vibrational circular dichroism of biopolymers: summary of methods and applications. *Vibrational Spectroscopy of Biological and Polymeric Materials* **2006**, 253-324.

49. Bax, A.; Davis, D. G., Mlev-17-Based Two-Dimensional Homonuclear Magnetization Transfer Spectroscopy. *J. Magn. Reson.* **1985,** 65, 355-360.

50. Smallcombe, S. H.; Patt, S. L.; Keifer, P. A., WET solvent suppression and its applications to LC NMR and high-resolution NMR spectroscopy. *Journal of Magnetic Resonance Series A* **1995,** 117, 295-303.

51. Hornak, V.; Abel, R.; Okur, A.; Strockbine, B.; Roitberg, A.; Simmerling, C., Comparison of multiple amber force fields and development of improved protein backbone parameters. *Proteins-Structure Function and Bioinformatics* **2006,** 65, 712-725.

52. Wang, J. M.; Cieplak, P.; Kollman, P. A., How well does a restrained electrostatic potential (RESP) model perform in calculating conformational energies of organic and biological molecules? *J. Comput. Chem.* **2000,** 21, 1049-1074.

53. Tsui, V.; Case, D. A., Molecular dynamics simulations of nucleic acids with a generalized born solvation model. *J. Am. Chem. Soc.* **2000,** 122, 2489-2498.

54. Koradi, R.; Billeter, M.; Wuthrich, K., MOLMOL: A program for display and analysis of macromolecular structures. *Journal of Molecular Graphics* **1996,** 14, 51-55.

55. Laskowski, R. A.; Rullmann, J. A. C.; MacArthur, M. W.; Kaptein, R.; Thornton, J. M., AQUA and PROCHECK-NMR: Programs for checking the quality of protein structures solved by NMR. *Journal of Biomolecular NMR* **1996,** 8, 477-486.

CHAPTER 3

SYNTHESIS AND EVALUATION OF α,α-DISUBSTITUTED AMINO ACIDS AS β-SHEET STABILIZING FACTORS

3.1 Introduction

A number of diseases arise by protein misfolding from a native structure to a predominantly β-sheet conformation. These protein conformational diseases include Alzheimer's disease (AD), type II diabetes, Parkinson's disease and prion disorders. In all these diseases the misfolded protein self-aggregates to amyloid fibrils and deposits as amyloid plaques in organs promoting tissue damage and organ dysfunction.[1-5] An increased understanding of what factors control or stabilize β-sheet structures may lead to valuable insights into the underlying causes of these diseases and suggest possible treatments for such protein misfolding disorders.[6-8]

Following protocols previously developed in the Hammer laboratory, α,α-diisobutylglycine (Dibg) was synthesized via palladium catalyzed allylic alkylation of ethyl α-nitroacetate with 2-methylallyl acetate and incorporated into various positions of a model β-hairpin peptide GHP, in order to determine the effectiveness of the tetrasubstituted amino acids as design elements in both the strand and turn portions of β-hairpins. β-Hairpins contain two-stranded antiparallel β-sheets connected by a two residue loop. β-Hairpins represent minimum increments of a β-sheet and therefore provide an excellent model system for evaluating the fundamental aspects of β-sheet formation and stabilization in isolated, well-defined molecular systems. Two novel peptides Leu^3-NG and $Dibg^3$-NG were also synthesized to investigate their ability to stabilize the β-hairpin peptides.

As part of our effort for understanding of the role of ααAAs on β-sheet propensity and adding to our ability to make peptide analogues of predictable structure, novel chiral ααAAs with bulky hydrophobic side chains, suitably protected for peptide synthesis, were synthesized via the catalytic approach. The synthesis of most chiral amino acids involve the use of chiral templates.[9, 10] This methodology requires the use of stoichiometric quantities of chiral template, which can cause difficulties in the preparation of highly functionalized ααAAs, due to incompatibility of conditions for template removal with existing side-chain protecting groups. Furthermore, preparative scale reactions to yield gram amounts of material for peptide synthesis are often expensive with template approaches. In contrast to utilizing chiral templates, the phase-transfer catalyst approach offers advantages, such as mild conditions, minimization of protection and deprotection chemistries, and the ability to scale up reactions.[11] Herein several chiral ααAAs were synthesized via the enantioselective phase-transfer catalytic alkylation of a Schiff base substrate in the presence of (*S,S*) –binaphthyl quaternary ammonium salt to streamline the synthesis of highly functionalized ααAAs.[12]

3.2 Results and Discussion

3.2.1 Molecular Modeling of Dibg-Containing Peptide

We modeled the peptide Ac-Val-Dibg-Ala-NHMe by first setting the peptide to a representative β-sheet conformation with $\phi = -125, \psi = 125$, locking these angles for the Val (ϕ_1,ψ_1) and Ala (ϕ_3,ψ_3) residues. Then the peptide was subjected to 200 cycles of simulated annealing. The low energy structure for each cycle of annealing was recorded. The structures within 6 kcal of the lowest energy structure (43 structures) are shown plotted as ϕ_2 vs. ψ_2 about the central Dibg residue (Figure 3.1). Not surprisingly

most of the lowest energy structures for this tripeptide (blue circles) fell in two domains, the fully extended conformation, ϕ, ψ = 180° and the gauche regime where ϕ_2, ψ_2 = ±30-60°. There were also several low energy conformations where one backbone dihedral angle was extended and the other one gauche; though these structures tended to be higher energy structures (yellow triangles, 4-6 kcal above the lowest energy structure).

Interestingly, when the same peptide was set into a right-handed helical conformation ($\phi_{1/3}$ = -57°, $\psi_{1/3}$ = -47) and subjected to simulated annealing, the resulting structures were all much higher in energy (>5 kcal) than the sheet-like conformations shown here.

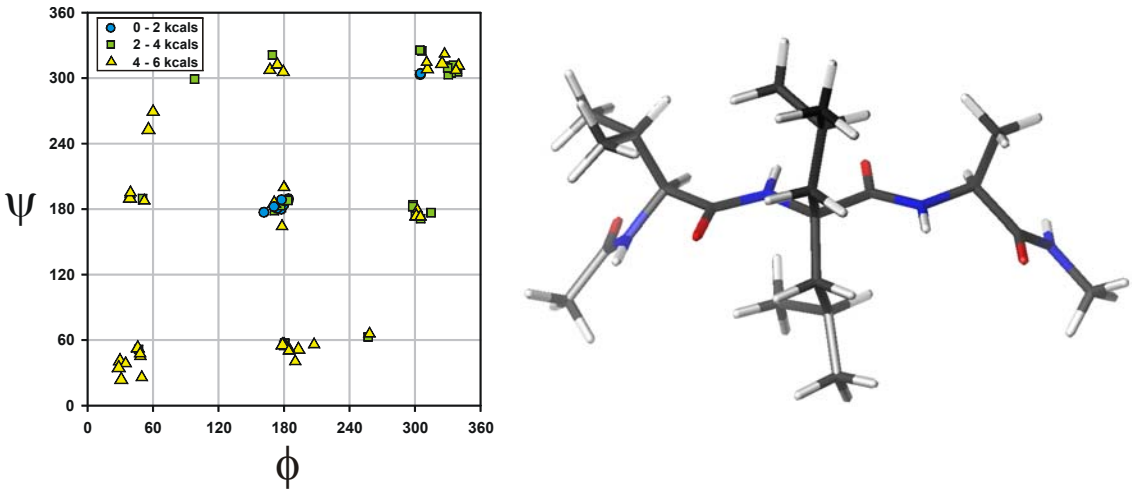

Figure 3.1 *Left:* Lowest energy conformations of Ac-Val-Dibg-Ala-NHMe plotted as ϕ_2 versus ψ_2. *Right:* stick representation of tripeptide in fully extended conformation

A representative space-filling model of one the ϕ_2, ψ_2 = 180° structures is shown in the bottom of Figure 3.2. This is compared to the minimized starting structure with all backbone angles locked in a proteinogenic β-sheet conformation at the top of Figure 3.3. Note how the isobutyl chains of the minimized structure wrap around the backbone and also force the isopropyl group of the N-terminal Val to rotate to accommodate the "lower" isobutyl group of the Dibg residue. The lower alkyl group should lead to

additional hydrophobic interactions or electrostatic interactions if it was a charged group in sheet structures, which are not normally present in proteinogenic sequences. The "C5" H-bond of the Dibg residue is clearly seen in the lower structure. Additionally the backbone is somewhat kinked relative to the "flat" sheet represented above. These modeling results suggest that ααAAs with larger side-chain groups can be accommodated into β-sheet structures.

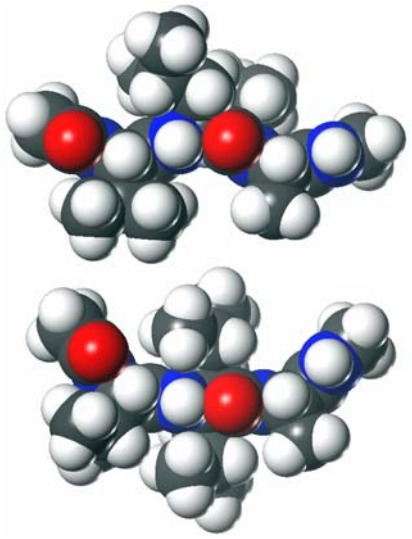

Figure 3.2 *Above*: Ac-Val-Dibg-Ala-NHMe in β-sheet conformation. *Below*: Same, in low energy conformation with ϕ_2, $\psi_2 = 180°$

3.2.2 Synthesis of α,α–Diisobutylglycine (Dibg)

α,α–Diisobutylglycine (Dibg) and α,α–dipropylglycine (Dpg) were traditionally synthesized from a ketone using the Bucherer-Bergs method via a hydantoin intermediate which then can be hydrolyzed to Dibg and Dpg.[13] This method was optimal for Dpg synthesis; however major flaws were associated with this approach in reference to Dibg due to the high resistance of formation and hydrolysis of hydantoin because of the two bulky isobutyl groups. The yields in hydantoin formation and hydrolysis for the Dibg

synthesis are only 12% and 11% respectively compared to those of 64% and 67% respectively in the Dpg synthesis as shown in Figure 3.3.

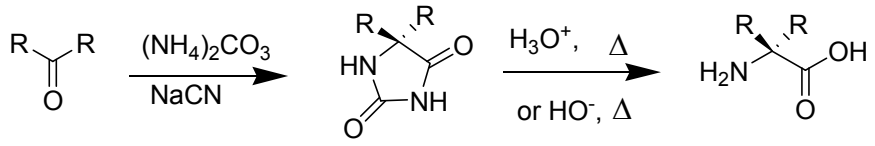

R = CH_2CH_3	64%	67%
R = $CH_2CH(CH_3)_2$	12%	11%

Figure 3.3 Synthesis of Dpg and Dibg via Bucherer-Bergs reaction

To overcome this problem, Dibg was synthesized via tetrakis-(triphenylphosphine)palladium(0)-catalyzed allylation of ethyl α-nitroacetate using 2-methylallyl acetate in excellent overall yield by following a method developed in Hammer's lab as illustrated in Figure 3.4.[14]

The first step in the synthesis is to form two new carbon-carbon bonds by palladium-catalyzed diallylation of ethyl α-nitroacetate in dry THF with 2-methylallyl acetate in the presence of 2 equiv of DIEA, and 0.1 equiv of $Pd(PPh_3)_4$. The highly acidic α-nitroacetate has been found to be a useful substrate for the formation of carbon-carbon bond in a variety of reactions in which the acidic proton was replaced by carbon-bond substituent. DIEA was used to remove two α-protons from nitroacetate to form α-nitroacetate anion, which acts as nucleophile to attack the palladium π-allyl complex of Pd (II) to give excellent yields of the diallylated α-nitroacetate. Previously, the palladium catalyst was removed using PS-PPh_3 resin. However, not all the palladium catalyst was scavenged using PS-PPh_3 resin and as a result, purification of the crude compound was problematic. A revised method was developed in order to overcome this problem. Crude oil was filtered through a flask fitted with a frit to capture all of the palladium catalyst.

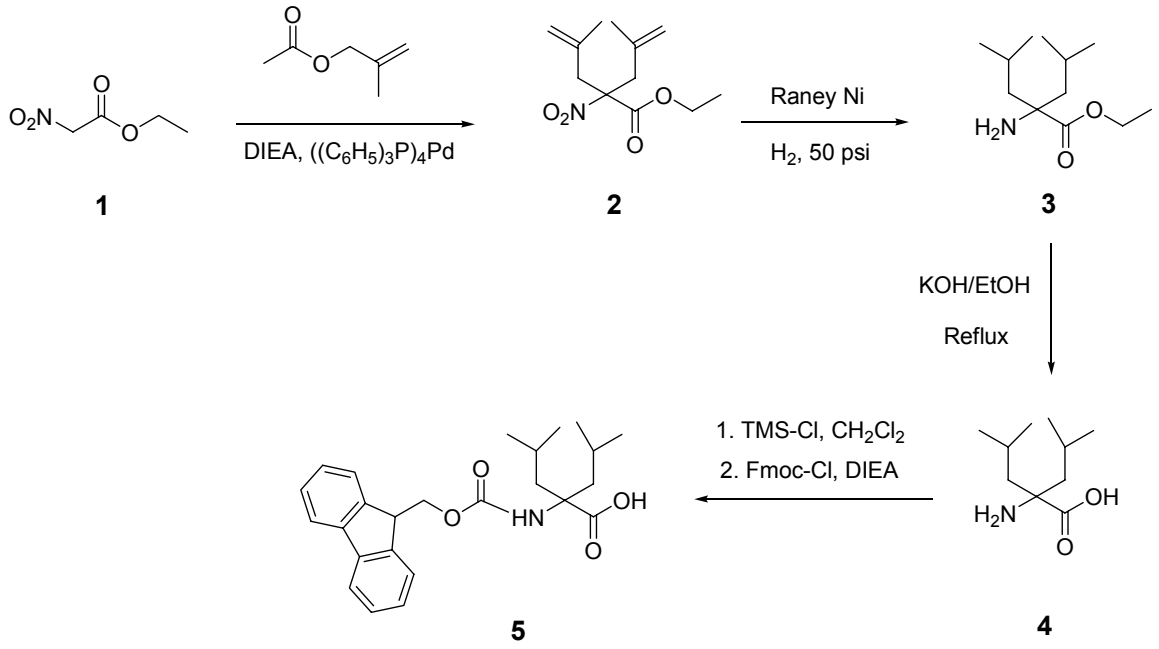

Figure 3.4 Synthesis of Dibg via $(Ph_3P)_4Pd$ catalyzed diallylation of ethyl nitroacetate

The next step involves the reduction of the nitro group and the side chain alkene to afford the amino ester in one step via hydrogenation over H_2 at 50 psi for 20 hrs with Raney nickel in 87% yield

The ester was hydrolyzed under strong basic conditionsb using 3M KOH. HCl was then added to the solution to precipitate the compound out as Dibg-HCl salt. The free Dibg was isolated in good yield by Dowex cation-exchange resin column with sulfonic acid functional group.

The free amino acid **4** was then N^{α} protected with an Fmoc group to allow for solid phase peptide synthesis. The N^{α}-protection of the amino group was carried out using an in *situ* silylation procedure affording Fmoc-Dibg in excellent 91% yield.[15] Two Equivalents of trimethylsilychloride (TMS-Cl) were added to form the intermediate O, N-bis-trimethylsilyl-Dibg. The TMS group was introduced in order to temporarily protect

the carboxyl group, which eliminated the oligomerization side reactions, such as the formations of di- or tripeptides as shown in Figure 3.5 below. TMS group can be readily removed by mild hydrolysis. The product **5** was verified by ^{1}H NMR and ^{13}C NMR and the purity of this compound was determined by elemental analysis.

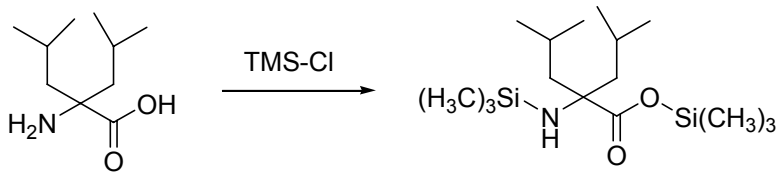

Figure 3.5 O, N-bis-trimethylsilyl-Dibg

3.2.3 Peptide Synthesis

Peptides listed in Table 3.1 were synthesized using Fmoc chemistry via solid-phase peptide synthesis on a peptide amide linker-polyethylene glycol-polystyrene (Fmoc-PAL-PEG-PS) resin as a solid support.

Table 3.1 Primary sequence of peptides

Peptide Name	Sequence
Dibg^{3}-GHP	H-Arg-Tyr-Dibg-Glu-Val-Pro-Gly-Orn-Lys-Ile-Leu-Gln-NH_2
Dibg^{6}-GHP	H-Arg-Tyr-Val-Glu-Val-Dibg-Gly-Orn-Lys-Ile-Leu-Gln-NH_2
Dibg^{3}-NG	CH_3CO-Arg-Thr-Dibg-Glu-Val-Asn-Gly-Lys-Lys-Ile-Thr-Gln-NH_2
Leu^{3}-NG	CH_3CO-Arg-Thr-Leu-Glu-Val-Asn-Gly-Lys-Lys-Ile-Thr-Gln-NH_2

All coupling reactions except the acylation of the N-terminus of Dibg and acylation of the N-terminus of peptide Dibg^{3}-NG peptide and peptide Leu^{3}-NG were carried out in DMF using PyAOP and DIEA as the coupling reagents. Fmoc removal was accomplished by a deblocking solution of 2% piperidine, 2% DBU in DMF. A double

coupling was performed for valine due to the difficult coupling of this amino acid to the peptide sequence because of its steric bulky side chain.

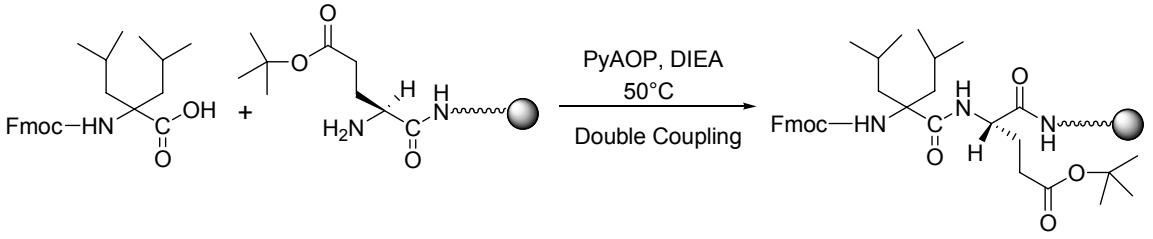

Figure 3.6 Coupling of Dibg to the peptide sequence in Dibg^3-GHP

The couplings before the Dibg residue were performed on the Applied Biosystem Pioneer Peptide synthesizer. The remaining amino acid residues were incorporated into the sequence manually. Coupling of Dibg to the resin-bound peptide was carried out using PyAOP as the activator in the presence of DIEA at 50°C on a shaker overnight due to the difficult coupling of the amino acid to the peptide sequence as shown in Figure 3.6. A double coupling was performed for Dibg coupling due to moderate coupling yields determined by UV analysis of Fmoc deprotection at 301 nm.[16]

Fmoc amino acid symmetrical anhydrides were found to be more efficient reagents for acylation N-terminus of highly hindered α,α-disubstituted amino acids, such as Dibg and Dbzg compared to the uronium salt HATU and phosphonium salt PyAOP.[17] Thus, amino acid symmetrical anhydrides were synthesized to acylate the N-terminus of Dibg. The symmetrical anhydride of Fmoc amino acids was prepared by treatment of 10 equivalents of the corresponding Fmoc amino acid with 5 equivalents of DCC in CH_2Cl_2 at room temperature for 2 hrs as shown in Figure 3.7. The resulting DCU precipitate was removed via filtration. Coupling of the symmetrical anhydride onto resin-bound peptide was carried out by adding preformed symmetrical anhydride to the resin-bound peptide in DCE-DMF (9:1) at 50 ˚C for 4 hrs while shaking. A double coupling procedure was

performed due to moderate coupling yields determined by UV analysis of Fmoc deprotection.

For the symmetrical anhydride coupling, the best coupling efficiency has been found to be an aprotic nonpolar solvent system of dichloroethane (DCE) and DMF (9:1). We propose that the enhanced reactivity of the symmetrical anhydride may result from the more effective amide bond formation via anchimeric assistance in aprotic nonpolar solvent. The formation of hydrogen bonding between the hydrogen of incoming amino acid and the oxygen of the symmetrical anhydride is more pronounced in the aprotic nonpolar solvent.

The crude Dibg[3]-GHP was 83% pure by HPLC analysis. The HPLC chromatogram and MALDI-MS spectrum for peptide Dibg[3]-GHP are shown in Figure 3.8 and Figure 3.9 respectively.

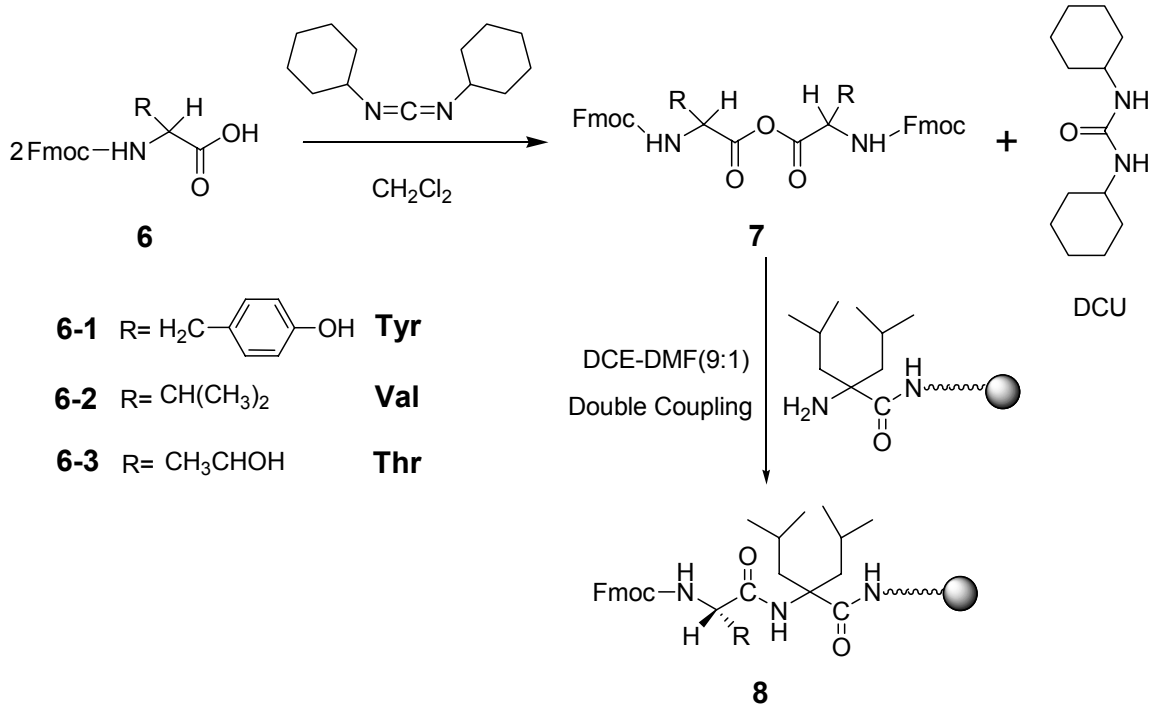

Figure 3.7 Acylation of N-terminus of Dibg via the Fmoc amino acid symmetrical anhydride

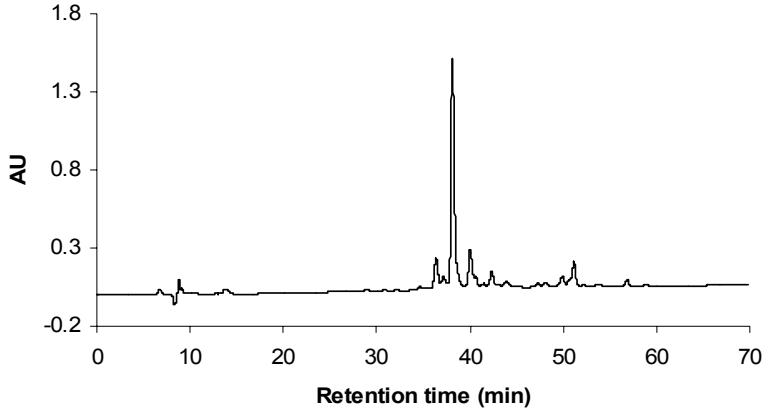

Figure 3.8 HPLC chromotogram of crude peptide Dibg[3]-GHP. Gradient: 90% A (H_2O, 0.1%TFA) and 10% B (CH_3CN, 0.1% TFA) to 30% A and 70% B over 60 mins at a flow rate 1mL/min.

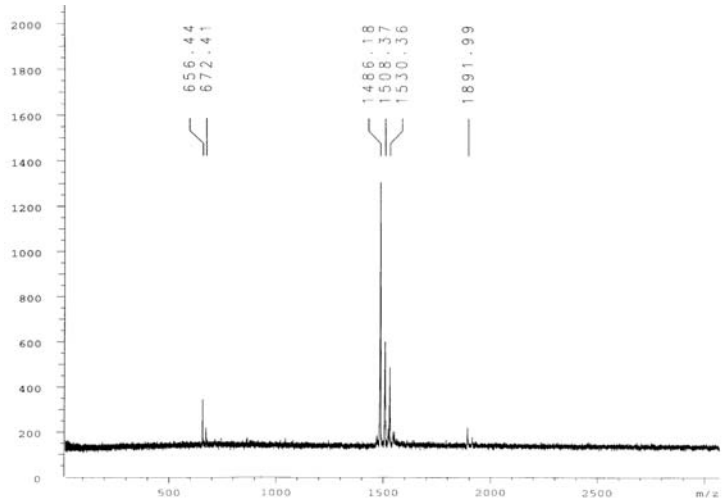

Figure 3.9 MALDI-MS spectrum of the main peak on HPLC. For MS of Dibg[3]-GHP, $[M+1]^+$ m/z calcd.1486.7 Obsd. 1486.2

3.2.4 Conformational Analysis of Peptides Containing Dibg

A well-defined peptide model is essential to elucidate peptide secondary structure propensities and systematically investigate the relationship between sequence, folded structure and stability of peptide conformations. Autonomously folding model systems for α-helix have been extensively studied and there are well-established principles for

designing synthetic peptides that adopt α-helical secondary structure. For example, α-helices display length-dependent stabilization; α-helices become more stable as the length of the helix grow longer. This length–dependent effect on conformational stability results from the balance between entropic cost of helix initiation and enthalpic benefit of helix propagation because helix initiation is thermodynamically unfavorable but helix propagation is favorable.[18] In contrast, model β-sheet peptides have only been developed until recently because of their tendency to aggregate and form discontinuous polypeptide segments. The first short peptide that folds into a monomeric β-hairpin in aqueous solution was reported by Blanco and coworkers in 1993.[19] This β-hairpin peptide has a sequence of YQNPDGSQA which was designed based on residues 15-23 (YQSWRYSQA) of a naturally occurring β-hairpin protein tendamistat. The four central residues in the tendamistat fragment were replaced by NPDG in order to maximize turn probability. More recently, several stable, non-aggregating, monomeric β-hairpins were synthesized and identified.[20-22] The general design strategies for these β-hairpin peptides are the incorporation of type I′ or type II′ β-turn and favorable long range side chain-side chain interactions to promote and stabilize anti-parallel β-hairpin formation.

β-Hairpins contain two-stranded antiparallel β-sheets linked by a β-turn and compose of the simplest model of β-sheet structures which therefore can provide fundamental insights into β-sheet stabilization. One particularly appealing β-hairpin model was developed by Gellman and co-workers; a 12-residue peptide, RYVEV^{D}PGOKILQ that adopts a β-hairpin conformation in aqueous solution with a two-residue loop, $_{D}$-Pro-Gly, which promotes formation of a “mirror image” β-turn (type

II' turn) as shown in Figure 3.10. This peptide is designated as GHP, the abbreviation of Gellman hairpin peptide.[23]

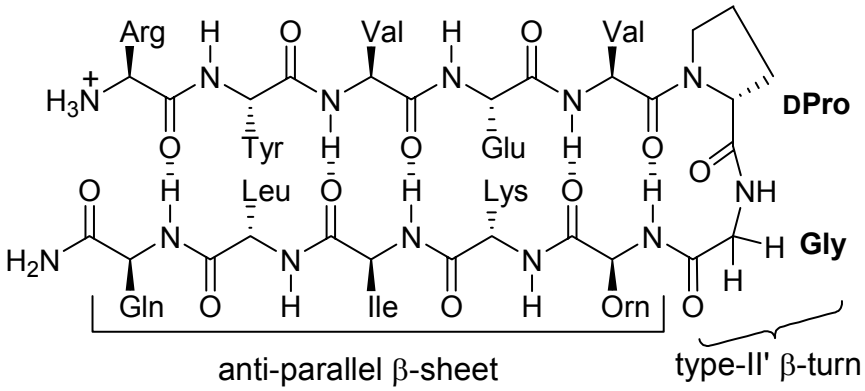

Figure 3.10 GHP: known to have a predominantly β-hairpin conformation in aqueous solution

GHP serves as an excellent model to study β-sheet structure as the β-hairpin conformation is highly populated and stable and exhibits low tendency to aggregate.[24] Because of these favorable properties of GHP, we have selected this model to probe the role of ααAAs as design elements in both the strand and turn portions of β-hairpin and study their effects on conformational stability. Incorporation of ααAAs into β-strand portion of β-hairpin structure is of interest for prevention of protein misfolding.

In the peptide Dibg[3]-GHP, Dibg was incorporated into position 3 of GHP in place of Val-3, while in the peptide Dpg[3]-GHP, Val-3 was replaced by Dpg (Figure 3.11).

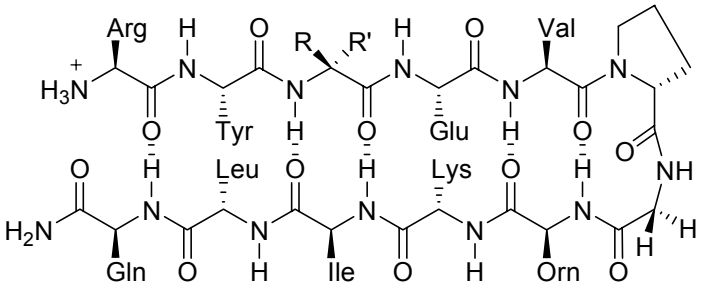

GHP R=*i*Pr R′=H Dibg[3]-GHP R,R′=*i*Bu Dpg[3]-GHP R,R′=Pr

Figure 3.11 Sequence of peptide GHP, Dibg[3]-GHP, and Dpg[3]-GHP

The conformational behavior of Dibg[3]-GHP and Dpg[3]-GHP was investigated by circular dichroism (CD) spectroscopy as shown in Figure 3.12. CD spectrum of Dibg[3]-GHP is characteristic of a β-sheet conformation with a maximum at 203 nm and a minimum at 217 nm. Dibg[3]-GHP possesses stronger intensities at both maximum (203 nm) and minimum points (217 nm) than GHP, suggesting that Dibg is readily accommodated into a β-hairpin structure. Peptide Dpg[3]-GHP, where Dpg was incorporated into position 3 replacing Val-3, gave a CD which was characterized by a stronger negative band at 190 nm and red-shifted band at 205 nm, suggesting that the Dpg residue reduced the amount of β-hairpin structure. This indicates that side chain branching of ααAA plays an important role in stabilization of the β-sheet portion of the hairpin.

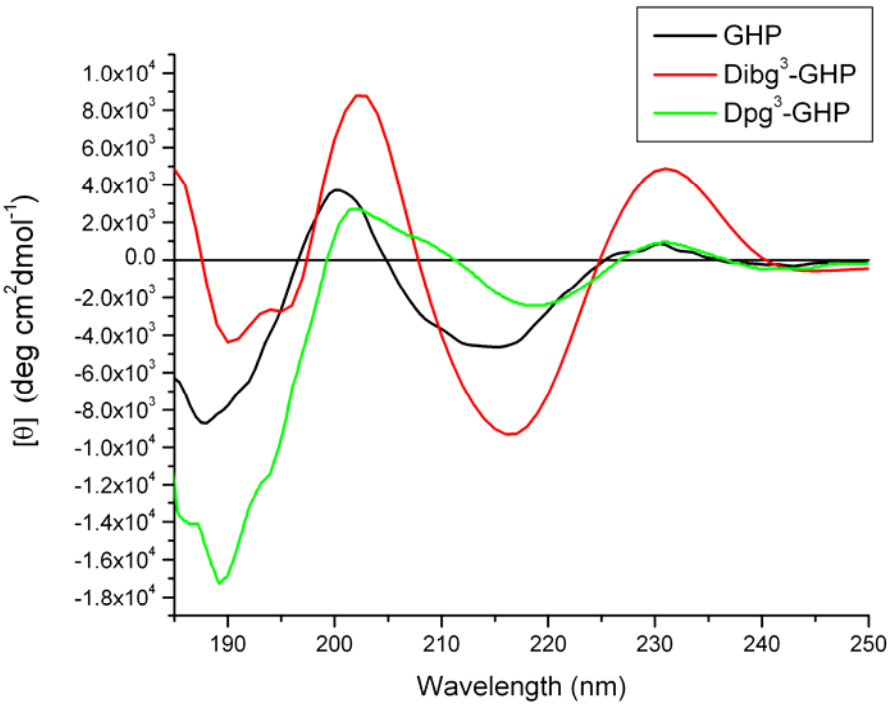

Figure 3.12 CD spectra of GHP, Dibg[3]-GHP and Dpg[3]-GHP in sodium acetate buffer. Condition: 100 μM peptide in 1 mM sodium acetate buffer, pH=3.8, 20˚C.[a]
[a] The CD of Dpg[3]-GHP were run by Marcus Etienne

α-Proton chemical shifts are found to be highly sensitive to conformational changes. α-Protons exhibit a downfield shift with respect to random coil conformations when in a β-sheet structure and an upfield shift when in helical and turn conformations.[25] Chemical shift deviations of α-protons from random coil values for the residues in the sheet portion of GHP, Dibg^3-GHP, and Dpg^3-GHP and the chemical shift difference between the two diastereotopic hydrogens of glycine are summarized in Figure 3.13. All α-protons for Dibg^3-GHP experience significant downfield shift (>0.10 ppm) relative to the random coil conformation with the exception of the terminal Arg-Gln pair, suggesting that Dibg^3-GHP is largely folded. The H_α of Leu-11 in Dibg^3-GHP displays a downfield shift, while this H_α in both GHP and Dpg^3-GHP display an upfield shift indicating that Dibg^3-GHP is more structured in comparison with GHP and Dpg^3-GHP. Wishart and coworkers have demonstrated that "chemical shift index" $\Delta\delta_{H\alpha} = \delta_{H\alpha(observed)} - \delta_{H\alpha(random\ coil)}$ (Equation 1) is an accurate technique to determine the types of secondary structures.[26] A group of adjacent residues containing three or more $\Delta\delta_{H\alpha} > 0.1$ are considered to be β-sheets. Wishart et al. also pointed out chemical shift indices of the residues at either N or C terminus are often opposite in magnitude to those of the corresponding secondary structure. This type of fraying at N- and C-termini is typically observed for the terminal residues in a β-hairpin, which is consistent with our observation for the terminal Arg-Gln pair. Both the pattern of the α-proton chemical shift deviations $\Delta\delta_{H\alpha}$ and the chemical shift index data for Dibg^3-GHP suggest that Dibg^3-GHP adopts a β-hairpin conformation and is largely folded in sodium acetate buffer at pH 3.8.

The separation of the diastereotopic α-proton resonances of glycine has been shown to correlate with the extent of folding in β-hairpins as illustrated in the following equation:[27, 28] Fraction folded(%)=$\delta Gly_{observed}$ /$\delta Gly_{fully\ folded}$; where fraction folded equals mole fraction of hairpin folded, $\delta Gly_{observed}$ is the chemical shift of the proton observed experimentally, and $\delta Gly_{fully\ folded}$ is the chemical shift of the proton in the fully folded state, which usually is the cyclic form of the peptide. The chemical shifts for diastereotopic α-protons of glycine are 3.75 ppm, 3.42 ppm respectively in GHP, 3.83 ppm, 4.03 ppm in Dpg^3-GHP and 3.70 ppm, 4.10 ppm in Dibg^3-GHP. The largest difference in chemical shift of the diastereotopic α-protons was observed in Dibg^3-GHP with 0.40 ppm and the least in Dpg^3-GHP with 0.20 ppm. The difference in GHP is 0.22 ppm indicating that Dibg^3-GHP is well folded and Dpg^3-GHP is less structured, which is in good agreement with the CD results.

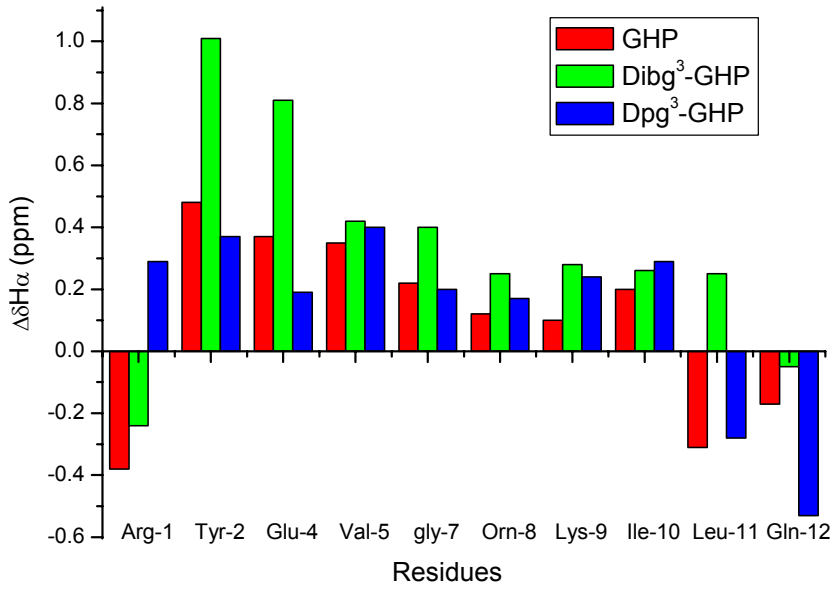

Figure 3.13 Chemical Shift Index ($\Delta\delta_{H\alpha}$) for GHP, Dibg^3-GHP, and Dpg^3-GHP at 3.5 mM in 100 mM aqueous sodium deuterioacetate buffer (H_2O: D_2O 9:1), pH 3.8 at 278 K. $\Delta\delta_{H\alpha}$ values were calculated using Equation 1 utilizing the random coil values of Dyson et al.[29] Gly values are the difference between the two diastereotopic hydrogens.

β-Sheet structures possess natural right-handed twist; Thornton et al. discovered that two-residue loops should adopt type I' or II' β-turn conformations in order to promote the formation of a β-hairpin because these β-turns match the natural right-handed twist of the β-sheet and promote sheet interactions between adjacent stands of the β-sheet.[30] Therefore design a stable β-turn with proper handedness is critical in order to generate stable β-sheet conformations. In GHP, the two-residue loop DPro-Gly promotes β-hairpin folding via a "mirror image" type II' turn in aqueous solution.

ααAAs were incorporated into the *i+1* position of the GHP loop in order to access the ability of ααAAs such as Dibg, Dpg, and Aib to stabilize the β-turn of β-hairpin peptides. In the peptide Dibg[6]-GHP, Dibg was incorporated into *i+1* position of the GHP loop in place of DPro, while in Dpg[6]-GHP and Aib[6]-GHP, DPro was replaced by Dpg and Aib respectively. The sequences of Dibg[6]-GHP, Dpg[6]-GHP, and Aib[6]-GHP are outlined in Figure 3.14.

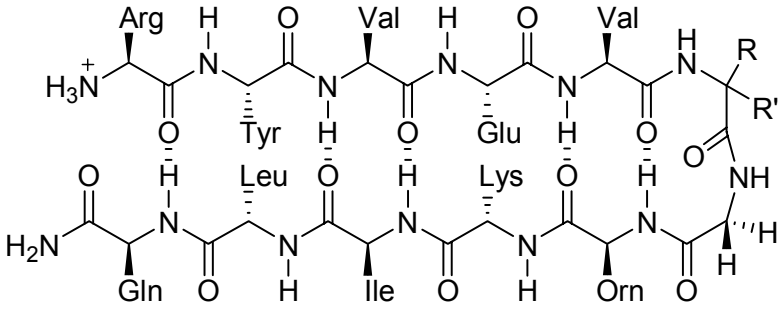

Dibg[6]-GHP R,R′=*i*Bu Dpg[6]-GHP R,R′=Pr Aib[6]-GHP R,R′=Me

Figure 3.14 Sequence of peptide Dibg[6]-GHP, Dpg[6]-GHP, and Aib[6]-GHP

The CD spectrum of Dibg[6]-GHP exhibits a maximum at 203 nm with an ellipticity at about -1000, while GHP displays a maximum at 201 nm with an ellipticity at about 4000. The significant decrease of the maximum of Dibg[6]-GHP with respect to the

GHP as shown in Figure 3.15, suggests that Dibg destabilizes the turn structure. It further proves the fact by our modeling studies that Dibg favors the extended structure, rather than the turn structures. Thus, we can conclude that Dibg disfavors type I' or II' β-turn conformation. CD spectrum of Dpg^6-GHP shows similar intensity at both maximum and minimum points as Dibg^6-GHP indicating that Dpg possesses the similar destabilizing effect on the β-turn as Dibg. CD spectrum of Aib^6-GHP exhibits similar CD band that almost overlays with GHP suggesting that they adopt similar structures. Masterson et al. have shown that Aib-Gly induces a type I' β-turn in GHP and shows equivalent folding as GHP based on CD and NMR analysis. The stabilizing effect of Aib on the type I' β-turn may be due to Aib is a strong promoter for turn or helical structures.

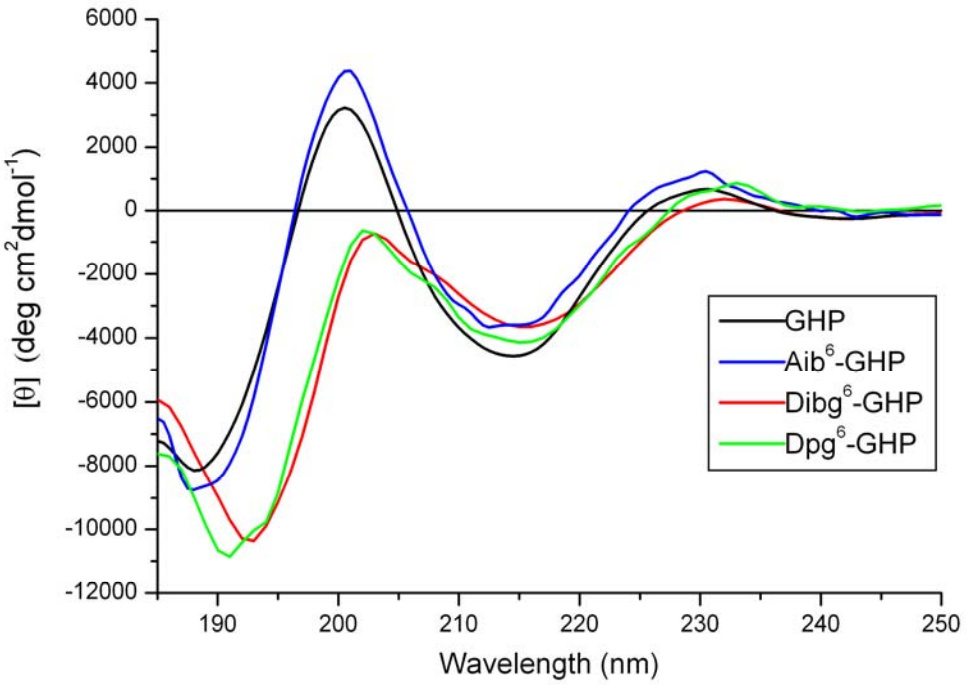

Figure 3.15 CD spectra of GHP, Aib^6-GHP, Dibg^6-GHP, and Dpg^6-GHP. Condition: 100μM peptide in 1mM sodium acetate buffer, pH=3.8, 20˚C.
[a] The CD of Aib^6-GHP and Dpg^6-GHP were run by Marcus Etienne.

The NMR analysis of GHP peptide revealed there are numerous NOEs between the side chains of Tyr-2 and Lys-9, Tyr-2 and Leu-11, indicating that interstrand side chain-side chain interactions resulting from those residues are critical in the stability of the β-hairpin. Waters and coworkers have found that aromatic interactions stemmed from the Phe-Phe cross-strand pair also contribute to the β-hairpin stability.[31] The peptide Leu[3]-NG was designed to probe whether non aromatic residue with high sheet propensity would exhibit the same stabilizing effects on an extended structure as the aromatic tyrosine. Russell et al. suggested that sheet propensities are more important than cross-strand interactions in the stability of the hairpin structure.[32] This peptide includes the proteinogenic LAsn-Gly two residue loop which has been shown to induce β-hairpin folding via a type I' turn in aqueous solution.(Figure 3.16) [19, 33-35] LAsn-Gly loop can avoid complications that arise in the determination of the peptide structure due to the tendency of the DPro-Gly bond to isomerize between the cis and trans conformations.

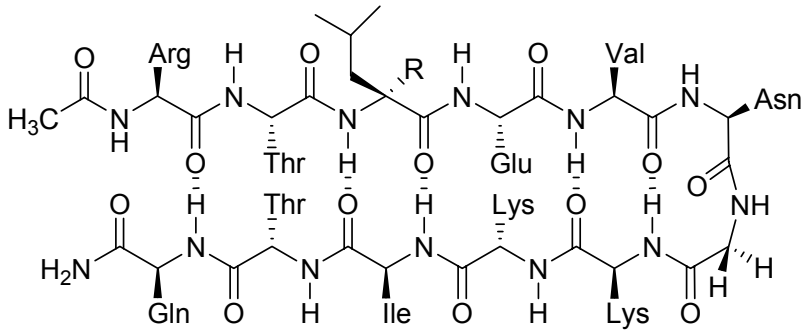

Leu[3]-NG R=H Dibg[3]-NG R= $CH_2CH(CH_3)_2$

Figure 3.16 Sequence of peptide Leu[3]-NG and Dibg[3]-NG

Tyr-2 and Leu-11 are replaced with two Thr respectively. Threonine possesses high sheet propensity allows us to probe the contribution of sheet propensities compared to interstrand side chain-side chain interaction and aromatic and aliphatic interaction. Thr

also has another favorable property in that it is not very hydrophobic, in contrast to other β-sheet promoting residues, such as valine and isoleucine.[36] Thus, it will not affect the solubility of this peptide in aqueous solution. Non-proteinogenic Orn-8 is replaced by Lys. Gellman et al. have shown that replacing Orn-8 by Lys has no effect on conformational stability of the β-hairpin.[24]

The CD spectrum of Leu^3-NG exhibits a minimum at 197 nm which is a signature band of random coil structure as shown in Figure 3.17**.** This suggests cross-strand interactions between Tyr-2 and Leu-11, between Tyr-2 and Lys-9 are essential for the stability of GHP. In Leu^3-NG, side chain of Thr might be too short to engage in a favorable diagonal inter-strand interaction with Lys compared to Tyr-2, thus cause the loss of conformational stability of the β-hairpin.

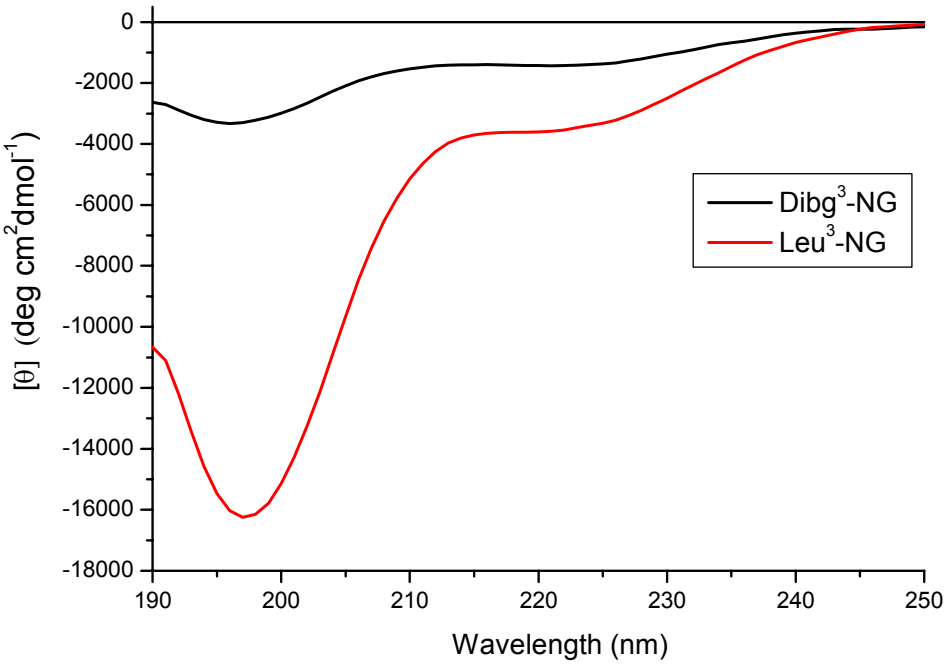

Figure 3.17 CD spectra of Dibg^3-NG and Leu^3-NG. Condition: 100 μM peptide in 1mM sodium acetate buffer, pH=3.8, 20˚C.

The contributions of Dibg to β-sheet stability have been examined with the peptide Dibg^3-NG. Dibg^3-NG contains Dibg at position 3 in place of Leu to probe structural effects of ααAA on the β-sheet formation. The CD spectrum of Dibg^3-NG shows a significantly diminishing of minimum at 197 compared to Leu^3-NG indicating Dibg is more structured than Leu^3-NG as illustrated in Figure 3.18. This suggests that the side chains of Dibg are able to impose backbone constraints to the peptide and make this peptide more structured compared to the non-constrained analogue.

3.2.5 Synthesis and Characterization of Novel Chiral α,α-Disubstituted Amino Acids

3.2.5.1 Enantioselective Synthesis of α,α-Disubstituted Amino Acids

First, Schiff base substrate **11** was prepared by a mild and efficient reaction of the corresponding amino ester hydrochloride salt **10** with 4-chlorobenzaldehyde **9** using Na_2CO_3 in H_2O & DCM as shown in Figure 3.18.[37] 4-Chlorobenzaldehyde is the limiting reagent; therefore it was not always detected by NMR. When excess 4-chlorobenzaldehyde determined by NMR, the excess 4-chlorobenzaldehyde was removed by washing with 30% sodium sulfite. The resulting carbon-nitrogen double bond in Schiff base has increased acidity of the α-proton, which allows the use of mild basic condition to remove the α-proton.

The enantioselective phase-transfer catalytic alkylation was performed by treatment of corresponding amino acid Schiff base **11** with 1.2 equivalents of alkyl halide along with chiral quaternary ammonium bromide salt (1 mol %)(Figure 3.19) in anhydrous toluene followed by addition of 5 equivalents of solid $CsOH{\cdot}H_2O$ at 0 °C. Reaction completion was verified via TLC and the resulting mixture was dissolved in water and extracted with DCM. Emulsion, caused by the fine solid particles of

$CsOH{\cdot}H_2O$ resulting in difficult in purifying compound **12**. Different solvent systems have been investigated, such as ether and water, ethyl acetate and water, and DCM and water. The least amount of emulsion occurred in the solvent system of DCM and water; therefore the extraction was carried out using DCM and water. After the extraction, the DCM layer was concentrated under reduced pressure.

In this reaction $CsOH{\cdot}H_2O$ was used to remove the α-proton to form the enolate ion pair intermediate with the chiral ammonium cation under the phase-transfer catalytic condition. The carbon-nitrogen double bond stabilized the carbanion of the enolate which was then reacted with alkyl halide to form a new carbon-carbon bond and generate a new stereogenic center. The reason for high enantioselectivity and absolute configuration is because the tight ion pair of chiral ammonium cation and the enolate only the *re*-face of the enolate is accessible for the alkylation reaction.[38]

The next step in the synthesis is to hydrolyze the imine under acidic condition using 0.5 M citric acid to provide the carboxyl protected chiral amino acid **13** in good yields with high to moderate enantiomeric excess as listed in Table 3.2.

The chiral amino acids were also synthesized via phase-transfer catalytic Michael addition. The Michael addition was performed under the same reaction conditions as the phase-transfer catalytic alkylation of amino acid Schiff base. The Michael addition only afforded the corresponding amino esters with 21% ee and 29% ee respectively as shown in Table 3.3 which are much lower enantiomeric excess compared to amino esters derived from the alkylation reaction as outlined in Table 3.2. The high reactivity of the *t*-butyl-3-bromopropionate possibly underwent a non-phase-transfer catalyst mediated

Michael reaction at the interface of the solid phase and solution phase phases, which may account for the substantial decrease in optical purity.

Three main steps have been proposed in the solid liquid phase-transfer alkylation process as illustrated in Figure 3.20:[39] 1) Deprotonation of α-proton of the Schiff base with $CsOH \cdot H_2O$ to form the enolate anion, which occurs at the interface between the solid-liquid layers; 2) Extraction of the enolate that formed as a result of the first step into the bulk organic phase by ion-exchange with the cation of the chiral quaternary ammonium salt to form a lipophilic ion-pair; 3) Creation of the new chiral center in the product by alkylation of the ion-pair at the re-face of the enolate with concomitant regeneration of the catalyst.

The corresponding racemic amino esters were synthesized via phase-transfer alkylation reaction in order to provide the references for enantiopurity analysis by ^{19}F-NMR. Alkylation of Schiff base with alkyl halide using 0.2 equivalent of tetra-n-butylammonium bromide (TBAB) as the phase-transfer catalyst, in the presence of nonnucleophilic base potassium carbonate in anhydrous acetonitrile (MeCN).[40] The reaction mixture was refluxed for 1hr. Cleavage of the imine with 0.5 M citric acid in tetrahydrofuran (THF) afforded the racemic amino ester in good yields as illustrate in Figure 3.21.

Fmoc-α-benzyl-leucine was synthesized from *tert*-butyl α-benzyl-leucinate to allow for solid phase peptide synthesis. First the t-butyl ester was removed by hydrolysis with HCl. The HCl salt was neutralized with DIEA to release the free amino acid. The free α-benzyl leucine was then N^{α}-protected using an in *situ* silylation procedure where Fmoc-Cl was added to the silylated ααAA in anhydrous DCM as shown in Figure 3.22.[15]

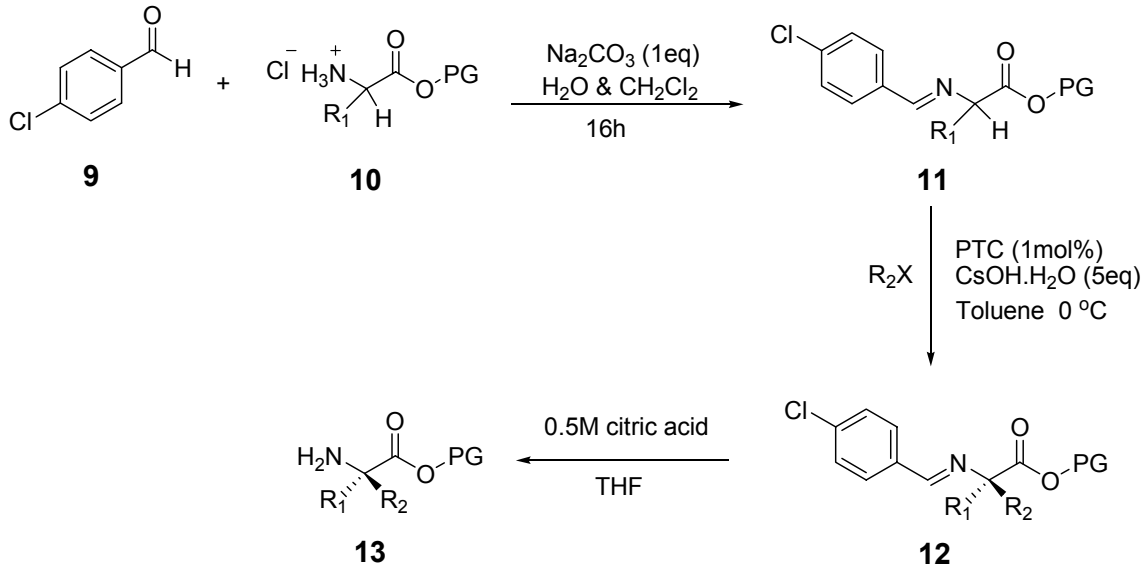

Entry	R_1	R_2	PG
13-1	$PhCH_2$		Bn
13-2	$PhCH_2$		Bn
13-3	*i*-Bu	$PhCH_2$	*t*-Bu
13-4	*i*-Bu		*t*-Bu
13-5	*i*-Bu		Bn

Figure 3.18 Synthesis of chiral amino acids via enantioselective catalytic phase-transfer alkylation

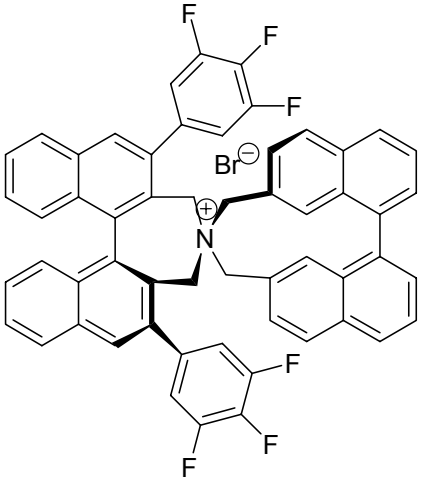

Figure 3.19 (*S,S*)-3,4,5-Trifluorophenyl-NAS bromide

Table 3.2 Alkylation of Schiff base to form chiral $C^{\alpha,\alpha}$-dialkylated amino ester

Entry	R_1	R_2X	PG	% Chemical yield	% ee[a]	Configuration
13-1	$PhCH_2$	allyl bromide	Bn	52	91	*S*
13-2	$PhCH_2$	1-bromopropane	Bn	60	89	*S*
13-3	*i*-Bu	benzyl bromide	*t*-Bu	66	78	*R*
13-4	*i*-Bu	allyl bromide	*t*-Bu	70	nd[b]	_
13-5	*i*-Bu	allyl bromide	Bn	68	nd	_

[a]Enantiopurities of entries 13-1, 13-2 and 13-3 were determined by ^{19}F-NMR analysis. The Enantiopurity of entry 13-3 was also analyzed by chiral HPLC. [b]nd=not determined

Table 3.3 Michael addition of Schiff base to form chiral amino ester[b]

entry	R_1	R_2	PG	%Chemical yield	% ee
13-6	$PhCH_2$	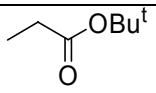	Bn	48	21
13-7	*i*-Bu	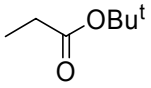	Bn	66	29

[b]Enantiopurity was determined by ^{19}F-NMR analysis of the corresponding amino esters.

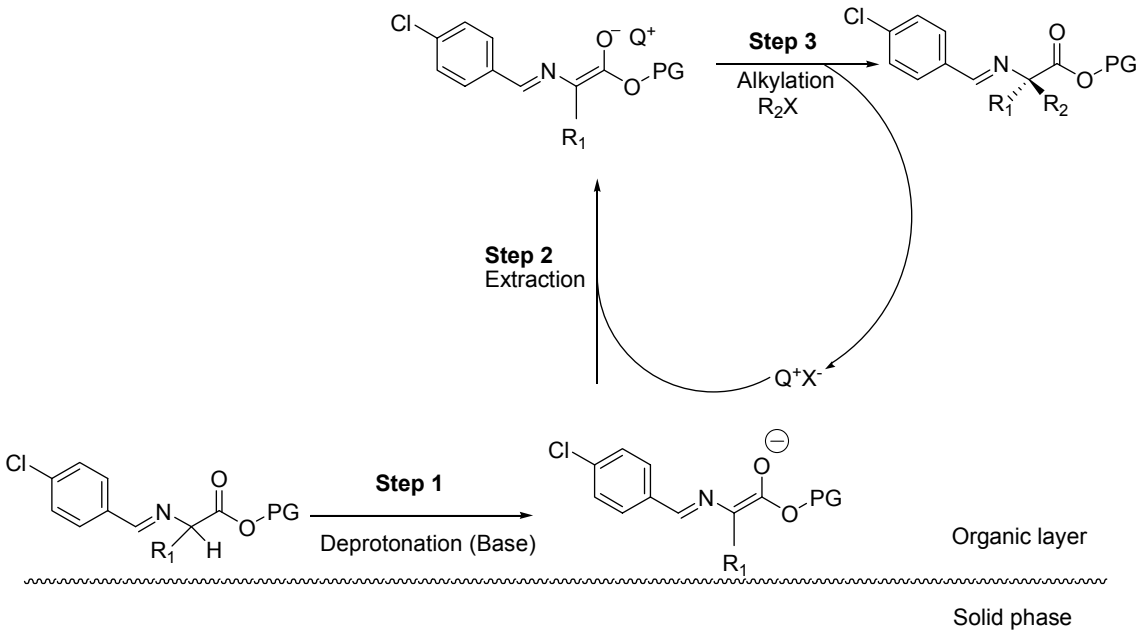

Figure 3.20 Mechanistic scheme for PTC alkylation

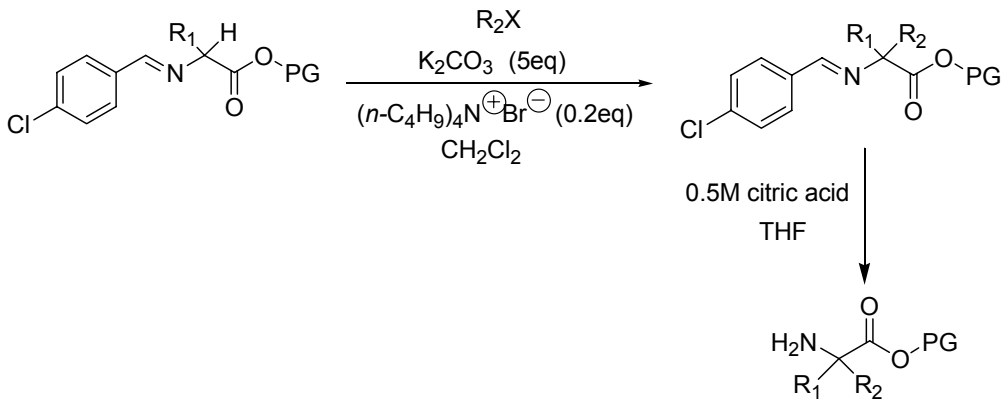

Figure 3.21 Synthesis of racemic amino esters via phase-transfer catalytic alkylation

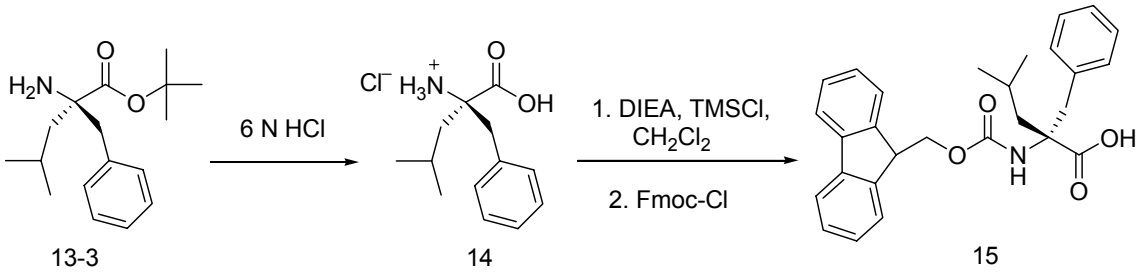

Figure 3.22 Preparation of Fmoc-α-benzyl-leucine

Crystal structures for *tert*-butyl α-benzyl-leucinate and Fmoc-α-benzyl-leucine are presented in Figure 23a and Figure 23b respectively. The crystals were obtained from DCM, ethyl acetate and hexanes respectively.

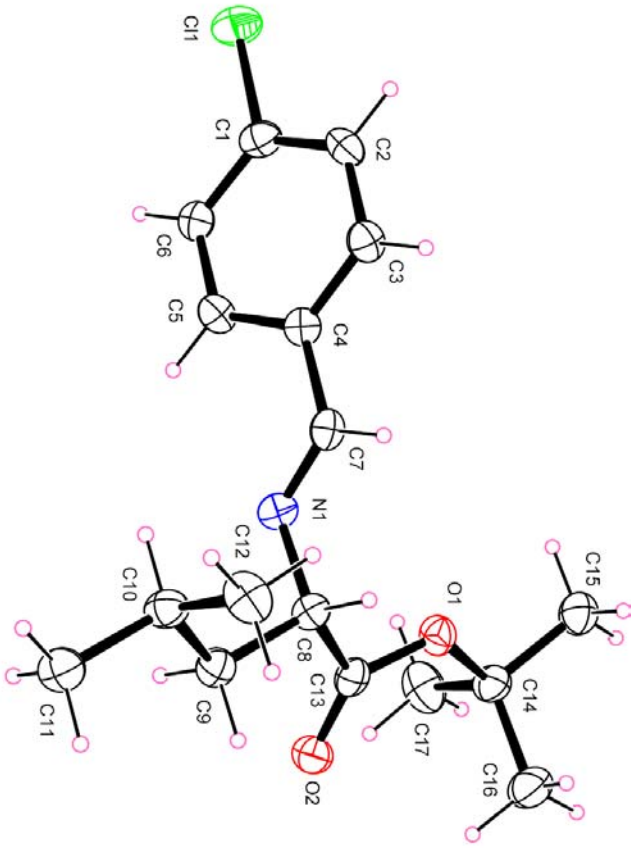

Figure 3.23a ORTEP diagram of *tert*-butyl leucinate *p*-chlorobenzaldehyde Schiff base

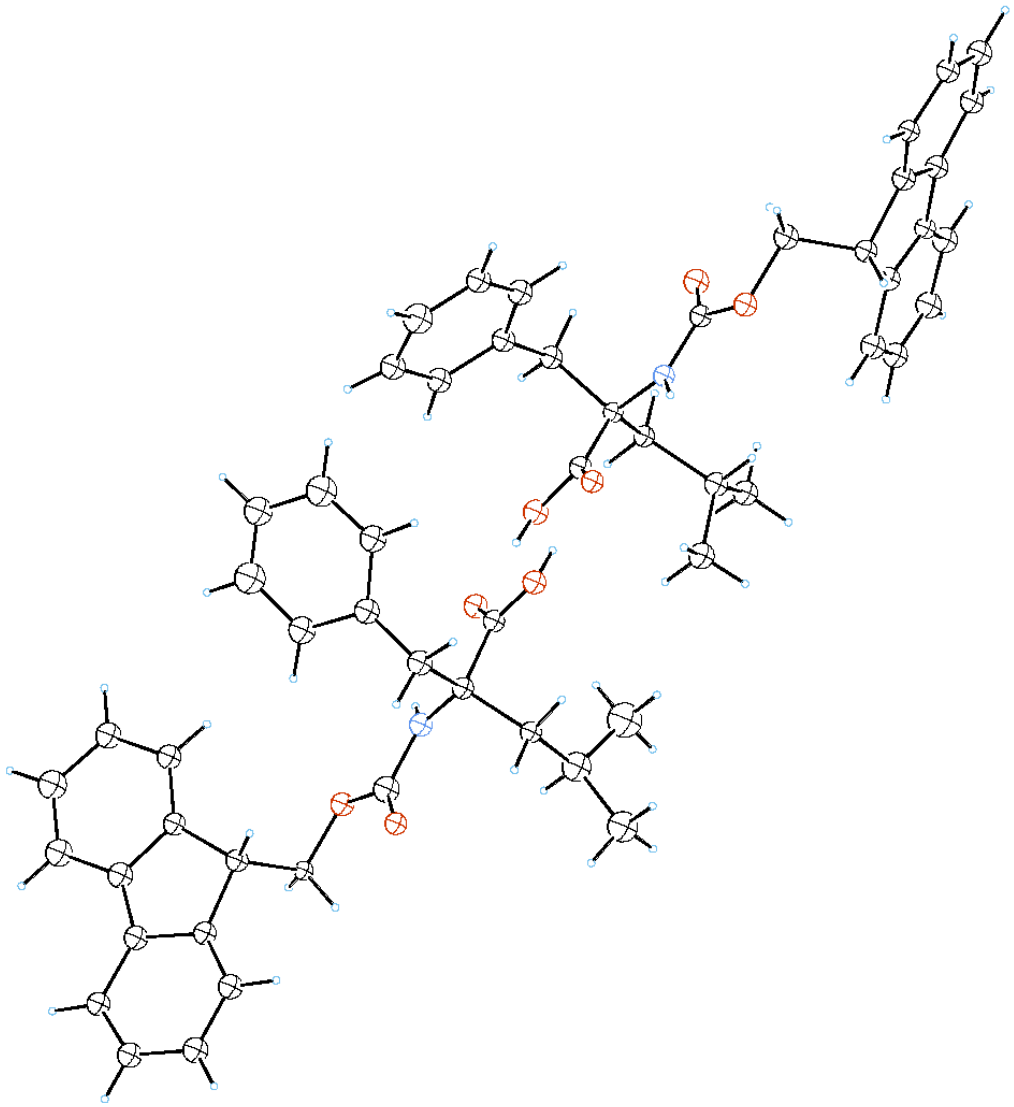

Figure 3.23b ORTEP diagram of Fmoc-α-benzyl-leucine dimer.

3.2.5.2 Enantiopurity Analysis of Chiral Amino Esters

The enantiopurities of amino esters in Table 3.2 and Table 3.3 were determined by quantitative ^{19}F-NMR analysis of the two diastereomeric Mosher amides, which have been prepared from an optically pure compound *R*-(-)-α-methoxy-α–trifluoromethylphenylacetyl chloride (MTPACl) with amino ester in the presence of DMAP in dry CH_2Cl_2 as shown in Figure 3.24.[41]

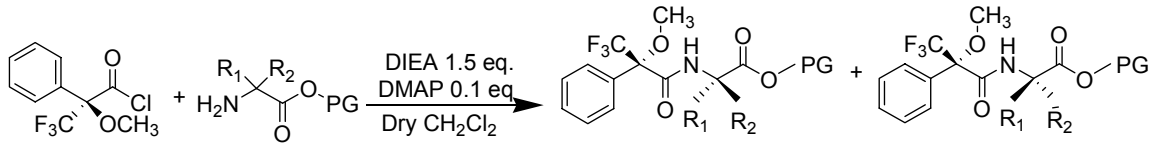

16

Entry	R_1	R_2
16-1	$PhCH_2$	
16-2	$PhCH_2$	
16-3	*i*-Bu	$PhCH_2$
16-4	$PhCH_2$	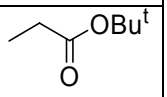
16-5	*i*-Bu	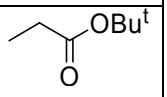

Figure 3.24 Preparation of Mosher amide for ^{19}F-NMR analysis

The ααAAs possess sterically hindered amino functions because the alpha carbon is disubstituted with two bulky groups; therefore 0.1 equivalent of 4-dimethylaminopyridine (DMAP) was used as a nucleophilic acylation catalyst to speed up this reaction as illustrated in Figure 3.25.[42] DMAP reacts with acyl chloride to form an acylpyridinium ion first. The acylpyridinium ion reacts with the amine rapidly to form the amide bond and regeneration of DMAP. The inclusion of DMAP in acylations by acid anhydrides and acyl chlorides have been shown to increase acylation rates by up to four orders of magnitude and permits successful acylation of tertiary and other hindered alcohols.

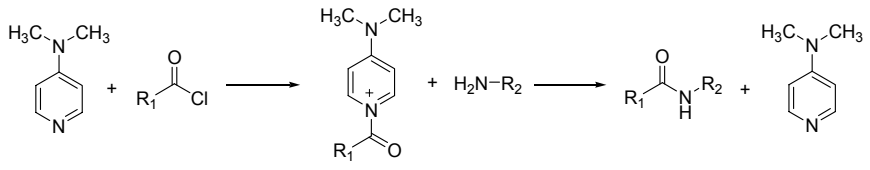

Figure 3.25 DMAP catalyzed acylation reaction

^{19}F NMR spectra of Mosher amides show two singlet signals for two diastereomeric Mosher amides *R*, *R* and *R*, *S* respectively. Integration of the two signals provides the enantiomeric excess of the two amino ester enantiomers. The peak areas for the two signals resulting from racemic amino esters are identical indicating that the enantiomeric excess for the racemic mixture is zero. The two diastereomers of Mosher amides formed from reacting the Mosher-chloride with the racemic amino ester have identical chemical shifts in reference to the two diastereomeric Mosher amides resulting from the chiral amino ester as shown in Figure 3.26.

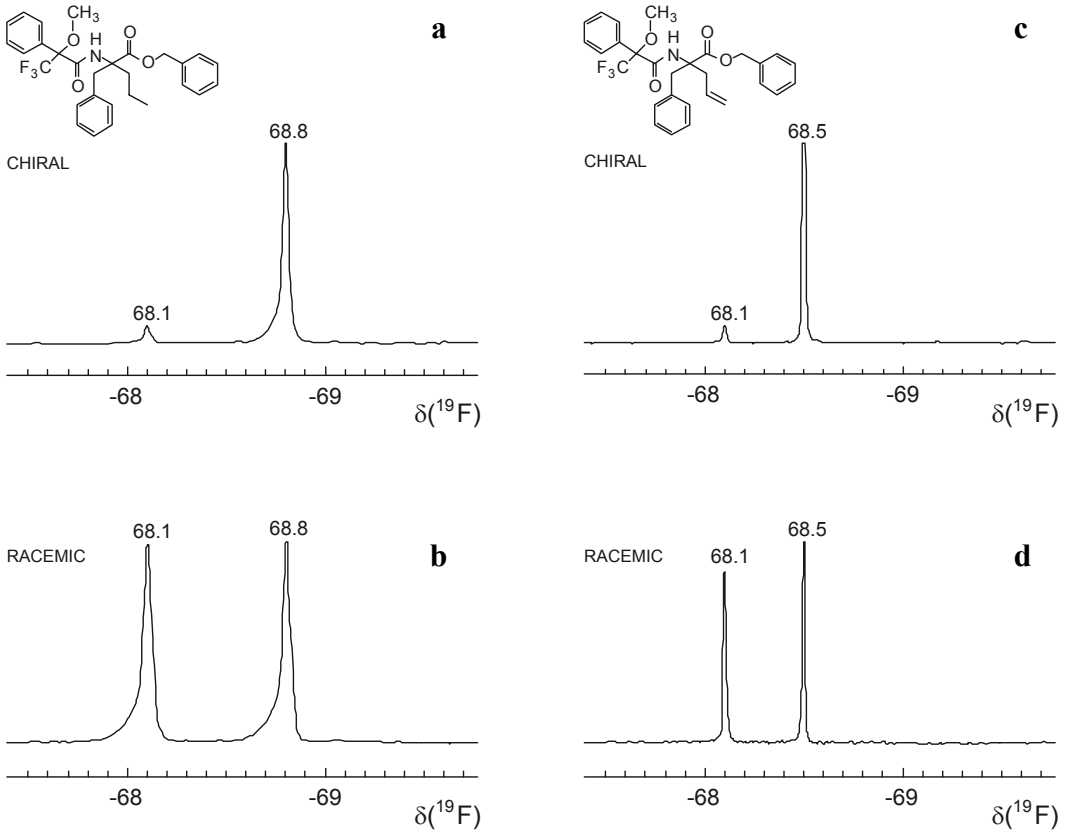

Figure 3.26 ^{19}F NMR spectra of diastereomers of Mosher amides

a. ^{19}F NMR spectrum of diastereomers of Mosher amides made from chiral benzyl α-propyl-phenylalaninate. **b.** ^{19}F NMR spectrum of diastereomers of Mosher amides made from racemic benzyl α-propyl-phenylalaninate. **c**.^{19}F NMR spectrum of diastereomers of Mosher amides made from chiral benzyl α-allyl-phenylalaninate. **d.** ^{19}F NMR spectrum of diastereomers of Mosher amides made from racemic benzyl α-allyl-phenylalaninate

Determination of enantiomeric excess based on fluorine resonance, is usually more reliable than proton resonances, because the fluorine signals are simple and located in an uncongested region. The fluorine NMR spectra taken at 235 MHz showed a chemical shift difference of 0.4-0.7 ppm between diastereotopic α-trifluoromethyl groups. Such differences permitted precise integrations of the fluorine signals. Comparable precision in measuring the signals from the diastereotopic proton was not always possible because of signal overlap.

The enantioselectivity of *tert*-butyl α-benzyl-leucinate (entry 13-3 in Table 3.2) was also determined by HPLC analysis. The HPLC profile and ^{19}F NMR spectrum for enantiomers of tert-butyl α-benzyl-leucinate are illustrated in Figure 3.27 and Figure 3.28 respectively. HPLC analysis was carried out using a chiral column (DAICEL Chiralpak AD-H) and monitored at 254 nm with hexanes: 2-propanol as a solvent, The enantiomeric excess is 79% from HPLC analysis and the enantiomeric excess is 78% based on ^{19}F NMR analysis. Therefore, the two methods give the almost identical results.

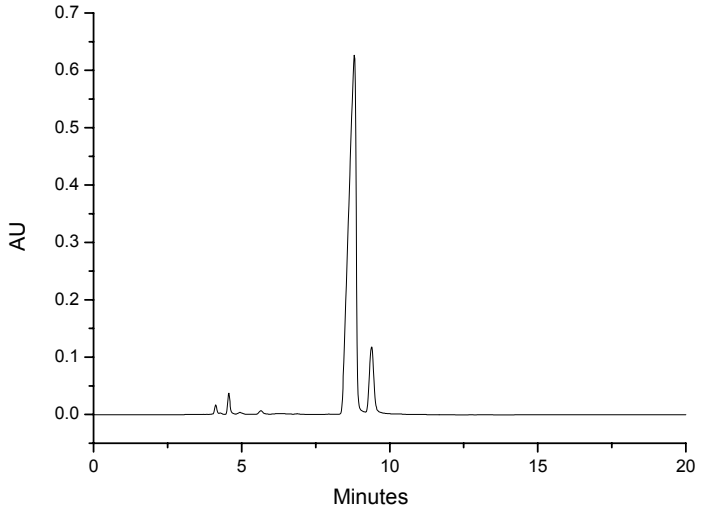

Figure 3.27 HPLC chromatogram of enantiomers of tert-butyl α-benzyl-leucinate. Conditions: hexanes:2-propanol(99:1), 25 °C

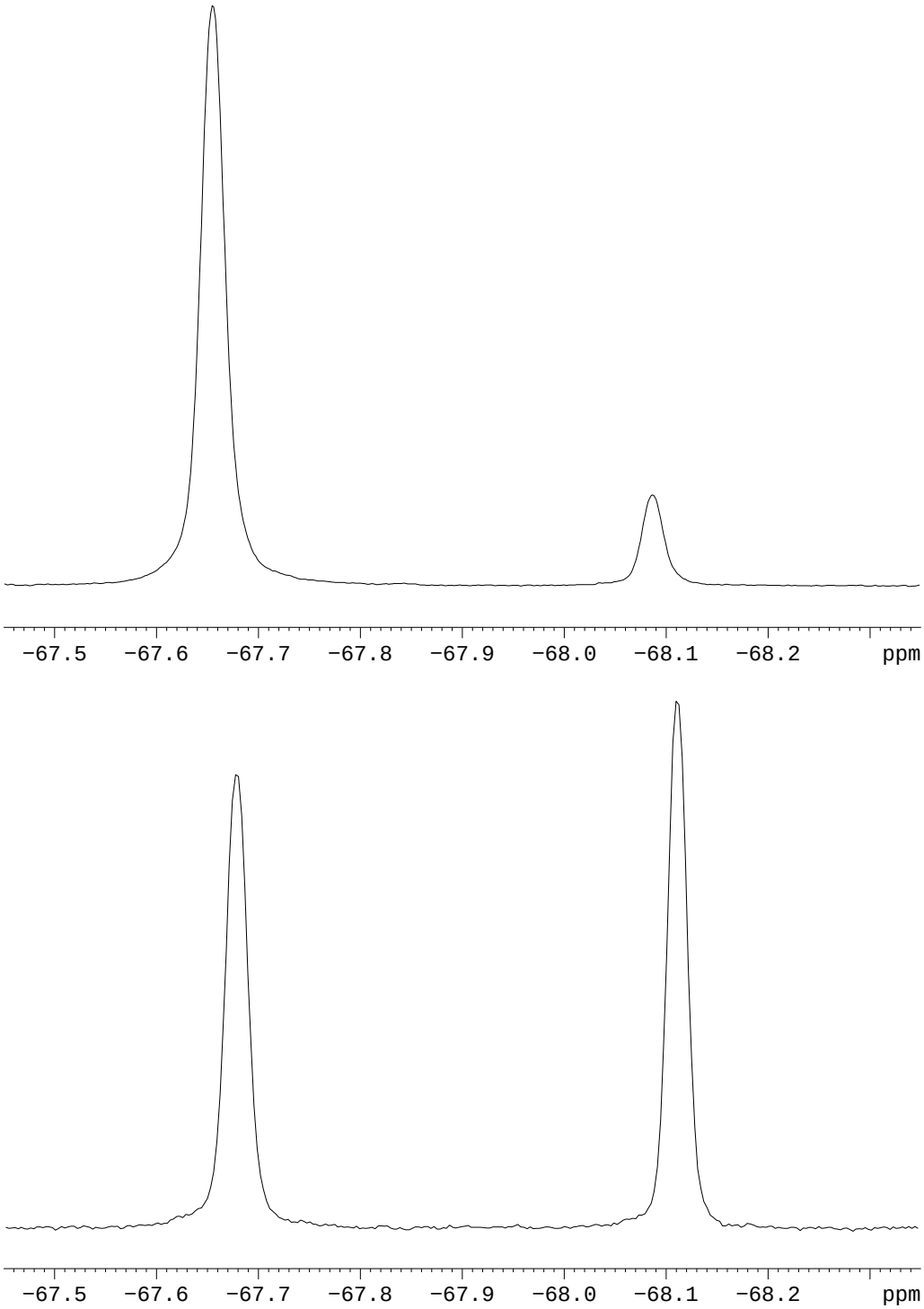

Figure 3.28a ^{19}F NMR spectrum of Mosher amides made from chiral tert-butyl α-benzyl-leucinate, **Figure 3.28b** ^{19}F NMR spectrum of Mosher amides made from racemic tert-butyl α-benzyl-leucinate

3.3 Conclusions and Future Research Direction

To summarize, Dibg was synthesized via palladium catalyzed allylation reaction with an excellent overall yield and incorporated into various positions of a model β-hairpin peptide GHP in order to determine the effectiveness of the tetrasubstituted amino acids as design elements in both the strand and turn portions of β-hairpins. CD and NMR data of Dibg containing peptides showed Dibg residue can contribute to the stability of the strand portion of a β-hairpin peptide and destabilize the β-turn in the GHP. The sheet stabilizing effect of Dibg may be due to the strong propensity of Dibg to have a fully extended conformation(ϕ/ψ= 180°). The unordered structures in Dibg^3-NG and Leu^3-NG suggest that the proteinogenic LAsn-Gly two residue loop, despite having a strong preference for a type I' turn formation in aqueous solution, is incapable generating the β-hairpin in the absence of the favorable interstrand side chain-side chain interaction and aromatic and aliphatic interaction.

Several chiral amino esters were prepared with high enantioselectivity by alkylation of the corresponding Schiff bases under chiral phase-transfer condition. The enantiomeric excess of these chiral amino esters was efficiently determined by ^{19}F-NMR analysis of the corresponding diastereomeric Mosher amides. The chiral ααAAs will be incorporated into the hydrogen bonding positions of the model β-hairpin peptide GHP to study their conformational effects on β-sheet peptides.

3.4 Experimental

- **General Methods**

TLC was performed on Merck silica gel 60 F_{254} plates and visualized by ultraviolet light, exposure to iodine vapor or ninhydrin test. Flash column

chromatography was performed using silica gel 60 (230-400 mesh). ^{1}H spectra were recorded on a 250 MHz spectrometer and ^{19}F spectra were recorded on a 235 MHz spectrometer.

- **Representative Procedure for Synthesis of Fmoc-Dibg Amino Acid**

To the solution of ethyl nitroacetate **1** (2 g, 15 mmol) in dry THF (100 mL) 2-methylally acetate (3.42 g, 30 mmol) and $Pd(PPh_3)_4$ (1.73 g, 1.5 mmol) were added and after 20 minutes DIEA (3.81 g, 30 mmol) was added and the reaction was stirred under argon for 10 hrs at 50˚C. The resulting solution was filtered over celite and washed with THF twice. The filtrate was concentrated, dissolved in 40 mL of EtOAc and washed with 10% K_2CO_3. To the organic layer PS-PPh_3 (1.3 mmol/g) Argonaut resin was added and shaken for 30 minutes. The resin was filtered off and the filtrate was purified via column chromatography (ethyl acetate-hexane 2:1) to provide ethyl 2,2-bis(2-methylallyl)-2-nitroacetate **2**, light yellow oil . Yield, 3.26g (90%). ^{1}H NMR (250 MHz, $CDCl_3$) δ 4.96-4.95(m, 2H) 4.80(m, 2H), 4.28-4.20(q, 2H), 3.03-3.02(m, 4H), 1.71(m, 6H), 1.31-1.26(t, 3H)

To a solution of **2** (3.26 g, 13.5 mmol) in absolute ethanol (15 mL) glacial acetic acid (2 mL) and a 50% (w/w) slurry of Raney nickel in water (2 g) were added. The solution was reduced via hydrogenation over H_2 (50 psi) for 20 hrs. The resulting solution was filtered carefully over celite and washed with ethanol. (Note: Raney nickel is very pyrophoric when dry). The solvent was removed under reduced pressure and the crude was dissolved in diethyl ether (25 mL). After washing with saturated sodium carbonate and brine, the organic fraction was dried over anhydrous sodium sulfate and rotary evaporated to yield ethyl 2, 2-diisobutylglycine ester (**3**) 2.53 g (87%). ^{1}H NMR (250 MHz, $CDCl_3$) δ 4.12-

4.10 (q, 2H), 1.75-1.68 (m, 6H), 1.49 (m, 2H), 1.32-1.26 (t, 3H), 0.95-0.94 (m, 6H), 0.93-0.81 (m, 6H).

A suspension of **3** (2.53 g, 11.8 mmol) in 3M KOH (50 mL) and ethanol (35 mL) was refluxed under argon for 12 hrs. The resulting mixture was concentrated to 10 mL and acidified to pH 6.5 with 12 N HCl. The solvent was evaporated and the residue was redissolved in a minimum amount of water. The mixture was added to an activated Dowex 50*8-400 ion-exchange resin (50 g). Resin was activated by the following procedure: 1. wash resin with 2N HCl till acidic, then wash resin with distill water and methanol. After sample was loaded, eluted resin with methanol (250 mL), H_2O (500 mL), and 2 N NH_4OH (500 mL) respectively. The collected 2 N NH_4OH fractions were evaporated under reduced prssure to give the free α,α–diisobutylglycine **4** as a white powder. Yield, 1.97 g (89%). ^{1}H NMR (250 MHz, DMSO-d_6) δ 7.3 (bs, 2H), 1.7-1.47 (m 6H), 0.85-0.83 (m, 12H). MALDI-MS of Dibg, $[M+1]^+$ m/z calcd.188.2, Obsd. 188.2.

Free Dibg (1.97g, 10.5mmol) was placed in a 2 neck round bottom flask fitted with a heating mantle and condenser. The solid was suspended in anhydrous CH_2Cl_2 (30 mL) and stirred vigorously. TMS-Cl (21 mmol, 2 eq) was added. The mixture was then refluxed for 6 hrs and allowed to cool in an ice bath. Diisopropylethylamine (3.2mL, 1.7eq) and Fmoc-Cl (1.9g, 0.7eq) were added. The solution was stirred with cooling for 20 min and warmed to room temperature overnight. The mixture was concentrated to remove CH_2Cl_2. The product was dissolved in ethyl acetate and the organic layer washed with 1N HCl twice. The organic layers were dried over anhydrous $MgSO_4$ and concentrated under reduced pressure. The crude product was triturated in hexanes to afford a white solid Fmoc-Dibg **5**. Yield, 3.91g (91%). ^{1}H NMR (250 MHz, DMSO-d_6)

δ 7.89–7.31 (m, 8H), 6.40 (s, 1H), 4.4 (d, 2H) , 4.2 (t, 1H), 2.01–1.99 (m, 2H), 1.62–1.44 (m, 4H), 0.79–0.75 (m, 12H). Elemental Analysis: Calcd for $C_{25}H_{31}NO_4$: C, 73.32; H, 7.63; N, 3.42. Found: C, 73.53; H, 7.49; N, 3.45.

- **Peptide Synthesis**

Peptides listed in Table 3.1 were synthesized using Fmoc chemistry via solid-phase peptide synthesis on a peptide amide linker-polyethylene glycol-polystyrene (Fmoc-PAL-PEG-PS) resin as a solid support. The side-chain protected amino acid derivatives utilized were Fmoc-Arg(Pbf)-OH, Fmoc-Dibg-OH, Fmoc-Glu(OtBu)-OH, Fmoc-Val-OH, Fmoc-$_D$-Pro-OH, Fmoc-Gly-OH, Fmoc-Orn(Boc)-OH, Fmoc-Ile-OH, Fmoc-Leu-OH, Fmoc-Gln(Trt)-OH, Fmoc-Lys(Boc)-OH, Fmoc-Orn(Boc)-OH, and Fmoc-Thr(tBu)-OH. Unless indicated otherwise, molar equivalents are given over resin-bound amine.

All coupling reactions except the acylation of the N-terminus of Dibg and acylation of the N-terminus of Dibg^3-NG and Leu^3-NG were carried out in DMF using four equivalents of Fmoc-amino acids and activation with 4 equivalents PyAOP, and 8 equivalents DIEA. A deblocking solution of 2% piperidine, 2% DBU in DMF was used for Fmoc removal. A double coupling was performed for valine due to the difficult coupling of this amino acid to the peptide sequence because of its sterically bulky side chain. The couplings before the Dibg residue were performed on the Biosystem Pioneer peptide synthesizer. The remaining amino acid residues were incorporated manually into the sequence. Dibg coupling was carried out using the PyAOP activator in the presence of DIEA at an elevated temperature of 50°C on a shaker for overnight due to the difficult coupling of the amino acid to the peptide sequence. A double coupling was performed for

Dibg coupling due to moderate coupling yields determined by UV analysis of Fmoc deprotection.

Symmetrical anhydride of Fmoc amino acids was prepared by treatment of 10 equivalents of corresponding Fmoc amino acid with 5 equivalents of DCC in CH_2Cl_2 at room temperature for 2 hrs. The resulting DCU precipitate was removed via filtration. Coupling of the symmetrical anhydride onto resin-bound peptide was carried out by adding preformed symmetrical anhydride to the resin-bound peptide in DCE-DMF (9:1) at 50 ˚C for 4 hrs while shaking. A double coupling procedure was performed due to moderate coupling yields determined by UV analysis of Fmoc deprotection.

After the symmetrical anhydride coupling, the resin-bound peptide was rinsed with DMF for 5 times. The deprotection solution, 10 mL 20% piperidine in DMF was added to the resin-bound peptide and shaken for 5 min, then the deprotection solution was filtered and the resin-bound peptide was washed with DMF for 3 times. A second treatment with deprotection solution to resin-bound peptide occurred for 20 mins while shaken then filtered and rinsed. After the resin was washed with DMF for 5 times, 4 equivalents of Fmoc-Arg(pbf)-OH, 8 equivalents of DIEA, 10 mL DMF were added to the resin and shaken for 2 hrs. The resin was then washed with DMF for 5 times and air dried for 10 min. The coupling efficiency was monitor by bromophenol blue test, ninhydrin test and Fmoc test described as below:

- **Bromophenol Blue Test Protocol[43]**

1. Add 1% bromophenol blue to acetonitril or N, N-dimethylacetamide to make bromophenol blue solution.
2. Sample a few resin beads and wash several times with DCM.

3. Transfer the resin to a test tube and add 3 to 5 drops of bromophenol blue solution.
4. The presence of resin-bound free amine is indicated by blue resin beads. Yellow stained resin beads indicate the completion of the coupling reaction.

- **Ninhydrin Test Protocol**[44]

1. Add 5 % ninhydrin in ethanol, 80 % phenol in ethanol, 15 % water together to a vial to make ninhydrin solution.
2. Sample a few resin beads and wash with ethanol 3 times in a syringe fitted with a frit and sit on an Erlenmeyer flask connected through a vacuum adaptor.
3. Transfer to a test tube and add 3 drops of ninhydrin solution.
4. Blue stained resin beads indicate the presence of resin-bound free amine. The α,α−disubstituted amino acid Dibg do not yield a positive reaction, thus give false negative results.

- **Fmoc Test Protocol**

1. Transfer small quantity of resin to a 10 mL syringe fitted with a frit and sit on an Erlenmeyer flask connected through a vacuum adaptor.
2. Wash resin 10 times with DCM, apply vacuum for each wash to drain off the DCM.
3. Dry resin for 1 hour under vacuo.
4. Weigh out 4 to 8 mg of dry resin; return any unused resin to reaction flask.
5. Treat the resin with 1 mL 20% piperidine in DMF solution for 30 mins.
6. Remove the piperindine/DMF solution and add to a graduated cylinder. Wash resin with 1 mL of MeOH for 6 times; combine the 6 portions to the graduated cylinder. This is the sample solution for UV analysis.
7. Prepare the reference solution of 1 mL piperindine in DMF in 6 mLs MeOH.

8. Place the reference solution into the UV cell and acquire UV spectrum form 240 nm to 350 nm. This is the back ground spectrum.

9. Acquire UV spectrum of sample solution in same wavelength range; correct for background.

10. Calculate the substitution level, coupling and percent coupling using the equations below.

$$\text{Substitution level} = \frac{[(\text{Absorbance@301 nm} \times 10^6) \times 0.007]}{[7800 \times \text{cell path length (cm)} \times \text{weight of resin (mg)}]}$$

Coupling efficiency = Substitution level per above/Substitution level of resin

Percent coupling efficiency = Coupling x 100%

Acetylation of N-terminus of Dibg^3-NG and Leu^3-NG was performed on the solid support by treatment with a solution of 0.2 M acetic anhydride and 0.28 M DIEA in DMF for 2 hrs. Once peptide assembly was completed, the peptide and side chain protecting groups were simultaneously cleaved off the resin with a cleavage cocktail: 88% trifluoroacetic acid, 5% phenol, 5% water and 2% triisopropylsilane (88:5:5:2 TFA:phenol:water:TIPS) and precipitated out from cold ether for overnight.

- **Peptide Purification and Characterization**

Crude peptides were purified by reverse-phase high-performance liquid chromatography (HPLC) on a Waters Delta-Pak C_{18} column (15 μm, 300Å, 8 x 100 mm) with a gradient from 90% A (H_2O, 0.1%TFA) and 10% B (CH_3CN, 0.1% TFA) to 30% A and 70% B over 60 mins at a flow rate of 1mL/min. Semi preparative conditions were carried out using a Waters preparative Delta-Pak C_{18} column (15 μm, 300 Å, 25x100 mm) at a flow rate of 20mL/min. The homogeneity (> 99%) was confirmed by analytical

reverse-phase HPLC monitoring at the wavelength of 220 nm with the scan wavelength from 200 to 400 nm using a Vydac C_{18} column (5 μm, 4.6 x 250 mm) and identity of the peptides was determined by matrix-assisted laser desorption ionization-time of flight (MALDI-TOF) on a Bruker Proflex III instrument with XMASS software.

Table 3.4 Analytical HPLC retention time and corresponding MALDI-MS results

Peptide	Retention time(min)	MALDI $(M+H)^+$ m/z	
		Calculated	Observed
Dibg^3-GHP	38.5	1486.7	1486.2
Dibg^6-GHP	40.8	1488.7	1488.6
Dibg^3-NG	24.9	1482.7	1483.3
Leu^3-NG	32.4	1427.7	1427.9

Representative Procedure for Preparation of Schiff Base

1. Preparation of *tert*-butyl leucinate *p*-chlorobenzaldehyde Schiff base.

Leucine hydrochloride *tert*-butyl ester (1 g, 4.47 mmol) and sodium carbonate (0.474 g, 4.47 mmol) were dissolved in water (50 mL), CH_2Cl_2 (50 mL) and 4-chloro-benzaldehyde (0.628 g, 4.47 mmol) was added. The mixture was stirred at 40 °C for 45 mins. The reaction was then allowed to react at room temperature for 16 hrs. The resulting mixture was extracted with CH_2Cl_2 and water. The organic layer was dried over $MgSO_4$ and evaporated under reduced pressure to afford the crude imine as a colorless oil. (1.2 g, 86.8%). ^{1}H NMR (250 MHz, $CDCl_3$) δ 8.24 (s, 1H) 7.75-7.70 (d, 2H), 7.42-7.40 (d, 2H), 3.99-3.94 (t, 1H), 1.83-1.77 (m, 2H) 1.63-1.52 (m, 1H), 1.49-1.45 (s, 9H), 0.97-0.89 (dd, 6H)

2. Preparation of benzyl phenylalaninate *p*-chlorobenzaldehyde Schiff base.

Phenylalanine hydrochloride benzyl ester (2 g, 6.85 mmol) and sodium carbonate (0.73 g, 6.85 mmol) were dissolved in water (50 mL), CH_2Cl_2 (80 mL) and 4-chloro-benzaldehye (0.994 g, 6.85 mmol) was added. The mixture was stirred at 40 °C for 45 mins. The reaction was then allowed to react at room temperature for 16 h. The mixture was then extracted with CH_2Cl_2 and water. The organic layer was dried over $MgSO_4$ and evaporated under reduced pressure to afford the crude imine as a colorless oil. Yield, 2.57 g (99.2%). ^{1}H NMR (250 MHz, $CDCl_3$) δ 7.87 (s, 1H), 7.76-7.60 (d, 2H), 7.38-7.15 (m, 12H), 5.19 (s, 2H), 4.23-4.19 (dd, 1H), 3.36-3.34 (dd, 1H), 3.19-3.16 (dd, 1H).

Representative procedure for catalytic enantioselective allylation of benzyl phenylalaninate *p*-chlorobenzaldehyde Schiff base under phase-transfer conditions to form benzyl α–allyl phenylalaninate. (entry 13-1)

To a mixture of benzyl phenylalaninate *p*-chlorobenzaldehyde Schiff base (800 mg, 2.12 mmol), chiral catalyst (19 mg, 0.0212 mmol) and allyl bromide (214 μl, 1.2 eq) in anhydrous toluene (10 mL), $CsOH{\cdot}H_2O$ (1.78 g, 5 eq) was added at 0 °C, and the reaction mixture was stirred vigorously for 1.5 hrs. Water was added and extraction was performed with CH_2Cl_2. CH_2Cl_2 was evaporated and the residue was re-dissolved into THF (10 mL). 0.5 M citric acid (20 mL) was added and stirred at room temperature for 1 h. The aqueous phase was separated and washed with ether. The aqueous phase was then basified by the addition of solid $NaHCO_3$ and extracted with CH_2Cl_2. The organic extracts were dried over Na_2SO_4 and concentrated. Purification of the residual oil was carried out via column chromatography on silica gel (ethyl acetate-hexanes 1:2) to yield product. Yield, 325 mg (52.32%). ^{1}H NMR (250 MHz, $CDCl_3$) 7.37-7.09(m 10H), 5.8-

5.6(m, 1H), 5.14 (m, 4H), 3.25-3.20 (d, 1H), 2.9-2.7 (m, 2H), 2.4 (m, 1H), 2.1-1.8(bs, 2H).

Representative procedure for catalytic enantioselective benzylation of *tert*-butyl leucinate *p*-chlorobenzaldehyde Schiff base under phase-transfer conditions to form *tert*-butyl α-benzyl leucinate. (entry13-3)

To a mixture of *tert*-butyl leucinate *p*-chlorobenzaldehyde Schiff base (300 mg, 0.97 mmol), chiral catalyst (8.9 mg, 0.0097 mmol) and benzyl bromide (138 μl, 1.164 mmol, 1.2 eq) in anhydrous toluene (4 mL), $CsOH{\cdot}H_2O$ (814.5 mg, 4.85 mmol) was added at 0 °C, and the reaction mixture was stirred vigorously for 1.5 hrs. Water was added and extraction was performed using CH_2Cl_2. The solution was concentrated and re-dissolved in THF (10 mL). 0.5 M citric acid (10 mL) was added and the mixture was stirred at room temperature for 1 h. The aqueous phase was separated and washed with ether.

The aqueous phase was then basified by the addition of solid $NaHCO_3$ and extracted with CH_2Cl_2. The organic extracts were dried over Na_2SO_4 and concentrated. Purification of the residual oil was carried out via column chromatography on silica gel (ethyl acetate-hexanes 2:1) to yield tert-butyl α-benzyl leucinate. Yield, 168.97 mg (63%).^{1}H NMR (250 MHz, $CDCl_3$) 7.27-7.24 (m, 5H), 3.16 (d, 1H), 3.11(d, 1H), 1.85-1.60 (m, 3H), 1.45 (s, 9H), 1.00-0.91(dd, 6H).

Benzyl α-propyl phenylalaninate (entry 13-2)

^{1}H NMR (250 MHz, $CDCl_3$) 7.36-7.34(m, 5H), 7.22-7.20(m, 3H), 7.08-7.05(m, 2H), 5.13(s, 2H), 3.19(d, 1H), 2.76(d, 1H), 1.97-1.85(ddd, 1H), 1.79(bs, 2H), 1.65-1.55(ddd, 1H), 1.50-1.32(m. 1H), 1.18-1.04(m, 1H), 0.92-0.86(t, 3H).

tert-Buty α-allyl leucinate (entry 13-4)

^{1}H NMR (250 MHz, $CDCl_3$) 5.73(m, 1H), 5.13(m, 2H), 2.55(dd, 1H), 2.16(dd, 1H), 1.72(m, 3),1.47(s, 9H), 0.97-0.87(dd, 6H)

Benzyl α-allyl leucinate(entry 13-5)

^{1}H NMR (250 MHz, $CDCl_3$) 7.31(m, 5), 5.54(m, 1H), 5.07(m, 3H), 3.90(m, 1H), 2.53(dd, 1H), 2.16(dd, 1H), 1.96(m, 1H), 1.85-1.53(m, 2H), 0.88-0.72(dd, 6H)

Benzyl α-*tert*-butyl propionate phenylalaninate (Entry 13-6)

^{1}H NMR (250 MHz, $CDCl_3$) 7.37-7.20(m, 10H), 5.14(s, 2H), 3.18(d, 1H), 2.81(d, 1H), 2.41(m, 1H), 2.19(m. 1H), 2.01(m, 2H), 1.82,(bs, 2H), 1.43(s, 9H)

If the compound is UV inactive, the reaction can be flollowed by ninhydrin test. First Spot the TLC with compound and then immerse TLC into the ninhydrin solution. The plates were then immediately heated by a heat gun, which completes the ninhydrin test where the primary amines appear as blue-purple spots on the TLC plates and the incompletion of the reaction is indicated by the yellow spot on the TLC plate.

Procedure for preparation of α-benzyl leucine HCl salt

To the *tert*-butyl α-benzyl leucinate, 50 ml of 6 N HCl was added. The reaction mixture was refluxed under argon for over night. The water layer was washed with ether, then the water was removed under reduced pressure, then redissolved in water and lyophilize to dryness.^{1}H NMR (250 MHz, D_2O) 7.30(m, 5H), 3.25(d, 1H), 3.01(d, 1H), 1.95(dd, 1H), 1.69(m, 2H), 0.84(dd, 6H)

Representative procedure for preparation of racemic amino ester

To the mixture of benzyl phenylalaninate *p*-chlorobenzaldehyde Schiff base (500 mg, 1.32 mmol), allyl bromide (243 mg, 2.01 mmol), 0.1 eq tetra-n-butylammonium bromide (42.5 mg, 0.132 mmol) in MeCN, finely ground technical grade potassium carbonate

was added and refluxed with stirring for 1h. The mixture was then cooled and filtered. 0.5 M citric acid (20 mL) was added and stirred at room temperature for 1h. The aqueous phase was separated and washed with ether. The aqueous phase was then basified by the addition of solid $NaHCO_3$ and extracted with CH_2Cl_2. The organic extracts were dried over Na_2SO_4 and concentrated. Purification of the residual oil was carried out via column chromatography on silica gel (ethyl acetate-hexane 1:2) to yield benzyl α–allyl phenylalaninate.^{1}H NMR (250, $CDCl_3$) 7.39-7.10 (m 10H), 5.8-5.6 (m, 1H) 5.15-5.11(m, 4H), 3.24-3.18 (d, 1H), 2.81-2.77 (m, 2H), 2.4-2.2 (m, 1H) 1.63 (s, 2H).

Representative procedure for preparation of Mosher amide in order to determine the enantioselectivity of the chiral amino esters

To *R*-(-)-α-methoxy-α–trifluoromethylphenylacetyl chloride (MTPA Cl, 0.032 g, 0.127 mmol), benzyl α–allyl phenylalaninate(0.025 g, 0.085 mmol), 4-dimethylaminopyridine (0.001 g, 0.0085 mmol) and DIPEA (14.7 μL, 0.085 mmol) were added and allowed to react overnight at room temperature. The crude product was extracted using 1 N HCl and CH_2Cl_2. The organic layer was washed with 4 N NaOH, dried over anhydrous $MgSO_4$, and evaporated under reduced pressure.^{19}F NMR (235 MHz, $CDCl_3$) -68.07(s), -68.52(s)

Entry 16-2 ^{19}F NMR (235 MHz, $CDCl_3$) -68.08(s), -68.75(s)

Entry 16-3^{19}F NMR (235 MHz, $CDCl_3$) -67.67(s), -68.12(s)

Entry 16-4^{19}F NMR (235 MHz, $CDCl_3$) -68.10(s), -68.74(s)

Entry 16-5^{19}F NMR (235 MHz, $CDCl_3$) -68.75(s), -69.02(s)

Chiral HPLC analysis of tert-butyl α-benzyl-leucinate was carried out using a chiral column (DAICEL Chiralpak AD-H) with hexanes:2-propanol = 99:1.0, flow rate= 0.5 ml/min, 25 °C, λ =254 nm, retention time: 16.13 min and 17.16 min respectively.

3.5 References

1. Sunde, M.; Blake, C. C. F., From the globular to the fibrous state: protein structure and structural conversion in amyloid formation. *Q. Rev. Biophys.* **1998,** 31, 1-37.

2. Rochet, J. C.; Lansbury, P. T., Amyloid fibrillogenesis: themes and variations. *Curr. Opin. Struct. Biol.* **2000,** 10, 60-68.

3. Gazit, E., The "Correctly folded" state of proteins: Is it a metastable state. *Angewandte Chemie-International Edition* **2001,** 41, 257-259.

4. Soto, C., Unfolding the role of protein misfolding in neurodegenerative diseases. *Nature Reviews Neuroscience* **2003,** 4, 49-60.

5. Stefani, M.; Dobson, C. M., Protein aggregation and aggregate toxicity: new insights into protein folding, misfolding diseases and biological evolution. *Journal of Molecular Medicine-JMM* **2003,** 81, 678-699.

6. Dinner, A. R.; Lazaridis, T.; Karplus, M., Understanding β-hairpin formation. *Proc. Natl. Acad. Sci. U. S. A.* **1999,** 96, 9068-9073.

7. Minor, D. L., Jr.; Kim, P. S., Context is a major determinant of β-sheet propensity. *Nature* **1994,** 371, 264-267.

8. Nesloney, C. L.; Kelly, J. W., Progress towards understanding β-sheet structure. *Bioorganic & Medicinal Chemistry* **1996,** 4, 739-766.

9. Duthaler, R. O., Recent developments in the stereoselective synthesis of α-amino acids. *Tetrahedron* **1994,** 50, 1539-1650.

10. Cativiela, C.; Diaz-De-Villegas, M. D., Stereoselective synthesis of quaternary α-amino acids. Part 2: cyclic compounds. *Tetrahedron: Asymmetry* **2000,** 11, 645-732.

11. O'Donnell, M. J.; Wu, S.; Huffman, J. C., A new active catalyst species for enantioselective alkylation by phase-transfer catalysis. *Tetrahedron* **1994,** 50, 4507-4518.

12. Ooi, T.; Takeuchi, M.; Kameda, M.; Maruoka, K., Practical catalytic enantioselective synthesis of α,α-dialkyl-α-amino acids by chiral phase-transfer catalysis. *J. Am. Chem. Soc.* **2000,** 122, 5228-5229.

13. Upham, S. D.; Dermer, O. C., A New Series of Anticonvulsant Drugs - Branched-Chain α−Aminoacetamides. *J. Org. Chem.* **1957,** 22, 799-802.

14. Fu, Y.; Etienne, M. A.; Hammer, R. P., Facile Synthesis of α,α-Diisobutylglycine and Anchoring its Derivatives onto PAL-PEG-PS Resin. *J. Org. Chem.* **2003,** 68, 9854-9857.

15. Bolin, D. R.; Sytwu, I. I.; Humiec, F.; Meienhofer, J., Preparation of oligomer-free N^{α}-Fmoc and N^{α}-urethane amino acids. *International Journal of Peptide & Protein Research* **1989,** 33, 353-9.

16. Wenschuh, H.; Beyermann, M.; Krause, E.; Brudel, M.; Winter, R.; Schumann, M.; Carpino, L. A.; Bienert, M., Fmoc Amino-Acid Fluorides - Convenient Reagents for the Solid-Phase Assembly of Peptides Incorporating Sterically Hindered Residues. *J. Org. Chem.* **1994,** 59, 3275-3280.

17. Fu, Y. W.; Hammarstrom, L. G. J.; Miller, T. J.; Fronczek, F. R.; McLaughlin, M. L.; Hammer, R. P., Sterically hindered $C^{\alpha,\alpha}$-disubstituted α-amino acids: Synthesis from α-nitroacetate and incorporation into peptides. *J. Org. Chem.* **2001,** 66, 7118-7124.

18. Zimm, B. H.; Doty, P.; Iso, K., Determination of the Parameters for Helix Formation in Poly-Gamma-Benzyl-L-Glutamate. *Proceedings of the National Academy of Sciences of the United States of America* **1959,** 45, 1601-1604.

19. Blanco, F. J.; Jimenez, M. A.; Herranz, J.; Rico, M.; Santoro, J.; Nieto, J. L., NMR Evidence of a Short Linear Peptide That Folds into a β-Hairpin in Aqueous Solution. *J. Am. Chem. Soc.* **1993,** 115, 5887-5888.

20. Venkatraman, J.; Shankaramma, S. C.; Balaram, P., Design of folded peptides. *Chem. Rev.* **2001,** 101, 3131-3152.

21. Searle, M. S.; Ciani, B., Design of β-sheet systems for understanding the thermodynamics and kinetics of protein folding. *Curr. Opin. Struct. Biol.* **2004,** 14, 458-464.

22. Hughes, R. M.; Waters, M. L., Model systems for β-hairpins and β-sheets. *Curr. Opin. Struct. Biol.* **2006,** 16, 514-524.

23. Stanger, H. E.; Gellman, S. H., Rules for antiparallel β-sheet design: D-Pro-Gly is superior to L-Asn-Gly for β-hairpin nucleation. *J. Am. Chem. Soc.* **1998,** 120, 4236-4237.

24. Syud, F. A.; Espinosa, J. F.; Gellman, S. H., NMR-based quantification of β-sheet populations in aqueous solution through use of reference peptides for the folded and unfolded states. *J. Am. Chem. Soc.* **1999,** 121, 11577-11578.

25. Wishart, D. S.; Sykes, B. D.; Richards, F. M., Relationship between Nuclear Magnetic Resonance Chemical Shift and Protein Secondary Structure. *Journal of Molecular Biology* **1991,** 222, 311-333.

26. Wishart, D. S.; Sykes, B. D.; Richards, F. M., The Chemical-Shift Index - a Fast and Simple Method for the Assignment of Protein Secondary Structure through NMR Spectroscopy. *Biochemistry* **1992,** 31, 1647-1651.

27. Griffiths-Jones, S. R.; Maynard, A. J.; Searle, M. S., Dissecting the stability of a β-hairpin peptide that folds in water: NMR and molecular dynamics analysis of the β-turn and β-strand contributions to folding. *Journal of Molecular Biology* **1999,** 292, 1051-1069.

28. Searle, M. S.; Griffiths-Jones, S. R.; Skinner-Smith, H., Energetics of weak interactions in a β-hairpin peptide: Electrostatic and hydrophobic contributions to stability from lysine salt bridges. *J. Am. Chem. Soc.* **1999,** 121, 11615-11620.

29. Merutka, G.; Dyson, H. J.; Wright, P. E., Random Coil H^1 Chemical-Shifts Obtained as a Function of Temperature and Trifluoroethanol Concentration for the Peptide Series GGXGG. *Journal of Biomolecular NMR* **1995,** 5, 14-24.

30. Sibanda, B. L.; Thornton, J. M., Beta-Hairpin Families in Globular-Proteins. *Nature* **1985,** 316, 170-174.

31. Tatko, C. D.; Waters, M. L., Selective aromatic interactions in β-hairpin peptides. *J. Am. Chem. Soc.* **2002,** 124, 9372-9373.

32. Russell, S. J.; Cochran, A. G., Designing stable β-hairpins: Energetic contributions from cross-strand residues. *J. Am. Chem. Soc.* **2000,** 122, 12600-12601.

33. Kortemme, T.; Ramirez-Alvarado, M.; Serrano, L., Design of a 20-amino acid, three-stranded β-sheet protein. *Science* **1998,** 281, 253-256.

34. Sharman, G. J.; Searle, M. S., Cooperative interaction between the three strands of a designed antiparallel β-sheet. *J. Am. Chem. Soc.* **1998,** 120, 5291-5300.

35. Griffiths-Jones, S. R.; Maynard, A. J.; Sharman, G. J.; Searle, M. S., NMR evidence for the nucleation of a β-hairpin peptide conformation in water by an Asn-Gly type I ' β-turn sequence. *Chemical Communications* **1998**, 789-790.

36. Chou, P. Y.; Fasman, G. D., Conformational Parameters for Amino Acids in Helical, β-Sheet, and Random Coil Regions Calculated from Proteins. *Biochemistry* **1974,** 13, 211-222.

37. Grigg, R.; Gunaratne, H. Q. N.; Kemp, J., X=Y-Zh Systems as Potential 1,3-Dipoles .1. Background and Scope. *Journal of the Chemical Society-Perkin Transactions 1* **1984**, 41-46.

38. Ooi, T.; Kameda, M.; Maruoka, K., Molecular Design of a C2-Symmetric Chiral Phase-Transfer Catalyst for Practical Asymmetric Synthesis of α-Amino Acids. *J. Am. Chem. Soc.* **1999,** 121, 6519-6520.

39. Odonnell, M. J.; Wu, S. D.; Huffman, J. C., A New Active Catalyst Species for Enantioselective Alkylation by Phase-Transfer Catalysis. *Tetrahedron* **1994,** 50, 4507-4518.

40. Odonnell, M. J.; Wojciechowski, K.; Ghosez, L.; Navarro, M.; Sainte, F.; Antoine, J. P., Alkylation of Protected α-Amino Acid Derivatives in the Presence of Potassium Carbonate. *Synthesis-Stuttgart* **1984**, 313-315.

41. Dale, J. A.; Dull, D. L.; Mosher, H. S., α-Methoxy-α-trifluoromethylphenylacetic acid, a versatile reagent for the determination of enantiomeric composition of alcohols and amines. *J. Org. Chem.* **1969,** 34, 2543-2549.

42. Hofle, G.; Steglich, W.; Vorbruggen, H., 4-Dialkylaminopyridines as Acylation Catalysts. 4,4-Dialkylaminopyridines as Highly Active Acylation Catalysts. *Angewandte Chemie-International Edition in English* **1978,** 17, 569-583.

43. Krchnak, V.; Vagner, J.; Lebl, M., Noninvasive Continuous Monitoring of Solid-Phase Peptide-Synthesis by Acid-Base Indicator. *International Journal of Peptide and Protein Research* **1988,** 32, 415-416.

44. Kaiser, E.; Colescot.Rl; Bossinge.Cd; Cook, P. I., Color Test for Detection of Free Terminal Amino Groups in Solid-Phase Synthesis of Peptides. *Anal. Biochem.* **1970,** 34, 595-598.

APPENDIX A
MALDI-MS SPECTRA OF PEPTIDES AND DIBG

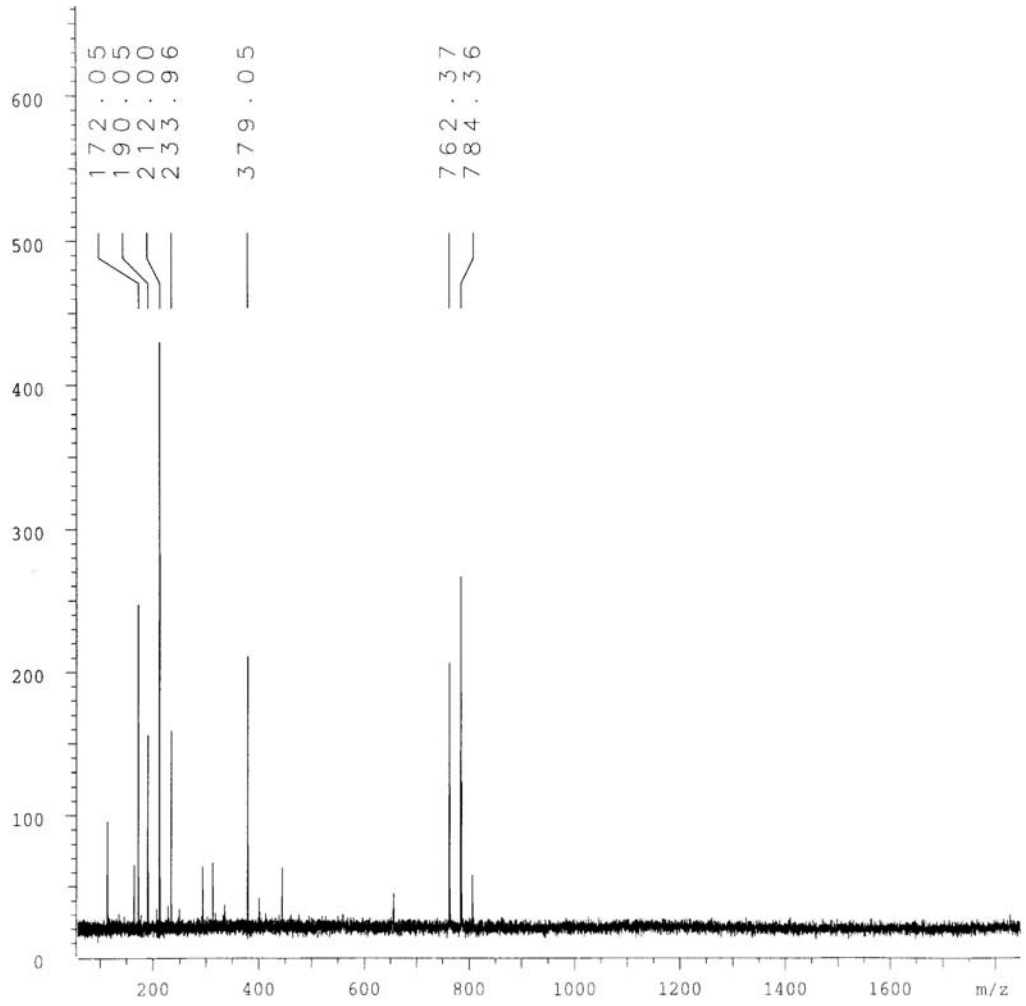

EK-Dpg-Y

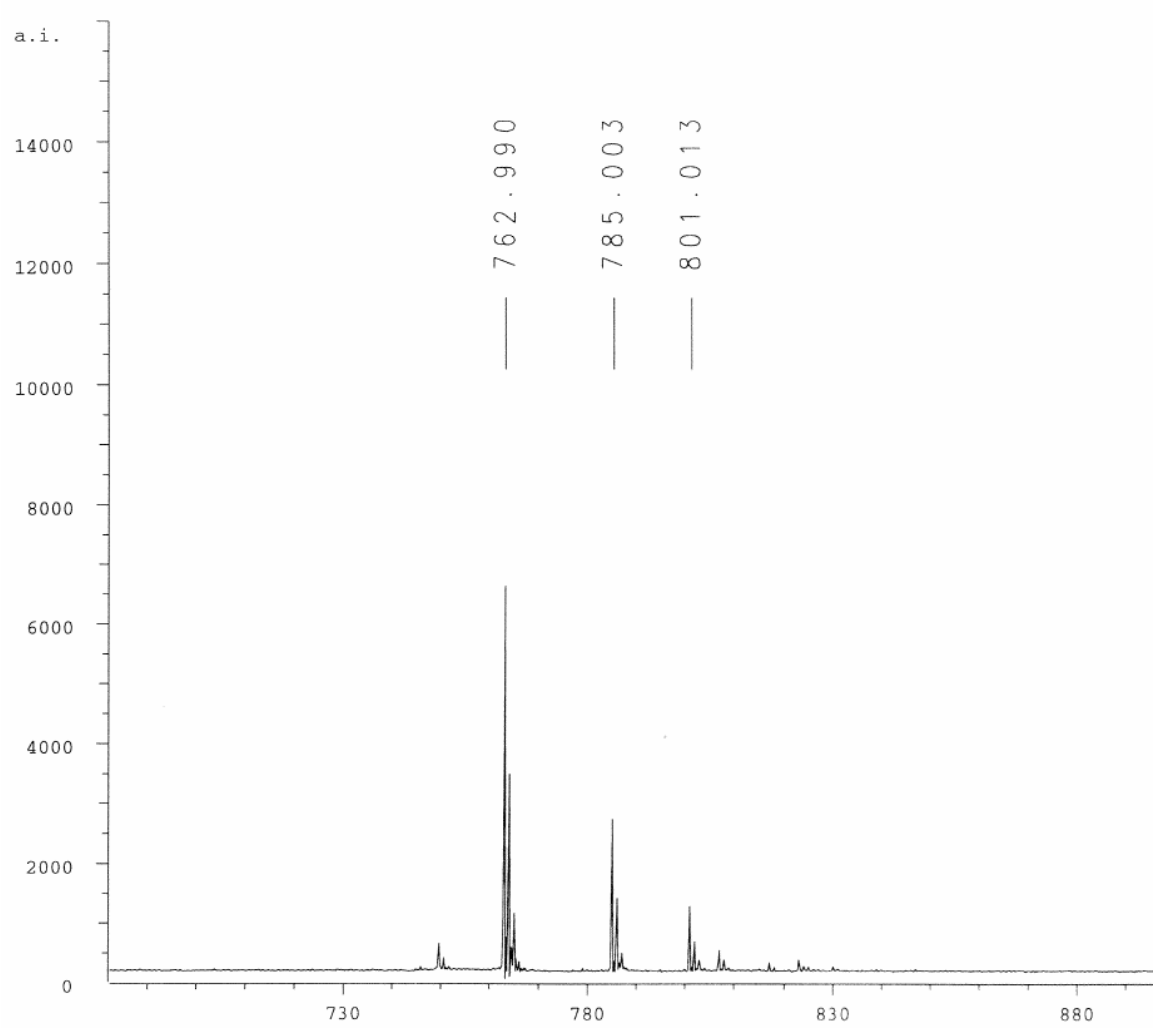
a.i.
14000
12000
10000
8000
6000
4000
2000
0
762.990
785.003
801.013
730
780
830
880

KE-Dpg-Y

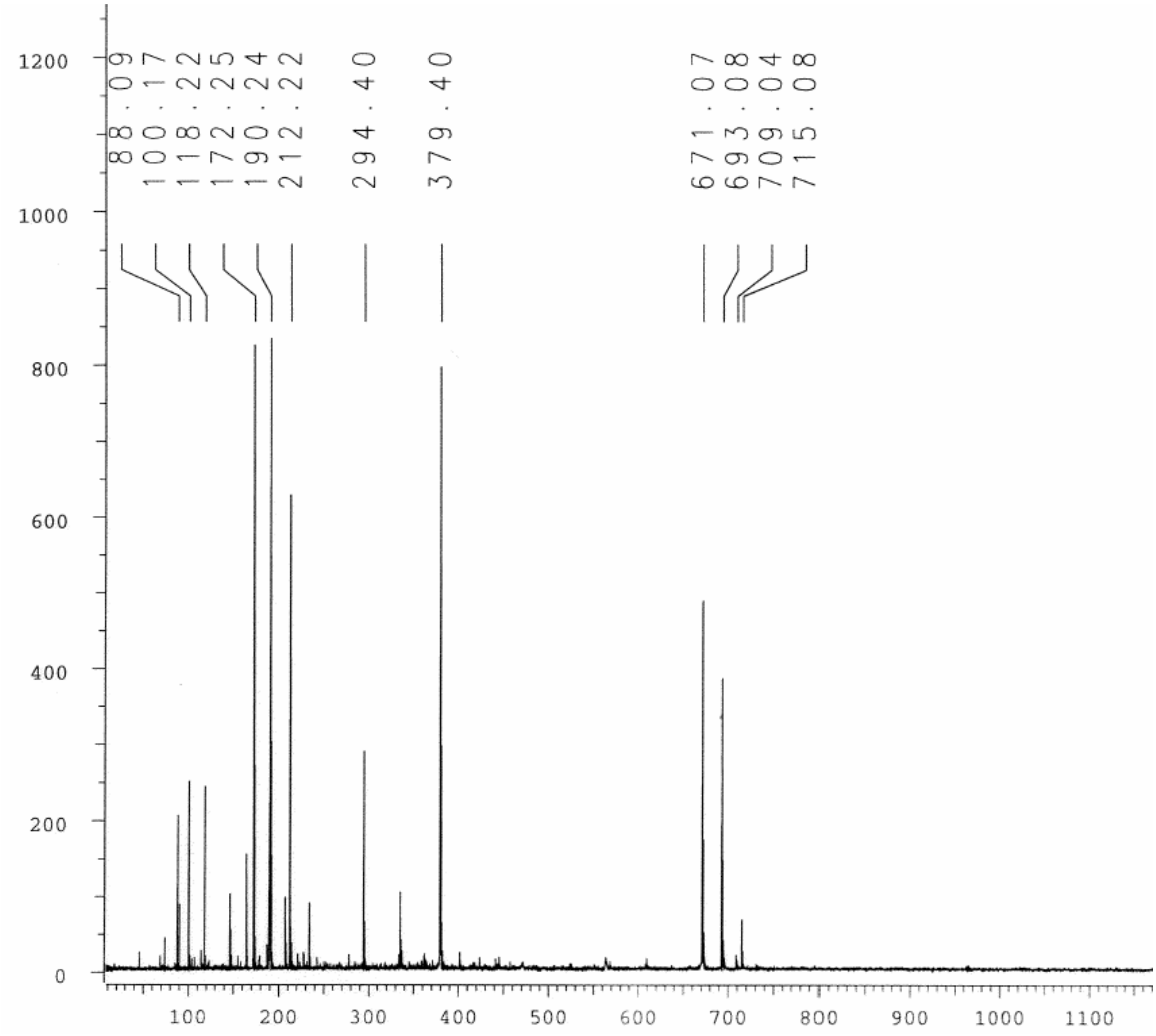
88.09
100.17
118.22
172.25
190.24
212.22
294.40
379.40
671.07
693.08
709.04
715.08
1200
1000
800
600
400
200
0
100
200
300
400
500
600
700
800
900
1000
1100

EK-Dpg-A

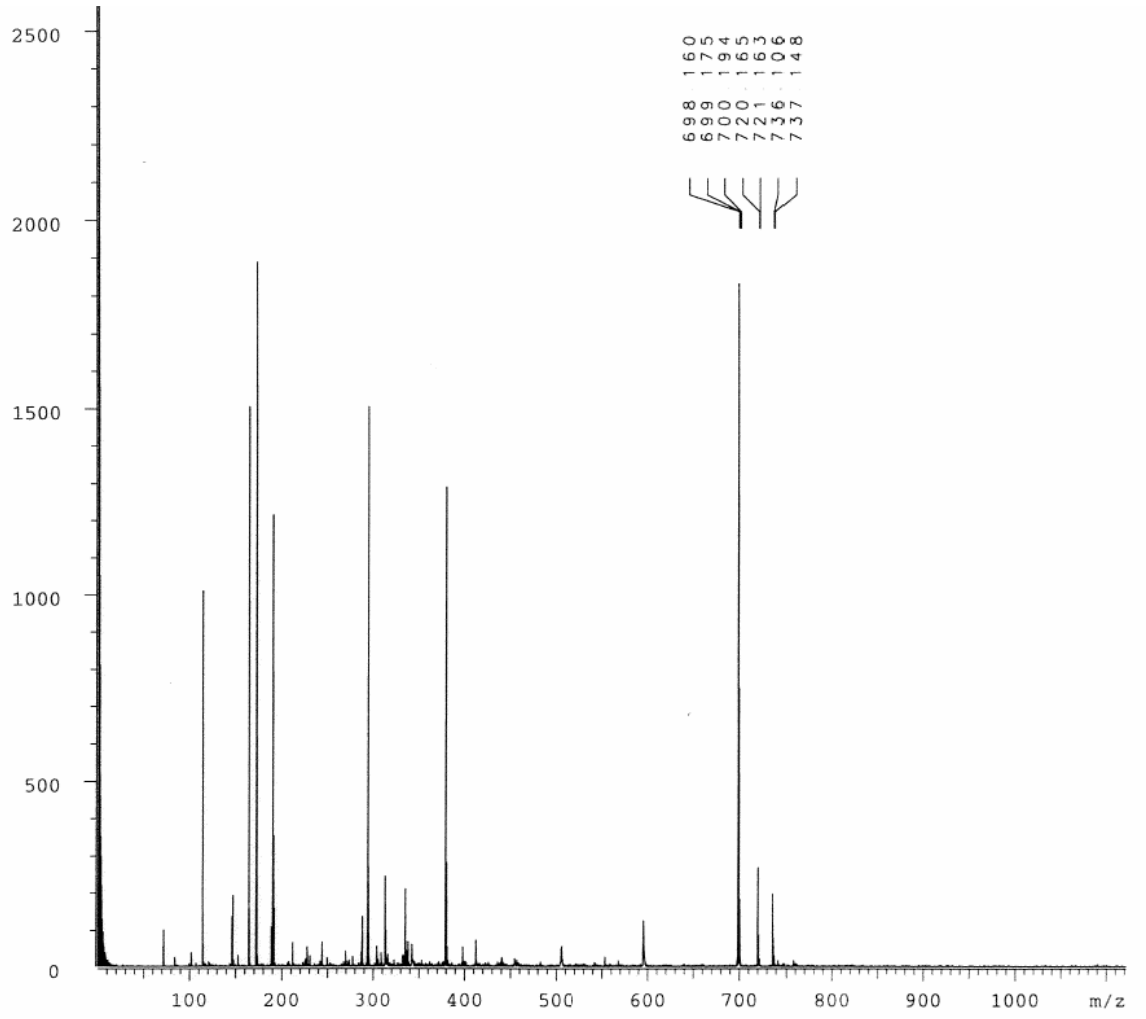
2500
2000
1500
1000
500
0
100
200
300
400
500
600
700
800
900
1000
m/z
698.160
699.175
700.194
720.165
721.163
736.106
737.148

EK-Dpg-V

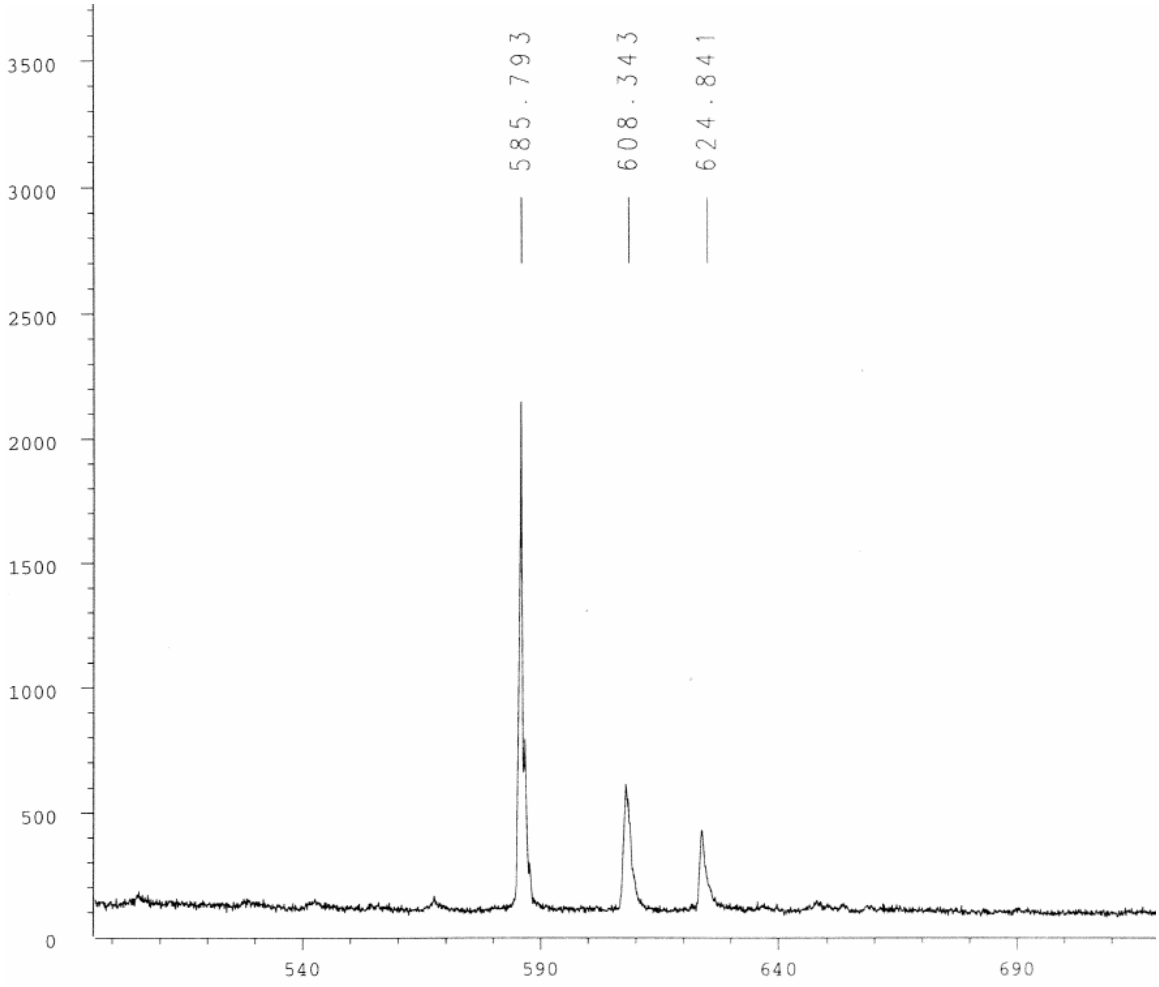
585.793
608.343
624.841
3500
3000
2500
2000
1500
1000
500
0
540
590
640
690

EK-Nva-A

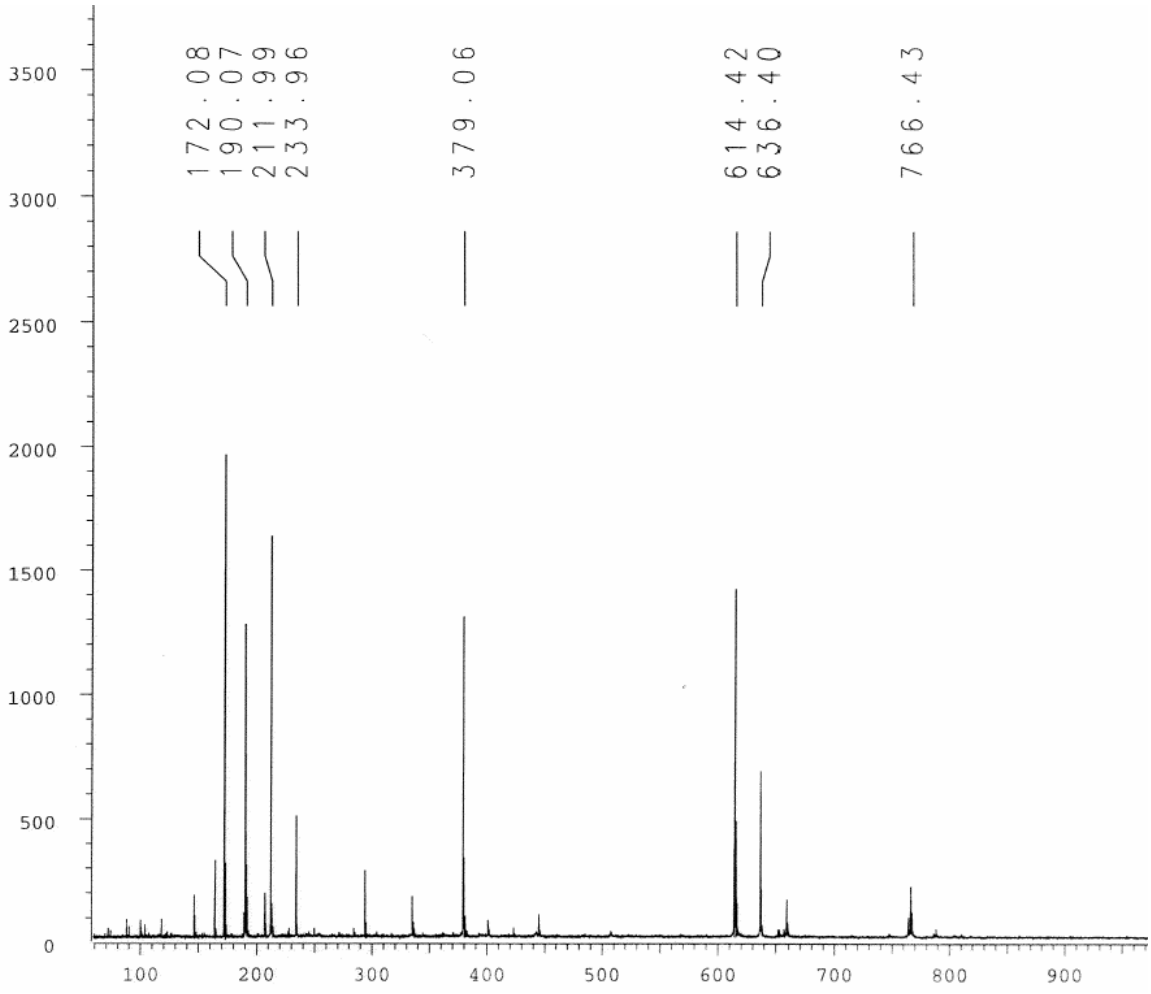
172.08
190.07
211.99
233.96
379.06
614.42
636.40
766.43
3500
3000
2500
2000
1500
1000
500
0
100
200
300
400
500
600
700
800
900

EK-Nva-V

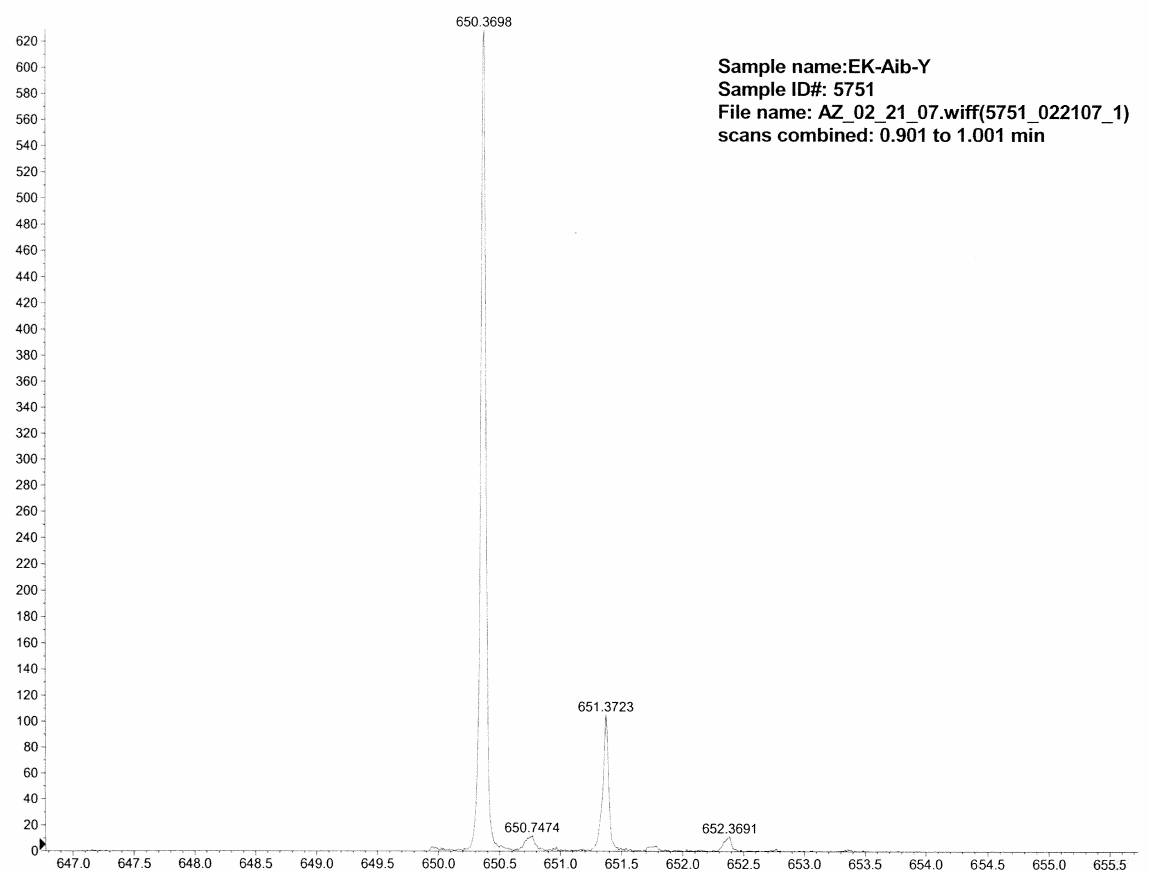
650.3698
Sample name:EK-Aib-Y
Sample ID#: 5751
File name: AZ_02_21_07.wiff(5751_022107_1)
scans combined: 0.901 to 1.001 min
651.3723
650.7474
652.3691

EK-Aib-Y

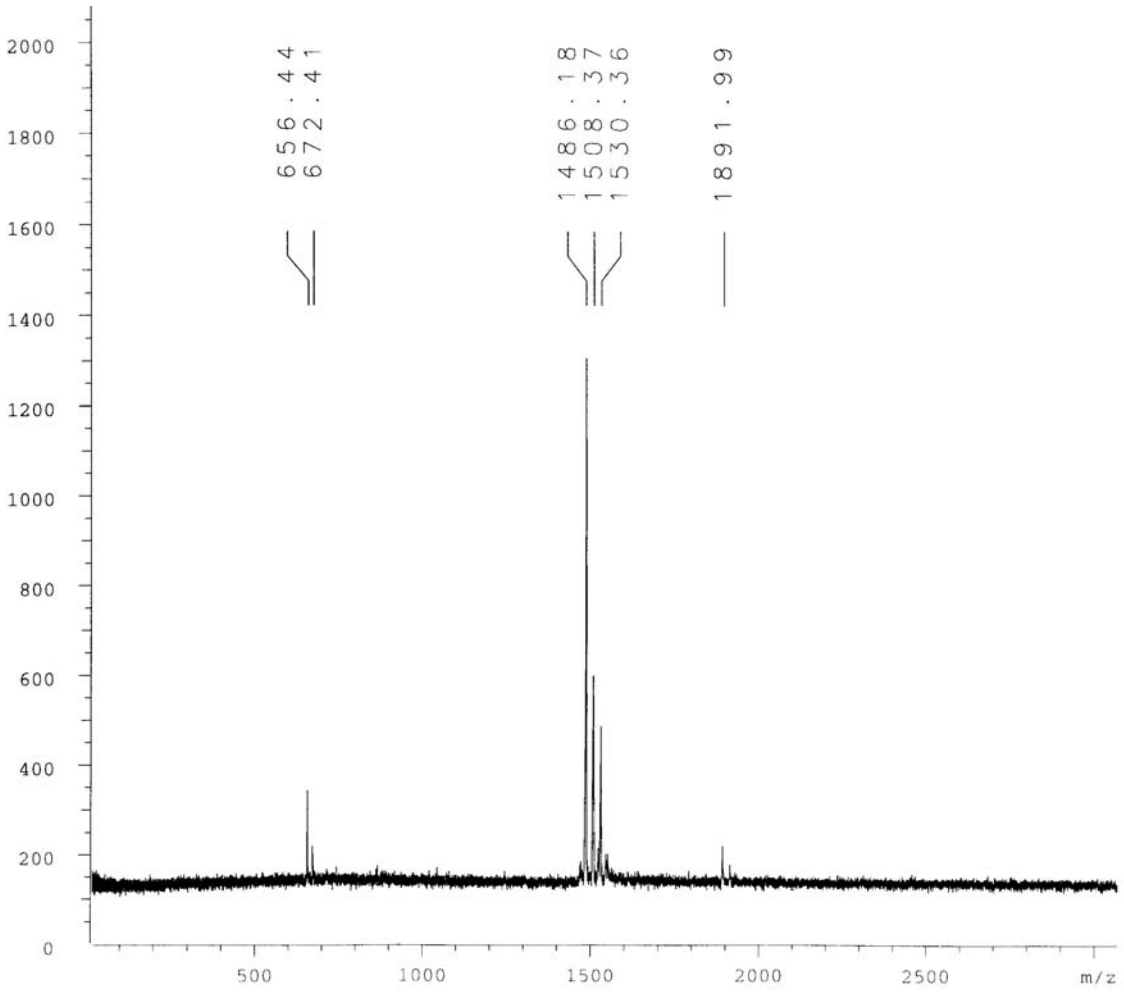
656.44
672.41
1486.18
1508.37
1530.36
1891.99
2000
1800
1600
1400
1200
1000
800
600
400
200
0
500
1000
1500
2000
2500
m/z

Dibg^3-GHP

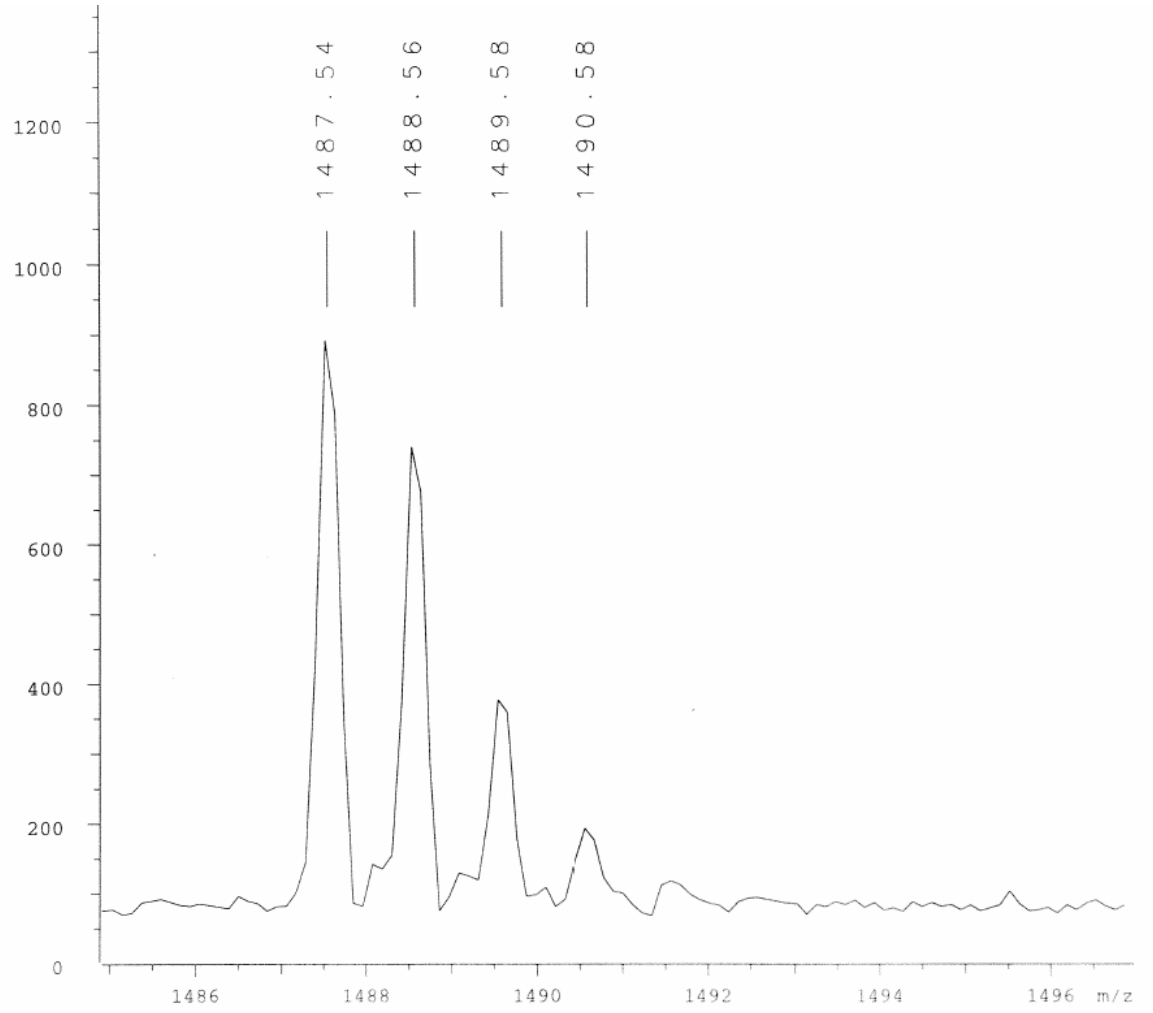
1487.54
1488.56
1489.58
1490.58
1200
1000
800
600
400
200
0
1486
1488
1490
1492
1494
1496
m/z

Dibg^{6}-GHP

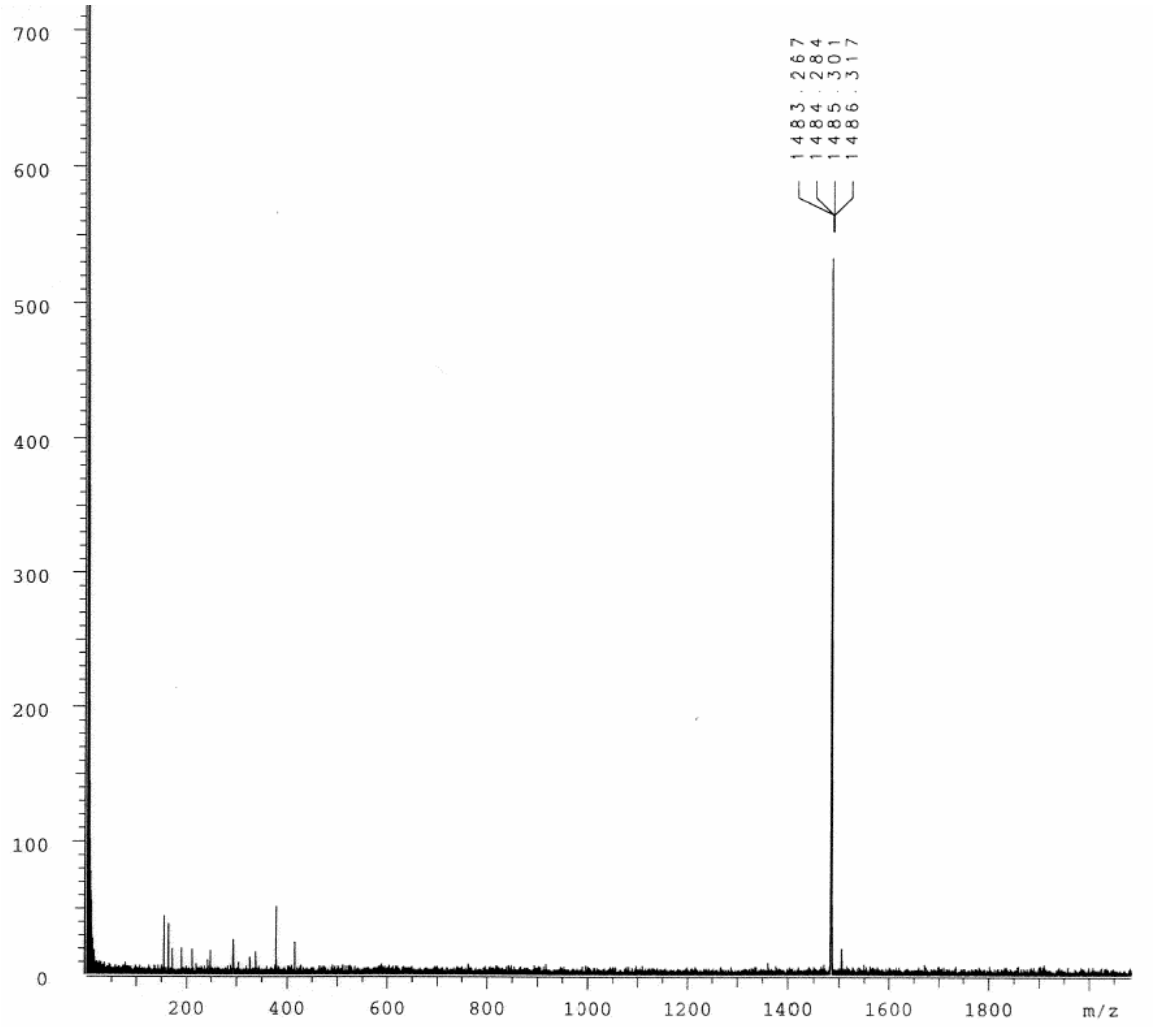
1483.267
1484.284
1485.301
1486.317
700
600
500
400
300
200
100
0
200
400
600
800
1000
1200
1400
1600
1800
m/z

Dibg^{3}-NG

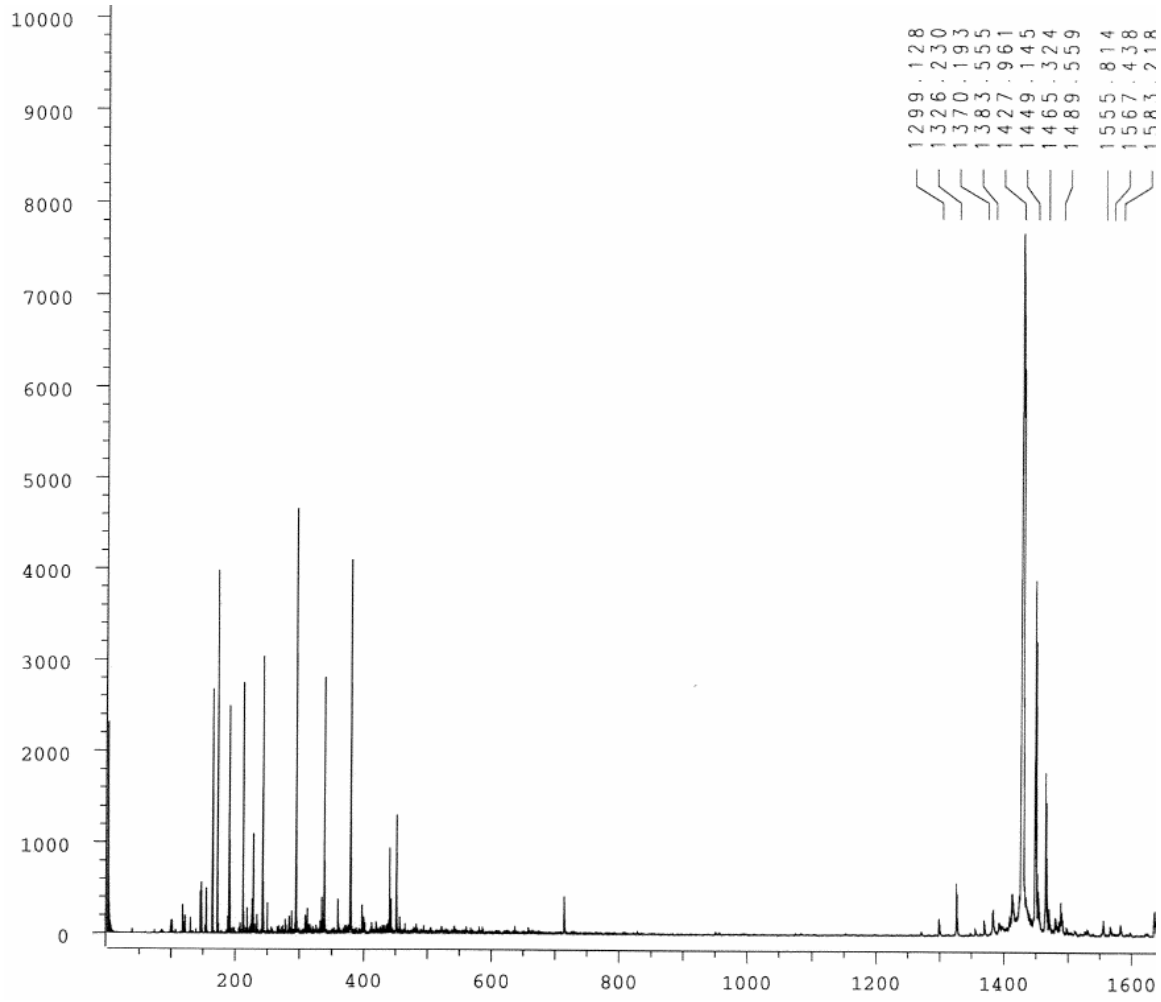
10000
9000
8000
7000
6000
5000
4000
3000
2000
1000
0
200
400
600
800
1000
1200
1400
1600
1299.128
1326.230
1370.193
1383.555
1427.961
1449.145
1465.324
1489.559
1555.814
1567.438

Leu^3-NG

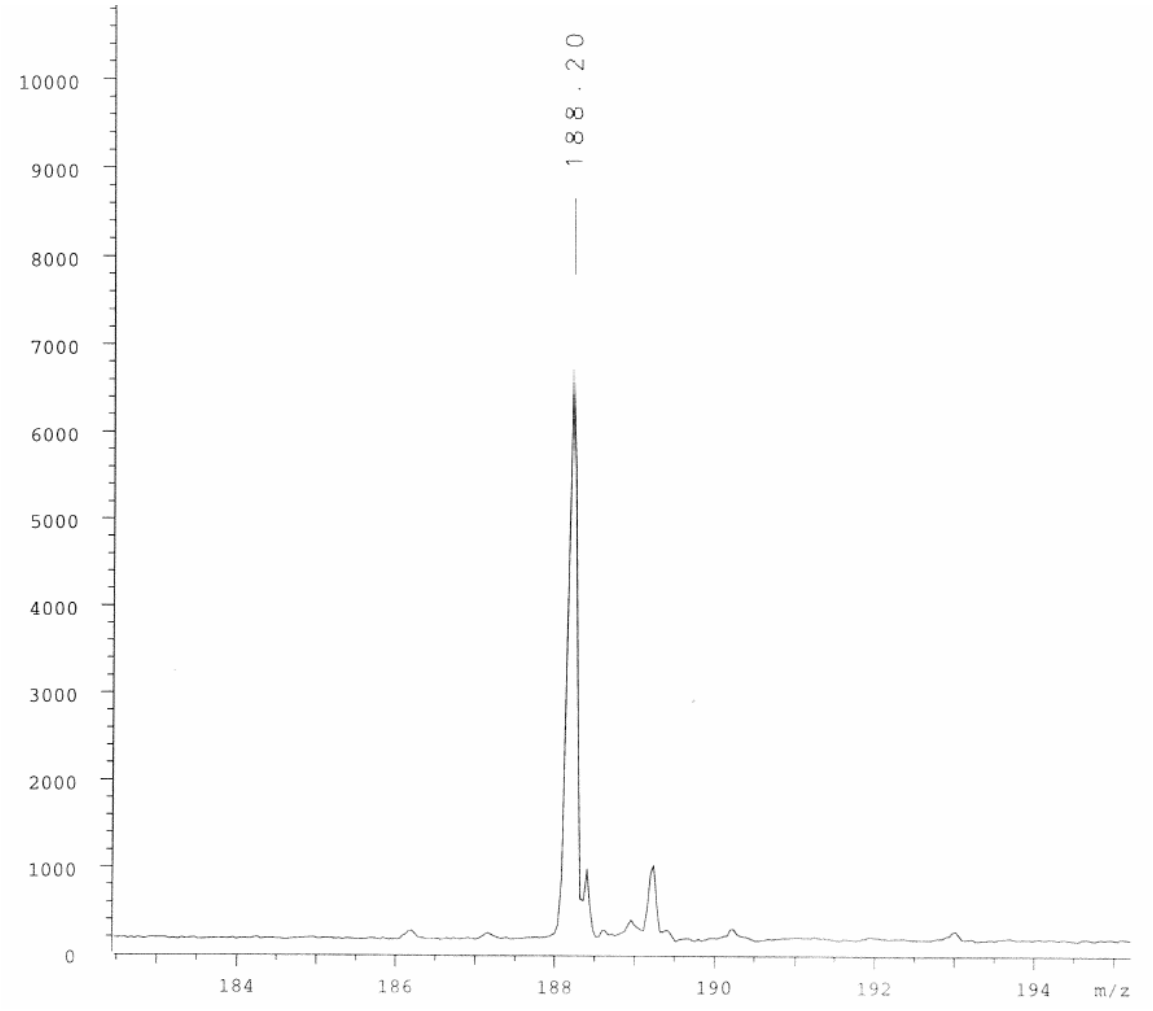
188.20
10000
9000
8000
7000
6000
5000
4000
3000
2000
1000
0
184
186
188
190
192
194
m/z

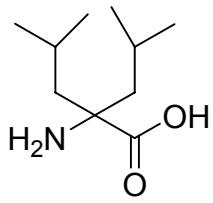
H2N
OH
O

Free Dibg

APPENDIX B
NMR SPECTRA OF COMPOUNDS AND PEPTIDES

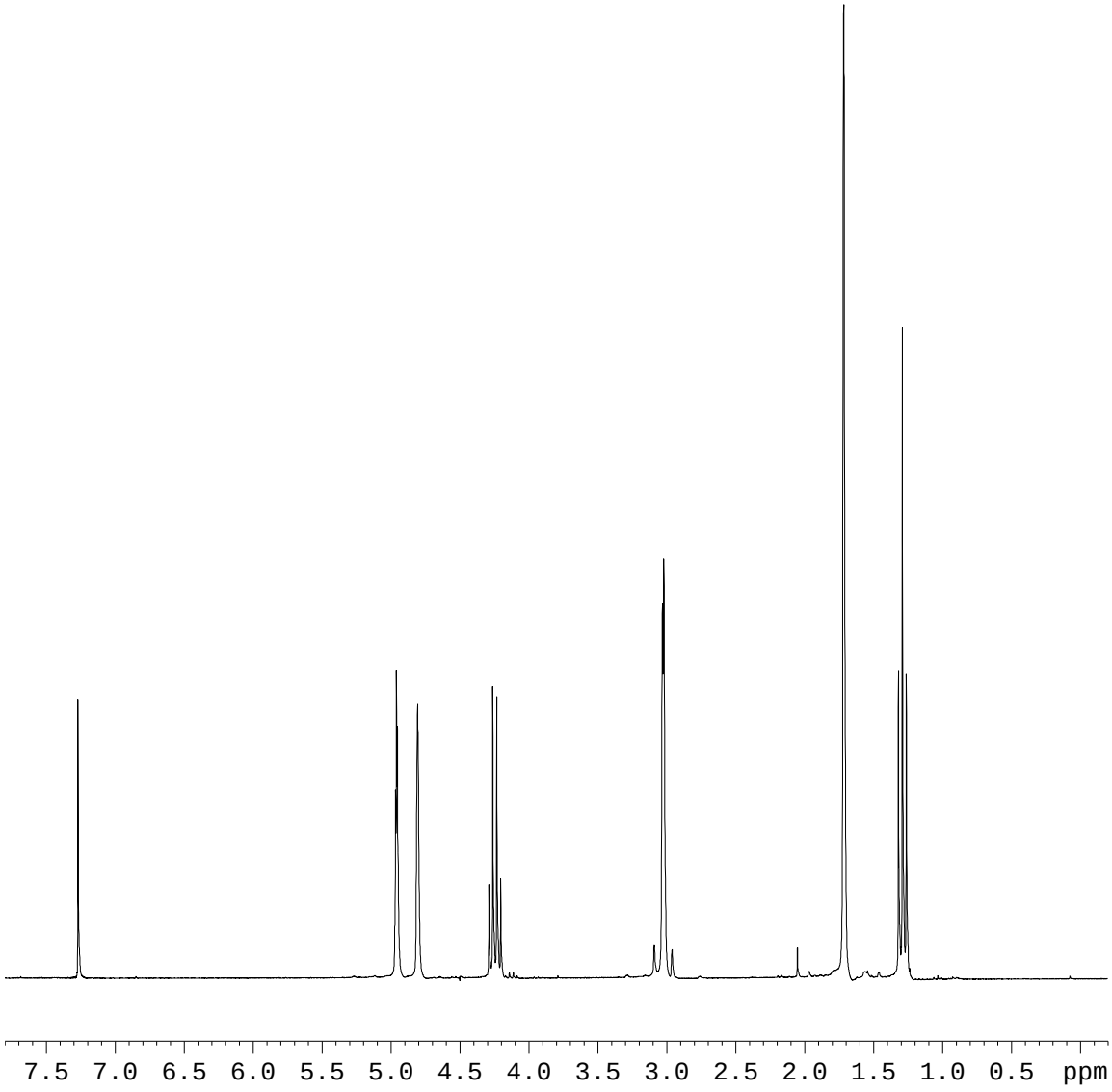

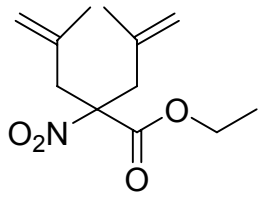

^{1}H NMR in $CDCl_3$

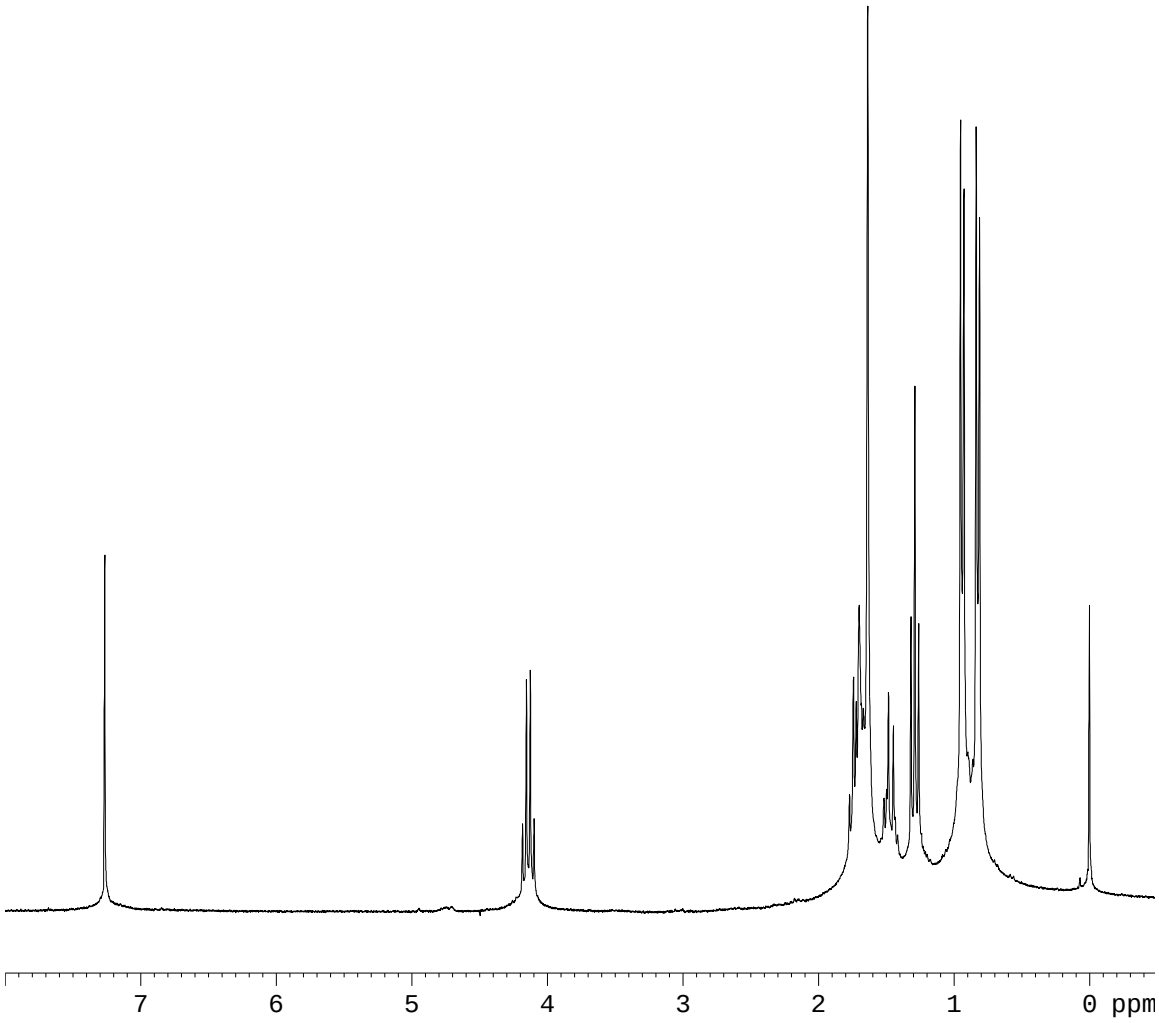

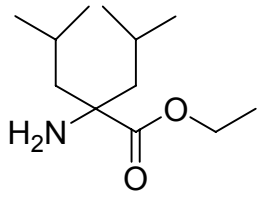

^{1}H NMR in $CDCl_3$

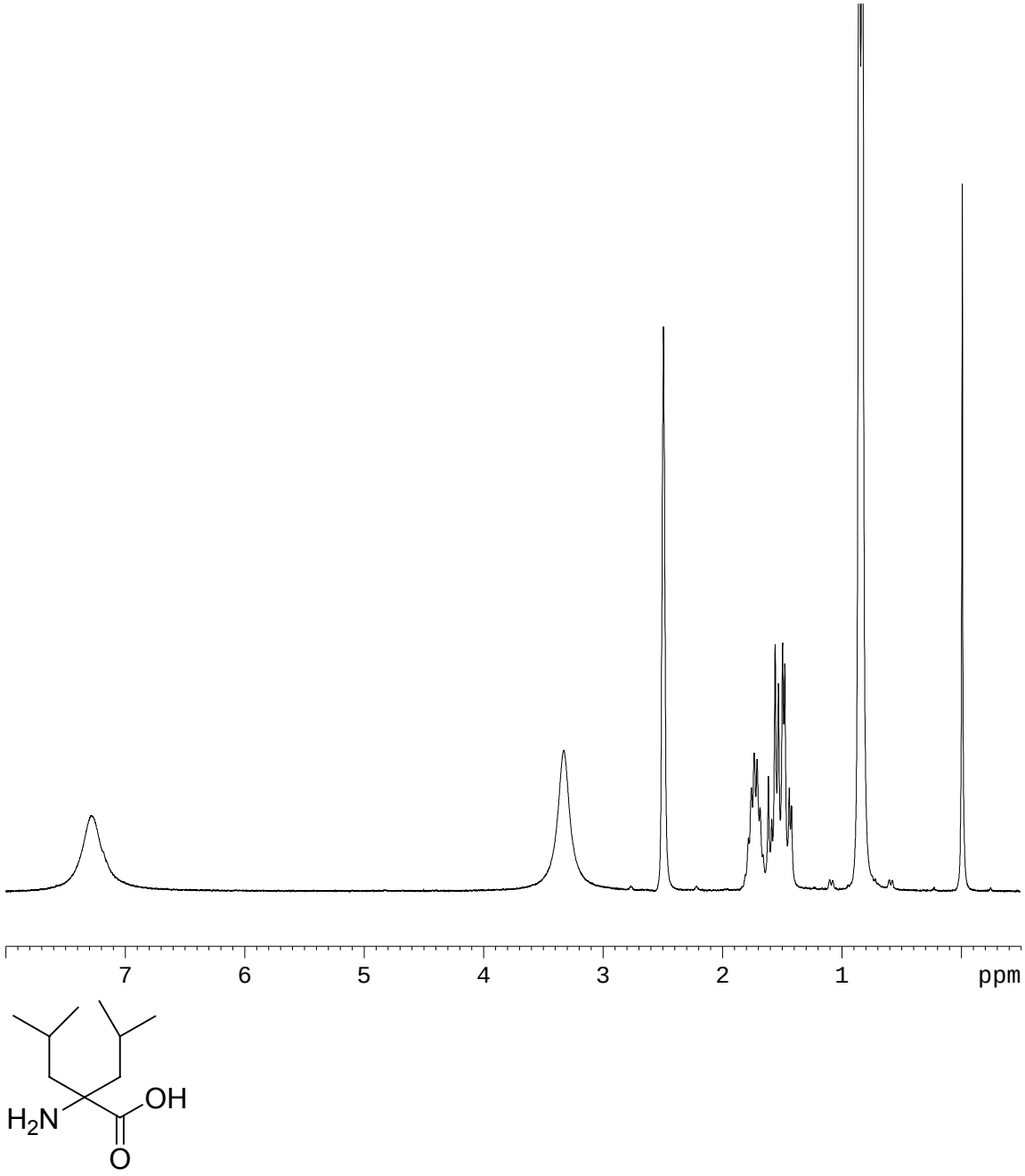

^{1}H NMR in DMSO-d_6

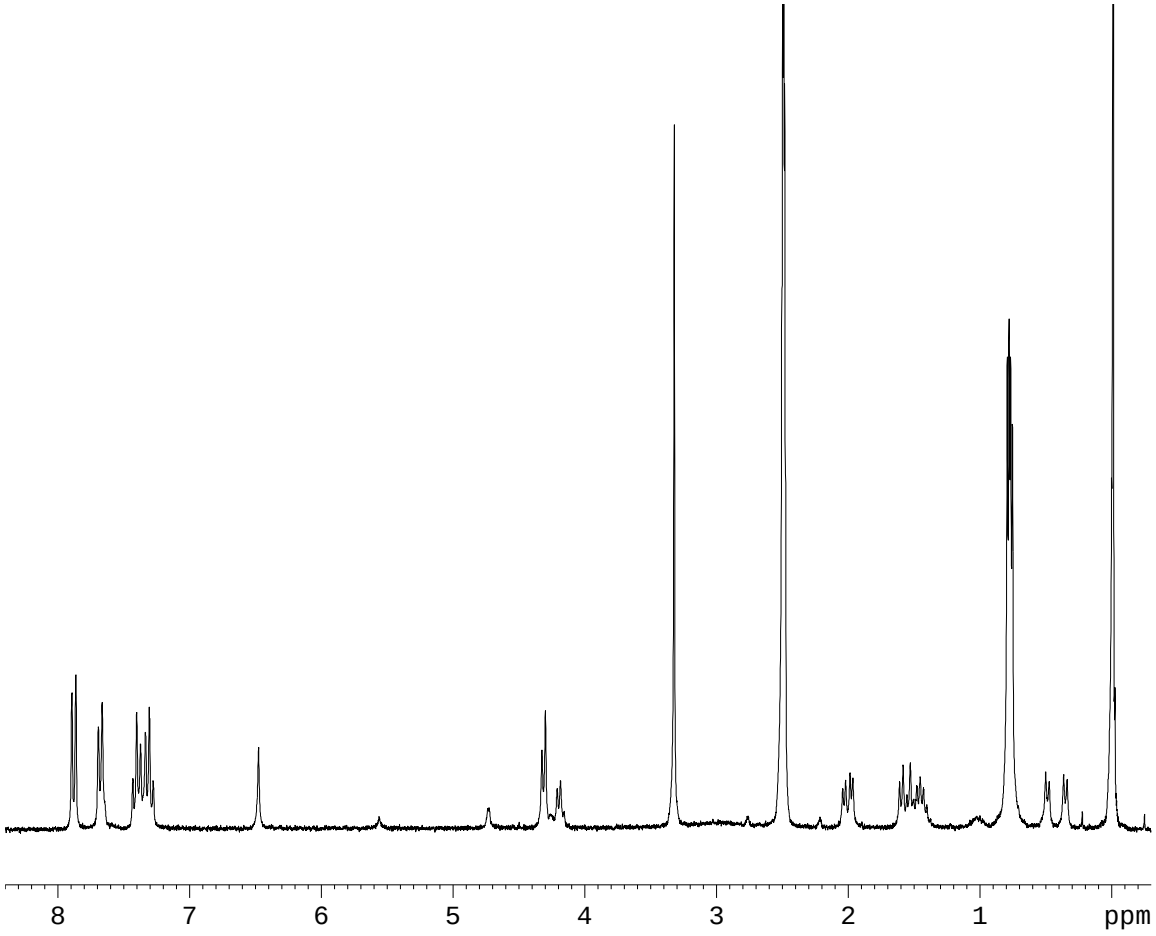

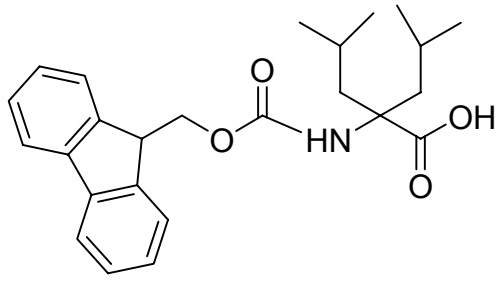

^{1}H NMR in DMSO-d_6

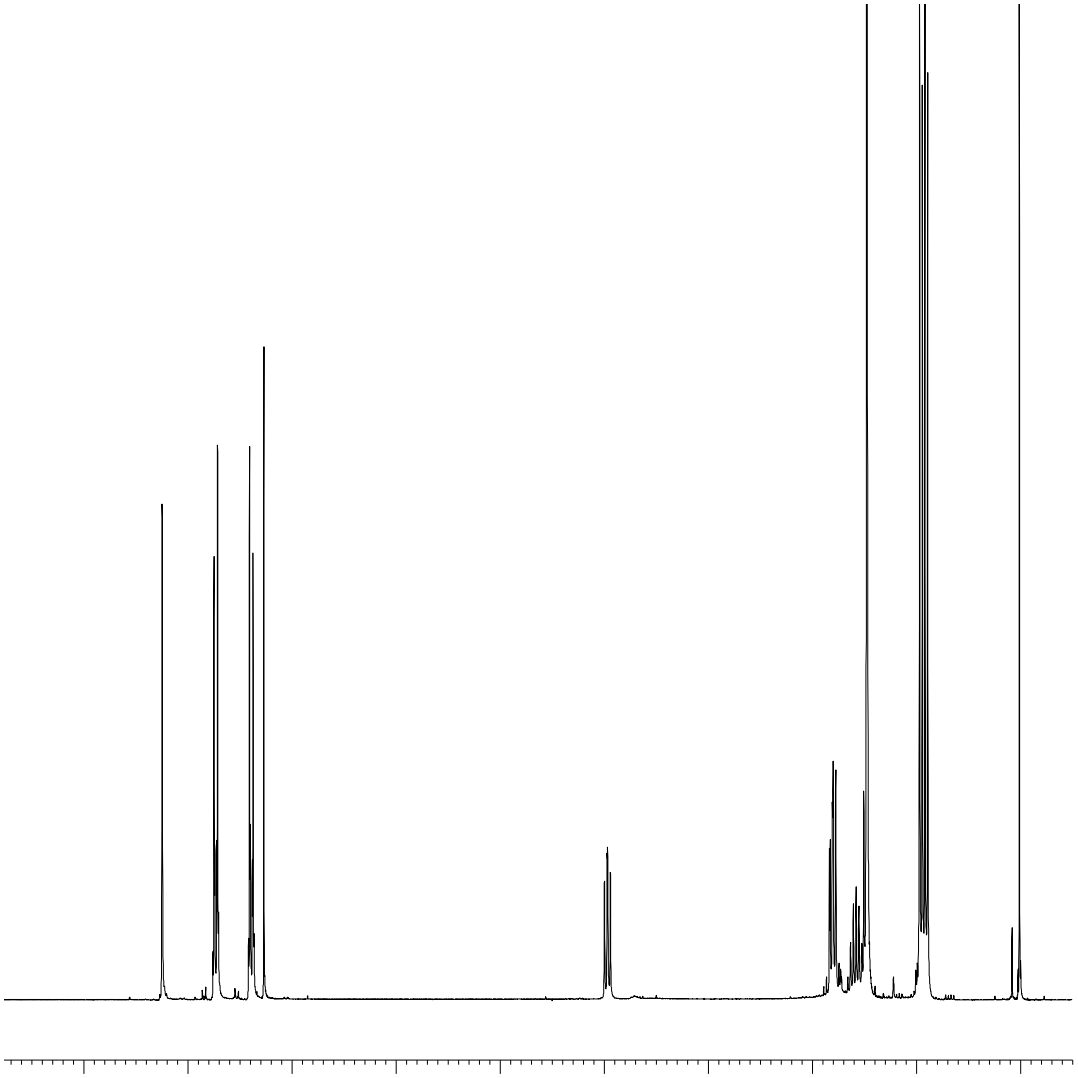

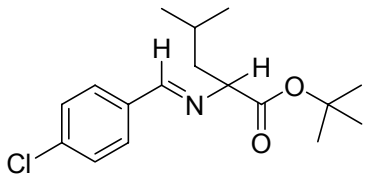

^{1}H NMR in $CDCl_3$

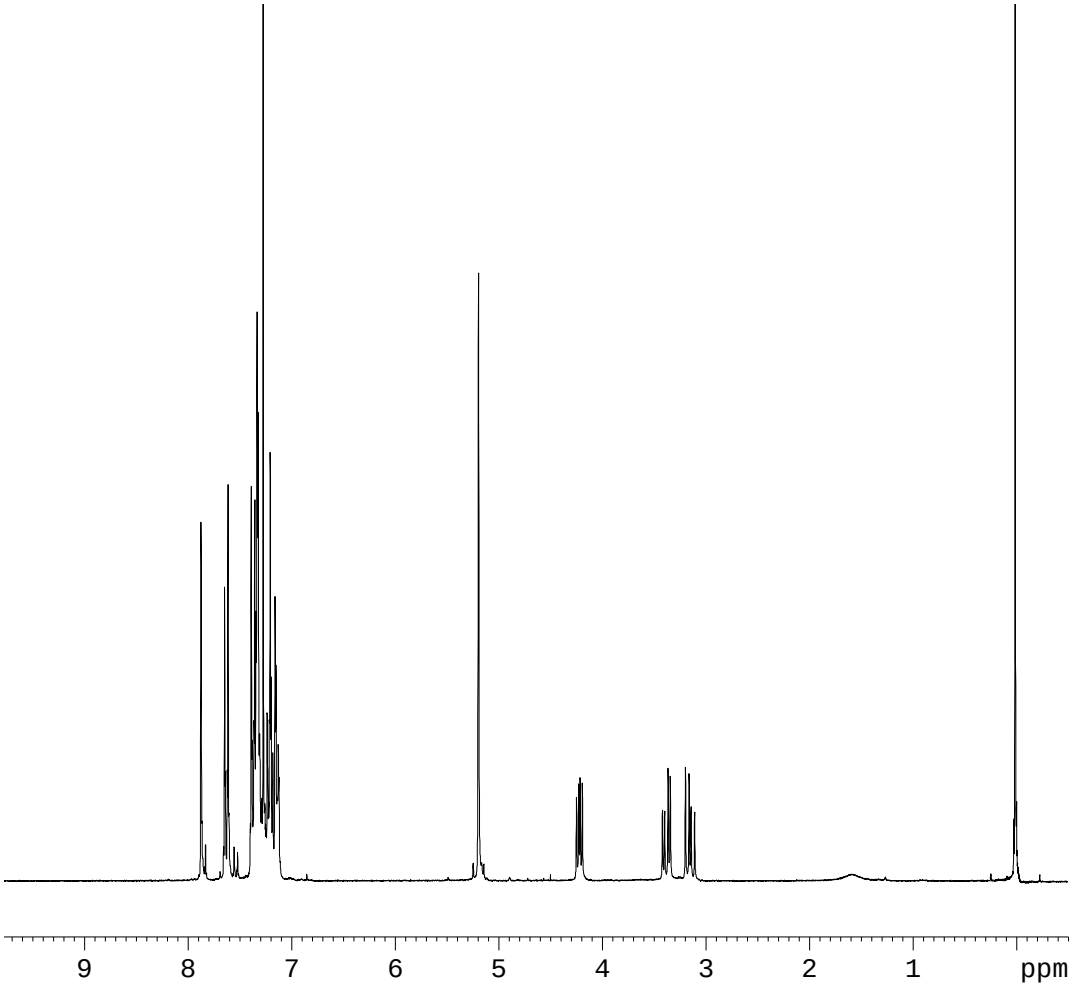

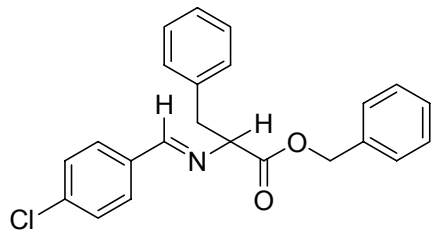

^{1}H NMR in $CDCl_3$

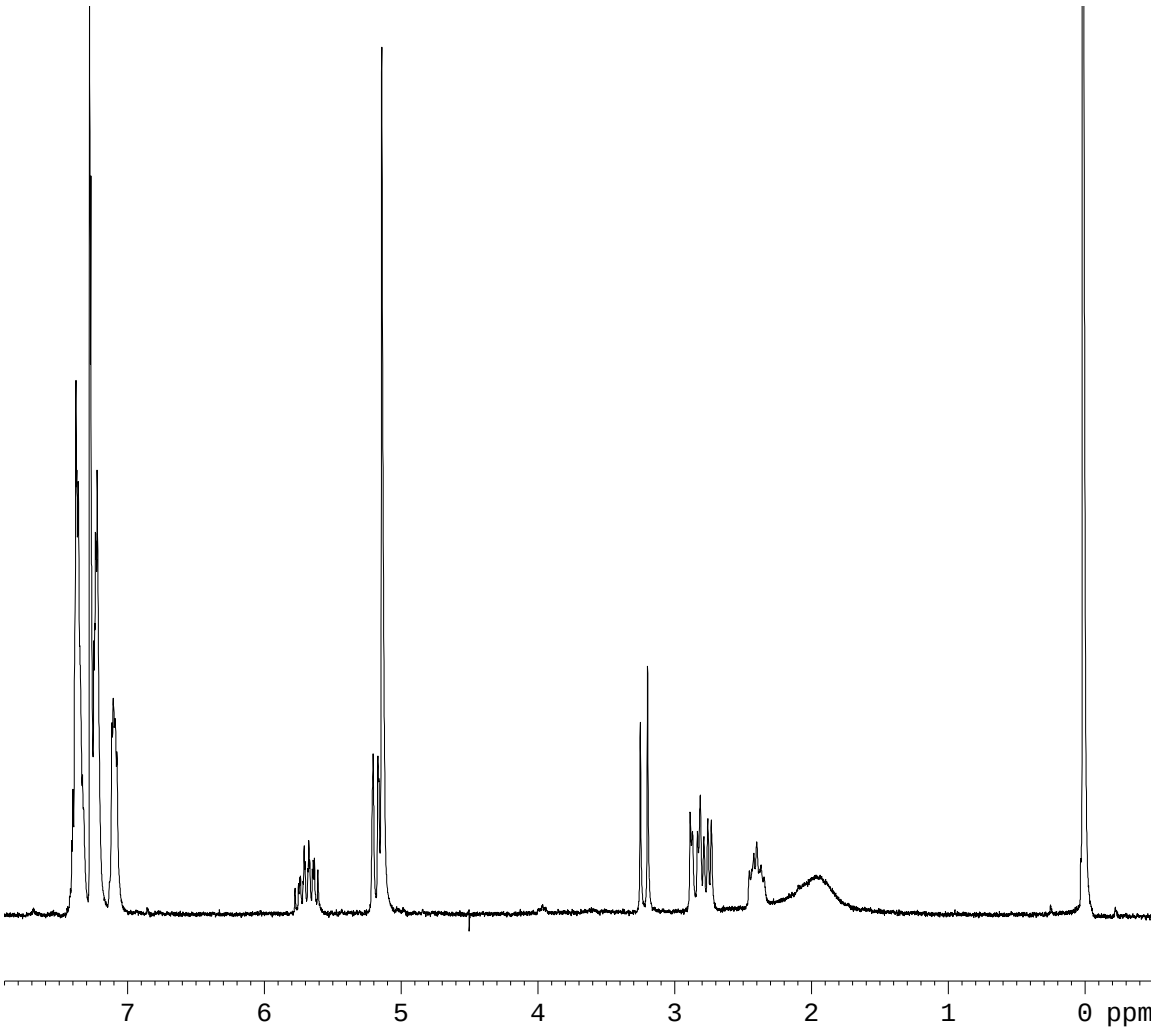

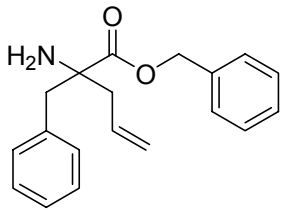

^{1}H NMR in $CDCl_3$

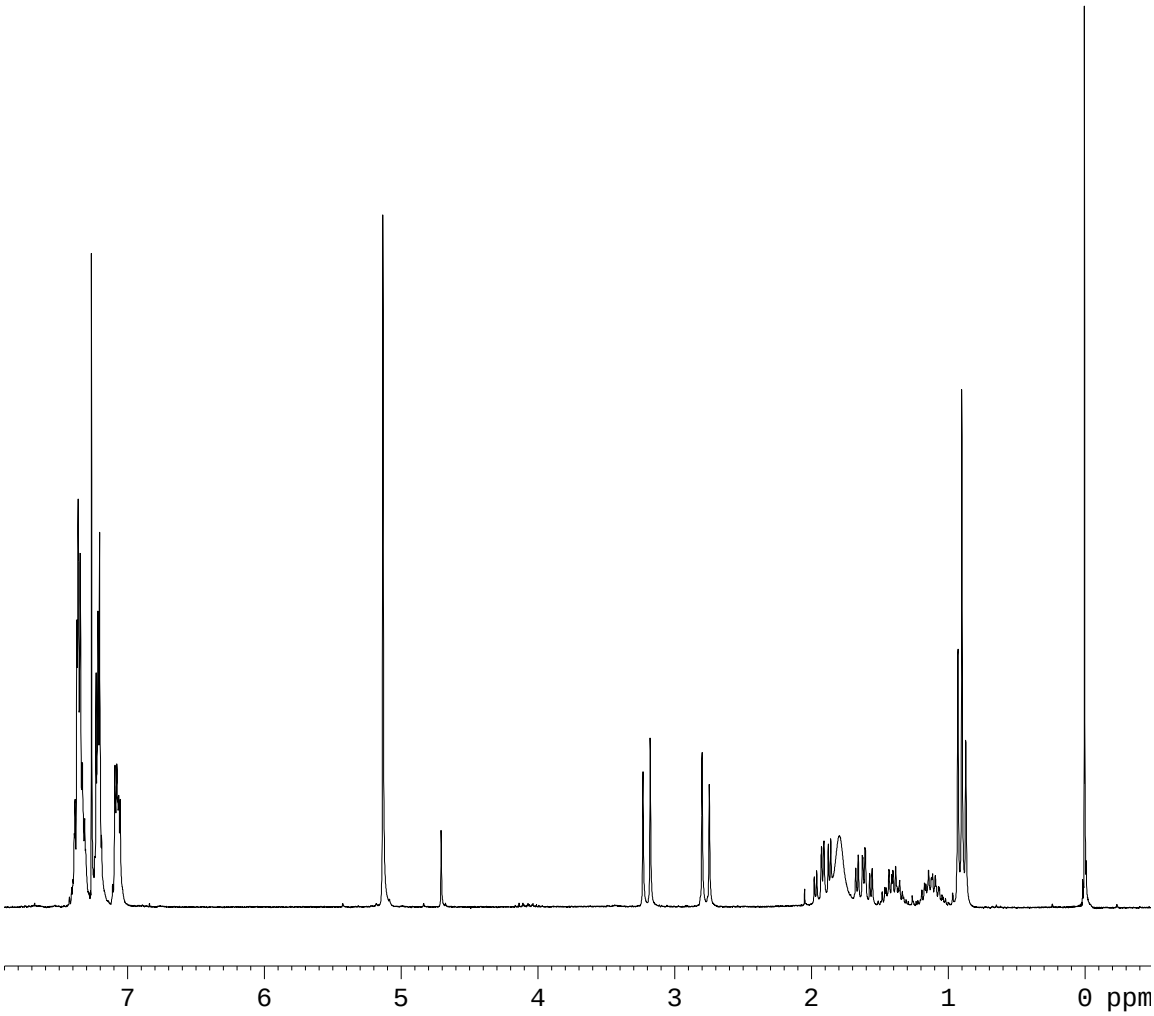

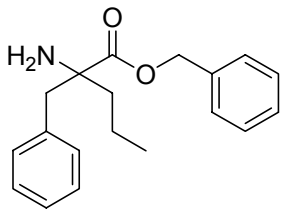

^{1}H NMR in $CDCl_3$

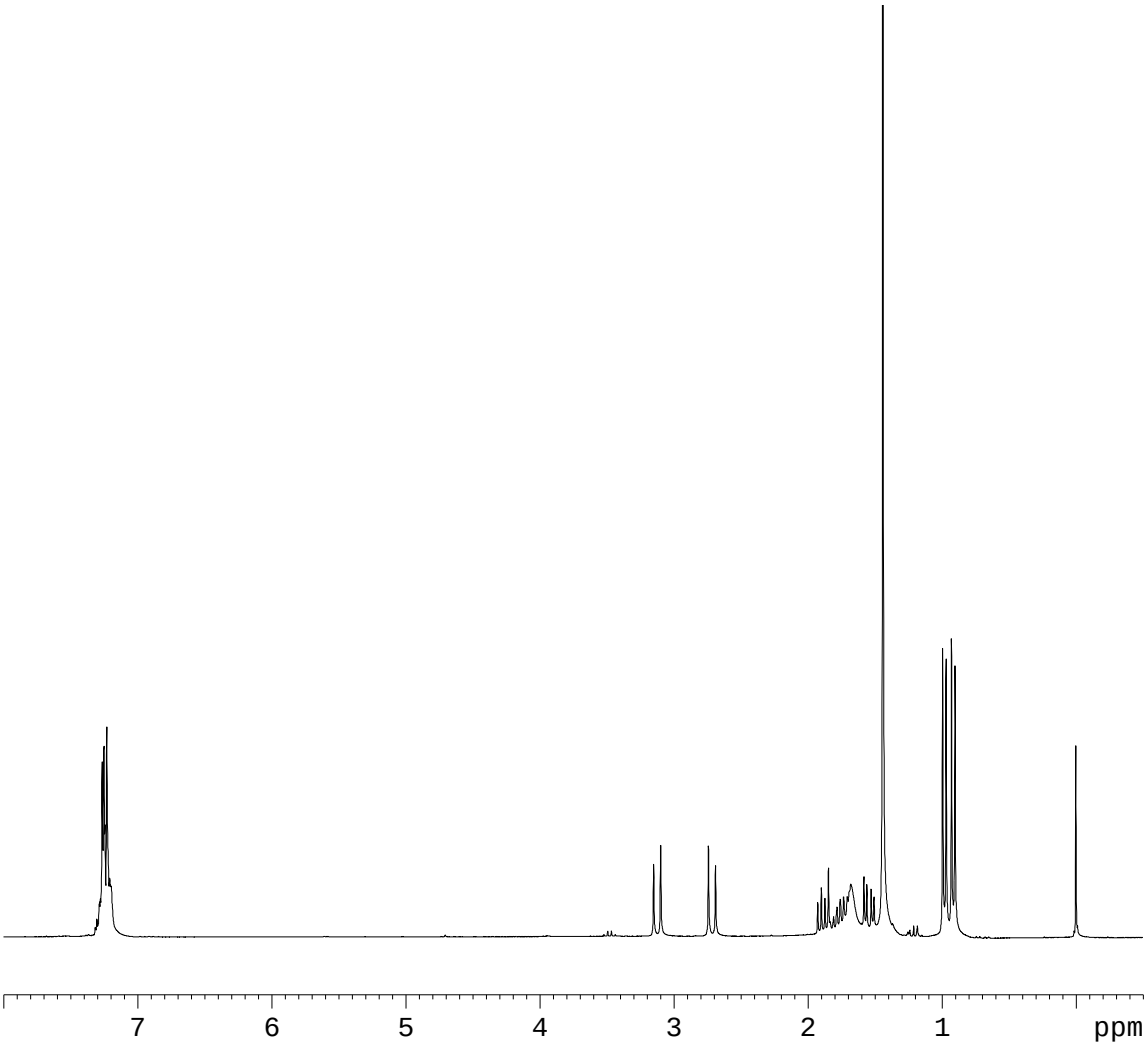

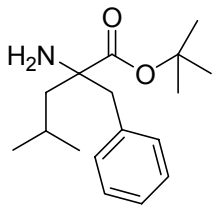

^{1}H NMR in $CDCl_3$

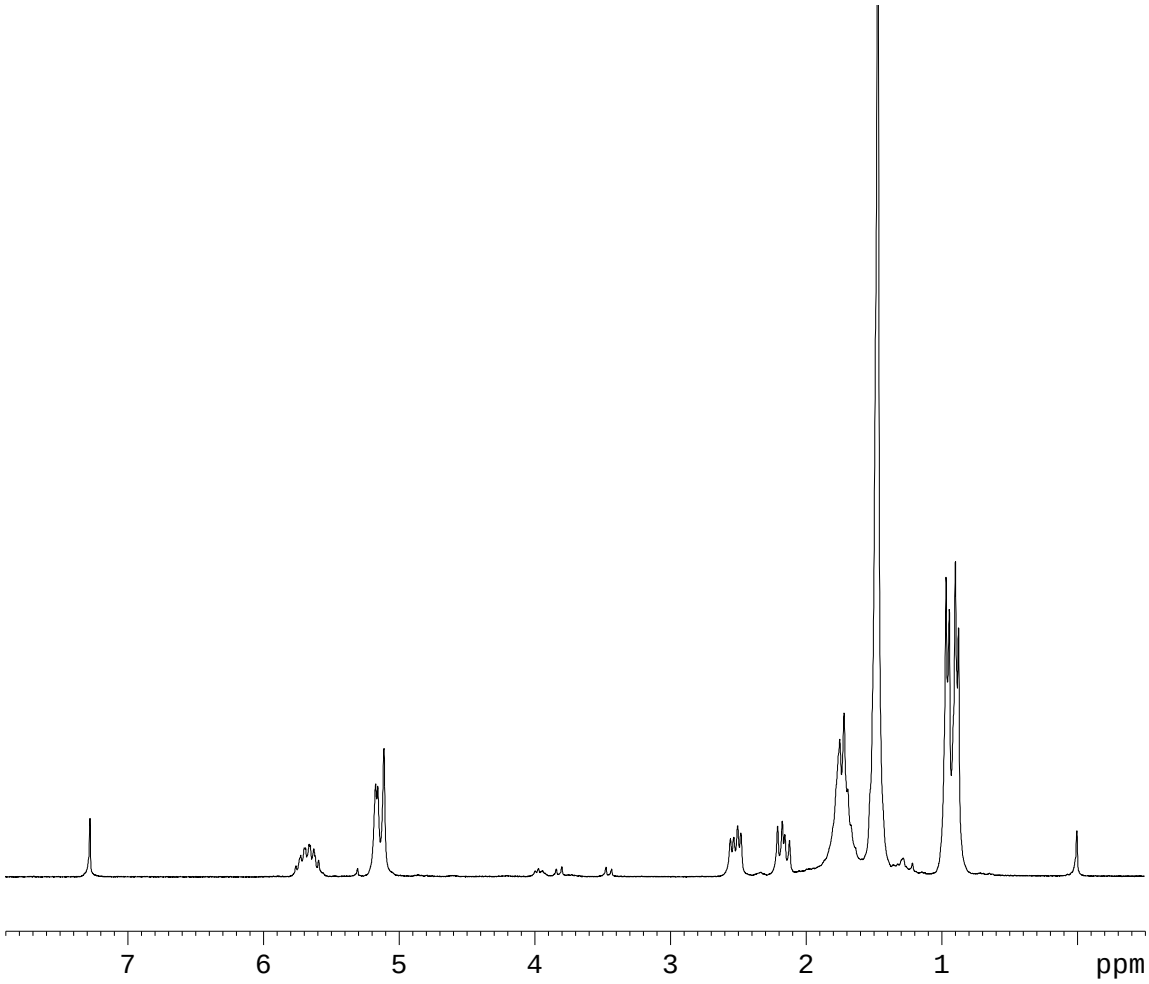

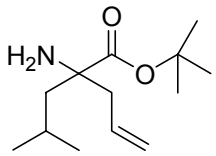

^{1}H NMR in $CDCl_3$

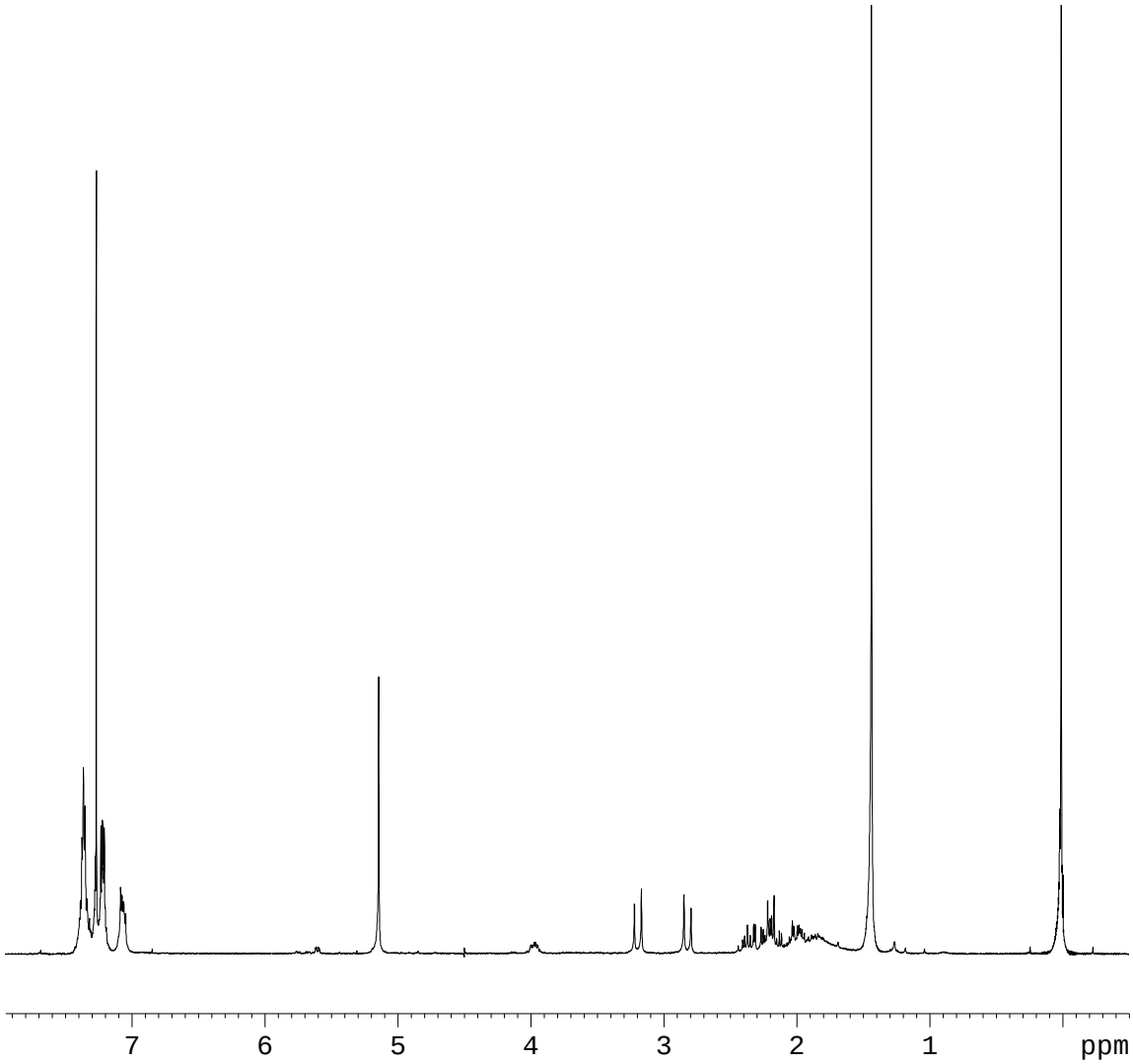

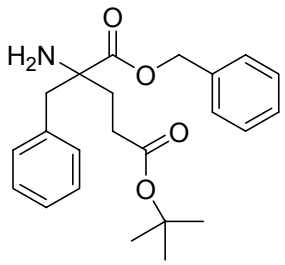

^{1}H NMR in $CDCl_3$

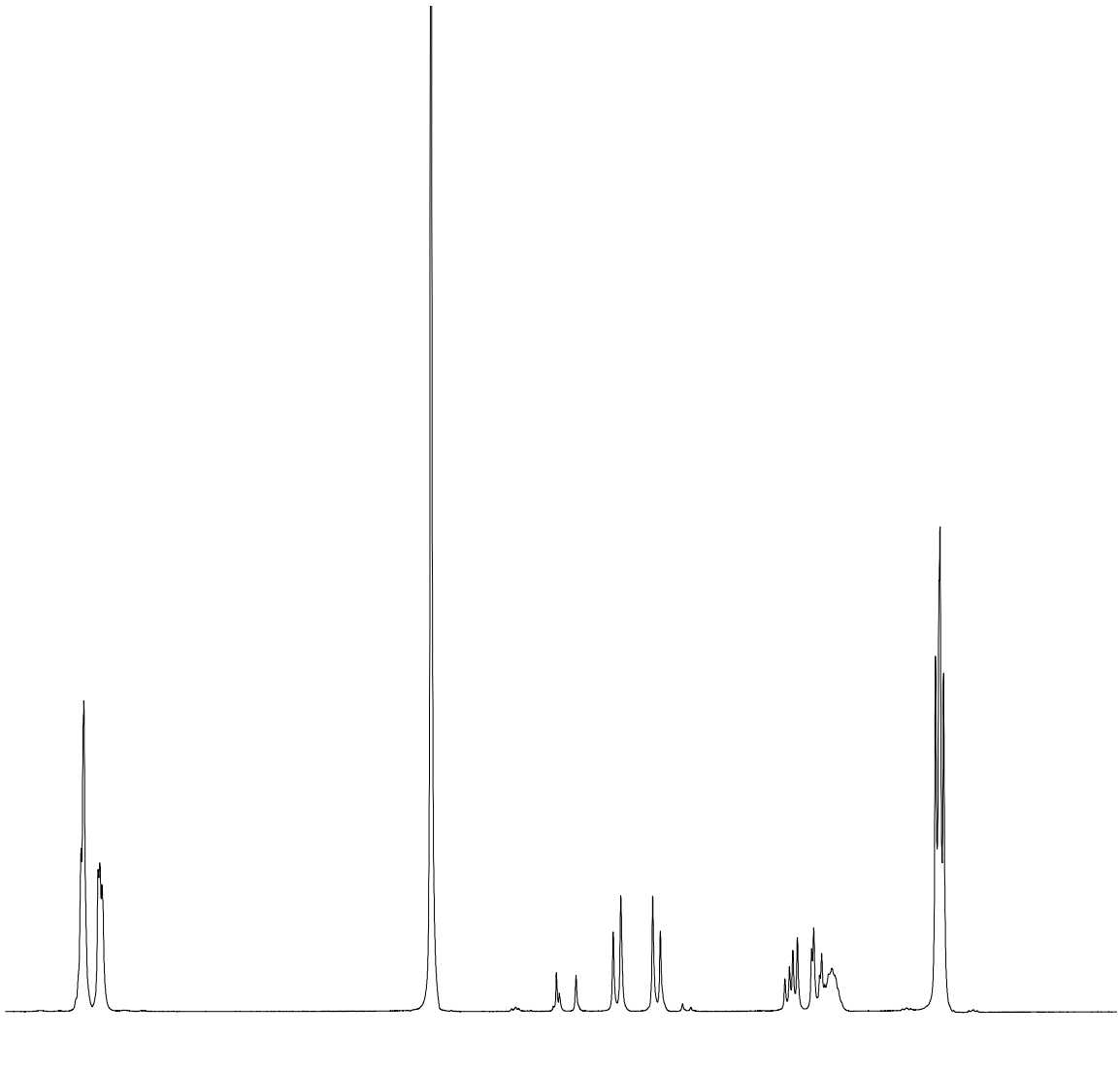

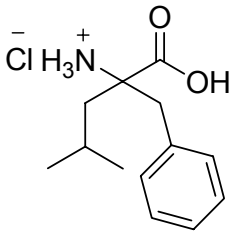

^{1}H NMR in D_2O

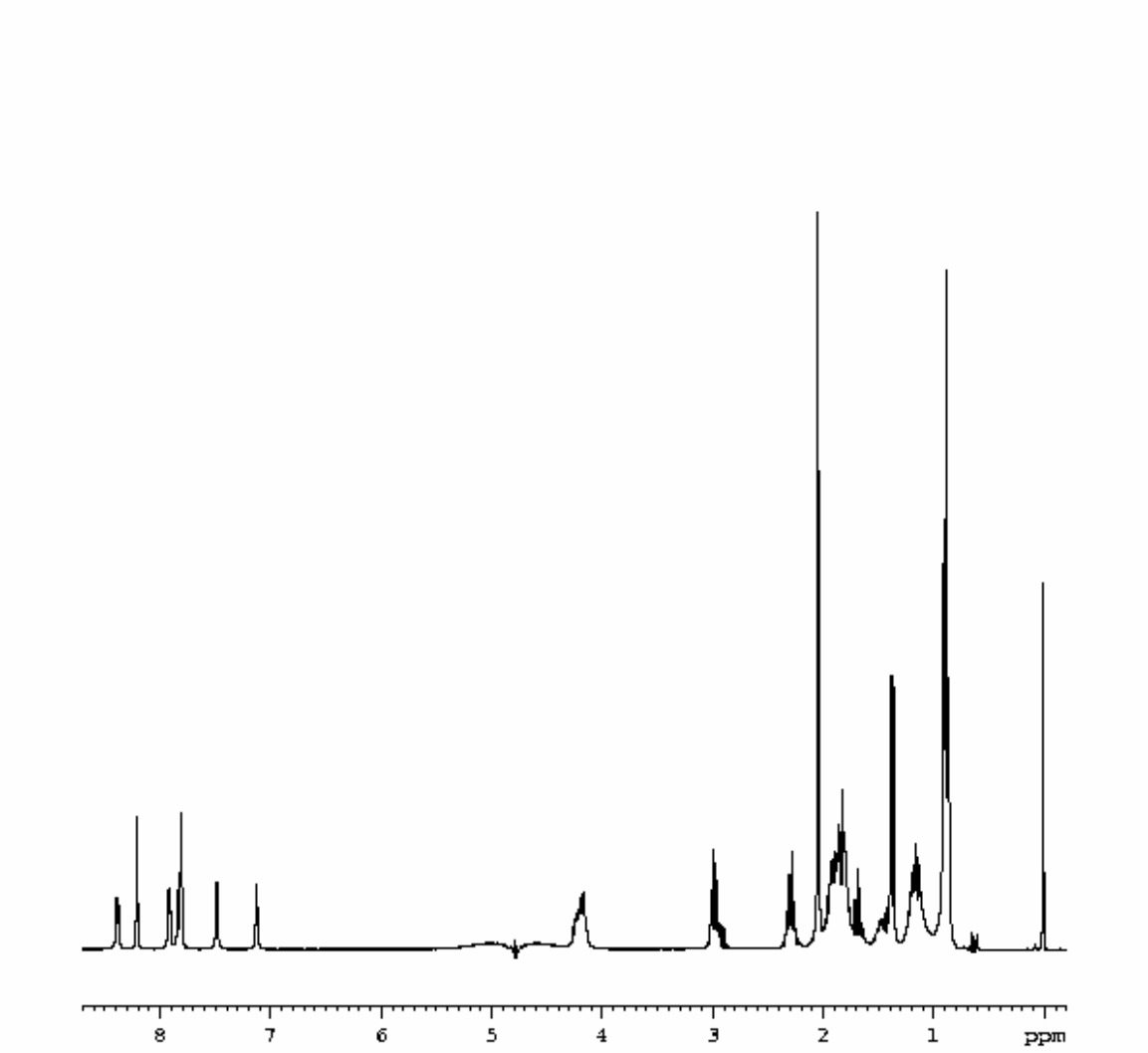

400 MHz ^{1}H NMR of 10 mM EK-Dpg-A in 30 mM phosphate buffer (H_2O: D_2O 9:1), pH 7.0 at 278K.

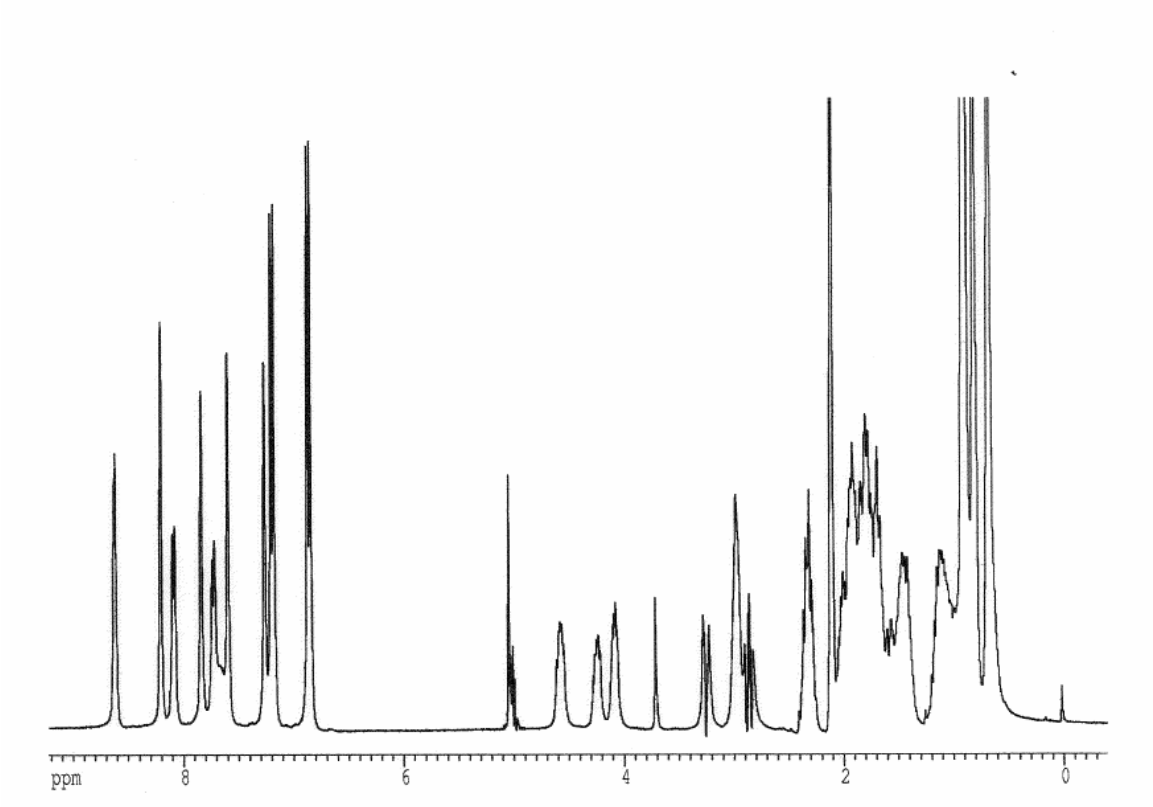

400 MHz ^{1}H NMR of 10 mM EK-Dpg-Y in 30 mM phosphate buffer (H_2O: D_2O 9:1), pH 7.0 at 278K.

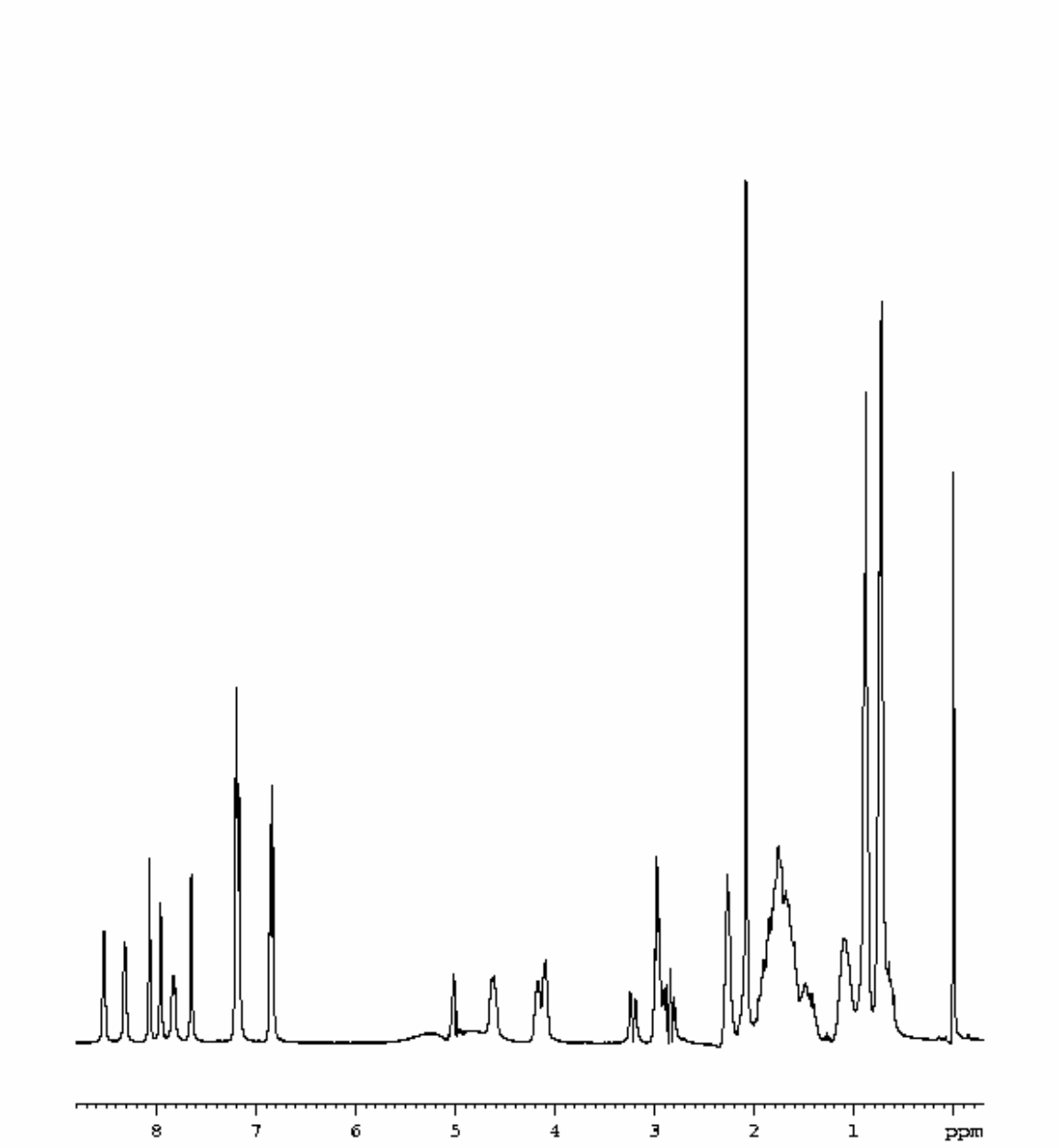

400 MHz ^{1}H NMR of 10 mM KE-Dpg-Y in 30 mM phosphate buffer (H_2O: D_2O 9:1), pH 7.0 at 278K.

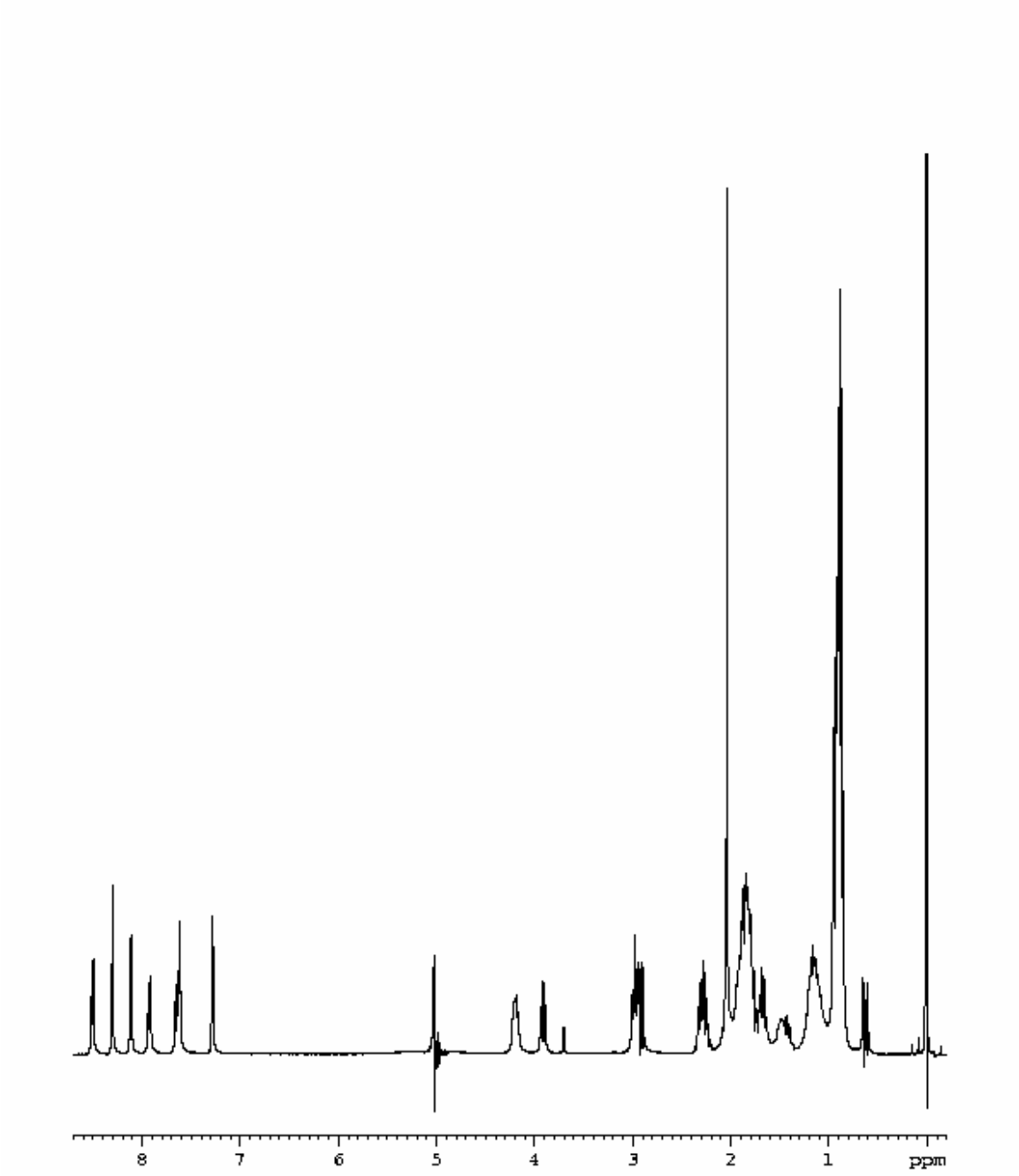

400 MHz ^{1}H NMR of 10 mM EK-Dpg-V in 30 mM phosphate buffer (H_2O: D_2O 9:1), pH 7.0 at 278K.

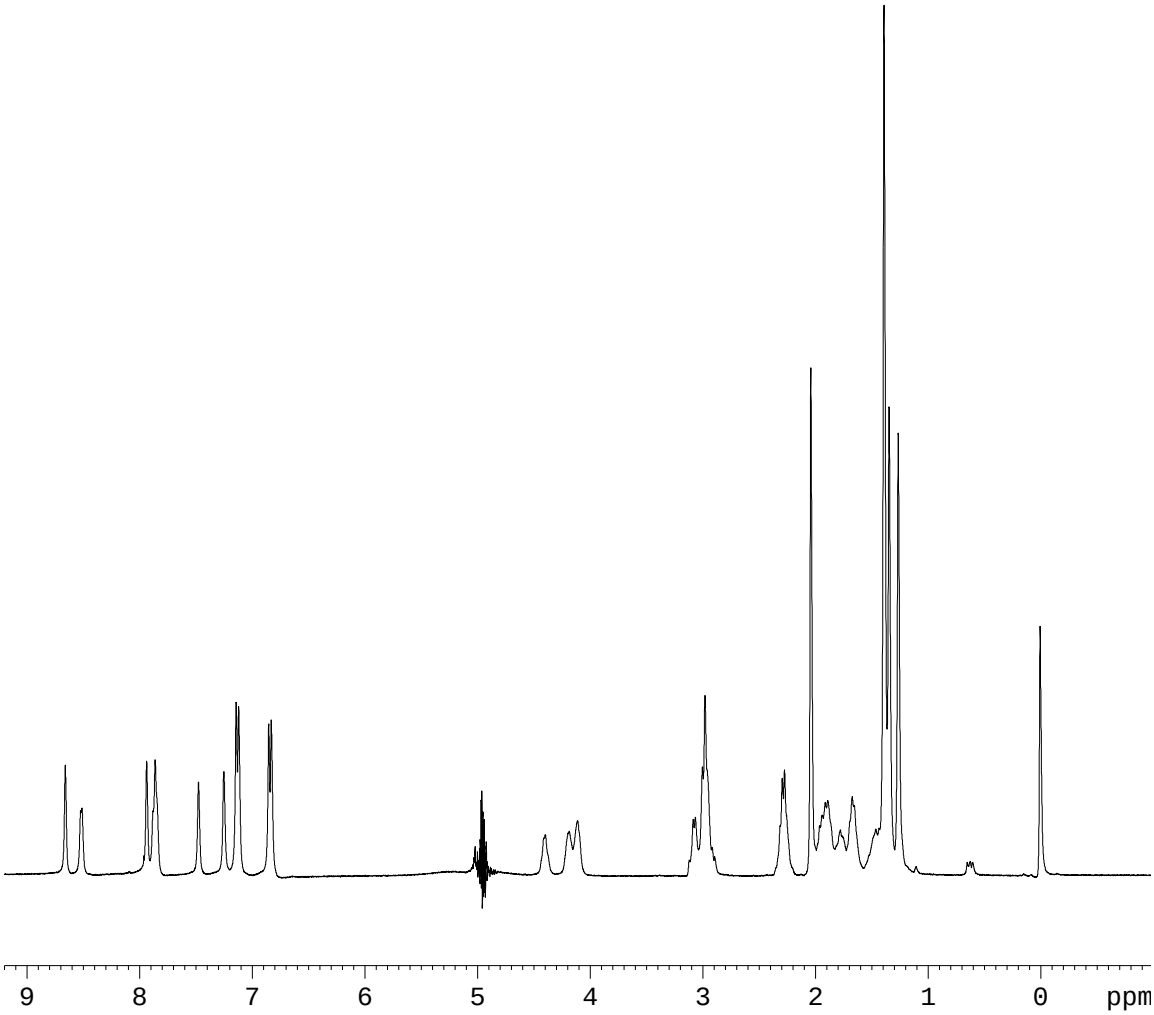

400 MHz ^{1}H NMR of 10 mM EK-Aib-Y in 30 mM phosphate buffer (H_2O: D_2O 9:1), pH 7.0 at 278K.

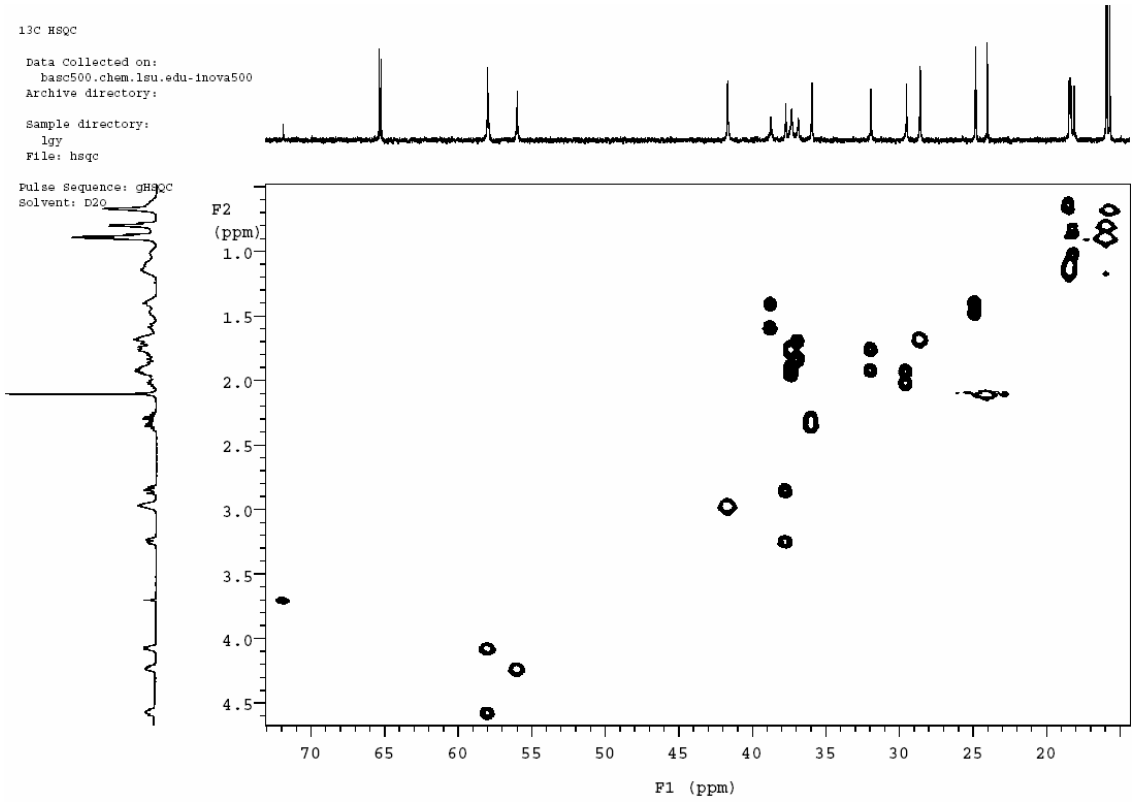

Portion of ^{1}H-^{13}C HSQC spectrum of EK-Dpg-Y in phosphate buffer (H_2O: D_2O 9:1), pH 7.0 at 278 K

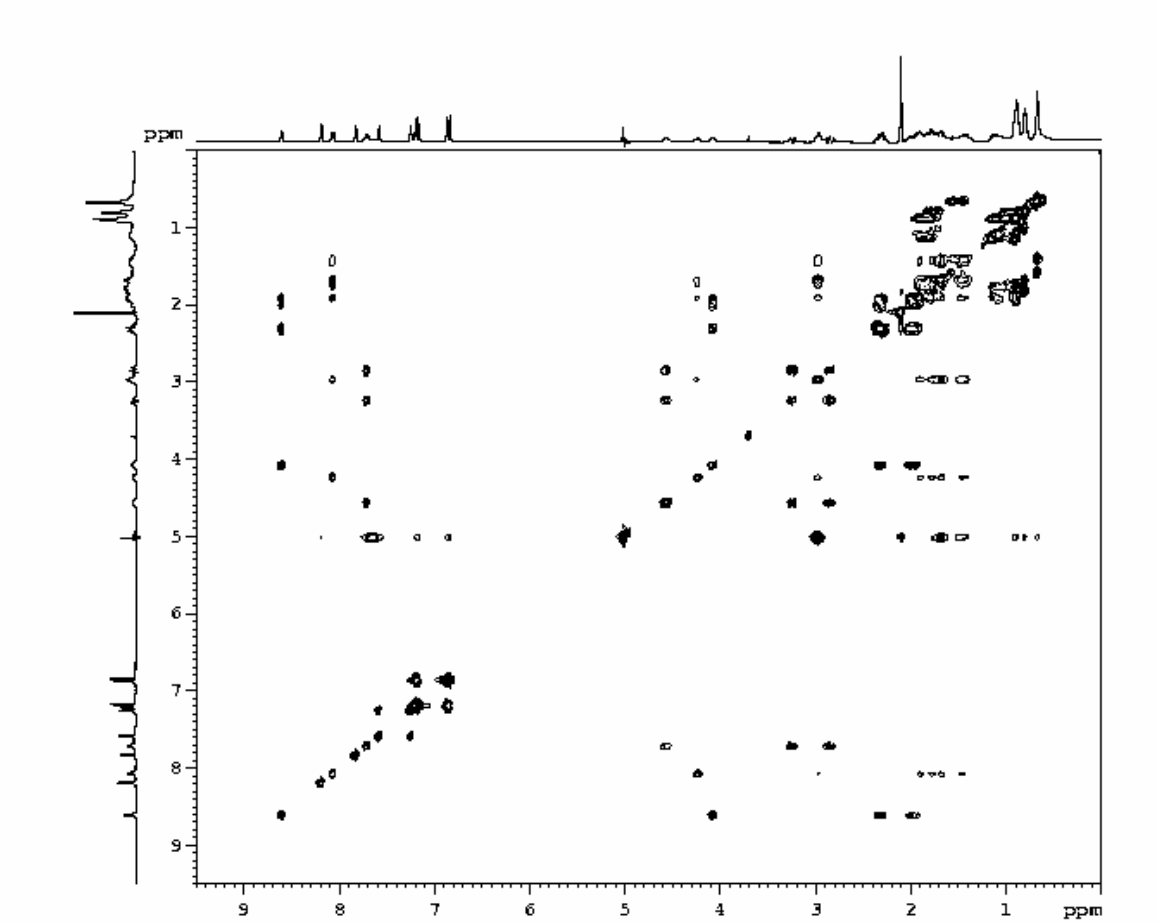

TOCSY spectrum of 10 mM EK-Dpg-Y in 30 mM phosphate buffer (H_2O: D_2O 9:1), pH 7.0 at 278 K. A spin –lock mixing time of 144 ms was used.

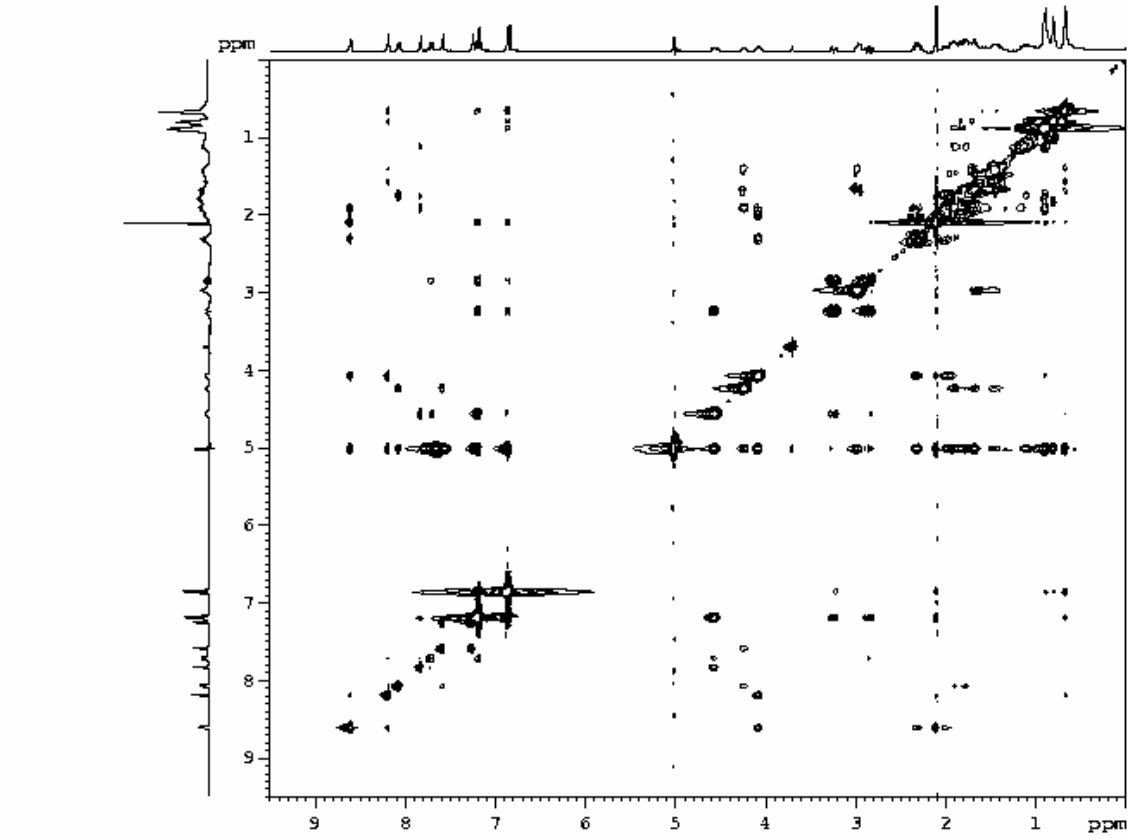

ROESY spectrum of 10 mM EK-Dpg-Y in 30 mM phosphate buffer (H_2O: D_2O 9:1), pH 7.0 at 278 K. A spin –lock mixing time of 400 ms was used.

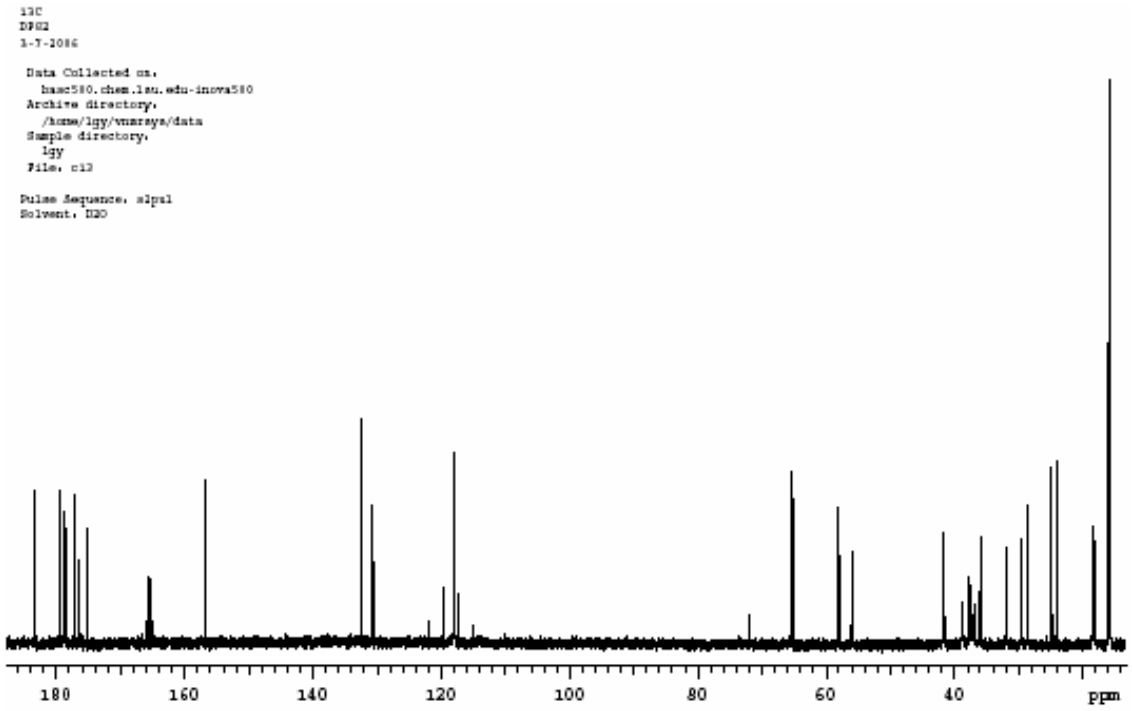

^{13}C NMR spectrum of 10 mM EK-Dpg-Y in 30 mM phosphate buffer (H_2O: D_2O 9:1), pH 7.0 at 278 K

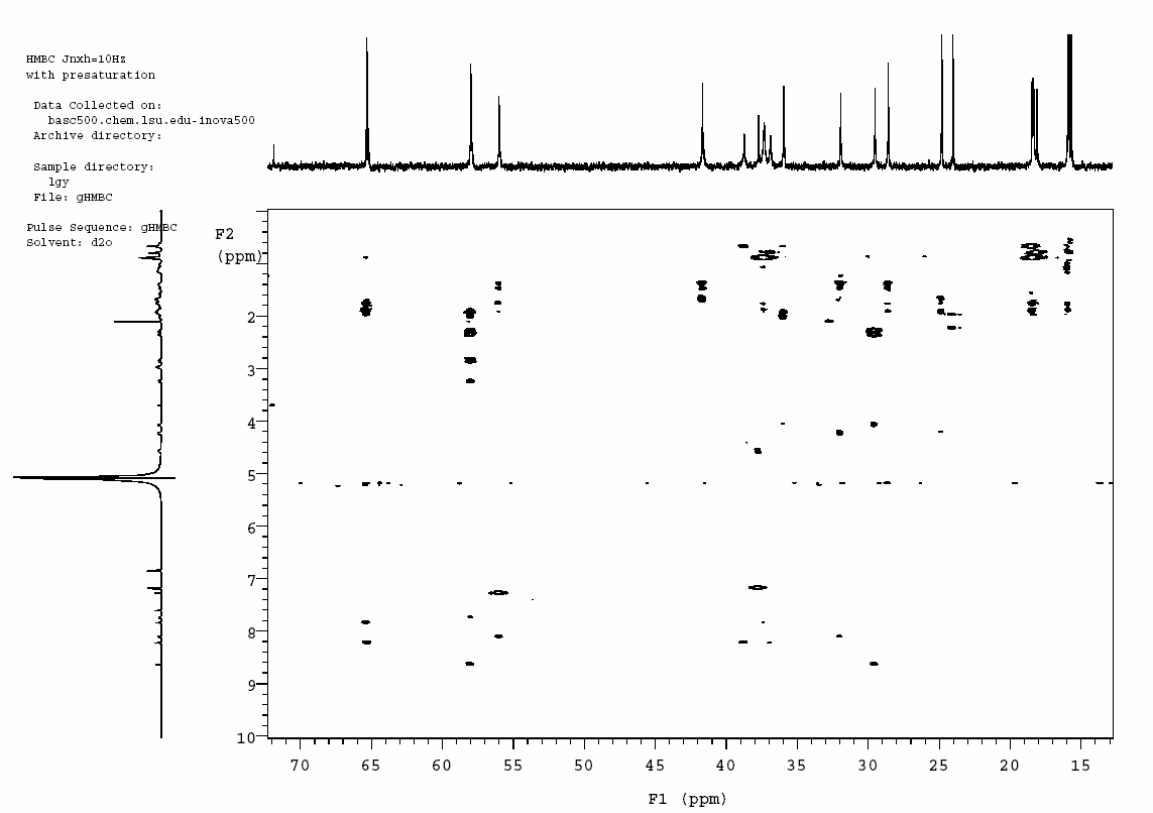

Portion of ^{1}H-^{13}C HMBC spectrum of 10 mM EK-Dpg-Y in phosphate buffer (H_2O: D_2O 9:1), pH 7.0 at 278 K

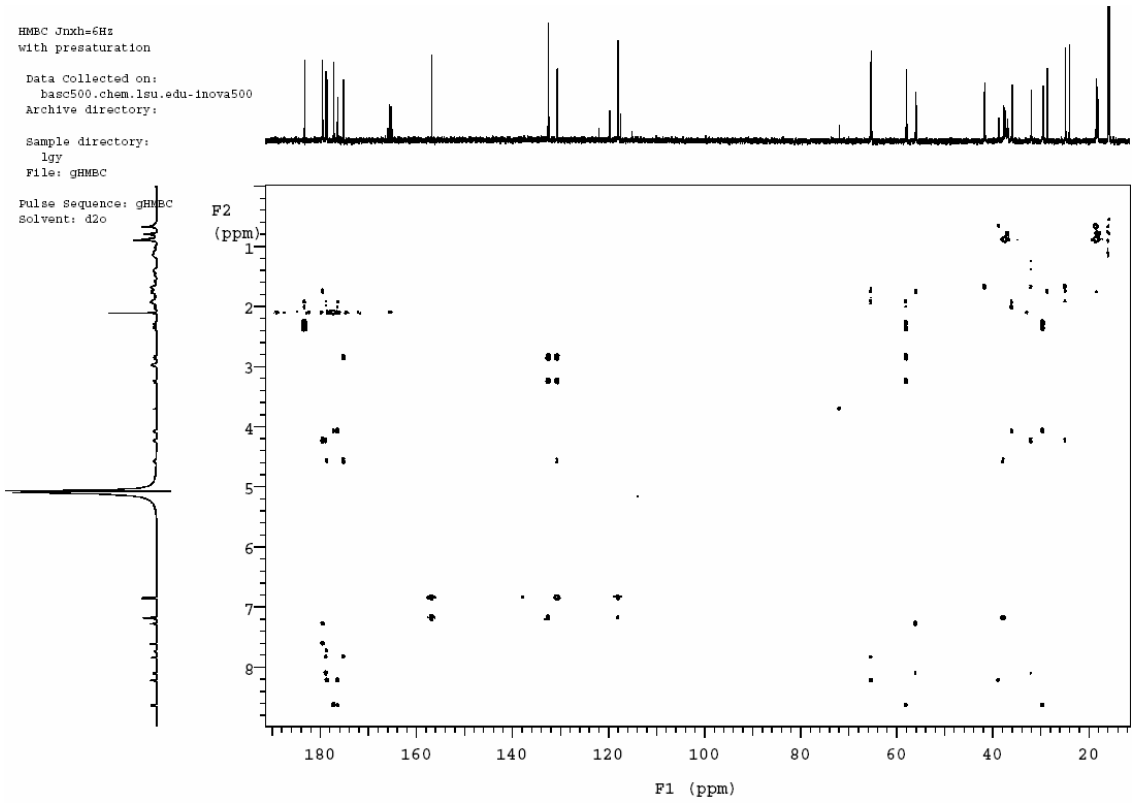

^{1}H-^{13}C HMBC spectrum of 10 mM EK-Dpg-Y in phosphate buffer (H_2O: D_2O 9:1), pH 7.0 at 278 K

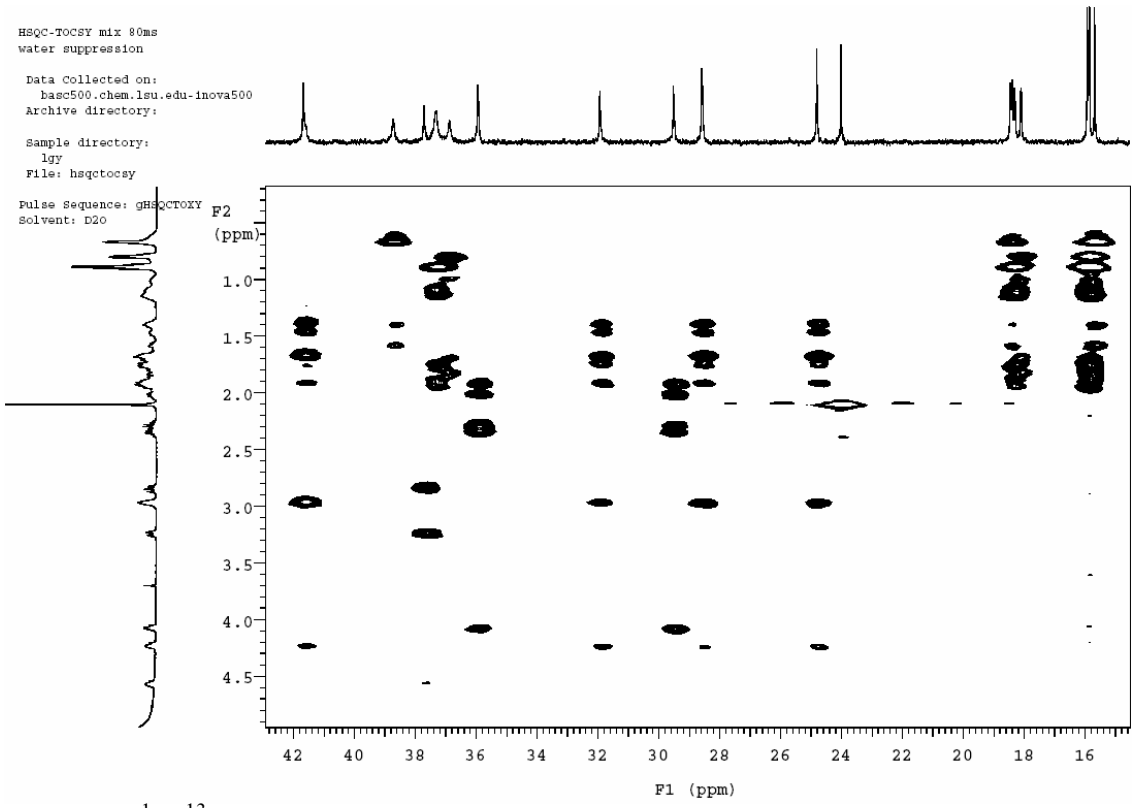

Portion of ^{1}H-^{13}C HSQC-TOCSY spectrum of 10 mM EK-Dpg-Y in phosphate buffer (H_2O: D_2O 9:1), pH 7.0 at 278 K

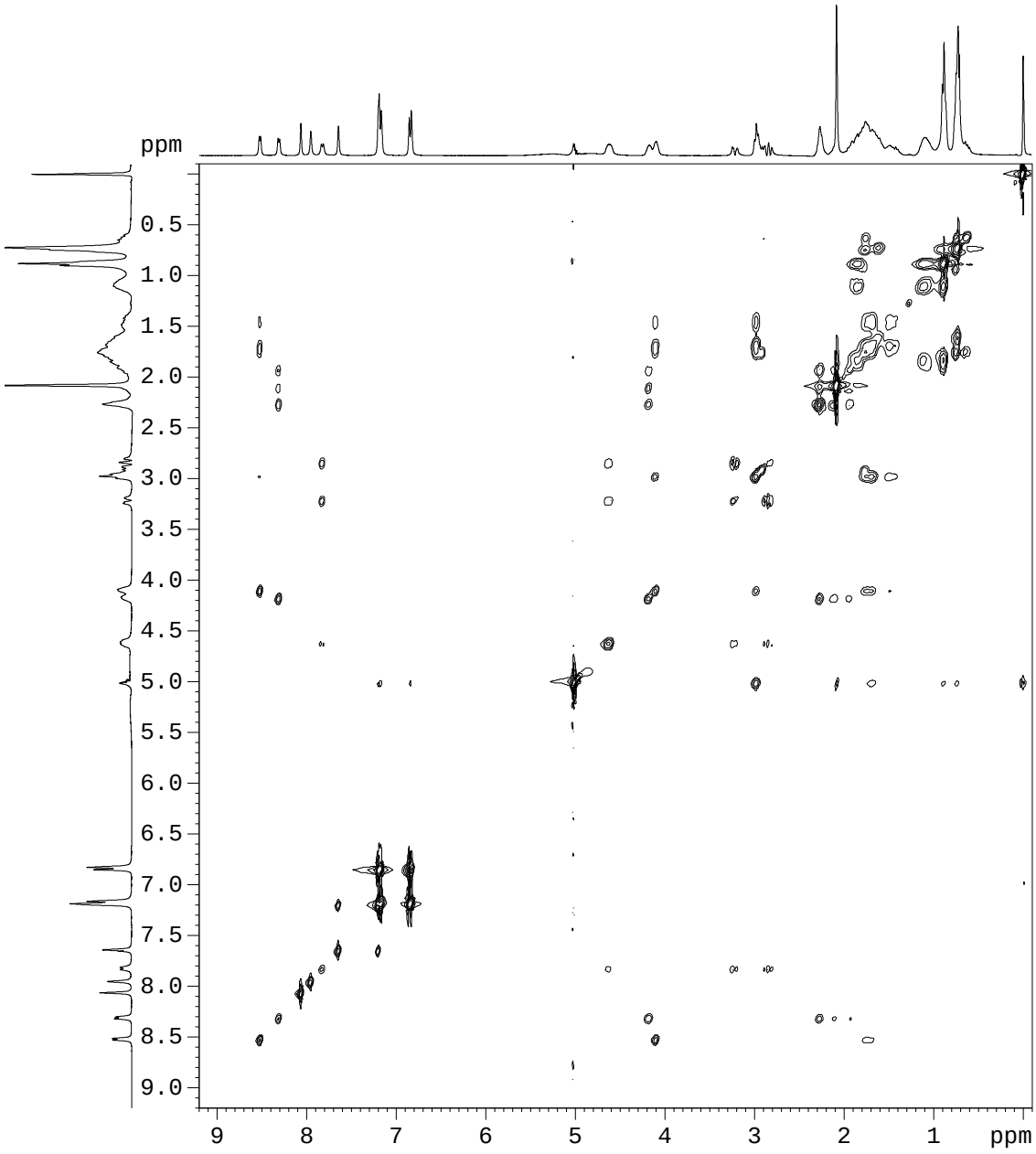

400 MHz TOCSY spectrum of 10 mM KE-Dpg-Y in 30 mM phosphate buffer (H_2O: D_2O 9:1), pH 7.0 at 278 K. A spin-lock mixing time of 144 ms was used.

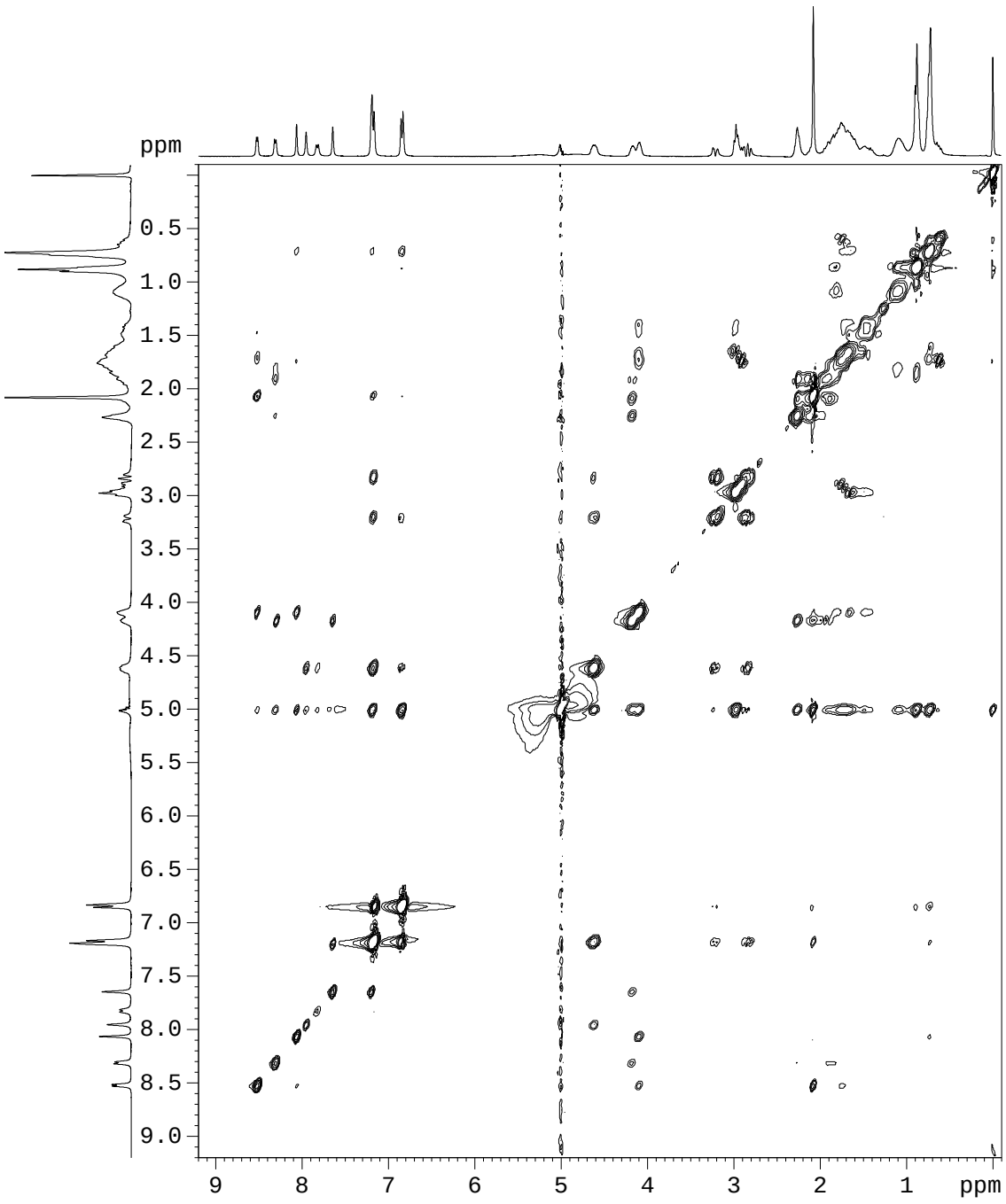

400 MHz ROESY spectrum of 10 mM KE-Dpg-Y in 30 mM phosphate buffer (H_2O: D_2O 9:1), pH 7.0 at 278 K. A spin-lock mixing time of 400 ms was used.

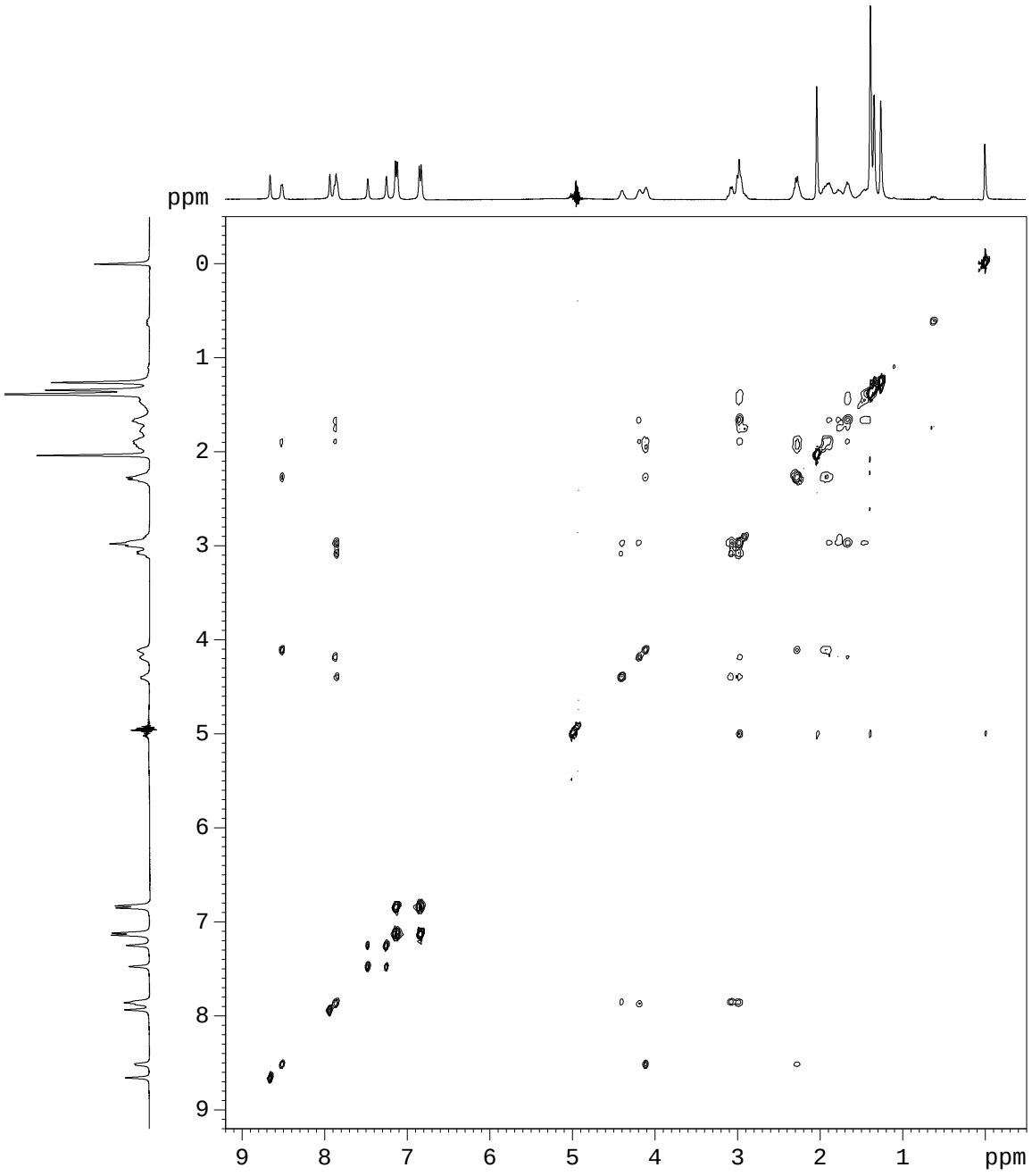

400 MHz TOCSY spectrum of 10 mM EK-Aib-Y in 30 mM phosphate buffer (H_2O: D_2O 9:1), pH 7.0 at 278 K. A spin-lock mixing time of 144 ms was used.

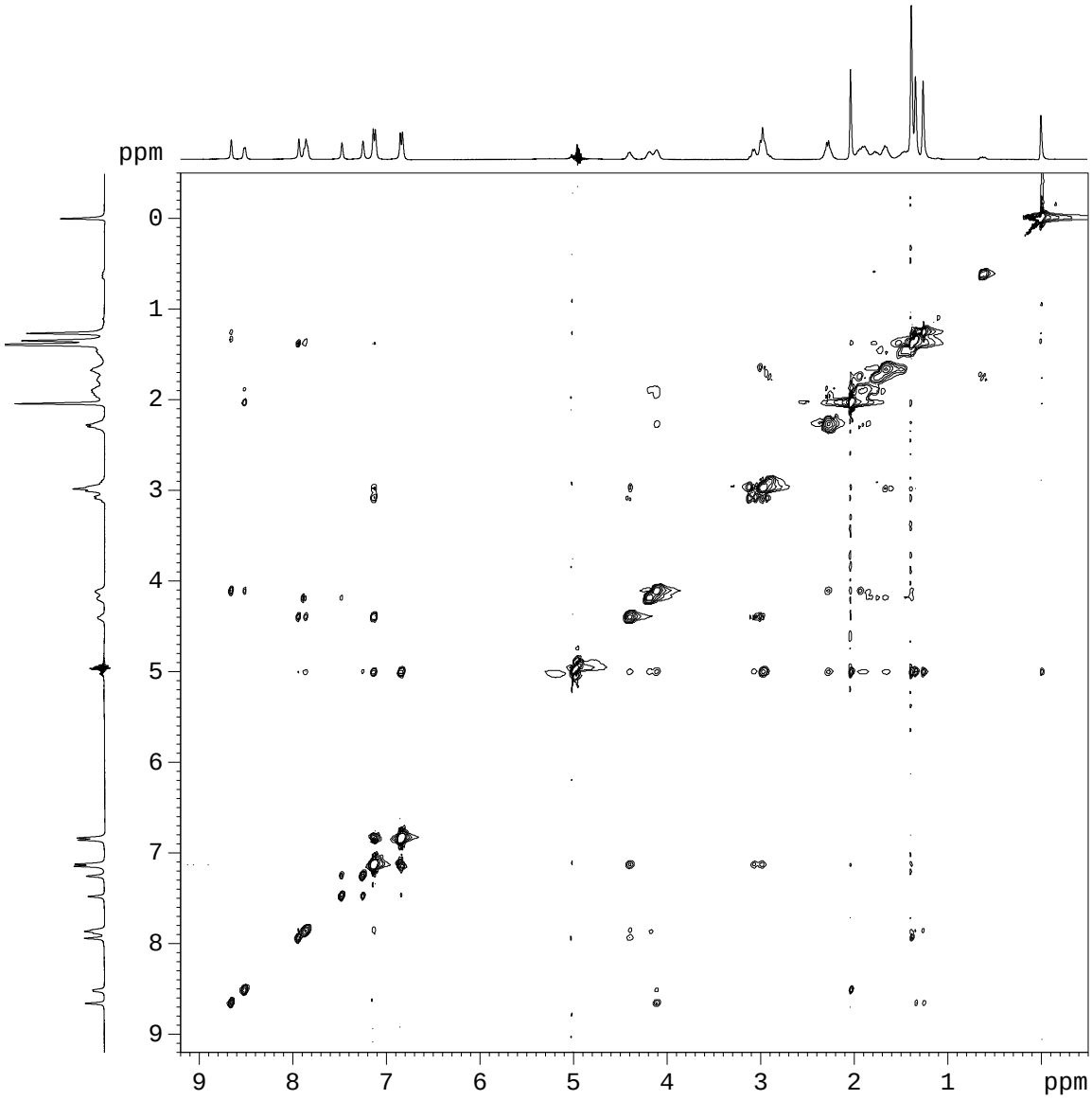

400 MHz ROESY spectrum of 10 mM EK-Aib-Y in 30 mM phosphate buffer (H_2O: D_2O 9:1), pH 7.0 at 278 K. A spin-lock mixing time of 400 ms was used.

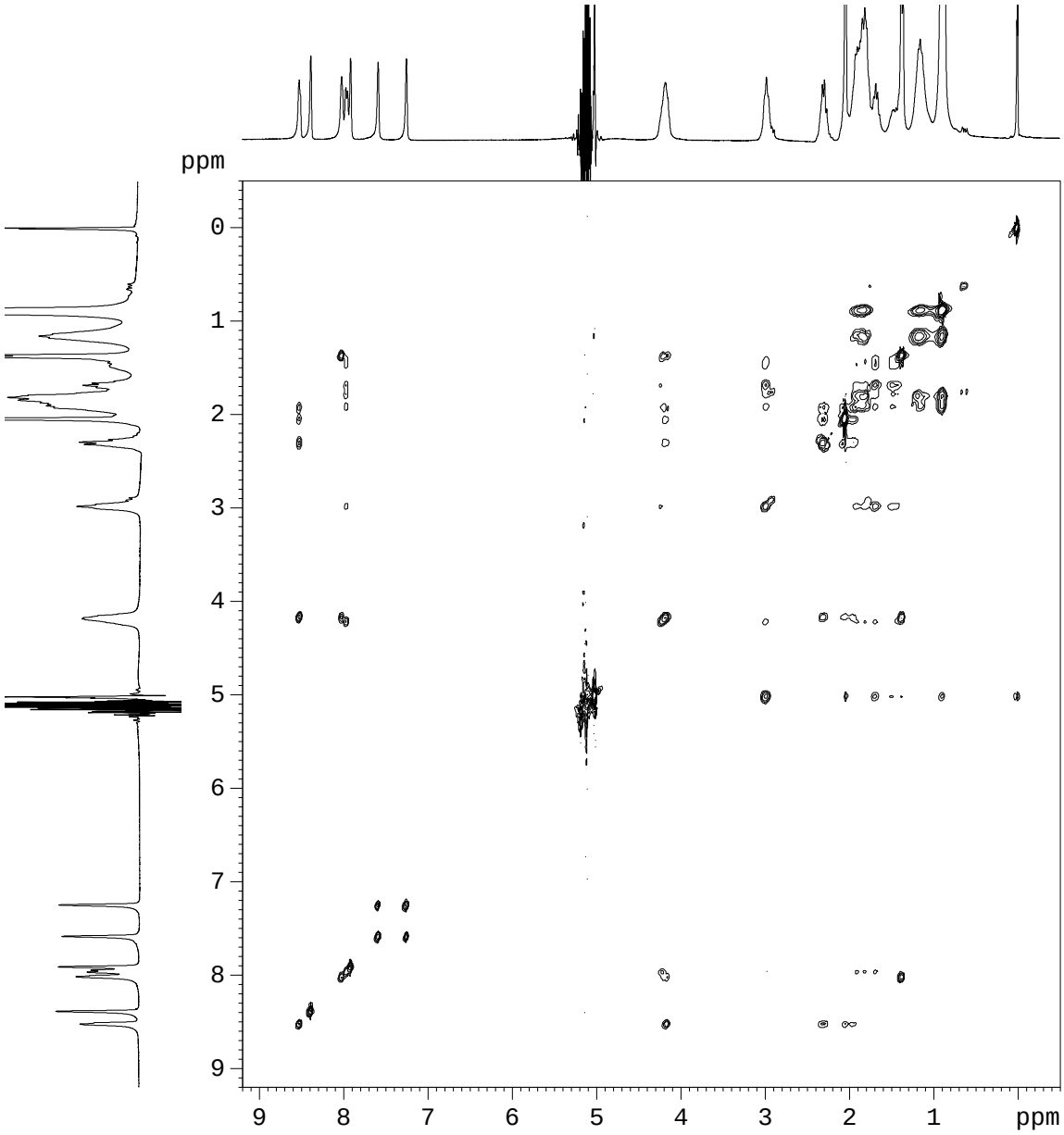

400 MHz TOCSY spectrum of 10 mM EK-Dpg-A in 30 mM phosphate buffer (H_2O: D_2O 9:1), pH 7.0 at 278 K. A spin-lock mixing time of 144 ms was used.

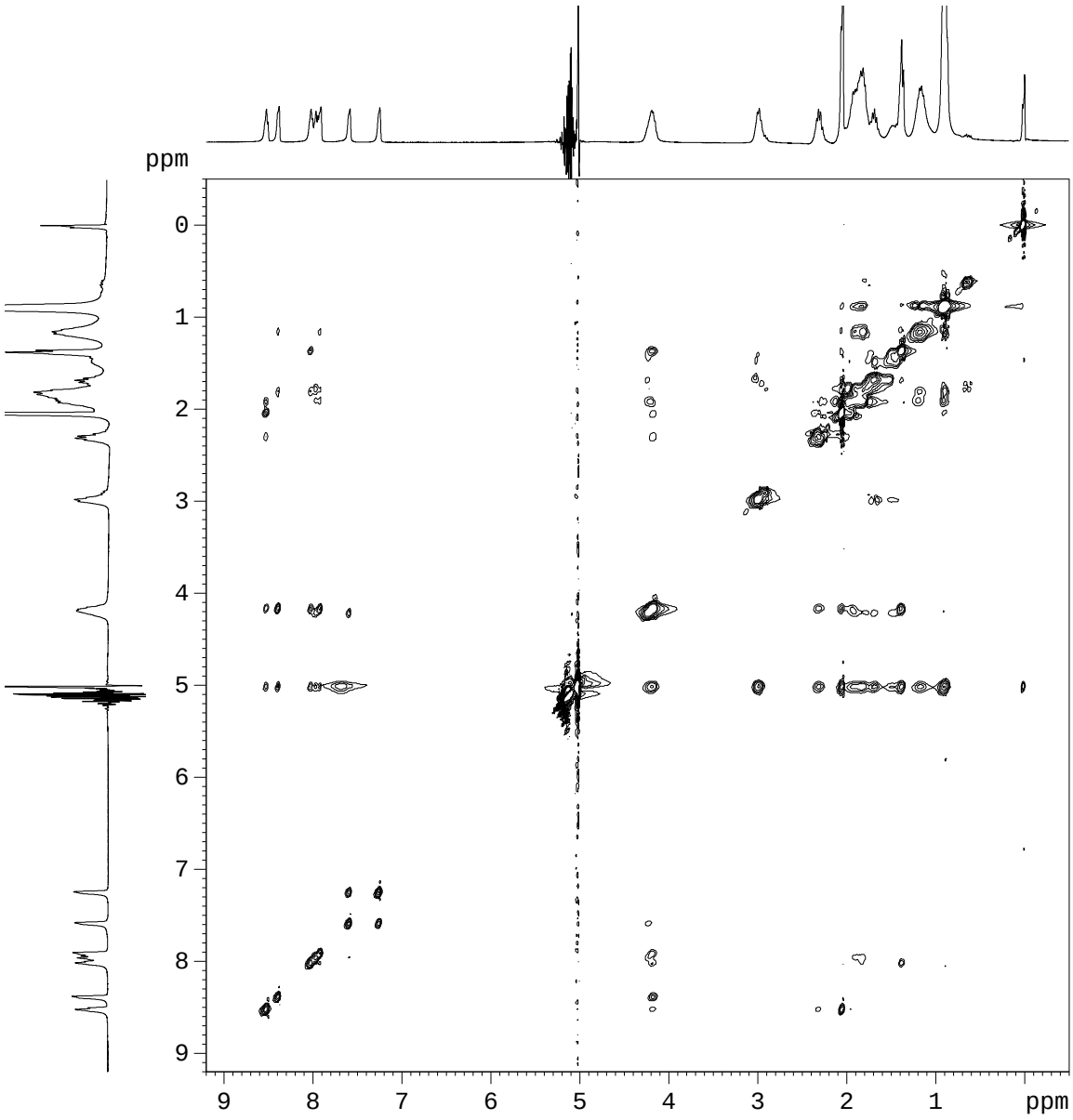

400 MHz ROESY spectrum of 10 mM EK-Dpg-A in 30 mM phosphate buffer (H_2O: D_2O 9:1), pH 7.0 at 278 K. A spin-lock mixing time of 400 ms was used.

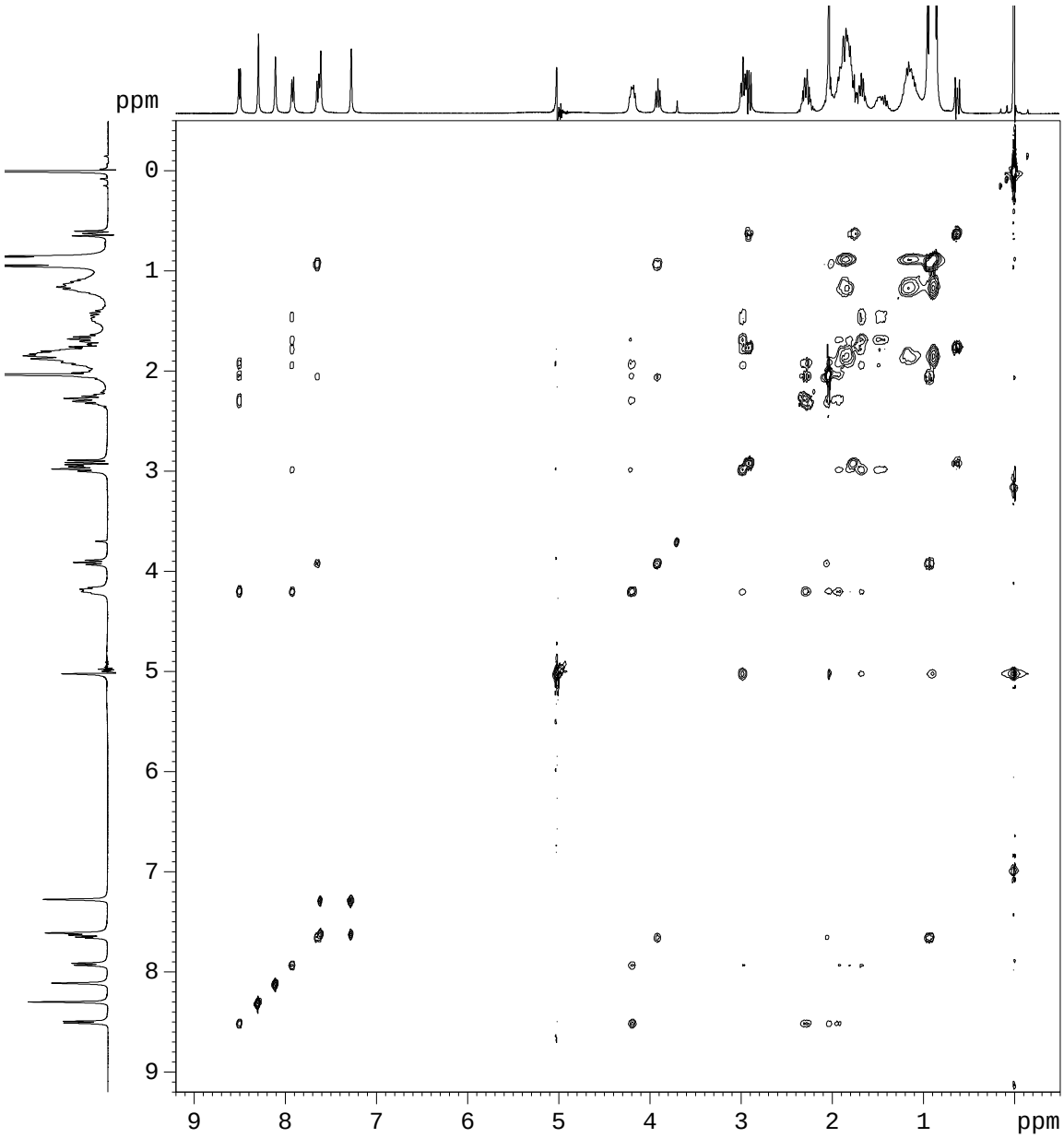

400 MHz TOCSY spectrum of 10 mM EK-Dpg-V in 30 mM phosphate buffer (H_2O: D_2O 9:1), pH 7.0 at 278 K. A spin-lock mixing time of 144 ms was used.

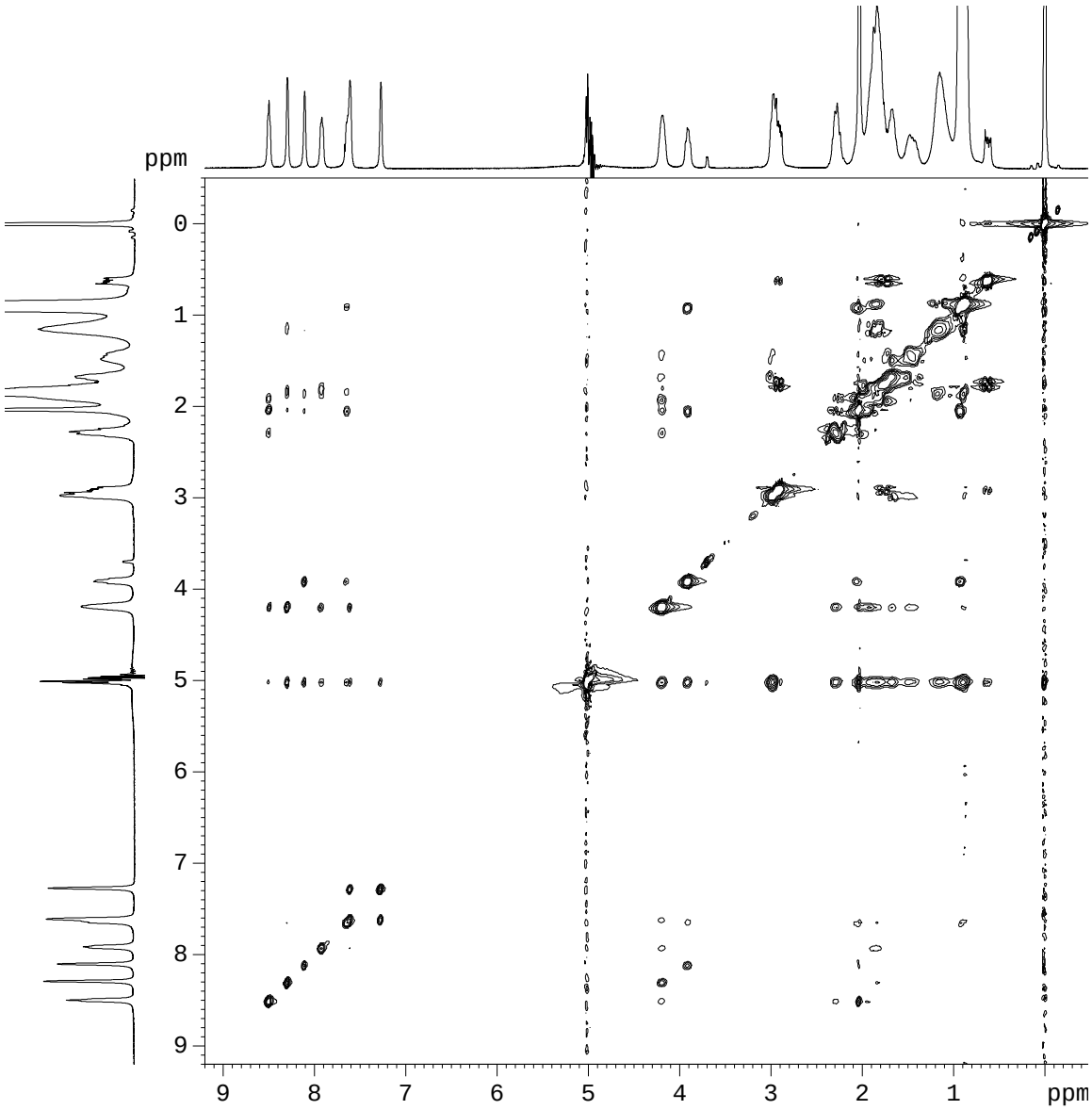

400 MHz ROESY spectrum of 10 mM EK-Dpg-V in 30 mM phosphate buffer (H_2O: D_2O 9:1), pH 7.0 at 278 K. A spin-lock mixing time of 400 ms was used.

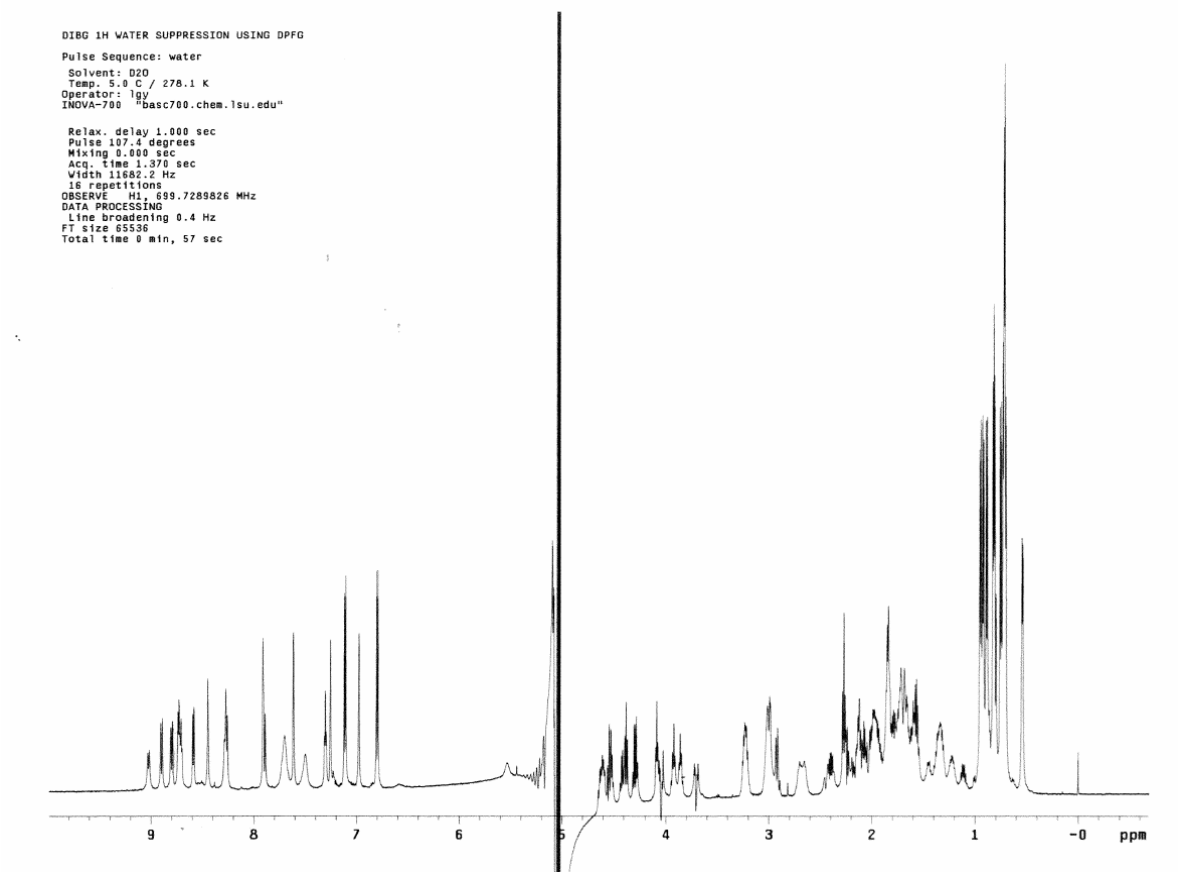

700 MHz ^{1}H NMR spectrum of 3.5 mM Dibg^{3}-GHP in 100 mM aqueous sodium deuterioacetate buffer (H_2O: D_2O 9:1), pH 3.8 at 278 K.

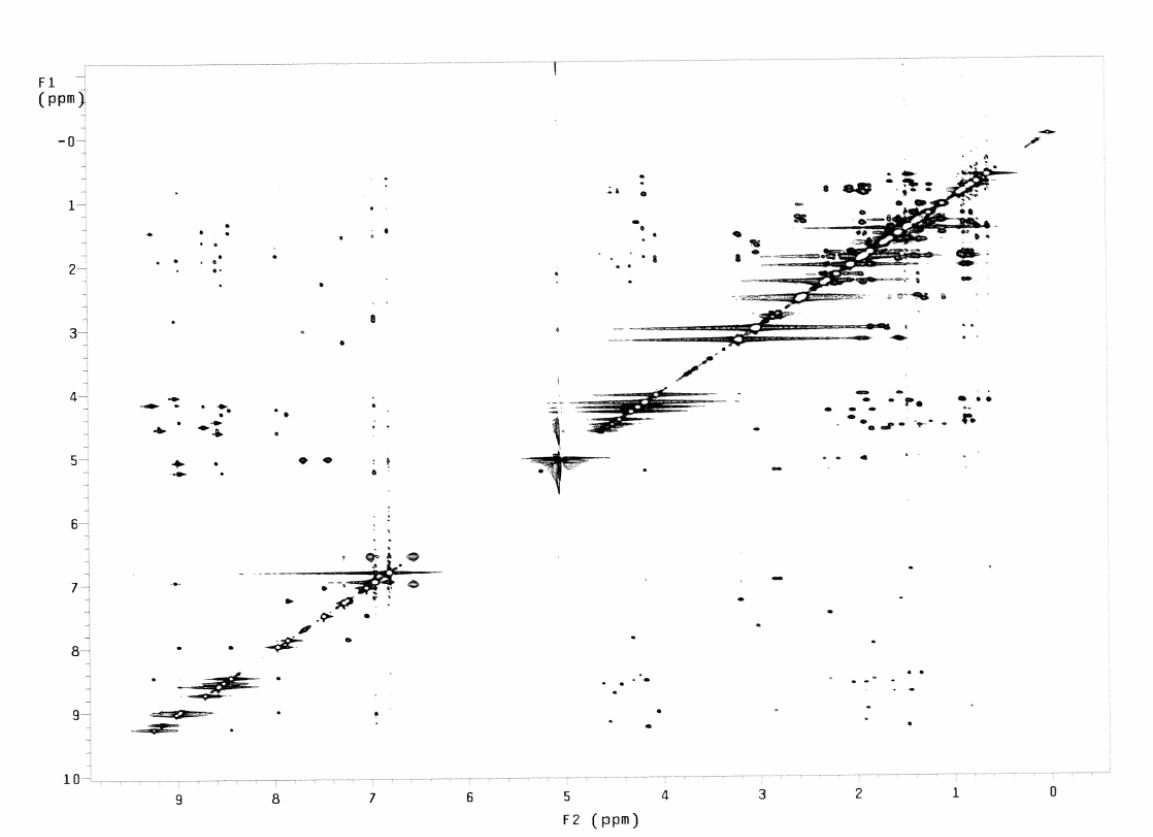

700 MHz ROESY spectrum of 3.5 mM Dibg^3-GHP in 100 mM aqueous sodium deuterioacetate buffer (H_2O: D_2O 9:1), pH 3.8 at 278 K.

VITA

Jia Wang received her Bachelor of Science degree in chemistry at Dalian University, China, in 1996. She joined the Department of Chemistry at Louisiana State University in Baton Rouge, Louisiana in 2002, where she is currently a candidate for the degree of Doctor of Philosophy in chemistry.